Characterization of the role of VEGFA isoforms in cell migration and metastasis using engineered microenvironments

Yu-Chin Lee

A thesis submitted in partial fulfilment of the requirements for the degree of Doctor of Philosophy

The University of Sheffield

Faculty of Medicine, Dentistry & Health

The Medical School

February 2023

Acknowledgement

First of all, I would like to express my gratitude to my supervisors Dr. Will English and Prof. Frederik Claeyssens for their support during my PhD. Their kindness, knowledge, encouragement and guidance gave me the courage to face any challenges optimistically over the 4-year journey. Their creativity also inspires me with many ideas for the project. I would also like to thank the rest of the group members, Claudia and Nada, for their help and accompany in the lab. It is very joyful to work with you two every day. You two are the best.

I would also like to thank the "Study Abroad Scholarship" received for 2-year during my PhD from the Taiwanese Government. Without their support for experiment consumables, I would not be able to complete my PhD and develop this project.

Finally, I am indebted to my friends and family for their support throughout the 4-year study. Always stand behind me providing the greatest spiritual support, especially during the pandemic lockdown. Thank you to whoever gives a hand wherever in or out of the lab. Love you all.

Abstract

Background: Mortality in cancer patients is predominantly caused by metastasis. Understanding mechanisms that lead to cancer cells gaining metastatic potential may lead to novel therapies that could prevent metastasis and improve overall survival. Increased cellular plasticity in adopting different modes of migration has been identified as an important factor in efficient metastasis. Although it is predominantly known as a major regulator of angiogenesis, Vascular Endothelial Growth Factor A (VEGFA) has also been shown to regulate cell migration and thus metastatic potential. *VEGFA* encodes for several isoforms through alternate mRNA splicing which exerts differences in signalling and biological activity. Using fibrosarcomas derived from mouse embryonic fibroblasts genetically engineered to express a single VEGFA isoform, previous research I contributed to showed there was an increased number of metastases to the lung from cells expressing only VEGFA120 (fs120 cells) compared to cells expressing VEGFA188 (fs188 cells) suggesting fs120 cells may have better metastatic potential. These studies also showed metastasis to the lung was selectively inhibited by anti-VEGFA antibodies in mice with fs120 tumours and this acted in part through inhibition of migration (English et al., 2017). During my MSc studies, I extended these studies of migration and found fs120 cells could migrate more efficiently in a custom non-adherent migration chamber than fs188 cells and this was inhibited by anti-VEGFA antibodies. As these suggested VEGFA120-expressing cells have greater plasticity in modes of cell migration and can adapt to more varied environments than VEGFA188-expressing cells, we hypothesised increased metastatic potential is VEGFA isoform-dependent and linked to an ability to adopt different migration modes in response to different microenvironments. However, as there are differences in embryonic development between mice expressing VEGFA120 and VEGFA188, and the mice were not isogenic, these findings needed to be confirmed in a new model with identical developmental and genetic backgrounds.

Objectives: To create new fibrosarcoma cell lines expressing single VEGFA isoforms to characterise differences in cell migration in comparison with embryonic-derived fibrosarcomas and to develop novel engineered microenvironments to test the plasticity of cell migration.

Methodology: Fibrosarcomas expressing only VEGFA120 or VEGFA188 were derived from *Vegfa* knockout (KO) adult mouse fibroblasts by stably introducing a VEGFA expression cassette using a transposon. Cellular functions, including cell proliferation, and the expression of cell migration-related proteins were characterized by MTT assay and western blotting in selected clones. PCL electrospinning of fibre scaffolds was used to mimic fibrillar collagen structures seen after imaging fs120 and fs188 mouse tumour sections by second-harmonic generation microscopy to generate a novel environment to characterise plasticity in migration. Cell migration capacity of adult- versus embryonic-derived fibrosarcomas expressing a single

VEGFA isoform was characterised using *in vitro* platforms by single-cell live imaging. Altered expression of cell migration-related proteins across cell lines on treatment with inhibitors targeting VEGFA signal transduction (VEGFA by antibody B20.4.1.1, VEGFR1 by antibody MF-1 and VEGFR/PDGFR/FGFR by receptor tyrosine kinase inhibitor pazopanib) were characterized by Western blotting.

Results: The expression of single VEGFA isoforms in new, fibrosarcoma cell lines, derived from *Vegfa* KO fibroblasts, were successfully generated to express VEGFA at comparable levels to the fs120 and fs188 cells as determined by ELISA and QRT-PCR. There was no difference in the expression of VEGFR1 across any of the cell lines, but the upregulated expression of NRP1 was seen in fs188 cells compared to other cell lines. Increased phosphorylated Akt was observed in all fibrosarcoma cells generated from embryonic fibroblasts and in adult *Vegfa* KO cells expressing VEGFA188. Moreover, fs120 cells expressed a higher level of SOX2 than all other cell lines. The migration capacity of cells on 2D surfaces coated with fibronectin or collagen and on 3D-aligned fibre scaffolds was similar between VEGFA120 and VEGFA188 expressing cells, and independent of their origin. Interestingly, suppressed migration capacity was detected only in cells expressing VEGFA120 on treatment with the anti-VEGFA antibody, B20.4.1.1, indicating VEGFA isoform selective response independent of cell origin. The anti-VEGFR1 antibody MF-1 did not inhibit migration. Increased phosphorylation of VEGFR1 in VEGFA120-expressing fibrosarcoma cells was observed on treatment with B20.4.1.1 and pazopanib, but not MF-1. However, increases in phosphorylated Akt were repressed only by pazopanib treatment.

Conclusions: Fibrosarcoma cells expressing different VEGFA derived from different origins share similar characteristics, suggesting VEGFA isoform-independent changes between models. Downregulated migration capacity in fibrosarcoma cells expressing VEGFA120 in response to anti-VEGFA antibody, B20.4.1.1, was also independent of cell origin. Fibrosarcoma cells expressing VEGFA120 and VEGFA188 have comparable capacity in 2D and fibrillar migration. The differential expression of a VEGFA single isoform may not contribute to the modulation of plasticity in cell migration modes. However, in previous results from the MSc thesis, the motility of fs188 cells was abolished in the confined non-adherent chamber compared with fs120 cells. This discrepancy suggests that the varying expression of VEGFA isoforms in fibrosarcoma cells may play roles in regulating the adaptation of amoeboid mode that is integrin-independent, as opposed to migrating on 1D fibrillar structures. Nonetheless, confirming this idea would necessitate evaluating the migratory abilities of new cell lines within the confined non-adherent chamber. Upregulation of p-VEGFR1 was observed in VEGFA120-expressing cells treated with anti-VEGFA antibody and pazopanib, whereas downregulation of p-Akt was observed only with the pazopanib treatment. These suggest another receptor also interacting with VEGFA120 participates in regulating cell migration. In

conclusion, the expression of VEGFA120 may potentially increase cell plasticity through another receptor, besides VEGFR, interacting with VEGFA. This signalling pathway is affected explicitly by the anti-VEGFA antibody and pazopanib. These outcomes open up a novel target for further treatment to prevent metastasis.

Table of contents

List of Figures

List of tables

Chapter 1

1. Introduction

1.1 Introduction to cancer

1.1.1 Hallmarks of cancer

Cancer is a leading cause of death worldwide, with the number of new cases diagnosed worldwide each year expected to increase from 17 million to over 30 million by 2040. Cancer is a disease in which cells gain new capabilities including uncontrolled proliferation, escape from growth suppressors, resisting cell death, becoming immortal, promoting angiogenesis, evading immunosurveillance, reprogramming metabolic mechanisms, evoking plasticity, invading surrounding tissues and metastasis, and triggering cellular senescence (Hanahan, 2022; Hanahan & Weinberg, 2011). Hanahan and Weinberg described these abilities as cancer hallmarks. Additionally, another four hallmarks are characterized as enabling characteristics, including genome instability and mutation, tumour-promoting inflammation, non-mutational epigenetic reprogramming and polymorphic microbiomes (Hanahan, 2022; Hanahan & Weinberg, 2011), which activate the ten emerging hallmarks listed above.

Genome instability and mutation are the dominant initiators of tumorigenesis that lead to the mutational activation of proto-oncogenes and loss of tumour suppressor genes, which regulate different cellular functions, such as proliferation, apoptosis, DNA repair and cell cycle checkpoints (Kontomanolis et al., 2020; Lee & Muller, 2010). The formation of tumours is an accumulation of multiple events of activation of oncogenes along with loss of tumour suppression genes. For example, *MYC* is a common oncogene that simultaneously controls proliferation and apoptosis (Vita & Henriksson, 2006). Activation of MYC, frequently through gene amplification, is often accompanied by the amplification of *Bcl2*, an oncogene that suppresses apoptosis (Li et al., 2019; Shortt & Johnstone, 2012; Strasser et al., 1990), or the loss of *TP53* function, a tumour suppressor gene and transcription factor that counters apoptosis and regulates the proliferation of cancer cells and disease progression in multiple types of cancer (Chen, Liu, & Tao, 2020; Hill et al., 2015). Moreover, *RAS* is a small GTPase and proto-oncogene family which frequently becomes active through mutation in human cancer and has three subsets, *K-RAS*, *H-RAS* and *N-RAS*. Besides enhancing cell proliferation and survival, the *RAS* family also participates in remodelling the tumour microenvironment, evading the immune system and promoting metastasis (Pylayeva-

Gupta, Grabocka, & Bar-Sagi, 2011). Upregulated expression of VEGFA mediated by oncogenic *KRAS* was observed in colon cancer that supported tumour growth (Ueyama & Nakamura, 2000). Oncogenic *KRAS* also downregulated the expression of antigen-presenting molecules, major histocompatibility complexes (MHC), on cancer cell surfaces resulting in an anti-immune response (Testorelli et al., 1997). Furthermore, acquired invasiveness and metastatic properties through the mutation of Ras and hyperactivation of its downstream PI3K signalling were found in breast cancer (Pylayeva et al., 2009). According to the thesis topic, the following sections will focus on metastasis and how cells gain metastatic potential.

1.1.2 Disease progression and metastasis

The National Health Service (NHS) in the UK has classified cancer progression into five stages from 0 to 4 based on the size of tumours and the distance of spread. When cancer remains *in situ* without spreading, it is classed between stage 0 to 2 based on the tumour size. However, once cancer invades the surrounding tissue, it is normally classed as stage 3, and metastasis has begun. Stage 4 is the last stage in which metastasis has been completed and is clinically detectable at tissue and organ sites distant from the primary tumour. Metastasis is a major cause of mortality in cancer patients, but it is difficult to prevent in advance and to treat due to its complex multi-step process, genetic heterogeneity of cancer cells, their adaptability and resistance to treatments, the influence of microenvironmental factors, difficulties in early detection, lack of specific targets, potential dormancy of metastatic cells, and the evolving nature of treatment resistance. These factors collectively hinder effective intervention against the spread of cancer to other parts of the body. Identification of the mechanisms that lead to cancer cells gaining metastatic potential is critical so that progression is prevented and to increase chances of treating metastatic disease. The events of disease progression from the primary tumour to metastasis are broken down into three steps described in the following sections: the acquisition of metastatic potential in the primary tumour, transit and survival, and formation of the metastatic niche allowing growth at the secondary site (Fares et al., 2020; Labelle & Hynes, 2012).

1.1.2.1 The acquisition of metastatic potential in the primary tumour

The first stage of cancer cells gaining metastatic potential is to exit from the primary tumour mass and invade the surrounding tissue. The efficacy of cancer cells

escaping from the primary tumour sites is modulated by several factors, including epithelial-mesenchymal transition (EMT), extracellular matrix (ECM) barrier, cell-ECM interaction, cell-cell adhesion and angiogenesis. It has been hypothesised that EMT is necessary, contributing to the disassociation of cancer cells from their neighbours and enhancing their mobility and invasiveness (Derksen et al., 2006). In carcinomas, downregulation of the cell-cell junction protein E-cadherin, a key event in which cells lose epithelial properties and gain mesenchymal properties, promotes metastasis in breast cancer (Onder et al., 2008). Hypoxia, which augments EMT is normally observed in large tumour masses which reach stage 2 and have the potential to develop to the higher stages. Overexpression of hypoxia-inducible factors (HIFs) in response to hypoxia initiates EMT and cell migration through activation of transcription factors that upregulate mesenchymal markers, including b-catenin, has been observed in multiple cancer types (Zhang et al., 2015; L. Zhang et al., 2013; Tsai & Wu, 2012; Krishnamachary et al., 2006). Besides direct HIF-induced EMT, HIF-activated autocrine TGF-β (Matsuoka et al., 2013) and Wnt/β-catenin (Q. Zhang et al., 2013) signalling also contribute to the regulation of EMT. Moreover, paracrine TGF-β expressed by tumour-associated macrophages (TAMs) (Liu et al., 2021; Cai et al., 2019) and cancer-associated fibroblasts (CAFs) (Huang et al., 2021) in the tumour microenvironment (TME) in response to hypoxia facilitates EMT and induces metastasis by increasing proteinase production, the release of TGF-β from extracellular stores and growth factors like HGF, formerly known as scatter factor.

Matrix metallopeptidases (MMPs) play roles in remodelling extracellular matrix (ECM). Overexpression of MMPs has been observed in multiple cancer types associated with poor disease survival and prognosis (Szarvas et al., 2021; Kasurinen et al., 2018; Pa, 2003). The expression of MMPs in cancer cells degrades the ECM barrier and the basement membrane (BM) supports the escape from the original site. MMPs are also responsible for the release of TGF-β and VEGFA from its binding proteins that sequester it in the ECM, as well as exposing cryptic integrin binding sites in the ECM that can promote migration. Downregulation of MMP expression suppresses invasion and metastasis in the breast (Lyu et al., 2019) and gastric cancer (Xia et al., 2015). The hypoxic condition in tumours also contributes to the regulation of MMP expression. Expression of HIF stimulates the expression of specific MMPs that promotes cell invasion in several different cell types (Shan et al., 2018; Wang et al., 2014; Choi et al.,

2011). By gaining invasiveness via the expression of MMPs, along with increased migration capacity through EMT, cancer cells are able to penetrate through the ECM barrier and BM reaching the circulation system and then metastasizing to distant sites.

1.1.2.2 Transit and survive

Survival under the shear stress generated by blood flow and the attack by the immune system is the top priority of cancer cells on reaching the circulation system (Wirtz, Konstantopoulos, & Searson, 2011). Cancer cells that have increased metastatic potential are capable of surviving until they arrive at distant sites via forming aggregates with platelets (Labelle & Hynes, 2012; Bambace & Holmes, 2011; Gay & Felding-Habermann, 2011) or cell clusters (Murlidhar et al., 2017; Wang et al., 2017; Aceto et al., 2014). The platelets in the aggregates act as a shield against the shear stress of blood flow but primarily evade immunosurveillance. Natural killer (NK) cells in the blood predominantly perform anti-tumoral activities against cancer cells showing "missing self" signals (Orr & Lanier, 2010). Platelets binding on cancer cell surface enhances the expression of MHC class I inducing "pseudo self" signals, that confound NK cells and increase cell survival (Placke et al., 2012; Nieswandt et al., 1999). Apart from coagulation with platelets, the formation of heterotypic cell clusters between cancer cells and CAFs or homotypic clusters of cancer cells prevents cell damage during transition. Duda *et al.* observed about twice as many viable cancer cells were detected in heterotypic clusters isolated from blood compared with singlet and doublet cells (Duda et al., 2010). Resistance to apoptosis and increased metastases are also detected from endogenous tumours and after tail vein-injection of circulating clusters in mice (Aceto et al., 2014). The detection of clusters and their sizes positively correlates to the disease prognosis in lung (Murlidhar et al., 2017), breast (Jansson et al., 2016) and prostate cancer (Aceto et al., 2014). Maintaining the expression of E-cadherin, an epithelial marker, would be another potential strategy to survive in the circulation system. However, invasiveness was repressed compared with breast cancer cells losing E-cadherin (Padmanaban et al., 2019). This suggests that cells having flexibility in between epithelial- and mesenchymal- properties may have a better chance of surviving during transit in the circulation system.

1.1.2.3 Arrival and formation of the metastatic niche

Circulating cancer cells end up entrapped in capillaries and undergo extravasation

(Massagué & Obenauf, 2016). Due to the characteristics of capillaries that are highly permeable, metastases commonly exhibit in the liver, lung and bones (Budczies et al., 2015; Denève et al., 2013), whereas metastasising to other organs may require support from expression of proteinases, cytokines and growth factors (Fouad & Aanei, 2017). The expression of VEGFA and ANGPTL4 induce permeability in capillaries (Padua et al., 2008; Weis et al., 2004), and COX2 and MMPs facilitate vascular remodelling (Gupta et al., 2007) in breast and colorectal cancer, promoting lung extravasation. Furthermore, platelets aggregated with cancer cells also cooperate with the extravasation process. Platelet-derived TGF-β promotes EMT by the activation of *Snail in vitro*. Depleted expression of TGF-β in platelets inhibits extravasation along with the downregulation of MMP9 *in vivo* (Labelle, Begum, & Hynes, 2011). The activation of endothelial $P2Y_2$ receptors by platelet-derived nucleotides disrupts cell-cell junctions allowing cancer cells to penetrate through the endothelial barrier (Schumacher et al., 2013). Metastatic cancer cells, either having abilities themselves or enlisting support from others, penetrate through endothelial barriers efficiently to arrive at distant sites.

According to the "seed and soil" theory proposed by Stephen Paget in 1889, the successful formation of metastases at the secondary site requires not only the arrival of cancer cells ("seed") at the distant site but also the well-prepared microenvironment ("soil"), like the supportive ECM architecture and the immunosuppressive condition (Langley & Fidler, 2011; Paget, 1989). The expression of LOX and PLOD2 in cancer cells that remodels the collagen structures establishes the pre-metastatic niche favouring metastases (Eisinger-Mathason et al., 2013; Erler et al., 2006a). Moreover, the recruitment of myeloid-derived suppressor cells (MDSCs) and regulatory T (T_{reg}) cells in response to platelet-derived TGF-β in the metastatic niche develops an immunosuppressive microenvironment supporting the colonization of metastatic cancer cells (Yamaguchi et al., 2020). Additionally, CAFs from the primary tumours that metastasise with cancer cells to distant sites or cancer cell-activated local fibroblasts acting as "soil" induce the production of CXCL9/10 and promote the formation of metastases (Pein et al., 2020; Duda et al., 2010). These pre-preparation processes at the distant site suggest organ-specific metastases.

The lack of any molecular mechanisms inducing the metastatic potential of cancer cells in the different steps of metastasis mentioned above may lead to insufficient metastasis. Overall, the architecture of ECM in the TME, migration capacity and plasticity of

cancer cells, the structure of vasculatures and the ability to evade immune response are primary rate-limiting factors of metastasis. This thesis will now focus on the mechanisms that regulate the migration capacity and plasticity of cells determining the metastatic potential of cancer cells.

1.2 Introduction to Vascular endothelial growth factors (VEGFs)

Vascular endothelial growth factor (VEGF) was found by Senger *et al.* in 1983 and named vascular permeability factor (VPF), secreted by tumours, and increased the permeability of vasculatures in guinea pigs and hamsters (Senger et al., 1983). Later in 1989, Ferrara *et al*. (Ferrara & Henzel, 1989) and Plouët *et al.* (Plouët, Schilling, & Gospodarowicz, 1989) reported a growth factor secreted by pituitary cells that was a mitogen specifically for vascular endothelial cells and named VEGF, and had similar amino acid sequence and functions in inducing vascular permeability and angiogenesis to VPF (Keck et al., 1989; Leung et al., 1989). Recent observations have identified a VEGF family that contributes to vasculogenesis and angiogenesis, including VEGFA, VEGFB, VEGFC, VEGFD and placental growth factor (PlGF) (Vempati, Popel, & Mac Gabhann, 2014). VEGFA is widely expressed by different cells initiating several biological functions. For example, the expression of VEGFA in tumours promotes angiogenesis and increases the permeability of vessels supporting tumour growth and metastasis (English et al., 2017; Tozer et al., 2008). Moreover, the recruitment and infiltration of TAMs by tumour-expressed VEGFA form an immunosuppressive TME exacerbating tumour progression (Okikawa et al., 2022). Because this project aims to identify the effects of VEGFA on cell migration and metastasis, this section will only focus on VEGFA, describing its transcriptional and translational regulation, interacting receptors and downstream signalling pathways in the following sections.

1.2.1 mRNA transcriptional regulation of *VEGFA*

The *VEGFA* is localized on chromosome 6 at 6p21.1 in humans and chromosome 17 in mice, organized by 8 exons and 7 introns (Vincenti et al., 1996). Instead of containing consensus TATA- and CCAAT-box initiating transcription, the VEGFA promoter is regulated by a proximal promotor region which has 88 GC-rich base pairs upstream of the initial transcription sequence. The activation of VEGFA transcription is adjusted by the interaction between specific transcriptional factors and the VEGFA promotor in response to growth factors, cytokines, tumour suppressor genes and

environmental stress (Shima et al., 1996). For instance, overexpression of TGF-β along with VEGFA is correlated to induced metastasis and angiogenesis in multiple cancer types. TGF-β-induced SMAD binding of Sp1 to the VEGFA promotor in the proximal promoter region switched on transcription in human cholangiocellular carcinoma (Benckert et al., 2003). Loss functions of tumour suppressor genes and gain activation of oncogenes launch tumorigenesis along with the increased expression of VEGFA (Rak et al., 2000). The binding of Sp1 to the VEGFA promoter in combination with p53 suppresses VEGFA expression (Zhang et al., 2000). On the contrary, Ras-increased VEGFA expression by the binding to Sp1 and AP2 via p42/p44 MAP kinase (Milanini et al., 1998). Hypoxia is a major environmental stress, that provokes angiogenesis during tumour growth. The activation of HIF-1 binding to the hypoxia-response element (HRE), located at the proximal promotor region, triggers the transcription of VEGFA (Forsythe et al., 1996). Tumour-derived effectors participating in VEGFA transcriptional regulation may be a potential target to inhibit the expression of VEGFA and its biological functions.

1.2.2 mRNA alternative splicing

It has been observed in multiple cancer types that cancer cells acquire characteristics of cancer hallmarks via undergoing alternative mRNA splicing (AS) (Zhang et al., 2021; Dvinge et al., 2016). There are two regions where AS occurs in *VEGFA* that develops different VEGFA isoforms with distinct biological properties. Splicing variation in exon 8 derives VEGFA isoforms with different C-terminal domains, $VEGFA_{xxx}a$ and $VEGFA_{xxx}b$, that show unique functions in pro-angiogenesis and anti-angiogenesis respectively, although the VEGFAxxxb variants are highly controversial and possibly not of physiological relevance (Dardente et al., 2020; Harris et al., 2012). On the other hand, the dominant VEGFA isoforms; VEGFA121, VEGFA165 and VEGFA189 in humans (an amino acid shorter in mice), show varied binding affinity to ECM, are generated by AS in exons 6 and 7 (Fig. 1.1) (Di Matteo et al., 2020; Vempati, Popel, & Mac Gabhann, 2014). The expression of these VEGFA isoforms plays an essential role in orchestrating angiogenesis not only during embryonic development and wound healing but also in cancer progression.

The lack of exons 6 and 7 in VEGFA121 decreases its binding affinity to ECM leading to better spatial distribution and the formation of the chemotactic gradient. On the

contrary, VEGFA164 and VEGFA188 can be sequestrated in ECM which may resist proteolysis and serve as ligands facilitating autocrine signalling (Vempati, Popel, & Mac Gabhann, 2014). In addition, the formation of vasculature induced by different VEGFA isoforms displays distinct features. Vessels generated by VEGFA120 in mice are enlarged, leaky and poor branching, whereas VEGFA164 and 188 induced vessels are narrow and well-branched (Gerhardt et al., 2003; Ruhrberg et al., 2002). Mice that only express VEGFA120 have fragile and leaky vessels resulting in a dysfunctional cardiovascular system and early death after birth in comparison to mice expressing VEGFA164 and VEGFA188 (Stalmans et al., 2002; Carmeliet et al., 1999). Leakage from the vasculature was also observed in mouse tumours expressing VEGFA120 which may lead to cancer cells being under hypoxic conditions (Tozer et al., 2008).

Regulation of the proportion of different VEGFA isoforms correlated to specific needs by AS is necessary. Induced expression of VEGFA188 during lung development in the postnatal stage is critical. However, the expression of VEGFA120 and VEGFA164 are dominant VEGFA isoforms in epithelial cells during the embryonic stage. The transition of the expression of VEGFA from shorter to longer isoforms in lung alveolar epithelial cells is regulated by RNA-binding proteins, *Cpeb4*, *Elavl2* and *Hnrnpa1*. Upregulation of *Cpeb4* and downregulation of *Elavl2* and *Hnrnpa1* transits the expression of VEGFA120 and VEGFA164 to VEGFA188 (Fidalgo et al., 2022). Moreover, the SR protein family and serine/arginine-rich splicing factor 1 (SRPK1) also regulate VEGFA splicing (Guyot & Pagès, 2015; Oltean et al., 2012). Reduced expression of SRPK1 and SRSF1 by knockout of Wilms' tumour suppressor 1 (WT1) in endothelial cells switches the expression of pro-angiogenic VEGFA164 to anti-angiogenic VEGFA120 resulting in induced apoptosis in endothelial cells (Wagner et al., 2019). The interaction between SRPK1 and SRSF1 also initiates the switch between VEGFA165a and VEGFA165b. Inhibition of SRPK1 with its inhibitor transitioning the expression of VEGFA165b to VEGFA165a promotes angiogenesis in HeLa cells and podocytes (Hatcher et al., 2018; Amin et al., 2011).

1.2.3 Post-translational processes

The post-translational modification of proteins is critical in the regulation of their bioactivity, such as enzyme activity, protein turnover rate and interaction and the activation of signalling pathways. Common post-translational modifications of proteins include phosphorylation, glycosylation, methylation and proteolysis. By undergoing proteolysis, in addition to mRNA splice variation, other VEGFA isoforms can be generated by proteases like plasmin and MMPs (Vempati, Popel, & Mac Gabhann, 2014). The cleavage of VEGFA isoforms alters their original bioactivity and binding affinity to receptors. VEGFA110 generated by cleavage of VEGFA165 by plasmin reduces its bioactivity and loses the binding site for heparin and NRP1, but also promotes endothelial cell mitogenesis (Keyt et al., 1996). The longer VEGFA isoforms that bind to ECM are the main target of proteolysis by MMPs. The cleavage of VEGFA164 and VEGFA188 from ECM by MMP3 generates VEGFA113. Unlike VEGFA188 and VEGFA164, the vasculature developed by VEGFA113 is leaky and enlarged sharing similar characteristics to VEGFA120-developed vasculature in *in vivo* models (Lee et al., 2005).

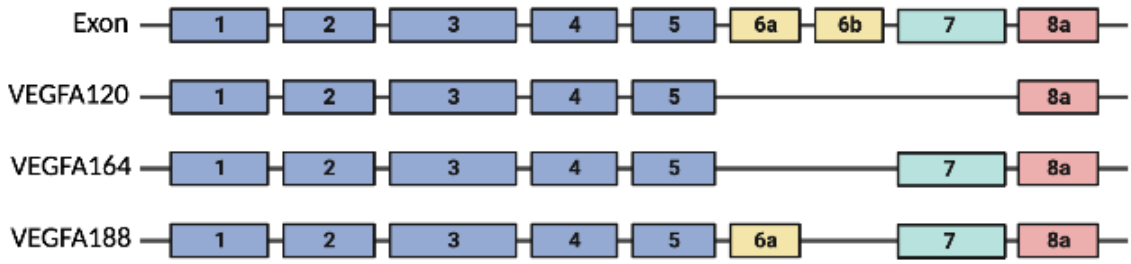

Figure 1.1 Splicing variation between different VEGFA isoforms

The structure of splicing variation corresponds to different VEGFA isoforms. Exons 1 to 5 (purple) encodes for the binding to VEGFR1 and VEGFR2. Exons 6 (yellow) and 7 (green) encode the heparin-binding sites. Exon 8 (red) encodes the neuropilin binding sites.

1.2.4 VEGFA receptors and its co-receptors

VEGF receptors (VEGFRs) consist of an extracellular domain that can bind with ligands, a transmembrane domain and multiple tyrosine kinases in an intracellular domain. The binding to ligands initiates a conformation change in the receptor, leading to the autophosphorylation of specific tyrosine residues, activating its downstream signalling pathways. There are three VEGFRs and VEGFA only interacts with VEGFR1(Flt-1) and VEGFR2 (Flk-1), as well as co-receptors, the neuropilins (NRP), controlling angiogenesis in endothelial cells. However, VEGFR3 predominantly binds to VEGFC and VEGFD and is expressed mainly on lymphatic endothelial cells participating in lymphomagenesis.

VEGFR1 interacts with multiple ligands, including VEGFA, PlGF and VEGFB. Although VEGFR1 showed a 10-fold higher binding affinity to VEGFA, the tyrosine kinase activity on VEGFA binding is weak compared to VEGFR2 (Ferrara & Davis-Smyth, 1997). Insufficient proliferation and migration of endothelial cells and tube formation through VEGFA-VEGFR1 signalling (Hiratsuka et al., 1998; Seetharam et al., 1995; Waltenberger et al., 1994), as well as overexpression of VEGFR1 under hypoxia (Gerber et al., 1997), suggest VEGFR1 negatively regulates angiogenesis. Moreover, soluble VEGFR1 (sVEGFR1), another form of VEGFR1 generated by splicing variation and proteinase cleavage, acts as a decoy receptor that competes with other receptors binding to VEGFA resulting in the downregulation of proangiogenic activities (Kendall & Thomas, 1993). Although the function of VEGFR1 negatively modulates angiogenesis, the expression of VEGFR1 is essential during embryonic development. Instead of promoting the differentiation of endothelial cells, VEGFR1 is critical in the organization of vascular structure. The abnormal vascular channels caused by mutated VEGFR1 lead to embryonic lethality (Fong et al., 1995). Instead of negatively regulating physiological angiogenesis, VEGFR1 is indispensable in tumour-derived angiogenesis and metastasis (Ceci et al., 2020; Hiratsuka et al., 2001). The activation of VEGFR1 induces the production of MMP9 in lung endothelial cells that favours organ-specific lung metastasis (Hiratsuka et al., 2002). In addition, VEGFR1 activation-induced MMP9 expression enhances invasiveness in hepatocellular carcinoma (Li et al., 2015) and melanoma (Hiratsuka et al., 2002).

Different to VEGFR1, VEGFR2 binds to VEGFA, VEGFC and VEGFD and mainly

regulates cellular functions of endothelial cells, such as proliferation, migration, survival and angiogenesis (Ferrara, Gerber, & LeCouter, 2003). Deficiency in VEGFR2 leads to a dysfunctional vascular system and early death in mouse embryos during vasculogenesis (Shalaby et al., 1995). VEGFR2, which plays a vital role in tumour-induced angiogenesis and metastasis, also acts as a target for anti-tumour therapy. Downregulation of VEGFR2 or inhibition of its signal transduction successfully represses cancer cell invasion and metastasis (Shiau et al., 2021; Volz et al., 2020). VEGFR2 also contributes to generating an immunosuppressive microenvironment in distant sites. The number of metastases to the lung and the expression of immune checkpoint ligand PD-L2 in the secondary tumours are repressed with the inhibition of VEGFR2 (Zheng et al., 2020).

Functional VEGFRs are formed not only of homodimers or heterodimers but also together with other co-receptors (Simons, Gordon, & Claesson-Welsh, 2016). Neuropilin-1 (NRP1) is one of the co-receptors to VEGFR2 that also have a high binding affinity to VEGFA. The binding site on VEGFA to NRP1 is encoded in exon 7 resulting in NRP1 as a VEGFA isoform-specific receptor (Soker et al., 1996, 1998). NRP1 is essential in VEGFA-facilitated cell migration in endothelial cells. Blocking the binding of NRP1 to VEGFA suppressed the migration capacity of endothelial cells *in vitro* and vascular remodelling in *vivo* (Herzog et al., 2011; Pan et al., 2007). VEGFA-activated NRP1 does not trigger any downstream signalling but acts as an enhancer amplifying the effects of the binding between VEGFA and VEGFR2 (Neufeld et al., 2002; Soker et al., 2002). Though tumour mass is decreased with anti-VEGFR2 therapy, the combined therapy of anti-VEGFR2 and anti-NRP1 augments the repression of tumour growth in multiple cancer types (Pan et al., 2007).

1.2.5 VEGFA-VEGFR signalling

VEGFA is a key regular of angiogenesis. It is essential in the development of vasculatures in embryos. Embryonic lethality occurs in the absence of VEGFA. Impaired expression of VEGFA also leads to early death in neonatal due to dysfunctional vascular structures. Induced VEGFA in tumours facilitates vascular sprouting and vessel formation transporting nutrients and oxygen for tumour growth. Anti-VEGFA therapy successfully inhibits angiogenesis in tumours and is widely used in treating multiple types of cancer in clinics. VEGFA signal transduction through VEGFR1/2 autophosphorylates different phosphorylation sites located in the intracellular domain. There are 7 phosphorylation sites in VEGFR1 of which Y794, Y1169 and Y1213 are important in VEGFA-mediated downstream signalling. On the other hand, the key phosphorylation sites in response to VEGFA activation in VEGFR2 are Y951, Y1175 and Y1214 in 10 sites (Fig. 1.2).

VEGFA-induced signal transduction through VEGFR2 regulates different biological functions by multiple tyrosine residues in endothelial cells (Wang et al., 2020). Cell survival is predominantly modulated by VEGFA-induced phosphorylation of Y951 in VEGFR2. Initiation of the downstream PI3K/Akt signalling pathway results in the activation of Bcl2 and the repression of apoptosis (Trisciuoglio et al., 2005). Activation of PLCγ by p-Y1175 initiates signal transduction to MAPK/ERK promoting cell proliferation in fibroblasts and endothelial cells (Sase et al., 2009; Takahashi et al., 2001; Takahashi & Shibuya, 1997). Multiple tyrosine residues contribute to the mediation of cell migration. The phosphorylation of Y951 in VEGFR2 on VEGFA binding activates Src signalling regulating the migration of endothelial cells by reorganizing the cytoskeleton (Matsumoto et al., 2005). The migration of endothelial cells is also promoted by the VEGFA-induced phosphorylation of Y1175 and Y1214, which increases the formation of stress fibres and focal adhesion by activating PI3K/FAK and MAPK pathways, respectively (Lamalice, Houle, & Huot, 2006; Holmqvist et al., 2004; Lamalice et al., 2004).

Besides phosphorylation of varied tyrosine residues, different signal transduction pathways and intracellular traffic control induced by VEGFA/VEGFRs are elicited in a VEGFA isoform-dependent manner. The phosphorylation of Y1175 in VEGFR2 acts as a dual regulator of cell proliferation and migration through distinct signalling pathways.

The phosphorylation of VEGFR2-Y1175 in response to VEGFA165 is significantly increased compared with VEGFA121. Cell proliferation of endothelial cells regulated by VEGFR2-Y1175 downstream signalling through the ERK pathway also increases after stimulation with VEGFA165 in comparison with VEGFA121. However, no difference was observed in the MAPK pathway that modulates cell migration (Fearnley et al., 2016). On the other hand, pY1175-VEGFR2 stimulated by VEGFA165 leads to endocytosis of VEGFR2, whereas VEGFA121-stimulated pY1175-VEGFR2 remains on the cell surface. VEGFA165-induced degradation, proteolysis and ubiquitylation of VEGFR2 are significantly upregulated but have negligible effects in endothelial cells stimulated with VEGFA121 (Fearnley et al., 2015). The production of soluble VEGFR1 (sVEGFR1) is upregulated in endothelial cells activated with VEGFA165 compared with VEGFA121. It is possible that VEGFA isoform-specific regulation in VEGFR trafficking and signal transduction results in different cellular functions in cancer cells (English et al., 2017; Kanthou et al., 2014), which may explain different sensitivity to the anti-angiogenesis therapy.

1.3 Introduction to modes of cell migration

Cell migration is a dynamic process regulated by different molecular and biophysical cues, which plays a critical role in a wide range of settings, including embryonic development, angiogenesis, tissue repair and immune response. However, cell migration also contributes to disease developments, such as inflammation and metastasis. A better understanding of regulatory mechanisms in cell migration may provide strategies to restore physiological processes or abrogate pathological progression. According to the migration pattern, cell migration modes are divided into collective and single-cell migration. Based on the interaction between cells and ECM, single-cell migration is further classified into three subtypes, mesenchymal, amoeboid and '1D migration' on fibres. This section will cover different modes of cell migration and determinants of favouring migration modes.

1.3.1 Collective cell migration

Collective cell migration is characterised by a group of cells migrating in a tube-, sheet- or chain-like structure in either 2D or 3D ECM microenvironments, and is commonly observed during organ formation (Theveneau & Mayor, 2013; Friedl & Gilmour, 2009). The stable structure of groups of cells is maintained by strong cell-cell interactions by forming adherens junctions (AJs) through cadherin binding. Cells migrating collectively rely highly on cell-cell communication. The polarization of cells generates stresses in response to the chemotactic gradient at the leading edge. Stresses then transmit to the mass of cells through AJs and guide the direction of movement (Trepat & Fredberg, 2011; Tambe et al., 2011). However, migration as a group of cells is commonly limited by the size of gaps in the ECM. The coordination of proteolytic activities to remodel the ECM is essential. Tumours originally from epithelial cells or connective tissue also migrate collectively during invasion and metastasis. The expression of MT1-MMP on the surfaces of the leading cancer cell degrades the ECM and forms tracks allowing cells to penetrate (Wolf et al., 2007). Furthermore, tumour-associated cells that have infiltrated can assume the role of degrading the extracellular matrix. Yet, cancer cells lacking proteolysis to widen gaps in ECM may undergo a collective-to-amoeboid transition allowing cancer cells to squeeze through the existing pores and keep the invasion progressing (Wolf et al., 2003; Ellerbroek et al., 2001). Therefore, initiating epithelial-to-mesenchymal transition (EMT) to escape from the

tumour mass is not the prerequisite for invasion and metastasis. Cancer cells can migrate as a group but require the accompanied ECM remodelling and plasticity in the mode of migration to overcome barriers in the TME.

1.3.2 Single-cell migration

Single-cell migration involves strong interactions between cells and the ECM. According to the dependency on integrins, single-cell migration is divided into mesenchymal and ameboid modes. The following sections focus on both mesenchymal and amoeboid modes of cell migration and how cells migrate on fibres.

1.3.2.1 Mesenchymal migration

Cells migrating in the mesenchymal mode, which is spindle-like and elongated, depend highly on the interaction between cells and the ECM. Integrin expressed at the leading edge of cells interacts with the ECM initiating the polarization of actin filaments and the formation of focal adhesions (FAs), which guides the direction of movement. The contraction of the cytoskeleton in the cell body generates traction forces moving the cell forward, followed by the recycling of FA complexes at the rear (Parri & Chiarugi, 2010). Mesenchymal migration is initiated by Rac and Cdc42, which are activated by binding the specific ECM substrate to its integrin (Keely et al., 1997). Activated Rac and Cdc42, facilitating the formation of lamellipodia at the leading edge, promote directional cell migration. Interference with the binding of β_1-integrin to the ECM matrix or blocking its downstream PI3K signalling impairs cell motility and invasion (Wolf et al., 2003; Keely et al., 1997). On the other hand, the Rho family regulates cell contractility by forming stress fibres at the trailing end of cells. Inactivating Rho in cells leads to the absence of stress fibre formation accompanied by downregulated migration capacity (Nobes & Hall, 1999). In addition, the migration of mesenchymal cells is normally protease-dependent. Activation of Rac1 promotes the transcription of MMPs through JNK signalling. Overexpression of MMP2 and MT1-MMP at the front of HT-1080 fibrosarcoma cells facilitates ECM remodelling and invasion (Wolf et al., 2003). Inhibition of the expression of MMPs transits cells migrating from mesenchymal to amoeboid modes, which is a proteolytic-independent mechanism of migration (Carragher et al., 2006).

1.3.2.2 Amoeboid migration

In contrast to mesenchymal migration, amoeboid migration is completely or partially independent of integrin-ECM substrate interaction and proteolytic activities (Graziani et al., 2022). The morphology of amoeboid cells is rounded or ellipsoid due to the lack of FAs. Instead of relying on "pull" forces generated from polarized actin, cells migrating in amoeboid utilise propulsive forces from contraction of the actomyosin cytoskeleton (Fackler & Grosse, 2008). In addition, melanoma cells migrating in amoeboid mode adopt the β1-integrin generating weak adhesion as a support for extra forces but no effect on the mobility with the blockade of integrin function in seen (Sanz-Moreno et al., 2008; Wolf et al., 2003). The expression of MMPs was also observed in amoeboid melanoma cells during their invasion (Orgaz et al., 2014). The formation of FAs and MMPs in amoeboid migration may not be absolutely required but may be a plus and could reflect the plasticity cancer cells have in their approach to migration. The dominant regulator of amoeboid migration is RhoA and its effector ROCK which participate in the control of actomyosin contractility (Sahai & Marshall, 2003). Because of the shortage in FAs and lack of ECM remodelling, the migration speed in ameboid mode is faster than in mesenchymal mode (Friedl, Zänker, & Bröcker, 1998). High migration speed allows leukocytes to arrive at the target sites facilitating immune response efficiently (Friedl & Weigelin, 2008). Multiple types of cancers that can migrate in amoeboid mode show higher metastatic potential (Gao et al., 2017; Kosla et al., 2013; Sanz-Moreno et al., 2008), suggesting interruption of mesenchymal-to-amoeboid transition together with abrogation of MMP expression can be a target to prevent metastasis. One of the key determinants of migration in ameboid versus mesenchymal modes is nuclear size and deformation. HT1080 cells will migrate in ameboid mode until they get stuck in the ECM as the nucleus cannot pass, at which point they resort to mesenchymal characteristics, using FA-directed proteolysis by MT1-MMP to enlarge the hole in the ECM to allow progress (Wolf et al., 2003).

1.3.2.3 1D migration on fibrillar structures

Recent studies have observed that cells can migrate along narrow linear structures, such as collagen fibrils and nerve fibres, both *in vitro* and *in vivo* (Hashimoto et al., 2022; Sharma et al., 2012; Weigelin, Bakker, & Friedl, 2012; Doyle et al., 2009). This type of migration has been classified as 1D migration and termed "contact guidance" (Yamada & Sixt, 2019). The morphology and polarity of cells while migrating on

fibrillar structures depend on the geometry of the ECM. The morphology of cells becomes elongated and polarized on aligned fibres. These cells do not form wide lamellipodia with a large number of FAs as seen in 2D migration when the fibre is narrower than 5 microns. This means the formation of only 1-2 FAs is needed at the narrow leading edge, making migration much more efficient and increasing migration speed significantly over 2D migration (Doyle et al., 2012). On the contrary, cells on random fibres are extended in varied directions, lose polarity and make multiple FA contacts, decreasing migration speed. The orientation of fibres also regulates the efficiency of 1D cell migration *in vivo*. Aligned fibres which are perpendicular to the tumour boundary promote invasion and metastasis in breast cancer patients (Esbona et al., 2018). The expression of the collagen-crosslinking enzyme (LOXL2) is crucial in collagen alignment (Cox et al., 2013; Kanapathipillai et al., 2012; Akiri et al., 2003). Inactivated functions of LOXL2 in breast cancer mouse model dysregulates the alignment of collagen fibrils resulting in inhibiting invasion and metastasis (Grossman et al., 2016; Riching et al., 2015). It has been reported the formation of protrusions and migration capacity of cells is orchestrated by ROCK-mediated myosin II contractility (Kubow et al., 2017; Ramirez-San Juan, Oakes, & Gardel, 2017). Although cell migration in breast cancer cells on aligned fibres is repressed with the ROCK inhibitor, the migration capacity is still better than cells on 2D surfaces (Wang & Schneider, 2017). 1D fibrillar migration in breast cancer and fibrosarcoma cells may be independent of myosin II.

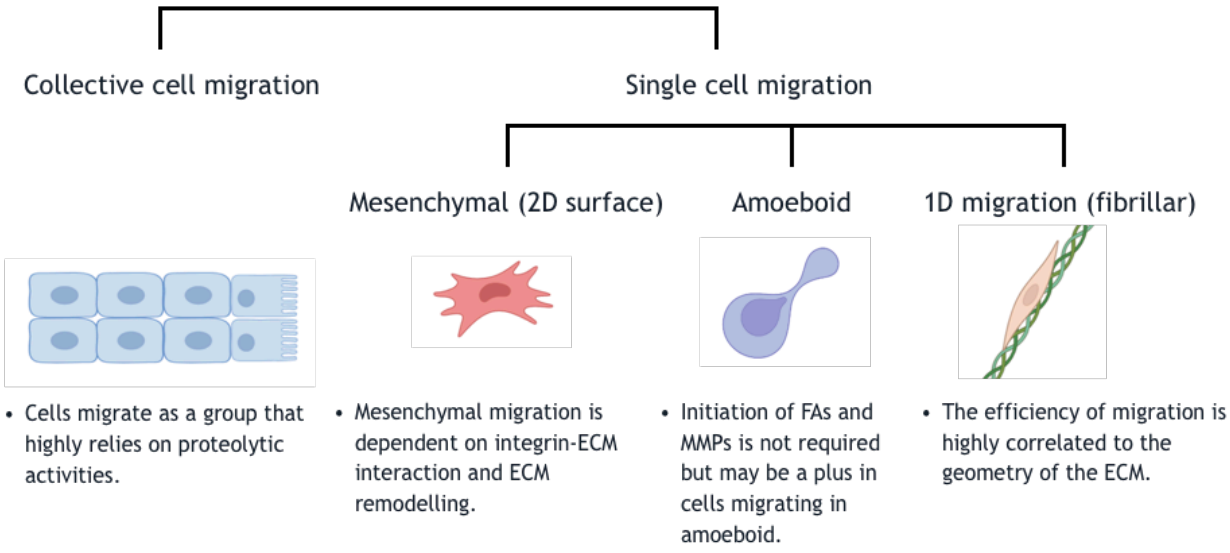

Figure 1.2 Different modes of cell migration

According to the number of cells migrating together, cell migration modes are distinguished into 2 groups, collective cell migration and single cell migration. Cells migrating as a group maintain an epithelial-like phenotype. The gaps between junctions regulate migration capacity control of collective cell migration. Hence, collective cell migration requires the participation of proteolytic enzymes. In addition, there are 3 distinct types of single cell migration based on the interaction between cells and ECM, mesenchymal modes, amoeboid and 1D migration. Mesenchymal migration is the most integrin-dependent mode, that highly relies on ECM remodelling. On the contrary, amoeboid is integrin-independent, which enables penetrating through gaps by shape-changed. 1D migration is a unique mode in which cells travel on a thin linear structure, such as collagen fibrils and nerve fibres. The architecture of the fibrils plays a critical role in regulating the migrating direction of cells travelling in fibres.

1.4 VEGFA and metastasis

VEGFA is a key growth factor that regulates angiogenesis (Carmeliet & Jain, 2011). Overexpression of VEGFA has been observed in clinical disease and positively correlates with disease progression and metastasis (Rosen, 2002). In addition, the development of abnormal vasculature corresponding to induced expression of VEGFA in tumours increases resistance to radiotherapy and chemotherapy, as this leads to decreased tumour pO_2 and increased interstitial fluid pressure (IFP). Although anti-VEGFA therapy was originally hypothesised to inhibit tumour growth by blocking angiogenesis, clinically its main effect is through a process called vascular normalisation, where poorly functioning vessels are pruned and pericyte coverage increases. This leads to increased tumour pO2 and reduced IFP, improving the response to therapy and reducing clinical problems like the build-up of ascites in ovarian cancer or intracranial pressure in glioblastoma. (Chekhonin et al., 2013; Toi, Matsumoto, & Bando, 2001). However, it has been reported that the promotion of metastasis can occur with anti-VEGFA therapy (Yang et al., 2016) which may be a potential explanation for the rare improvement in the overall survival of cancer patients with the therapy (Gilbert et al., 2014; Motzer et al., 2013; Perren et al., 2011). VEGFA has been identified that is essential in the induction migration capacity of endothelial cells during angiogenesis (Hayakawa et al., 2011; Oommen, Gupta, & Vlahakis, 2011). However, little is known about the roles of VEGFA in the biological functions of cancer cells. This section will summarize the observation of VEGFA contributing to cancer cell migration and metastasis.

1.4.1 Roles VEGFA play in the regulation of cell migration *in vitro*

Migration capacity and invasiveness are the most important factors *in vitro* utilised to determine the metastatic potential of cancer cells. Wound healing (scratch) assays and transwell assays with the Boyden chamber are basic methods to measure the mobility and invasion of cancer cells, respectively. Targeting VEGFA successfully inhibits cell migration and invasion in multiple cancer types. Direct or indirect downregulation of VEGFA signalling transduction through VEGFR2, resulting in repressed activation of Akt, inhibits mobility and invasion in lung cancer and renal clear cell carcinoma (Zeng et al., 2016; Chen et al., 2009). Blocking the interaction between VEGFA and α_9-integrin subunit expressed on colorectal cancer cells also decreases the

number of cells invading through matrigel and the wound assay closing efficiency (Oommen, Gupta, & Vlahakis, 2011). Moreover, the expression of MMP2 that degrades the ECM is regulated by the expression of VEGFA in glioblastoma. Downregulated invasive ability, as well as the expression of MMP2, was observed by silencing VEGFA expression (Gong et al., 2014). VEGFA modulates cell migration and invasion by regulating EMT, activating focal adhesion kinase proteins and producing ECM degradation proteins.

Interestingly, the regulation of the migration capacity in cancer cells is VEGFA isoform dependent between varied types of cancer. The absence of total VEGFA in breast cancer cells causes loss of filopodia at the leading edge of cells leading to the inhibition of mobility. The migration capacity of these VEGFA knockout cells is rescued with the application of VEGFA165 recombinant protein but failed with VEGFA121 due to the lack of exon 7 binding to NRP1 (Kiso et al., 2018a), suggesting the necessity of VEGFA/NRP1 signalling in cell migration in breast cancer cells. In addition, plasticity in the mode of cell migration is another determinant of the efficiency in metastasis. Fibrosarcoma cells expressing VEGFA120 have better plasticity that can switch migration mode from mesenchymal to amoeboid in response to migrating from adhesive to non-adhesive surfaces. In contrast, cells expressing longer isoforms can only migrate in mesenchymal mode and are trapped on non-adhesive surfaces (unpublished data, Yu-Chin Lee MSc thesis). The molecular properties between VEGFA isoforms show distinct strategies in modulating cell migration capacity.

1.4.2 Roles VEGFA plays in the regulation of metastasis *in vivo*

Overexpression of VEGFA and its receptors has been detected in various cancer types in clinical disease and is highly correlated to poor disease progression and metastasis (Goel & Mercurio, 2013). Blocking the signal transduction of VEGFA through VEGFR2 to ERK successfully suppressed metastases of gastric cancer cells to the lung in mice (Yu et al., 2022). Lack of VEGFA/VEGFR signalling decreases the metastatic potential of gastric cancer cells by impairing EMT and attenuating their stemness. Furthermore, fibrosarcoma cells expressing VEGFA120 have greater metastasis to the lungs from primary tumours and are more resistant to cell death caused by the arrest in the lung vasculatures in comparison to cells expressing VEGFA188 (English et al., 2017). The expression of VEGFA or its specific isoforms affects the

metastatic potential of cancer cells in clinics and experimental mouse models.

1.5 Extracellular matrix remodelling in the tumour microenvironment

The ECM in TME plays important roles in either facilitating or limiting tumorigenesis and metastasis by regulating its biochemical (e.g. growth factors) and biophysical (e.g. topography) parameters (Winkler et al., 2020). Analysing the architectures of ECM in TME has been widely used in identifying the stage of tumour progression and predicting the therapeutic outcome in the clinic. (Naba et al., 2012; Bergamaschi et al., 2008). Processes of ECM remodelling that regulate cell migration and metastasis are described below.

1.5.1 ECM deposition

Cancer cells modulate the composition of the ECM in the TME to favour tumour growth, invasion and metastasis by altering the expression of different ECM proteins. Fibrosarcomas expressing different VEGFA isoforms show distinct ECM expression patterns affecting cell behaviours. Fibrosarcoma cells expressing VEGFA120 have a mesenchymal-like morphology on laminin and better migration capacity and invasiveness compared to an epithelial-like morphology on collagen-I. Although the morphology remains mesenchymal-like in VEGFA188-expressing fibrosarcoma cells between laminin and collagen, these cells are more invasive in collagen-I gels (English et al., 2017). The more metastatic VEGFA120-expressing fibrosarcoma cells retain their metastatic potential by creating a laminin-rich TME which favours their migration. On the other hand, cancer cell-recruited stromal cells also contribute to building up ECM components. Tumour-secreted growth factor, TGF-β, activates the differentiation of stromal cells into cancer-associated fibroblasts (CAFs) that deposit fibrotic collagen, increasing ECM stiffness and promoting metastasis in varied cancer types (Zhou et al., 2017; Calvo et al., 2013; Provenzano et al., 2008). In addition, stiffening of the ECM in the TME facilitates the formation of invadopodium in breast cancer cells, resulting in gains in metastatic potential (Parekh et al., 2011). The deposition of the ECM would be the first initiator of cancer cells acquiring metastatic properties.

1.5.2 ECM modification

The architecture of the ECM acts as a rate control of cancer progression, especially during metastasis. The synthesized ECM proteins in TME undergo different types of post-translational modifications that assist cancer cells in escaping from the primary tumour. ECM modification can be done by either modifying ECM surface molecules

or cross-linking ECM proteins through the expression of specific proteins or cell self-generated forces during cell-ECM interaction, which alters ECM biophysical properties and topographies. These processes involve the expression of specific proteins dominantly, and cell self-generated forces during cell-ECM interaction. It has been reported that 3T3 fibroblasts and Human Umbilical Vein Endothelial Cells (HUVEC) enable to align collagen fibres by the forces generated from cell-ECM interaction leading to the increase of ECM density (Malandrino et al., 2017; Nam et al., 2016). Interestingly, the reoriented structure may still remain even after decellularization. Phosphorylation of fibronectin by Casein Kinase II increases cell attachment and traction force leading to the enhancement of metastatic potential has been observed in many types of cancer (Yalak et al., 2019; Yalak & Vogel, 2015; Kraning-Rush, Califano, & Reinhart-King, 2012). Furthermore, glycosylated fibronectin facilitates EMT in prostate cancer cells (Freire-de-Lima et al., 2011) and increases invasiveness in urothelial carcinoma (Richter et al., 2008). The induction of ECM cross-linking correlates to increased metastasis and poor disease survival. Collagen-I is the dominant ECM protein that forms cross-linking 3D topography by Lysyl oxidase (LOX), lysyl oxidase homologues (LOXLs) and procollagen-lysine 1, 2- oxoglutarate 5-dioxygenases (PLODs) (Qi & Xu, 2018; Barker, Cox, & Erler, 2012), that is curly in normal tissue but becomes organized and fibrillar in tumours. Induced expression of PLODs, LOX and LOXLs cross-links collagen, stiffens the ECM and increases the integrin-dependent migration capacity of cells and metastasis (Levental et al., 2009). Moreover, fibrotic-induced ECM stiffness promotes EMT by activating TWIST1 signalling, leading to enhanced cell invasion and metastasis in breast and pancreatic cancer cells. Overexpression of these proteinases is seen in response to hypoxic conditions (Qi & Xu, 2018; Erler et al., 2006a), illustrating the abrogation of ECM modification may be a potential method to inhibit hypoxia-induced metastasis.

1.5.3 ECM degradation

ECM degradation is essential in remodelling the architecture of the ECM during tissue remodelling and morphogenesis of which proteinases, like MMPs, ADAM TS and other proteinases like amino peptidases or cathepsins cleaving specific amino acid residues, participate in this process. Overexpression of ECM-degrading proteases is known to exacerbate disease progression and increase metastasis in various cancer types (Qin et al., 2016; Stadlmann et al., 2003). Upregulation of MMP9 was observed

in primary metastatic hepatocellular carcinomas and enhanced the invasiveness of carcinoma cells *in vitro* (Takafuji et al., 2007). Inhibition of MMP2 and MMP9 impairs migration and invasion capacity in retinoblastoma (Webb et al., 2017). The absence of support from proteinases like MT1-MMP to widen pore sizes or gaps, allowing cells to pass through, especially for cells only migrating in mesenchymal modes, prevented progress through the ECM (Wolf et al., 2013; Wolf & Friedl, 2011). Moreover, tumour-associated cells such as CAFs and TAMs also participate in ECM degradation (Afik et al., 2016; Burke et al., 2013). Suppression of MT1-MMP in CAFs abrogates collagen remodelling and invasion in breast cancer cells and oral squamous cell carcinoma (Feinberg et al., 2018; Sabeh et al., 2004). Besides taking charge of producing proteases, CAFs-expressed TGF-β initiates the expression of MMPs in cancer cells increasing their invasive properties (Yamahana et al., 2021; Yu et al., 2014).

1.6 Introduction to engineered microenvironments of 3D *in vitro* Model

1.6.1 Limitation in 2D and animal models

The TME comprises neoplastic cells as well as recruited cell types such as fibroblasts, immune cells, and vascular cells that are held within a supportive matrix of connective tissue or ECM. The interaction and communication between cancer cells, stromal cells, and ECM play a critical role in regulating the rate of cancer progression. In research, 2D models are widely used due to their ease of use, high replicability, and cost-effectiveness. Nonetheless, these models have their limitations as they cannot fully encompass the intricate and dynamic interactions between cancer cells and ECM, which govern cell morphology and polarity. On the other hand, animal models, including syngeneic and Genetically Engineered Mouse Models (GEMM), provide a more physiologically relevant environment by incorporating these elements. However, these models also have critical shortages. For example, animal models might not entirely mimic the human TME due to inherent differences between species. Moreover, ethical concerns arise regarding animal usage in research, and there are gaps in translating findings from animals to humans. While these models offer valuable insights, understanding cell migration and metastasis necessitates the development of innovative in vitro models that can bridge the gap between simplicity and physiological relevance, minimising the shorts associated with both 2D and animal models.

1.6.2 Types of tumour microenvironment-mimicking 3D engineered models

Recent novel 3D *in vitro* cancer models offer the potential to recapitulate the natural tumour microenvironment, including the complexity of the cell populations, extracellular matrix components, signalling gradients, and physical cues, in contrast to traditional 2D approaches (Rodrigues et al., 2021; Albritton & Miller, 2017). The following paragraphs provide an overview of different systems of 3D models mimicking the tumour microenvironment. Techniques for generating 3D tumour models and their application in cancer research, ranging from multicellular-based to cell/extracellular-based and microfluidic models, are discussed below.

1.6.2.1 Multicellular-based 3D models

Tumours exhibit a high degree of heterogeneity, encompassing a diverse array of cell populations. In addition to cancer cells, which themselves may display intratumoral variability, cancer-associated fibroblasts (CAFs) and various immune cell types

dominate this cellular population. The interplay between cancer cells and these neighbouring cells orchestrates their survival, proliferation, and invasive potential, brought about by alterations in the biochemical attributes and structural composition of the surrounding ECM.

Spheroids, as 3D models, not only mirror the morphology of solid tumours but also capture their properties, such as cellular diversity, spatial arrangement of cell populations, and gradients of biochemical cues. Successfully inducing a shift in macrophages from an M1-like to an M2-like phenotype, effectively fostering an immunosuppressive milieu that bolsters cancer cell survival, has been observed in multicellular spheroids comprising non-small cell lung cancer cells, monocytes, and CAFs (Rebelo et al., 2018). Nonetheless, the uneven distribution of cell populations introduces complexities in achieving data reproducibility.

In contrast to spheroids, where the cellular aggregation is externally induced, tumour organoids take shape from patient-derived samples, naturally self-organizing into a 3D structure that closely mimics native tumour formation (Chamoun et al., 2019). Notably, Mazzocchi et al. documented enhanced chemoresistance within organoids of lung cancer cells extracted from patients, surpassing outcomes seen in the 2D monolayer model (Mazzocchi et al., 2019). This observation indicates the ability of organoids to mirror phenomena observed in patients. Yet, the lack of vascular structure restricts the length of the culture period and the size of the 3D structure which may interfere with the outcome of drug screening.

1.6.2.2 Cell/Extracellular matrix-based 3D models

Interactions between cells and their surrounding structure, known as the ECM, play a crucial role in how cancer spreads. The way the ECM, which acts as a barrier around the primary tumour, behaves mechanically and biochemically is critical for cancer cells' ability to survive and escape from their origin. The replication of ECM properties in TME within 3D tumour models has become imperative for investigating cancer cell ECM interaction. They use different methods like embedding cells in hydrogel and making frameworks with biomaterials. These methods help researchers understand how cells behave in a controlled environment.

Hydrogel, a widely utilised substitute of ECM, replicates the physical parameters of the *in vivo* ECM environment, thereby facilitating the investigation of both cell-ECM and

cell-cell interactions critical to tumour progression. This model involves the encapsulation of cancer cells or spheroids within a 3D hydrogel matrix that mirrors the ECM structural complexities of the TME (Hutmacher et al., 2010; Peppas et al., 2006). As a result, it improves the study of cell behaviour and intricate signalling pathways in comparison to 2D cell cultures. Notably, the arrangement of luminal cells and MCF-7 cells in co-culture with tumour-associated fibroblasts within a 3D collagen hydrogel showed distinct spatial distributions, different from the 2D platform, recapitulating cell organizations seen in breast cancer. Moreover, the expression of MMPs by tumour-associated fibroblasts not only sustains cell distribution but also triggers the invasive potential of breast cancer cells (Holliday et al., 2009). While hydrogels effectively mimic key physical cues, such as stiffness, porosity, and crosslinking, thereby establishing a reproducible platform for investigating diverse factors of cancer progression, the multifaceted architecture of the ECM *in vivo* might still influence the outcomes of experiments.

Synthetic polymetric biomaterials, such as degradable polyethylene Glycol and polycaprolactone, are common polymers applied to create scaffolds that imitate the ECM's structure and chemical properties (Long et al., 2014; S. Feng et al., 2013). The scaffolds enable to undergo various modifications, for instance, functionalised the scaffolds with RGD (Arg-Gly-Asp) peptides or fibronectin induces cell adhesion and proliferation (Rodenhizer et al., 2018; Caicedo-Carvajal et al., 2011). In comparison to cells cultured on 2D surfaces, oral squamous cell carcinoma and mouse Lewis Lung carcinoma cells pre-cultured on the 3D scaffold induced expression of growth factors resulting in increased tumour growth in mice (Fischbach et al., 2007). Besides synthetic scaffolds, decellularized ECM (dECM), a ECM from tissues with cells removed, is another alternative that recapitulates both biochemical cues and ECM architecture relative to *in vivo* properties (Ferreira et al., 2021; Ferreira, Gaspar, & Mano, 2020). This approach mimics more factors in the natural TME, but the process of removing cells can damage its ECM properties by enzymes.

1.6.2.3 3D bioprinting models

3D Bioprinting is a novel technique capable of producing consistent *in vitro* models that replicate spheroids/organoids and extracellular matrix (ECM) topography, fulfilling the benefits of both multicellular and cell/ECM-based 3D models. Langer *et al.* demonstrated the bioprinting of multicellular 3D structures, including patient-

derived pancreatic ductal adenocarcinoma cells surrounded by HUVECs and normal human primary pancreatic stellate cells. Cancer cells in the printed multicellular structures gained migration capacity but also recreated patient phenotypes (Langer et al., 2019). Beyond cell printing, this method also enables the reconstruction of the ECM architecture observed within the *in vivo* TME (Zhou et al., 2016; Asghar et al., 2015). For instance, when colorectal cancer cells were cultured on 3D-printed scaffolds emulating ECM architecture, they induced the expression of stem cell-like markers, resulting in heightened tumorigenicity and drug resistance. Moreover, the upregulation of MMP2 and promotion of pre-vascularisation exhibited in CAFs and tumour-associated endothelial cells were also detected on 3D scaffolds compared with 2D platforms (Chen et al., 2020). Hence, 3D bioprinting not only preserves cell population composition and dispersion, along with ECM components but also overcomes the limitations seen in irregular constructs generated by spheroids/organoids and conventional fabrication processes.

1.7 Background

Previous observations in the group pointed out that the expression of different single VEGFA isoforms in fibrosarcoma cells altered their cellular functions both *in vitro* and *in vivo*. Fibrosarcoma cells expressing VEGFA188 had better migration capacity on non-coated plastic and collagen-I whereas VEGFA120-expressing cells were better on fibronectin and laminin (English et al., 2017; Kanthou et al., 2014). However, the number of tumour cells that metastasized to the lung was significantly increased compared with cells expressing VEGFA188 in mice indicating VEGFA120 expressing tumour cells may have greater metastatic potential (English et al., 2017). VEGFA120 cells were better able to survive initial arrest in the lung vasculature compared to VEGFA188 expressing cells. The observation of tumour cells with better migration capacity *in vitro* conflicted with cells with better metastatic potential *in vivo*. Interestingly, fibrosarcoma cells expressing VEGFA120 displayed different morphologies in response to distinct protein-coated surfaces whereas VEGFA188-expressing cells maintained mesenchymal-like morphology (Kanthou et al., 2014). Unlike VEGFA188-expressing cells, VEGFA120-expressing cells appear to utilise different migration modes to adapt to diverse environments. In my previous MSc studies, I showed VEGFA120 cells were able to migrate faster than VEGFA188 expressing cells in a non-adherent chamber, supporting the hypothesis that the more metastatic cells enabled migrating in varied modes indicating increased plasticity, another factor that participated in the regulation of metastatic potential. another factor that participated in the regulation of metastatic potential. However, the previously generated fibrosarcoma cells expressing a single VEGFA isoform were obtained from mice that had differences in development and were not isogenic, factors that may alter their plasticity, meaning new cell lines expressing a single VEGFA isoform that have the same isogenic background are needed for comparison. In addition, 2D microenvironments are unable to identify if cells have better plasticity. New microenvironments enabling to challenge of cells are also needed.

1.8 Hypothesis and aims

According to previous findings, we hypothesized that the increased metastasis of VEGFA120-expressing cells within the lungs of mice is linked to their ability to switch between different modes of migration in response to different topographies in the microenvironments more efficiently than VEGFA188-expressing cells.

Objectives:

1. To establish new fibrosarcoma cell lines expressing single VEGFA isoforms but with similar developmental and genetic backgrounds.
2. To create engineered microenvironments mimicking the TME observed in mouse tumours.
3. To measure the migration capacity of cells between the previous and newly generated cell lines on different microenvironments.
4. To identify a potential mechanism initiated by VEGFA-VEGFR signalling that regulates cell plasticity.

Chapter 2

2. Materials and Methods

Table 2.1. List of Reagents

Reagent	Company	Cat. No.
3-(trimethoxysilyl) propyl methacrylate (MAPTMS)	Sigma-Aldrich	440159
Ammonium Persulphate (APS)	Sigma-Aldrich	A3678
B20-4.1.1	Genentech	PUR27594
BE5	Genentech	PUR66443
BioMix™ Red	Meridian BioScience	BIO-25006
Bovine Serum Albumin (BSA)	Sigma-Aldrich	A3059
Collagen I, Rat Tail	Corning	354236
cOmplete™ ULTRA Tablets, Mini, EDTA-free, *EASYpack* Protease Inhibitor Cocktail	Roche	05892791001
DC101	Imclone/Ely Lilly	
Dichloromethane	Sigma-Aldrich	270997
Dimethyl Sulfoxide (DMSO)	Sigma-Aldrich	D8418
Diphenyl(2,4,6-trimethylbenzoyl) phosphine oxide/2-hydroxy-2-methylpropiophenone	Sigma-Aldrich	405663
Dithiothreitol (DTT)	Sigma-Aldrich	D9163

DNase I, Amplification Grade	Invitrogen™	18068015
Dulbecco's Eagle's Medium (DMEM)	Corning	10-013-CV
Ethanol	Fisher Scientific	AC615100010
Ethylenediaminetetraacetic Acid (EDTA)	Sigma-Aldrich	3690
Fibronectin	Merck	FC010
G418	TOKU-E Merk	G048 A1720
Gel Loading Dye (6x, no SDS)	New England BioLabs	B7025
Halt™ Phosphatase Inhibitor Cocktail	Thermo Fisher	78420
HBSS (with Ca^{2+}/Mg^{2+})	Gibco	14025092
Heat-inactivated fetal bovine serum	Sigma-Aldrich	F9665
Horse Serum	Sigma	H0146
Hydrogen peroxide (H_2O_2)	Sigma-Aldrich	H1009
Laemmli Buffer (4x)	Bio-Rad	1610747
Laminin	Sigma	L2020
Low Temperature Gelling	Sigma-Aldrich	A9414
Methanol	Fisher Scientific	A412

MF-1	Imclone/Ely Lilly	
Nitrocellulose Membrane	Bio-Rad	1620112
NuPAGE® Transfer Buffer	Thermo Fisher	NP0006
Penicillin-Streptomycin	Sigma-Aldrich	P4333
Phosphatase-Buffered Saline	Lonza	17-516F
Poly (ethylene glycol) diacrylate (PEGDA) (700 g/mol)	Sigma-Aldrich	455008
Protogel (40%)	National Diagnostics	EC-891
Protogel Resolving Buffer	National Diagnostics	EC-892
Protogel Stacking Buffer	National Diagnostics	EC-893
Puromycin	Sigma-Aldrich	P8833
Restore™ PLUS Western Blot Stripping Buffer	Thermo Fisher	46430
RIPA Lysis and Extraction Buffer	Thermo Fisher	89900
Sulphuric acid (H_2SO_4)	Sigma-Aldrich	339741
Suramin Salt	CalBiochem	574625
SYBR Green PCR Master Mix	Thermo Fisher	4385612
SYBR Safe	Invitrogen	S33102

T4 DNA Ligase	New England BioLabs	M0202S
T4 DNA Ligase Buffer	New England BioLabs	B0202S
Tetramethylethylenediamine (TEMED)	Sigma-Aldrich	T9281
Toluene	Fisher Scientific	T324-1
TransIT-2X	Mirus	MIR6000
Tris-Buffer Saline (TBS) Buffer	Chem Cruz	SC-362305
Triton™ X-100 Surfact-Amps™ Detergent Solution	Thermo Fisher	28314
Trypsin-EDTA	Sigma-Aldrich	T3924
Tween -20	Sigma-Aldrich	P9416

Table 2.2. List of Kits

Kit	Company	Cat. No.
ECL™ Western blotting detection Kit	Amersham	GERPN2209
GnenFlute™ Mammalian Total RNA Miniprep Kit	Sigma-Aldrich	RTN70
High Capacity cDNA Reverse Transcription Kit	Applied Biosystem™	4368814
In-Fusion® HD Cloning Kit	Takara Bio	639650
Mouse VEGF DuoSet ELISA kit	R&D Systems	DY493
MTT Vybrant® Cell Proliferation Assay	Thermo Fisher	V-13154
PierceTM BCA Protein Assay	Thermo Fisher	23227

2.1 Cell Culture

2.1.1 Sources of cell lines and their maintenance

Mouse fibrosarcoma cells expressing single VEGFA isoforms (fs120 and fs188) derived from single VEGFA isoforms expressing embryonic fibroblasts were kindly provided by Dr. Kanthou from the University of Sheffield, UK. Both fs120 and fs188 cells were cultured in Dulbecco's Eagle's Medium (DMEM) containing 10% (v/v) heat-inactivated fetal bovine serum (FBS), 2 mM L-glutamine, 1% (v/v) penicillin-streptomycin (100 units), 600 μg/mL G418 and 2 μg/mL puromycin (Tozer et al., 2008). Total *Vegfa* knockout mouse fibrosarcoma (*Vegfa* KO) cells were obtained from Prof. Cao from the Karolinska Institute, Sweden. *Vegfa* KO cells were cultured with DMEM containing 10% (v/v) heat-inactivated fetal bovine serum (FBS), 2 mM L-glutamine and 1% (v/v) penicillin-streptomycin (100 units) (Yang et al., 2013). VEGFA120 and VEGFA188 cells described in this thesis, the fibrosarcoma cell lines developed expressing single VEGFA isoforms from mature skin VEGFA KO fibroblast provided by Prof. Cao, were cultured with the same medium recipe as the fs120 and fs188 cells.

H5V cells were donated by Dr. Kanthou and used as the positive control of inhibitors. These cells were cultured with DMEM supplemented with 10% (v/v) heat-inactivated fetal bovine serum (FBS), 2 mM L-glutamine and 1% (v/v) penicillin-streptomycin (100 units) (Kanthou et al., 2014).

All cell lines were incubated with 5% CO_2 at 37 ℃ before reaching 75% for passage.

2.1.2 Cell passage

When cells reached 75% confluency, they were ready to passage to a new flask. The remaining medium was removed from the flask, and trypsin-EDTA (TE) (0.5 g/L trypsin and 0.2 g/L EDTA) was added to detach the cells. Because H5V cells adhered harder to the flask, cells were washed with PBS before adding TE. Cells with TE in the flask were incubated at 37 ℃ for 5 minutes and checked down the microscope if cells were mostly detached. Gentle taps to the flask may be needed to detach the cells. Then the pre-warmed medium was added to the flask to quench the reaction to TE. The mixture was then transferred to a falcon tube and centrifuged at 1500 rpm for 5 minutes. The supernatant was carefully removed from the tube and the cell pellet was

resuspended with fresh medium. Cells were transferred into a new flask with fresh medium at the desired density.

2.1.3 Cell storage

This method used steps described in the cell passage with the following changes; the cell pellet was resuspended with 10% (v/v) dimethyl sulfoxide (DMSO) in heat-inactivated FBS. 1 mL of cell mixture containing approximately 1×10^6 cells was transferred into a cryotube and placed in a Mr. Frosty™ freezing container (Thermo Fisher) before storing at -80 ℃. For storage longer than 2-3 months cells were transferred to the department's biorepository in Liquid N_2 vapour.

2.2 Cell Transfection

2.2.1 Vector digestion and ligation

For the construction of a system which stably expressed a single VEGFA isoform in the *Vegfa* KO cells, $[HRE]_5$-minCMV-VEGFA or CMV-VEGFA was cloned into the pCLIIP plasmid by replacing the Luciferase2-E2A-mStrawberry-pA fragment (English et al., 2017). Details of the steps are described below.

2.2.1.1 Restriction digestion enzyme

Both 1 µg pCLIIP-C-LS and pUC57+$[HRE]_5$-minCMV-VEGFA plasmids (customized from Eurofins Scientific) were double digested with 10 unites FseI and MluI digestion enzymes in 10 x CutSmart Buffer respectively. The mixture was gently mixed with the pipette and incubated at 37 ℃ for 2 hours. The digested plasmids were mixed with DNA loading dye (6 x, no SDS) and purified on a 1 % (w/v) agarose gel in TBE with SYBR Safe. The desired product was cut from the gel under UV light and transferred to microcentrifuge tubes for extraction. The DNA gel extraction processes followed the protocol provided in the kit. Further purification processes may be required if the ratio of 260/230 was too low. The DNA cleanup processes followed the protocol provided in the kit. The digested vector and DNA insert sequence were mixed in a ratio of 1:5. 1 µL T4 DNA ligase was added into a total of 20 µL mixture and incubated at room temperature for 1 hour. The reaction was heat inactivated at 65 ℃ for 10 minutes. The construct could be stored at -20 ℃ for later transformation.

2.2.1.2 In-fusion enzyme cloning

The vector pCLIIP-[HRE]$_5$-minCMV-VEGFA was linearized with 10 units of restriction enzymes MluⅠ and NotⅠ in 10 x CutSmart Buffer at 37 ℃ for 2 hours. The digested vector was purified on 0.8 % (w/v) agarose gel in TBE with SYBR Safe. DNA gel extraction processes followed the protocol provided in the kit. The DNA sequence of CMV from plasmid pcDNA 3.1 (Clontech) was amplified by Q5 High-Fidelity DNA Polymerase (NEB) and the designed primer pairs (Table 2.1) with 15 bp extensions homologous to vector ends. The PCR processes were listed below (Table 2.2). The amplified product was gel purified on 1 % (w/v) agarose gel in TBE with SYBR Safe following the protocol provided in the kit. Digested vector and DNA insert sequence were mixed in a weight ratio of 1:4 with 5x In-Fusion enzyme premix in a total volume of 10 μL. The mixture was incubated at 50 ℃ for 15 minutes and stored at -20 ℃ for later transformation.

Table 2.3. Designed Primer Pairs for In-fusion Cloning

Gene	Sequence (5'-3')	Product (bp)
CMV	CCGGGGATCTACGCGTGACATTGATTATTGACTAGTTAT	617
	CCTACCGGTGCGGCCGCAGCTCTGCTTATATAGACCTC	

Table 2.4. PCR Amplification of CMV

Step	Temperature (°C)	Time	Cycles
Denaturation	98	30 sec	
Annealing	98	10 sec	35
	72	30 sec	
	72	20 sec	
Extension	72	2 min	
Hold	4	∞	

2.2.2 Transformation

5 µL of the plasmid was mixed with 30 µL of DH5α competent *E. coli* cells in a 1.5 mL Eppendorf tube. The mixture was incubated on ice for 30 minutes and heat shocked at 42 ℃ for 45 seconds. *E. coli* cells were then incubated in ice again for 2 minutes. S.O.C medium was added to the mixture tapped up to 1 mL and incubated at 37 ℃ for another 2 hours on the shaker. Serially diluted mixtures were plated on an LB agar plate with 50 µg/mL (w/v) ampicillin respectively and incubated at 37 ℃ overnight. Up to 8 single colonies were picked and individually incubated in 5 mL of LB medium with 50 µg/mL (w/v) ampicillin at 37 ℃ for about 12 hours. *E. coli* cells in LB medium were pelleted by centrifuging at 6,800 x g at room temperature for 3 minutes. The extraction of plasmids from *E. coli* followed the protocol provided by the kit.

2.2.3 Colony PCR and Sanger sequencing

100 ng of extracted plasmids were mixed with specific primer pairs (Table 2.5) and 2 x master mix in a total reaction of 30 µL. The mixture was incubated in the PCR machine with the programme listed in Table 2.5 and 2.6. PCR products were run on 1.3% (w/v) agarose gel in TBE with SYBR Safe to confirm whether the interest gene was successfully inserted in the vector.

Colony PCR-checked plasmids were diluted with deionized water to 80 ng/µL (w/v) in a total volume of 10 µL. Primers were also diluted with deionized water to 5 µM in a total volume of 10 µL and mixed with the construct in a 1.5 mL Eppendorf tube. Samples were sent to Genewiz (Azenta Life Sciences) for Sanger sequencing. Both forward and reverse sequencing results were aligned with the theoretical sequence to identify the sequence of the newly made plasmid. The plasmids that had the correct sequence were used for transfection.

Table 2.5. Primer Pairs for Colony PCR and Sanger Sequencing

Gene	Sequence (5'-3')	Product (bp)	Annealing Temperature (℃)
CMV	CCGGGGATCTACGCGTGACATTGATTATTGACTAGTTAT	807	62
	CTCAATCGGACGGCAGTAGC		
VEGFA120	CACGACAGAAGGAGAGCAGAAG	348	60
	GGCTTGTCACATTTTTCTGG		
VEGFR164	CACGACAGAAGGAGAGCAGAAG	239	62
	TCCGCATAATCTGCATGGTG		
VEGFR188	CACGACAGAAGGAGAGCAGAAG	425	60
	AACAAGGCTCACAGTGAACGCT		

Table 2.6. Programme of Colony PCR

Step	Temperature (℃)	Time	Cycles
Denaturation	94	3 min	
Annealing	94	15 sec	30
	60	20 sec	
	72	1 min	
Extension	72	5 min	
Hold	4	∞	

2.2.4 Transfection

Cells were seeded with a density of 5 $\times 10^4$ cells in 2 mL of medium per well in a 6-well plate and ready for transfection when reached 70% confluency. 2.5 μg of plasmid DNA was mixed with 7.5 μL of TransIT-X2, and 1 μg of PmBP in 250 μL of the pre-warmed serum-free medium in an Eppendorf tube and incubated at room temperature for 30 minutes in the hood. The mixture was then added dropwise onto different areas of cells. When cells in the well reached 90% confluency, cells were transferred to a T25 flask and cultured with the medium including selection agents. Surviving cells reaching 90% confluency were ready for single clone selection.

2.2.5 Single clone selection

Transfected cells were diluted to a concentration of 0.5 cells per 100 μL of medium and then 100 μL of the diluted cell suspensions were pipetted into each well of a 96-well plate. The number of colonies in each well was monitored every 3 days. Cells which grew only in 1 colony in a well were transferred into a T25 that was selected for further expansion when reaching 50% confluency. At least 10 colonies were picked for each construct. The characteristics of cells from each colony were analysed by methods described in section 2.3.

2.3 Cell Characterization

To avoid selecting clones whose phenotype was due to random insertion of the transposon and selection, clones that shared similar characteristics were selected for further functional assays.

2.3.1 Characterisation of and quantification of mRNA expression by quantitative real-time PCR

2.3.1.1 mRNA extraction and quantification

Cells were seeded in T25 flasks grown to 90% confluency. The cultured medium was removed, and cell pellets were harvested for mRNA extraction. The extraction processes followed the instructions provided in the kits. Extracted mRNA was kept on ice for cDNA preparation. The concentration of mRNA from different VEGFA-expressing clones was quantified by measuring the wavelength at 260 nm in Nanodrop 1000 UV-Vis system. mRNA samples (n=3) were stored at -80℃ for later use.

2.3.1.2 cDNA preparation

mRNA samples were treated with DNase I, Amplification Grade, at the concentration of 1 U/μL at room temperature for 15 minutes. The reaction was inactivated by applying 25 mM EDTA at 65℃ for 10 minutes. mRNA was reverse transcribed into cDNA by using the High Capacity cDNA Reverse Transcription Kit. DNase I treated mRNA was mixed with 10 x RT random primer, 25 x dNTP mix, 10 x RT buffer, 1μL MultiScribe Reverse Transcriptase and 1 μL RNase inhibitor in a total volume of 20 μL. Mixtures were incubated as described in Table 2.7. The concentration of cDNA was quantified by measuring the wavelength at 260 nm in a Nanodrop 1000 UV-Vis system. cDNA samples were stored at -20℃ for later use.

Table 2.7. Program of Reverse Transcription

	Step 1	**Step 2**	**Step 3**	**Step 4**
Temperature (℃)	25	37	85	4
Time	10 min	120 min	5 min	∞

2.3.1.3 PCR amplification of cDNA for sequencing

PCR was performed to identify the presence of the gene. 100 ng of cDNA was mixed with 0.5 μM primer pairs (Table 2.6) and 2x BioMix^{TM} Red Master Mix in a total volume of 20 μL. The mixture was incubated as processes listed in Table 2.7. qPCR products were run on 1.3% (w/v) agarose gel in TBE with SYBR Safe. The agarose gel was imaged under UV light to check the size of the PCR product.

Table 2.8. Primer Pairs for Colony PCR and Sanger Sequencing

Gene	Sequence (5'-3')	Product (bp)	Reference
VEGFR1-1	CTTTCTCAAGTGCAGAGGGG'	302	(Zips et al., 2005)
	TCATGTGCACAAGTTTGGGT		
VEGFR1-2	ACATGGGACAGTAGGAGA	425	(Kim et al., 2011)
	ACGGAGGTGTTGAAAGAC		
VEGFR2-1	GGGGATTGACTTCAACTGG	211	(Zhang et al., 2014)
	GACCCTGACAAATGTGCTG		
VEGFR2-2	GACCTGGACTGGCTTTGG	342	(Kim et al., 2011)
	TCTCTTTTCTGGATACCT		

Table 2.9. Programme for PCR detection of amplified cDN

Step	Temperature (℃)	Time	Cycles
Denaturation	94	3 min	
Annealing	94	15 sec	35
	60	20 sec	
	72	40 sec	
Extension	72	5 min	
Hold	4	∞	

2.3.1.4 Real-Time PCR

RT-PCR was performed with the SYBR Green system. 15 ng of cDNA was mixed with 200 nM of primer pairs (Table 2.8) and 5 μL of SYBR Green PCR Master Mix in a total volume of 10 μL in a 384-well plate. cDNA was then amplified following the program described in Table 2.9, performed by Applied Biosystems 7900HT Sequence Detection system. All samples were run in triplicate on the same plate. GAPDH was used as a housekeeping gene to calculate ΔCT value which was then subtracted with the ΔCT of fs188 cells and earned ΔΔCT.

Table 2.10. Real-Time PCR Primers

Gene	Sequence (5'-3')	Product (bp)	Reference
Mouse VEGFA120	GCCAGCACATAGGAGAGATGAGC	94	(Darland et al., 2011)
	GGCTTGTCACATTTTTCTGG		
Mouse VEGFA188	GCCAGCACATAGGAGAGATGAGC	171	(Darland et al., 2011)
	AACAAGGCTCACAGTGAACGCT		
Mouse Total VEGFA	CACGACAGAAGGAGAGCAGAAG	82	(Brennan et al., 2009)
	CTCAATCGGACGGCAGTAGC		
Mouse GAPDH	TAGGTGAAGGTCGGTGTGAACG	233	(Brennan et al., 2009)
	CGCTCCTGGAAGATGGTGATGG		

Table 2.11. Program of Real-Time PCR

Step	Temperature (°C)	Time	Cycles
Enzyme Activation	95	20 sec	

Denaturation	95	1 sec	40
Annealing	60	20 sec	

2.3.2 Characterisation of protein expression

As described in the sections below, ELISA and Western blotting measured the protein expression of secreted and endogenous proteins.

2.3.2.1 Secreted protein detection

Cells were seeded in the density of 4×10^5 cells in 5 mL of medium in a T25 flask and incubated with 5% CO_2 at 37 ℃ until reaching 70% confluency. The existing medium was replaced with 2 mL of fresh medium and incubated for 24 hours. The medium was then collected and placed in a 5 ml bijou tube for storage at -20 ℃. With the additional treatment of suramin salt, cells were treated with 6 mmol/L of suramin salt for 3 h before collecting medium. The medium was stored at -20 ℃ for later analysis. The number of cells in the flask while collecting medium was counted for normalization. Three independent replicates from different passage numbers of each cell line were collected (n=3).

The expression of the secreted protein in the collected medium was measured by using the Mouse VEGF DuoSet ELISA kit. All medium samples were analysed as technical replicates in triplicate in addition to the three biological replicates. Protein detection followed the protocol provided by the manufacturer.

2.3.2.2 Detection of proteins in cell lysates

The detection of endogenous proteins was performed by Western blotting. The steps of Western blotting were described more in detail in section 2.4.

2.3.3 Cell Viability

Responses of cells across cell lines to the same culturing conditions were monitored by measuring changes in the proportions of healthy cells within the population over time using two different methods.

2.3.3.1 Cell proliferation measured using viable cell counts

Cell proliferation was determined by measuring the number of live cells over a period of 72 hours. Cells across different cell lines were seeded in the same density of 4×10^5 cells in 5 mL of medium in the T25 flask. Cells were harvested following the steps described in Section 2.1.2. Cell pellets were resuspended with 1 mL fresh medium. A small portion of the cell suspension was mixed with Trypan Blue at a 1:1 volume:

volume ratio. 10 µL of the mixture was applied to counting slides and counted with an automated cell counter, TC20 (Bio-Rad). The number of viable cells was recorded.

2.3.3.2 Cell proliferation measured using a metabolic assay.

Instead of distinguishing between dividing and non-dividing cells, viable cells are identified by mitochondrial activity, which measures the rate of metabolising colourimetric substrate dyes by mitochondrial enzymes. The yellow tetrazolium dye 3-(4,5-Dimethylthiazol-2-yl)-2,5-Diphenyltetrazolium Bromide (MTT) used in the metabolic assay enables to be reduced by oxidoreductase enzymes to insoluble purple formazan in viable cells. Relative numbers of viable cells present in the well were determined by the absorbance at 540 nm of the soluble purple formazan in the reagent.

MTT working solution was made by dissolving MTT powder in PBS at the concentration of 5 mg/mL (w/v) in the dark a day before experiments and stored at 4 ℃ in the dark. 4,000 cells in 100 µL of medium were seeded in triplicate in each well of the 96-well plate. The proportion of viable cells across cell lines was measured after 24-, 48- and 72-hour incubation. The existing medium in the well was removed and replaced with 100 µL of fresh medium containing 10 µL of MTT working solution. Cells with MTT dye were incubated at 37 ℃ for 4 hours with 5% CO2. Unmetabolized soluble MTT dye in the medium was removed from each well; insoluble purple formazan was dissolved with 100 µL of DMSO and incubated at 37 ℃ for another 10 minutes. The plate was well mixed and read the absorbance at 540 nm on a plate reader.

2.4 Western Blotting

2.4.1 Collection of cell lysates

Cell lysates were collected when cells in the T75 flask reached 90% confluency. For samples with treatments, e.g. inhibitors (Table 2.10) these were applied into the medium when cells reached 70% confluency and incubated overnight. Cells were then passage into a new flask and cultured in fresh medium with inhibitors and incubated overnight again. Cell lysates were then harvested as described below.

The flasks and samples were kept on ice for the following steps. The existing medium in the T75 flask was removed, and the cells were washed with 2 mL of ice-cold PBS. The cells were then scraped in 1 mL of RIPA lysis buffer supplemented with 5 mM EDTA, protease inhibitors (2 x recommended concentration) and phosphatase inhibitor (1 x). Lysates were passed through a 23-gauge needle 3 times and centrifuged at 10,000 x g at 4 ℃ for 10 minutes in 1.5 mL microcentrifuge tubes. Supernatants were aliquoted into 100 µL each and stored at -20 ℃ for further experiments.

Table 2.12. The concentration of inhibitors used

Inhibitors	Lot.	Stock Concentration (mg/mL)	Working Concentration (µg/mL)
BE5	PUR86443	16.1	40
B20-4.1.1	PUR27594	17.26	40
MF-1	110519	9.2	40
DC-101	141023	13.5	40
Pazopanib		1 mM	1 µM

2.4.2 Protein quantification

The protein concentration of cell lysates was measured by BCA assay following the protocol from the kit. The standard curve was established by known BSA standards in 8 different concentrations. 25 μL of lysates/standards were mixed with 200 μL of BCA working reagent in each well in the 96-well plate. The plate was covered with parafilm and incubated at 37 ℃ for an hour. The absorbance of samples on the plate was measured at 562 nm by the plate reader. If the absorbance of lysates were out of the range of the standards, lysates were diluted with PBS and measured again. The standard curve was generated by fitting the concentration versus absorbance of known BSA standards via linear regression. The concentration of lysates was calculated by fitting the absorbance of the samples into the linear regression formula.

2.4.3 Sample preparation

Loading buffer was made with Laemmli Buffer (4x) with 10% (v/v) DTT. 30 μg of protein was mixed with 10 μL of loading buffer in a total volume of 50 μL and incubated at 95 ℃ for 5 minutes. Once samples were cool, they were centrifuged at 13,000 x g for 10 seconds.

2.4.4 SDS-PAGE gel electrophoresis

According to the molecular weight of the target protein, samples were resolved using different percentage of SDS-polyacrylamide gel (SDS-PAGE). The SDS-PAGE gel was made with 8 to12% (v/v) of resolving gel with 0.5% (v/v) of 10% (w/v) APS and 0.05% (v/v) of TEMED and 4% (v/v) stacking gel with 0.5% (v/v) of 10% (w/v) APS and 0.1% (v/v) of TEMED. 35 μL of samples and reference protein ladder were loaded in the well of gels and run in Tris-Glycine SDS-PAGE buffer at 120 V for about 80 minutes.

2.4.5 Protein transfer

Transfer buffer was made by NuPAGE transfer buffer (1x) with 10% (v/v) of methanol. Resolved protein samples were transferred onto a nitrocellulose membrane in the transfer buffer at 15 V for an hour by a semi-dry transfer system (Invitrogen). The membranes were then blocked with 5% (w/v) fat-free dried milk or 3% (w/v) BSA in Tris-buffer saline (TBS) with 0.1% (v/v) of Tween-20 (TBS-T) for 30 minutes on the shaker.

2.4.6 Immunodetection and analysis

The membranes were incubated with diluted primary antibodies in 5% (w/v) dried milk or 3% (w/v) BSA at 4 ℃ overnight (Table. 2.13). The membranes were washed with TBS-T for 10 minutes thrice and incubated with diluted secondary antibodies in 1:10,000 in 3% (w/v) dried milk at room temperature for an hour. The membranes were then washed again with TBS-T for 10 minutes thrice. All incubations were performed on a shaker. The membrane was incubated with ECL reagent at room temperature for a minute and its chemiluminescent signal was detected with the Bio-Rad ChemiDoc system. If the signal was too weak to be detected using the ChemiDoc system, it was detected by incubation with x-ray film overnight and developed using a film auto processor.

The density of detected protein bands was quantified by the “Gel Analysis Tool” in Image J. Each band were marked and plotted as a peak. The area under the peak representing its density was calculated. The densities of bands between samples were normalized by GAPDH.

2.4.7 Membrane stripping and re-probing

The membrane was incubated with stripping buffer at room temperature for 10 minutes and washed thrice with TBS-T for 10 minutes on the shaker. The membrane was then blocked with 5% (w/v) dried milk or 3% (w/v) BSA in TBS-T for 30 minutes and ready to re-prob another primary antibody. Protein detection and analysis were the same as described in section 2.4.6.

Table 2.13. List of Antibodies and Working Concentration for Western Blotting

Protein	Company	Cat. No.	Dilution	MW (kDA)
Fibronectin	Abcam	ab2413	1:1000 (milk)	262
N-cadherin	Abcam	ab18203	1:1000 (milk)	130
Vimentin	Cell Signalling	5741	1:1000 (milk)	57
p-Src	Cell Signalling	9843	1:1000 (BSA)	60
t-Src	Cell Signalling	2109	1:1000 (milk)	60
p-Akt	Cell Signalling	9271	1:1000 (BSA)	60
t-Akt	Cell Signalling	9272	1:1000 (milk)	60
p-p44/42 MAPK	Cell Signalling	9101	1:1000 (BSA)	42, 44
t-p44/42 MAPK	Cell Signalling	4695	1:1000 (milk)	42, 44
Sox2	Abcam	ab97959	1:1000 (milk)	34
Rac1	BD Bioscience	R56220	1:1000 (BSA)	21
RhoA	Cell Signalling	2564	1:1000 (BSA)	21
p-VEGFR1 (Y1213)	Sigma-Aldrich	07-758	1:1000 (BSA)	66
t-VEGFR1	Abcam	ab32152	1:1000 (milk)	180
p-VEGFR2 (Y1059)	Cell Signalling	3817	1:1000 (BSA)	230

Protein	Company	Cat. No.	Dilution	MW (kDA)
p-VEGFR2 (Y1175)	Cell Signalling	2478	1:1000 (BSA)	230
t-VEGFR2	Cell Signalling	2479	1:1000 (milk)	210, 230
NRP1	Cell Signalling	3725	1:1000 (milk)	120
GAPDH	Abcam	ab8245	1:10,000 (milk)	37
Anti-rabbit HRP	Jackson Immunoresearch	715035152	1:10,000 (milk)	
Anti-mouse HRP	Jackson Immunoresearch	715045150	1:10,000 (milk)	

2.5 Immunofluorescent Staining

2.5.1 Cell preparation

2.5.1.1 8 chamber slides

8 chamber slides (ibidi) were pre-coated with diluted fibronectin, collagen and laminin in PBS at room temperature or 37 ℃ for 2 hours respectively (Table 2.14). The chamber slides were washed with PBS 3 times and the culture medium once. 3×10^4 cells in 300 μL of medium were seeded in each well of slides and incubated overnight for cell attachment and stabilization.

Table 2.14. Working Solution for Coating

Protein	Stock Concentration (mg/mL)	Desired Concentration (µg/mL)
Fibronectin	1	5
Collagen	3.71	20
Laminin	1	5

2.5.1.2 Fibre scaffolds

Fibre scaffolds were fastened on the CellCrown Insert and pushed to the bottom of the 12-well plate. Scaffolds were then coated with 10 µg/mL (w/v) of fibronectin in PBS at room temperature overnight on the shaker. Each well was washed with PBS thrice and the medium once. 5×10^4 cells in 500 µL of the medium were evenly seeded on top of the scaffolds. 1mL of the medium was filled around the scaffolds gently. The cells were incubated overnight before staining.

2.5.2 Staining

The existing medium was removed from the well and washed cells with HBSS (with Ca^{2+}/Mg^{2+}) for 3 minutes twice. Cells were fixed with 4% (v/v) PFA in PBS at room temperature for 20 minutes and washed with HBSS (with Ca^{2+}/Mg^{2+}) for 5 minutes twice. Cells were then incubated with 0.1% (v/v) Triton™ X-100 in 1% (w/v) BSA for 5 minutes and washed with PBS for 5 minutes twice. The cells were blocked with 1% BSA in PBS for 20 minutes. The working concentration of primary antibody was added to each well and incubated at room temperature for an hour in the dark (Table 2.15). The cells were washed with PBS for 5 minutes thrice. The working concentration of secondary antibody was added to each well and incubated at room temperature for another hour in the dark (Table 2.15). The cells were washed with PBS for 5 minutes thrice again. Phalloidin (1 x) diluted in 1% BSA was added to each well and incubated at room temperature for 30 minutes in the dark after incubating with the secondary antibody if needed. The cells were incubated with DAPI overnight in the dark with the

coverslips/lids on the top. The coverslips/lids were sealed with clear nail polish and stored at 4 ℃ away from light.

Table 2.15. List of Antibodies and Working Concentration for Immunofluorescent Staining

Protein	Company	Cat. No.	Dilution
Fibronectin	Abcam	ab2413	1:200
N-cadherin	BD Bioscience	BD610920	1:50
β-catenin	Cell Signalling	8480	1:100
p-paxillin	Cell Signalling	69363	1:200
β-integrin	BD Bioscience	BD 553837	1:50
Alexa Fluor™ 633 Phalloidin	Invitrogen	A22284	1:400
Alexa Fluor 488 Dye	Invitrogen	A11034 (Rab)	1:500
		A11001 (M)	
Alexa Fluor 555 Dye	Invitrogen	A31572 (Rab)	1:500
Alexa Fluor 633 Dye	Invitrogen	A21052 (M)	1:500

2.6 Characterisation of Collagen Fibril Structures in Mouse Tumours

2.6.1 Tumour slide preparation

Paraffin-embedded tumour sections are required to be deparaffinized and rehydrated before any further actions. The slides with tumour sections were bathed in 100% xylene for 3 minutes twice and then 50% (v/v) xylene diluted in 100% ethanol for 3 minutes. Leftover xylene on the slides was removed by bathing slides in 100% ethanol for 3 minutes twice. Rehydration was performed by bathing slides in ethanol followed by a concentration of 95, 70, and 50% for 3 minutes each. The slides were rinsed with running tap water for a few minutes. The remaining water on the sides was removed with a tissue. Tumour sections were then mounted with PBS under a coverslip and sealed with clear nail polish (Narice et al., 2016). The tumour slides were also stained with hemidactyline and eosin (H&E) as a reference, performed by the Histology Core in the medical school.

2.6.2 Imaging with Second Harmonic Generation (SHG) microscopy

Fibril collagen is a non-centrosymmetric structure that enables the production of strong second-harmonic (SH) signals detected by SH microscopy without any labelling. The morphology and topography of fibril collagen in tissue stroma can be identified by SHG microscopy (Garcia et al., 2018; Williams et al., 2005). All slides were imaged under 40 x oil lenses with a Zeiss LSM 510 META confocal microscope excited with Chameleon laser tuned at 940 nm. The SHG signals of fibril collagen were collected at 470 nm (Narice et al., 2016). The H&E stained slides were scanned by a slide scanner acted as a reference to determine whether images were taken in necrotic or viable areas. Multiple images were taken in both necrotic and viable areas in the same tumour section (n=4, from different cell lines).

2.6.3 Analysis of collagen fibril structure

Analysis of SHG images was performed in Image and its plugin Orientation J (Rezakhaniha et al., 2012). The average diameter of collagen fibres in each image was calculated by manually measuring 100 positions on fibres. The orientation of collagen fibres was analysed by Orientation J Distribution of fibres was displayed with different colours corresponding to different orientations.

2.7 *In vitro* Engineered Environment Models

According to previously unpublished SH data collected from live imaging of tumours using the dorsal skinfold window chamber by the Tumour Microcirculation Group, collagen in the TME formed fibrillar structures, particularly in the fs120 tumours (Lunt, SJ and Tozer, GM, unpublished). Moreover, recent observations suggested cells can invade through a narrow confined space in ECM (Holle et al., 2019). The confined non-adherent chamber mimicked this space observed *in vivo* has been made during my MSc study (unpublished data, Yu-Chin Lee MSc thesis). We aimed to recapitulate fibrillar collagen in TME and rebuild the chamber adopting the previous design using different engineered environments with the application of techniques from Biomaterial Science.

2.7.1 Confined non-adherent chamber

The confined non-adherent chamber was made of 2 coverslips coated with the non-adherent material spacing with a layer of 3M Scotch tape (approximately 50 μm thick). The cells were seeded in between 2 coverslips for experiments.

2.7.1.1 Functionalization of coverslips

13 mm rounded coverslips were hydroxylated in Piranha solution which was made by slowly mixing sulphuric acid and hydrogen peroxide in a 3:1 volume ratio. The coverslips were incubated for 90 minutes and rinsed with deionised water 2 times for 5 minutes. Each coverslip was dipped into methanol and dried on a paper towel. The coverslips were then silanated in a mixture of MAPTMS and toluene at a 1:9 weight ratio for at least overnight. The coverslips were then stored in MAPTMS/toluene away from light before use.

2.7.1.2 Preparation of polyethylene glycol (PEG)-coated coverslips

5% (w/v) Poly (ethylene glycol) diacrylate (PEGDA) with a molecular weight of 700 g/mol was dissolved in deionized water. The photoinitiator, diphenyl(2,4,6-trimethylbenzoyl) phosphine oxide/2-hydroxy-2-methylpropiophenone was then added to the PEG solution at the concentration of 1% (w/w) over the polymers and stirred for an hour away from light. A little amount of food colour dyes may be added to the PEG solution as a coating reference. The leftover PEG solution was stored at -20 ℃.

The coverslips were removed from the MAPTMS/toluene mixture and rinsed with methanol. These were ready for coating once the coverslips were dried. The PEG solution was spin-coated onto functionalized coverslips using a spin coater, Model WS-400B-6NPP/Lite. The PEG solution was transferred into a 1 mL syringe with a 20-gauge blunt end needle. Approximately 500 µL of PEG solution per coverslip was coated by spinning at 4000 rpm for a minute. Coated coverslips were then photocured under UV light for 300 seconds and stored at room temperature away from light.

2.7.2 Electrospinning fibre scaffolds

Electrospinning is a technique of fabricating polymer fibres from solutions with the application of high voltage. The positively charged ejected polymer solution is guided by an electric field and lands on a negatively charged collector. The 3D structure of the fibre scaffold can highly mimic the topography of collagen fibres in TME.

2.7.2.1 Preparation of Polycaprolactone (PCL)

3 g of PCL was mixed with 20 mL of DCM in a glass bottle with a lid and gently shaken on a shaker at room temperature overnight until fully dissolved. During this process, any air bobbles were avoided to be generated in the solution. The solution was stored at 4 ℃ sealing the lids with parafilm.

2.7.2.2 Electrospinning

Electrospinning was set by a syringe on a pump and a rotational collector covered with foil 15 cm on the other side. The solution was put in a 1 mL syringe with a 20-gauge blunt end needle, set on a pump with a pump rate of 1 mL per hour, and applied with 12.7 kV. Depending on the needs of fibre scaffolds in different alignments, electrospinning fibres were collected on the collector at rotational speeds between 2000 and 200 rpm.

2.7.2.3 Fibronectin Coating

Because there is fibronectin attached to the collagen fibres observed in TME (Shi et al., 2010; Velling et al., 2002), the fibre scaffolds were coated with fibronectin for further experiments. The fibre scaffolds were fastened in the CellCrown Insert and pushed to the bottom of the 12-well plate. The fibronectin coating process was

similar to that described in section 2.5.1.2.

2.8 Migration Assay via Single-Cell Live Imaging

2.8.1 Cell seeding

Migration assays on 2D ECM-coated surfaces were performed in 24-well plates, and the 3D fibre scaffolds, and the non-adherent chambers were in 12-well plates. The coating process of the plates and scaffolds was similar to that described in section 2.5.1. The cells were washed following the steps described in section 2.1.2. For 2D surfaces, 1×10^4 cells in 500 µL of medium were seeded in each well and incubated at 37 ℃ overnight. For the 3D fibre scaffolds, 4×10^4 cells in 500 µL of medium were evenly seeded on top of the scaffold. 1 mL of medium was then filled around the CellCrown Insert and incubated at 37 ℃ overnight. The existing medium in both 2D and 3D systems was replaced with serum-free medium and with 40 µg/mL (v/v) of inhibitors or their controls and incubated for another 2 hours. For the non-adherent chamber, 1×10^4 cells in 50 µL of serum-free medium with inhibitors were seeded on top of a PEG-coated coverslip. The other coated coverslip was applied on the top and the entire sandwich structure was fastened in the CellCrown Insert. 1 mL of serum-free medium with 40 µg/mL (v/v) inhibitors or their controls was filled around the CellCrown Insert. The concentration of inhibitors was listed in Table 2.12.

2.8.2 Generation of a chemotactic gradient

Chemotaxis during live cell imaging was provided by a horse serum agarose gel on the side of the well-studied. The low-gelling temperature agarose was dissolved in PBS at the concentration of 10 mg/mL (w/v). 10% (v/v) Horse serum was added to the agarose solution once getting cool. Then autoclaved plastic cloning rings were filled with the serum/agarose solution and removed once the agarose solidified. The horse serum agarose gel was applied at one side of each well and incubated at 37℃ for 30 minutes before imaging.

2.8.3 Setup of live cell imaging

Live cell imaging was performed on the microscope, Zeiss CellDiscoverer 7, with the 10-x lens. The microscope was pre-warmed to 37℃ and pre-set CO_2 concentration to 5%. The stage was set to move at 3% maximum speed with 7% maximum acceleration. Once the well plate was placed in the microscope, the bottom

of the well was measured first as the focusing reference. At least 6 positions per well were marked and focused manually. Images of each position were taken every 10 minutes for a total duration of 2 hours for non-adherent chambers and fibre scaffolds and 3.5 hours for 2D surfaces.

2.8.4 Cell migration analysis

For each well, 30 randomly picked cells were analysed using cell tracking and chemotaxis tools (ibidi) in Image J. The position of a single cell on each image was selected using the mouse and tracked through the cell tracking plugin. The migration distance, speed and directionality were calculated with the chemotaxis tool of those positions using data exported from the cell tracking tool. Distance cells travelled and their speed was displayed in a bar chart for comparison. The directionality of cell migration was presented as a rose plot. Data from each experiment were from 3 independent experiments (n=3).

2.9 Statistical Analysis

All statistical analysis was performed on GraphPad Prism 9. Before performing statistical analysis, all samples were checked if they fit a normal distribution. Samples with 2 independent groups were analysed by unpaired t-test for parametric data or Mann-Whitney test for non-parametric data and plotted with standard error of the mean (SEM). Samples with multiple independent groups were analysed by One-Way ANOVA for parametric data or the Kruskal-Wallis test for non-parametric data and plotted with SEM. Multiple comparisons between groups were made by using Uncorrected Dunn's test. Statistically significant differences between groups were marked as $P<0.05$ (*), $P<0.01$ (**), $P<0.001$ (***) and $P<0.0001$ (****).

Chapter 3

3. Development of a novel single VEGFA isoform expressing fibrosarcomas

Upregulation of soluble VEGFA in tumours, leading to leaky vasculature, promoted cancer metastasis (Akerman et al., 2013; Cooke et al., 2012). Besides regulating the modification of vasculature structures in endothelial cells, the expression of different VEGFA isoforms also affected the functions of cancer cells in TME (Kiso et al., 2018b). English *et al* have observed that fibrosarcoma cells expressing soluble VEGFA had greater metastatic potential and response to anti-VEGFA therapy (English et al., 2017). However, the effects of expressing different VEGFA isoforms on the metastatic potential of fibrosarcoma cells are still not fully understood.

Previous efforts from Tozer *et al* successfully developed fibrosarcoma cells expressing a single VEGFA isoform from embryonic fibroblasts but they may have gone through different stages of selection and differentiation which altered their cell plasticity (Tozer et al., 2008). To overcome varied developmental and differential backgrounds between fibrosarcoma cells expressing different single VEGFA isoforms, new fibrosarcoma cell lines were derived from mature skin VEGFA KO fibroblasts. This chapter will describe the methods of inducing VEGFA expression in VEGFA KO fibrosarcoma cells and the comparison of cellular functions between fibrosarcoma cells derived from different origins.

3.1 Introduction

Fibrosarcoma cells expressing a single VEGFA isoform were successfully generated from embryonic fibroblasts followed by immortalizing and oncogenically transforming by h-Ras and SV40 (Tozer et al., 2008) (Fig. 3.1). The heterozygous $VEGFA^{+/120}$ mice were generated by removing exons 6 and 7 in embryonic stem (ES) cells using *Cre/LoxP* system (Carmeliet et al., 1999). The heterozygous $VEGFA^{+/188}$ mice were generated by replacing new exons 4 to 8 with a *lox P*-flanked neomycin phosphotransferase which was then excised by *Cre* expression plasmids (Stalmans et al., 2002). Unlike normal neonates carrying $VEGFA^{188/188}$, $VEGFA^{120/120}$ mice died because of severely impaired cardiac performance and bleeding issues. Therefore, fibroblasts expressing a single VEGFA isoform were isolated from heterozygous breeding embryos in 13.5 dpc.

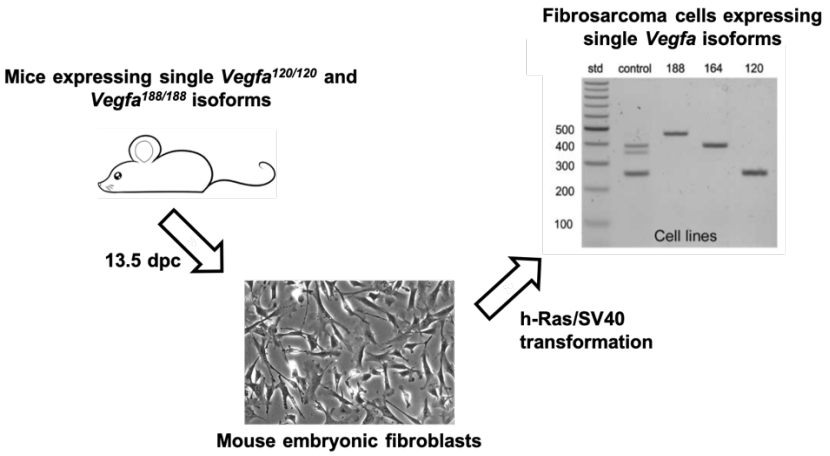

Figure 3.1 Generation of fibrosarcoma cells expressing a single VEGFA isoform from embryonic fibroblast

Embryonic fibroblasts expressing a single VEGFA isoform were isolated in 13.5 dpc and immortalized and oncogenically transformed by h-Ras/SV40. The mRNA expression of *Vegfa* isoforms in fibrosarcomas expressing a single VEGFA isoform was verified by gel electrophoresis.

Because of the significant correlation between cell plasticity and the extent of cell differentiation and self-renewal, it is crucial to consider cells utilised in complex migrations across diverse modes within engineered microenvironments. (Shiozawa et al., 2013; Mani et al., 2008; Morel et al., 2008). Autocrine VEGFA signalling has been reported, which was critical in regulating cell differentiation through different lineages (Liu et al., 2012; Bryan et al., 2007). However, previous fibrosarcoma cells expressing a single VEGFA isoform, fs120 and fs188, derived from embryonic fibroblasts exposed under only a single VEGFA isoform may have already experienced different levels of differentiation and selection. It increased the risks of determining whether the response to different microenvironments was VEGFA isoform-dependent alone, or if other factors such as the expression of stem cell-like traits were also involved. Generating new cell lines expressing a single VEGFA isoform from the same lineage was required.

New fibrosarcoma cell lines expressing a single VEGFA isoform were derived from *Vegfa*$^{-/-}$ fibrosarcoma cells which were immortalized and oncogenically transformed by h-Ras from mature skin *Vegfa*$^{-/-}$ fibroblast (Yang et al., 2013; Viloria-Petit et al., 2003) (Fig. 3.2). These skin *Vegfa*$^{-/-}$ fibroblasts were isolated from *Vegfa*$^{+/+}$/*Vegfa*$^{-/-}$ chimeric mice generated by aggregation of *Vegfa*$^{+/+}$ and *Vegfa*$^{-/-}$ ES cells and selected by G418-resistance (Tanaka et al., 1997; Carmeliet et al., 1996; Nagy et al., 1993). The fibrosarcoma cell lines expressing a single VEGFA isoform from the same lineage were then successfully made by transfection with a plasmid carrying the sequence of a single VEGFA isoform.

The expression of VEGFA was induced in response to hypoxia facilitating angiogenesis that was regulated by the transcription factor, hypoxia-inducible factor 1 (HIF-1) (Liu et al., 1995). Once cells experienced hypoxia, the heterodimer HIF-1 subunits bond to hypoxia response elements (HRE) in the promoter and activated transcription of VEGFA (Forsythe et al., 1996). Cancer cells transfected with the plasmid containing 5 copies of a 35-bp HRE fragment expressed maximum hypoxia-induced VEGFA (Shibata et al., 1998). To fulfil the inducible response to hypoxia, plasmids to transfect cells expressing a single VEGFA isoform were constructed with [HRE]×5 linked to a minimal human cytomegalovirus promoter (minCMV). Of which cells continuously expressing a single VEGFA isoform were transfected with plasmids constructed with a human cytomegalovirus promoter (CMV) alone. The expression of VEGFA in cells transfected between hypoxia-induced and conserved systems was similar under

hypoxia (Shibata, Giaccia, & Brown, 2000). Cells may be transfected with plasmids constructed with different promoters according to the needs of VEGFA expression under certain environmental conditions.

The expression of VEGFA highly affects the characteristics of cells (Kanthou et al., 2014). New cell lines with a similar mRNA and protein expression of VEGFA to Fs120 and Fs188 cells were selected for further experiments. Their proliferation rate, morphology on different ECM-coated surfaces and expression of cell migration-related proteins were compared with Fs120 and Fs188 cells and described in the following.

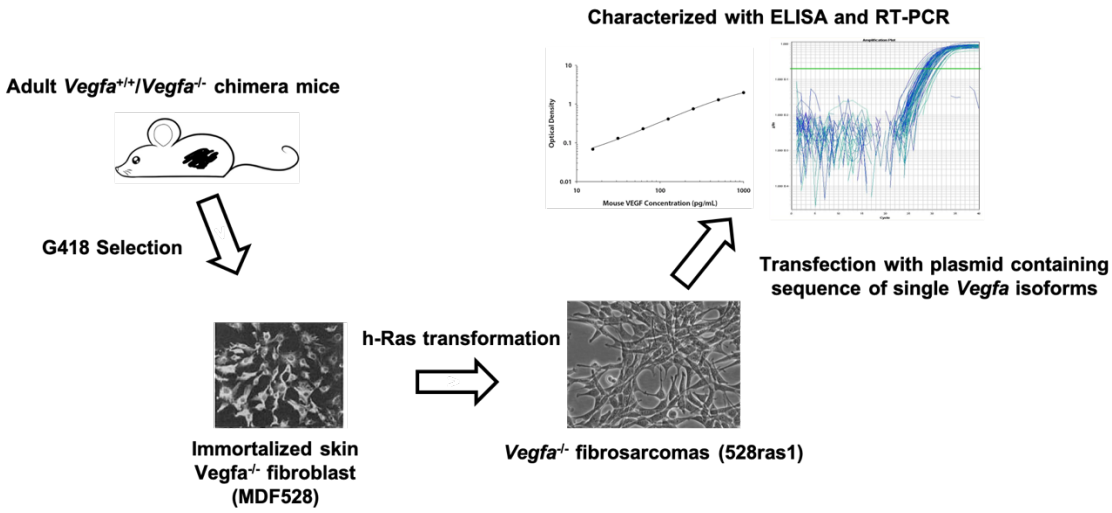

Figure 3.2 Generation of fibrosarcoma cells expressing a single VEGFA isoform from mature skin *Vegfa*$^{-/-}$ fibroblast

Mature skin *Vegfa*$^{-/-}$ fibroblasts were isolated from VEGFA$^{+/+}$/VEGFA$^{-/-}$ chimeric mice and immortalized and oncogenically transformed by h-Ras. *Vegfa*$^{-/-}$ fibrosarcomas selected by G418 were transfected with the plasmid carrying a sequence of a single *Vegfa* isoform. The mRNA and protein expression of a single VEGFA in transfected *Vegfa*$^{-/-}$ fibrosarcomas were characterized by RT-PCR and ELISA respectively.

3.2 Development of fibrosarcomas expressing a single VEGFA isoform

3.2.1 Construction of plasmids containing a single VEGFA isoform

Plasmids were synthesised using the DNA sequence of a single VEGFA isoform with different promotors generated using ligation-dependent and ligation-free cloning into the piggyBac (PB) transposon vector pCLIIP (Section 2.2). The target DNA sequence was integrated into the chromosome by the PB transposase via a "cut-and-paste" mechanism (Zhao et al., 2016). In comparison to viral vectors, the PB transposon system is more stable and easier to prepare. In addition, better transposition efficiency, larger cargo, long-term stable expression and footprint-free insertion into the genome compared with other transposon systems are pluses (Li et al., 2013; Maragathavally et al., 2006).

3.2.1.1 Preparation of the pCLIIP-[HRE]×5-minCMV-VEGFA plasmid

The PB transposon vector, pCLIIP-C-LS (English et al., 2017), was prepared as a cargo carrying the target DNA sequence [HRE]×5-minCMV-VEGFA. The Luciferase2-E2A-mStrawberry fragment located between MluI and FseI sites on the vector was removed by restriction enzymes and replaced with [HRE]×5-minCMV-VEGFA by T4 ligase (Fig. 3.3A). The expression of the inserted VEGFA fragment was regulated by 5 copies of HRE following a minCMV promotor. The sequence of the plasmid was verified by sequencing with primers recognizing VEGFA all isoforms and VEGFA isoform-specific primers in different directions (Fig. 3.3B).

3.2.1.2 Preparation of the p-CLIIP-CMV-VEGFA plasmid

As described in the introduction to this chapter, to achieve the continuous expression of VEGFAs at a higher level, the [HRE]×5-minCMV promotor was substituted with CMV. The plasmid with minCMV promotor was linearized by removing [HRE]×5-minCMV between MluI and NotI sites. The DNA sequence of the CMV promotor with 15 bp extensions homologous to both cut vector ends was amplified with customized primer pairs from the donor vector, pcDNA 3.1 zeo+. The [HRE]×5-minCMV promotor was successfully replaced with the CMV promotor by forming homologous pairs between donor and recipient DNA (Fig. 3.4A). The sequence of plasmid was verified by sequencing with primers recognizing the CMV promotor and VEGFA isoform-specific primers in different directions (Fig. 3.4B).

(A)

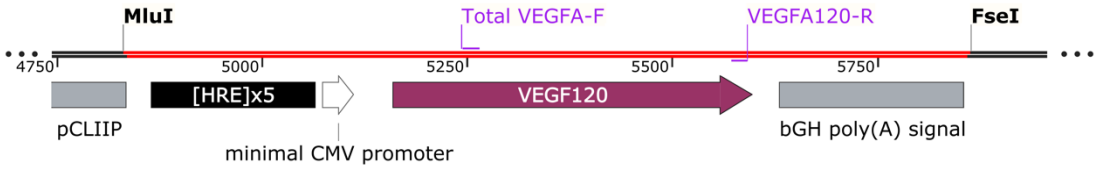

(B)

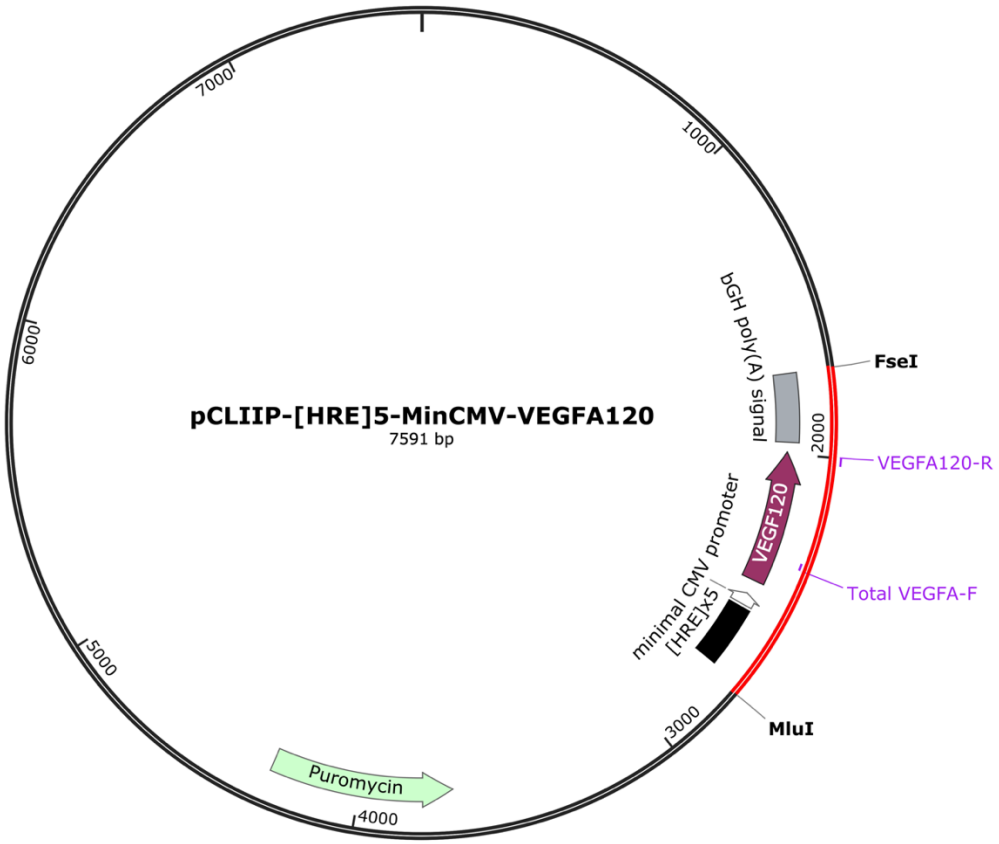

Figure 3.3 pCLIIP-[HRE]×5-minCMV-VEGFA plasmid

Plasmids containing the DNA sequence of different single VEGFA isoforms were generated with the same processes. The pCLIIP-[HRE]×5-minCMV-VEGFA120 plasmid is shown as representative. (A) The sequence of [HRE]×5-minCMV-VEGFA (Red) (Eurofins Scientific) was inserted between FseI and MluI sites in the pCLIIP vector (Black). (B) The plasmid was verified by sequencing with primers (Purple) respectively which have specificity to VEGFA isoforms. The region that coded for the puromycin-resistant gene was marked in green. Cells successfully transfected by the plasmids were selected with the application of puromycin in the cell culture media.

(A)

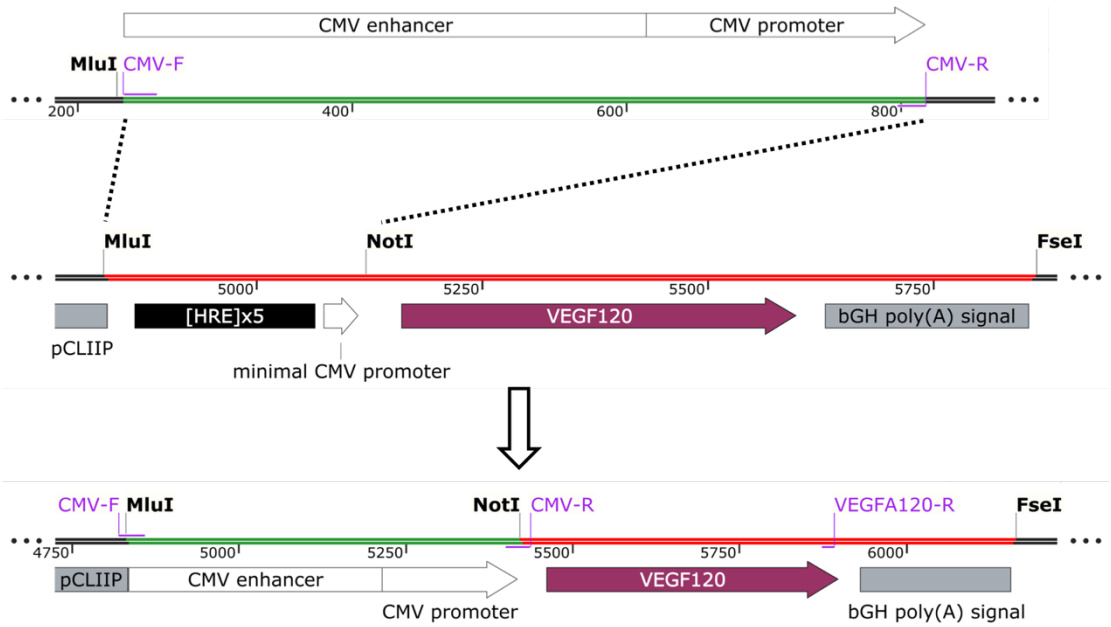
CMV enhancer
CMV promoter
MluI
CMV-F
CMV-R
200
400
600
800
MluI
NotI
FseI
5000
5250
5500
5750
pCLIIP
[HRE]x5
minimal CMV promoter
VEGF120
bGH poly(A) signal
CMV-F
MluI
NotI
CMV-R
VEGFA120-R
FseI
4750
5000
5250
5500
5750
6000
pCLIIP
CMV enhancer
CMV promoter
VEGF120
bGH poly(A) signal

(B)

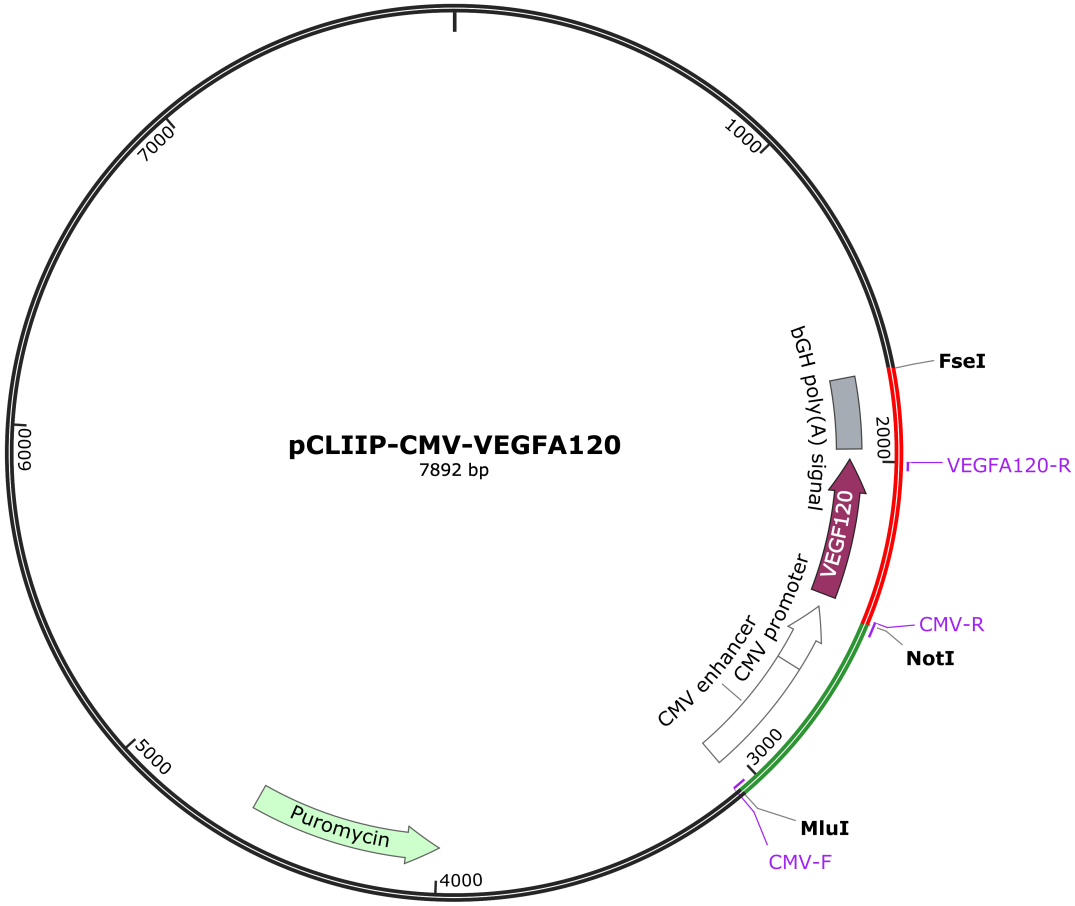
pCLIIP-CMV-VEGFA120
7892 bp
1000
2000
3000
4000
5000
6000
7000
FseI
VEGFA120-R
CMV-R
NotI
MluI
CMV-F
bGH poly(A) signal
VEGF120
CMV promoter
CMV enhancer
Puromycin

Figure 3.4 pCLIIP-CMV-VEGFA plasmid

Plasmids containing the DNA sequence of different single VEGFA isoforms were generated with the same processes. The pCLIIP-CMV-VEGFA120 plasmid was shown as representative. (A) The sequence of minCMV promotor with $[HRE]_5$ between MluI and NotI sites (Red) was replaced by the CMV promotor (Green) amplified from the donor pcDNA 3.1. MluI and NotI restriction digestion sites remained in the newly formed pCLIIP-CMV-VEGFA120 plasmid for further practice. (B) The plasmid was verified by sequencing with primers (Purple) respectively which have specificity to VEGFA isoforms and CMV promotor. The region that coded for the puromycin-resistant gene was marked in green. Cells successfully transfected by the plasmids were selected with the application of puromycin in the cell culture media.

3.2.2 Characterisation of VEGFA expression by ELISA in stably transfected VEGFA knockout cells

The goal of the experiment was to generate new mouse fibrosarcomas stably expressing a single VEGFA isoform with an approximately similar VEGFA expression level to fs120 and fs188 cells but sharing the same genetic background. $VEGFA^{-/-}$ (KO) cells were transfected with plasmids carrying a sequence of single VEGFA isoforms to reach this goal. Successfully transfected cells survived after puromycin selection and their VEGFA expression were measured. At least 10 single-cell colonies were selected and characterized to avoid any artefacts from clonal selection and ensure VEGFA expression was comparable to their fs120 or fs188 counterparts.

3.2.2.1 Characterisation of VEGFA expression in cells transfected with the pCLIIP-[HRE]×5-minCMV-VEGFA plasmid

Protein expression of VEGFA in VEGFA KO cells transfected with the pCLIIP-[HRE]×5-minCMV-VEGFA120 plasmid was measured by ELISA. As expected, there was no detection of VEGFA in VEGFA KO cells. Mouse VEGFA expression was successfully detected in puromycin-selected clones after transfection with the plasmid compared with VEGFA KO cells. However, expression of VEGFA was between 10-30-fold less than in Fs120 cells in all selected clones (Fig. 3.5). As protein expression of VEGFA was unable to reach a similar level as Fs120 cells under normoxia, cells transfected with the CMV promoter containing plasmid were characterised as described in the following sections.

3.2.2.2 Characterisation of VEGFA expression in cells transfected with the pCLIIP-CMV-VEGFA plasmid

VEGFA KO cells were transfected with pCLIIP-CMV-VEGFAs plasmid restoring the expression of VEGFAs or pCLIIP-C-LS plasmid acting as a transfection control. Their expression of different VEGFA isoforms was detected by ELISA. There were three clones (1.2,1.3 and 1.4) in cells transfected with the plasmid carrying VEGFA120 that showed similar VEGFA expression levels compared to fs120 cells, while three clones (2.2 and 2.5-2.8) had higher expression levels (Fig. 3.6). Similar VEGFA expression level to fs188 cells in VEGFA KO cells transfected with the plasmid carrying VEGFA188 was only observed in clones 2.4 and 2.5 (Fig. 3.7).

Unlike soluble VEGFA120, VEGFA188 binds to cell surfaces and the ECM and is

rarely detected in the culture medium by ELISA (Ferrara, 2010). However, the application of suramin salt transforms VEGFA188 into a soluble form (Tozer et al., 2008). To release VEGFA188 into the medium, cells were treated with suramin salt for 3 h before collection of the culture medium. VEGFA KO cells transfected with pCLIIP-C-LS were used as a transfection and selection control. No VEGFA expression was detected in the medium from both VEGFA KO and control cells. Significantly increased expression of VEGFA in cells expressing VEGFA188 was detected compared with cells expressing VEGFA120. In addition, no significant differences in the expression of VEGFA between VEGFA-rescued KO cells and fs cells were seen (Fig. 3.8). In conclusion, under normoxia, transfection of VEGFA KO cells with pCLIIP-CMV-VEGFA plasmids rescued the expression of VEGFA to similar expression levels seen in fs120 and fs188 cells and these were used in further experiments.

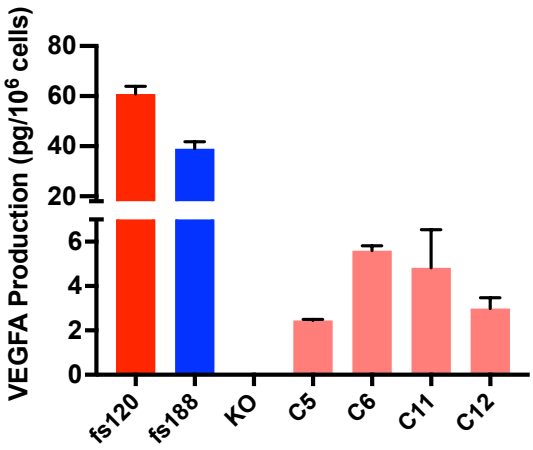

Figure 3.5 VEGFA expression in pCLIIP-[HRE]×5-minCMV-VEGFA120 stably transfected cells

4 clones as representatives were selected from the pool of VEGFA KO cells stably transfected with the pCLIIP-[HRE]×5-minCMV-VEGFA120 plasmid. Mouse VEGFA expression was measured by ELISA in the medium after 24 h incubation in atmospheric O_2. VEGFA detected was divided by the number of viable cells. Data is from 3 independent experiments. The average of triplicates was expressed as mean ± mean standard error.

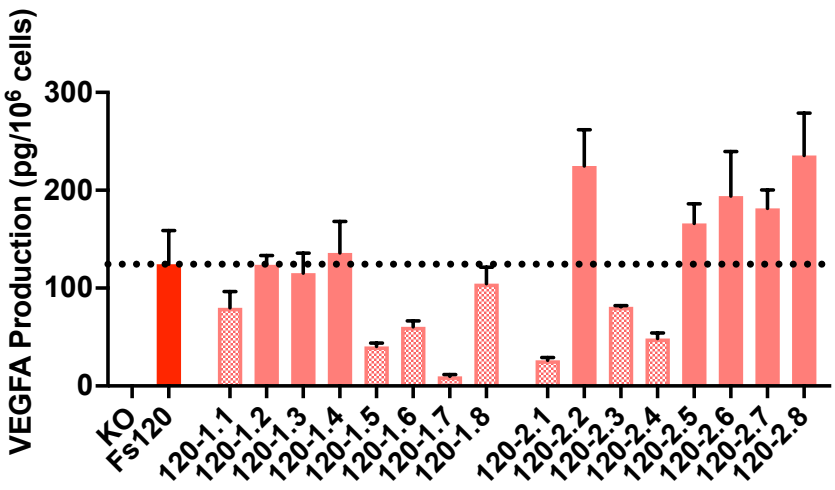

Figure 3.6 VEGFA protein expression in pCLIIP-CMV-VEGFA120 stably transfected cells.

The expression of mouse VEGFA in the medium collected after 24 h incubation in atmospheric O_2 in cells was quantified by ELISA. The culture medium from cells was collected from 3 independent experiments. VEGFA detected was divided by the number of viable cells. Data shown are mean ± SEM. The black dotted line was the mean VEGFA expression in fs120 cells.

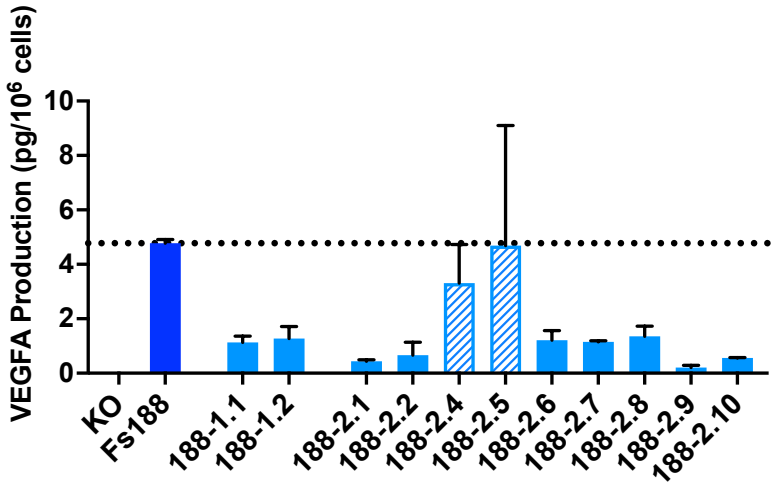

Figure 3.7 VEGFA protein expression in pCLIIP-CMV-VEGFA188 stably transfected cells.

The expression of mouse VEGFA in the medium collected after 24 h incubation in atmospheric O_2 in cells was quantified by performing ELISA. Medium samples of cells were collected in 3 independent experiments. VEGFA detected was divided by the number of viable cells. The average of triplicates was expressed as mean ± mean standard error. The black dotted line was the mean VEGFA expression in fs188 cells.

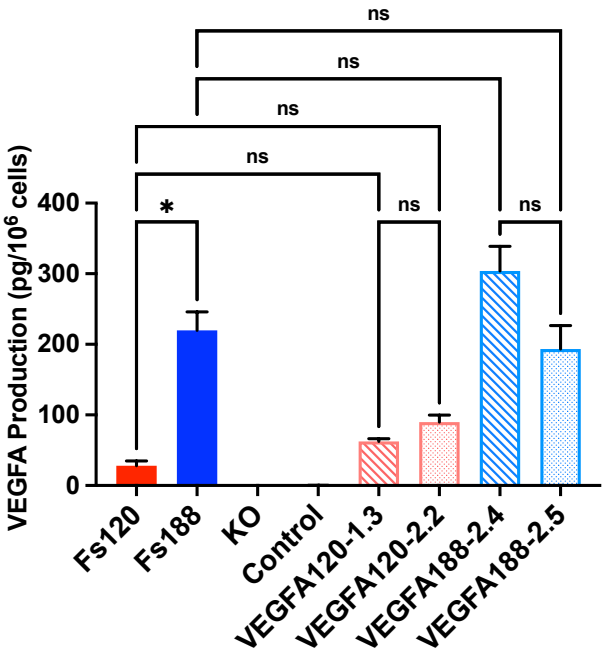

Figure 3.8 VEGFA protein expression in pCLIIP-CMV-VEGFA stably transfected cells treated with suramin salt

The expression of mouse VEGFA was quantified by performing ELISA in the medium from stably transfected cells collected after 3 h incubation with suramin salt in atmospheric O_2. VEGFA detected was divided by the number of viable cells. Medium samples of cells were collected in 3 independent experiments. The average of triplicates was expressed as mean ± mean standard error. A non-parametric Kruskal-Wallis test with multiple comparisons made using an Uncorrected Dunn's test was performed. * p-value <0.05.

3.2.3 mRNA expression of VEGFA isoforms in stably transfected *Vegfa* KO cells

As described in section 3.2.2.2, detecting the protein expression of VEGFA by ELISA in the medium is less sensitive in cells expressing VEGFA188. Therefore, the expression of VEGFA in VEGFA188-expressing cells was characterized by mRNA quantification via RT-PCR. The mRNA expression of *Vegfa* in VEGFA188 expressing cells was measured by the primers detecting total *Vegfa* and $Vegfa_{188}$ - specific primers. The mRNA expression of total *Vegfa* was significantly increased in clones 2.4 and 2.5, while clones 1.1 and 2.2 showed no difference compared with fs188 cells (Fig. 3.9A). Moreover, only clones 2.4 and 2.5 expressed similar levels of $Vegfa_{188}$ compared with fs188 cells, but others were significantly reduced (Fig. 3.9B). Although measuring the protein expression of VEGFA by ELISA is less accurate, both mRNA and protein expression of VEGFA shared similar trends (Fig. 3.5 and 3.7).

(A)

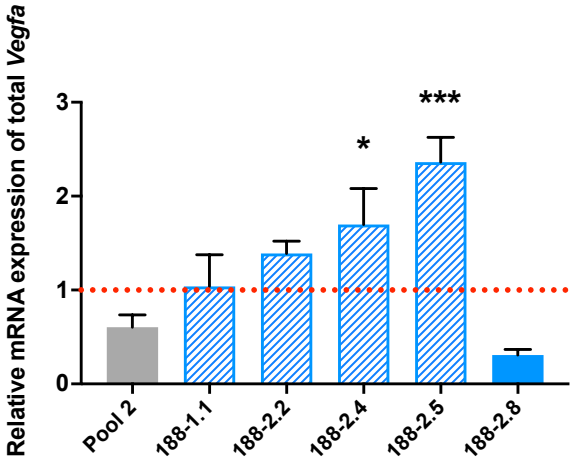

(B)

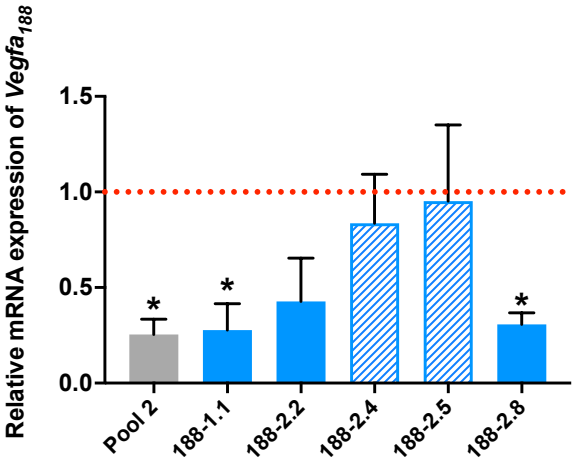

Figure 3.9 Total *Vegfa* and *Vegfa$_{188}$* mRNA expression in pCLIIP-CMV-VEGFA transfected cells

The mRNA expression of (A) total *Vegfa* and (B) *Vegfa$_{188}$* in cells under atmospheric O_2 was quantified by performing QRT-PCR. The expression of *Vegfa* in fs188 cells was used as the reference which was marked as the red-dotted line. Relative mRNA expression (ΔΔCT) of *Vegfa* in selected clones was calculated by, first normalizing with GAPDH, second subtracting ΔCT of fs188 cells and converting to the folds of changes. mRNA samples of cells were collected in 3 independent experiments. The average of triplicates was expressed as mean ± mean standard error. A one-way ANOVA with multiple comparisons using Fisher's LSD post-test was performed. * p-value <0.05, ** p-value <0.01, *** p-value <0.001.

3.3 Comparison of functional characteristics between fibrosarcoma cell lines expressing single VEGFA isoforms.

To characterize the effects of expressing a single VEGFA isoform in the clones selected from the VEGFA KO in comparison with the fs120 and fs188 cells, different functional assays were performed. Cell morphology, proliferation rates, the expression and phosphorylation of signalling participants downstream of VEGFA and VEGFRs and cell migration-related markers are described in the following sections.

3.3.1 Cell morphology and localisation of signalling proteins on different ECM of fibrosarcomas expressing single isoforms

3.3.1.1 Cell morphology and localisation of cadherins and b-catenin in fibrosarcomas expressing single VEGFA isoforms

Cell-cell adhesion plays an important role in the regulation of morphogenesis and cell migration. E-cadherin, a cell-cell adhesion molecule, is a major participant in forming adherens junctions (AJs) between neighbouring cells. The interaction between the extracellular domain of E-cadherin from neighbouring cells facilitates β-catenin binding to its cytoplasmic domain that stabilizes cell-cell junctions (Gumbiner, 2005; Conacci-Sorrell, Zhurinsky, & Ben-Ze'ev, 2002). Yet, when cell invasion occurs and cell-cell junctions are lost, β-catenin is translocalized to the nucleus activating transcription of factors that facilitate EMT (Brabletz et al., 2001). β-catenin trafficking in cancer cells is essential for EMT and metastasis. Unlike E-cadherin, N-cadherin is a hallmark of a mesenchymal-like phenotype. Upregulation of N-cadherin disrupts cell-cell adhesion and enhances the invasiveness and migration capacity of carcinoma cells (Hazan et al., 2004). Co-staining of β-catenin with E or N-cadherin in fibrosarcomas expressing different VEGFA isoforms would provide information on which morphology and if cells prefer to be single or adhere together on different ECM-coated surfaces.

VEGFA KO and transfection control cells, which did not express any VEGFA isoforms, displayed atypical mesenchymal features. Although cells were elongated and spindle-shaped, they grew side-by-side with each other. After the expression of either VEGFA120 or VEGFA188, VEGFA KO cells retained similar atypical mesenchymal features. However, cells expressing VEGFA188 grew in less close association with each other compared with cells expressing VEGFA120 on plastic, suggesting they were

slightly more mesenchymal in characteristic. In addition, fs120 cells, derived from embryonic fibroblasts, also showed atypical mesenchymal features forming long multicellular chains. In contrast, fs188 cells grew in a classic mesenchymal morphology which showed spindle-shaped and no cell-cell interactions (Fig. 3.10). The area of cells suggests how well cells spread on the surfaces. Fibrosarcoma cells derived from embryonic fibroblasts expressing VEGFA188 spread wider than cells expressing VEGFA120 on the plastic. In addition, restored the expression of VEGFA in VEGFA KO fibrosarcomas induced the cell area on the plastic compared to the transfection control cells (Fig. 3.11). Although there were significant differences in cell area on the plastic in cells expressing the same VEGFA isoform between different origins, the mean of cell area was alike across all cell lines.

All fibrosarcomas were then seeded on different ECM protein-coated surfaces to further characterise their morphology. There was a strong expression of N-cadherin in all fibrosarcomas on all ECM protein-coated surfaces indicating the cells were predominantly mesenchymal in morphology. The staining of β-catenin could identify the cell-cell interactions between fibrosarcomas. β-catenin was mainly distributed in the cytoplasm across all fibrosarcomas on all coated surfaces. Interactions between neighbouring cells in all fibrosarcomas seeded on uncoated plastic are marked with red arrows in Fig. 3.12. Moreover, cell-cell junctions were observed in VEGFA120 expressing cells on laminin-coated surfaces and in fs120 cells on collagen-coated surfaces (Fig. 3.13 and 3.15). β-catenin accumulating at the plasma membrane was displayed in all VEGFA isoform-expressing cells but not VEGFA KO fibrosarcomas on uncoated plastic and collagen (Fig. 3.12 and 3.15). In addition, both fs120 and fs188 cells displayed the accumulation of β-catenin at the membrane, whereas only the transfection control and VEGFA120 expressing KO cells showed similar features on laminin and fibronectin (Fig. 3.13 and 3.14). Interestingly, VEGFA120 clones on laminin and fs188 cells on collagen showed translocalization of β-catenin to the nucleus marked with white arrows in Fig. 3.13 and 3.15. Unlike on other ECM-coated surfaces, there were also cell pieces from fibrosarcomas that adhered to the surfaces. These could be membrane fragments left behind after cell death or torn from cells during migration. (Fig. 3.14).

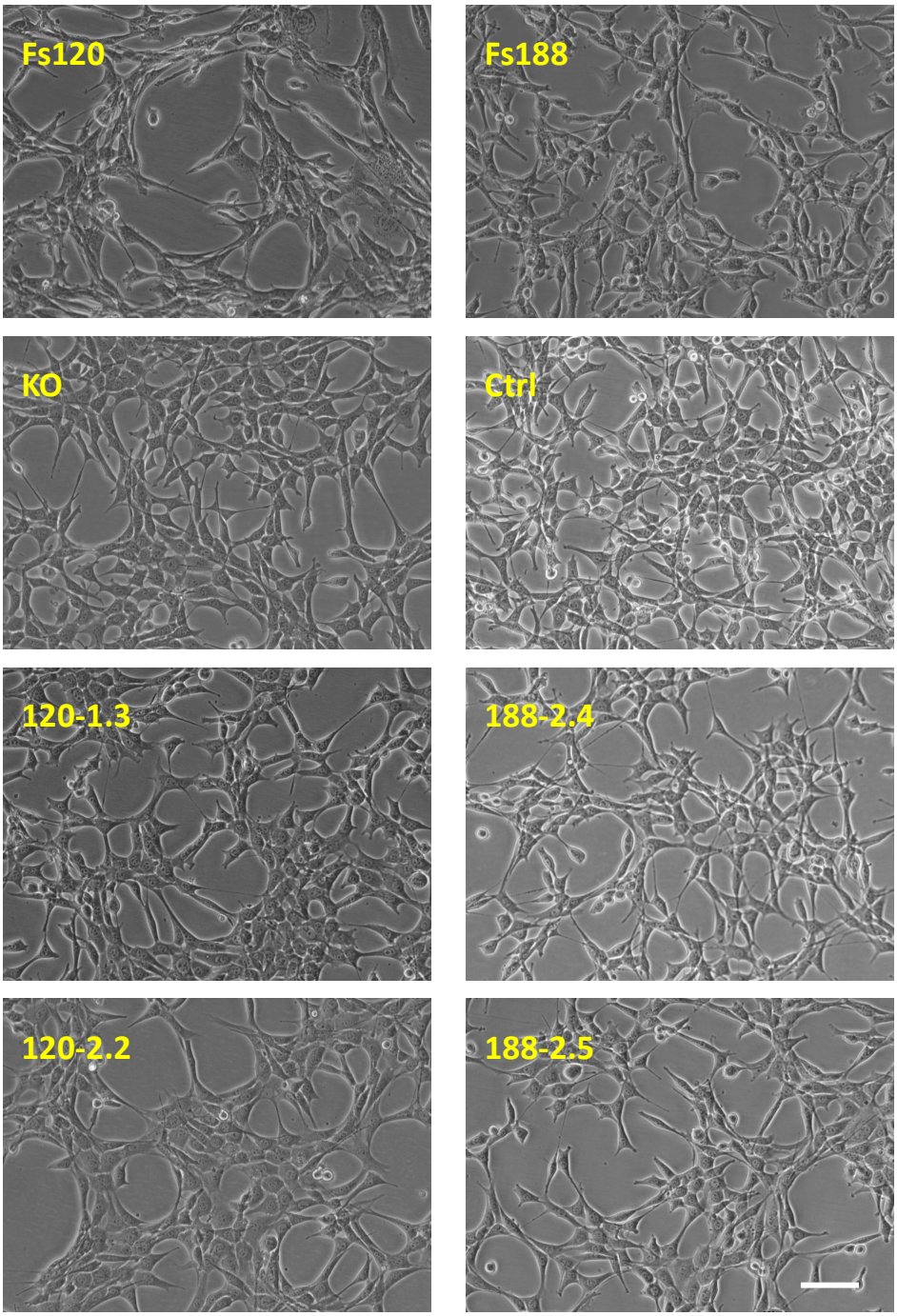

Figure 3.10 Cell morphology of fibrosarcomas expressing a single VEGFA isoform on non-coated plastic

Phase contrast images of 8 selected clones cultured with DMEM supplemented with FBS, glutamine and p/s at 37 °C under 5% CO_2 cell culture conditions on non-coated plastic. Scale bar = 50 μm (20X).

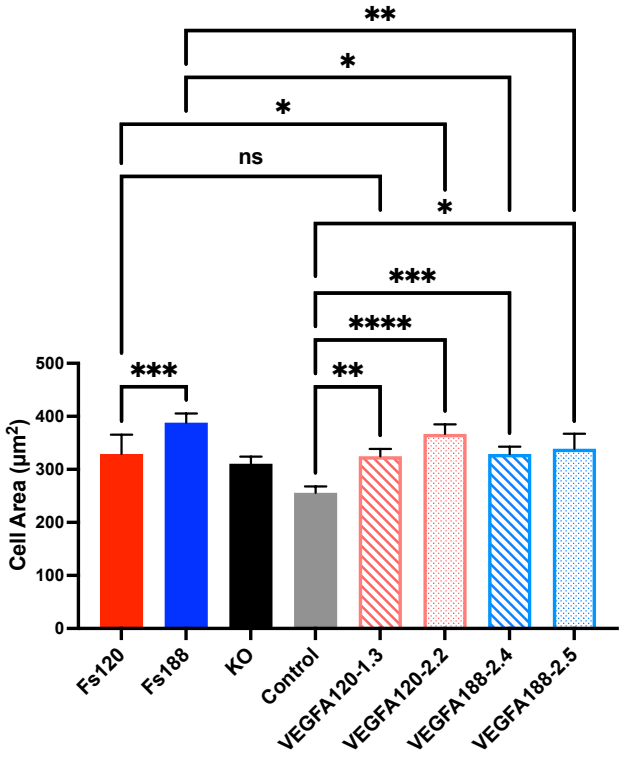

Figure 3.11 Cell area of fibrosarcomas expressing a single VEGFA isoform on non-coated plastic

The area of fibrosarcoma cells expressing different VEGFA isoforms was marked by freehand and calculated by the Image J. The average of calculated area was expressed as mean ± SEM (n=30). A non-parametric Kruskal-Wallis test with multiple comparisons followed by an Uncorrected Dunn's test was performed to determine statistical differences. * p-value <0.05, ** p-value <0.01, *** p-value <0.001, **** p-value <0.0001.

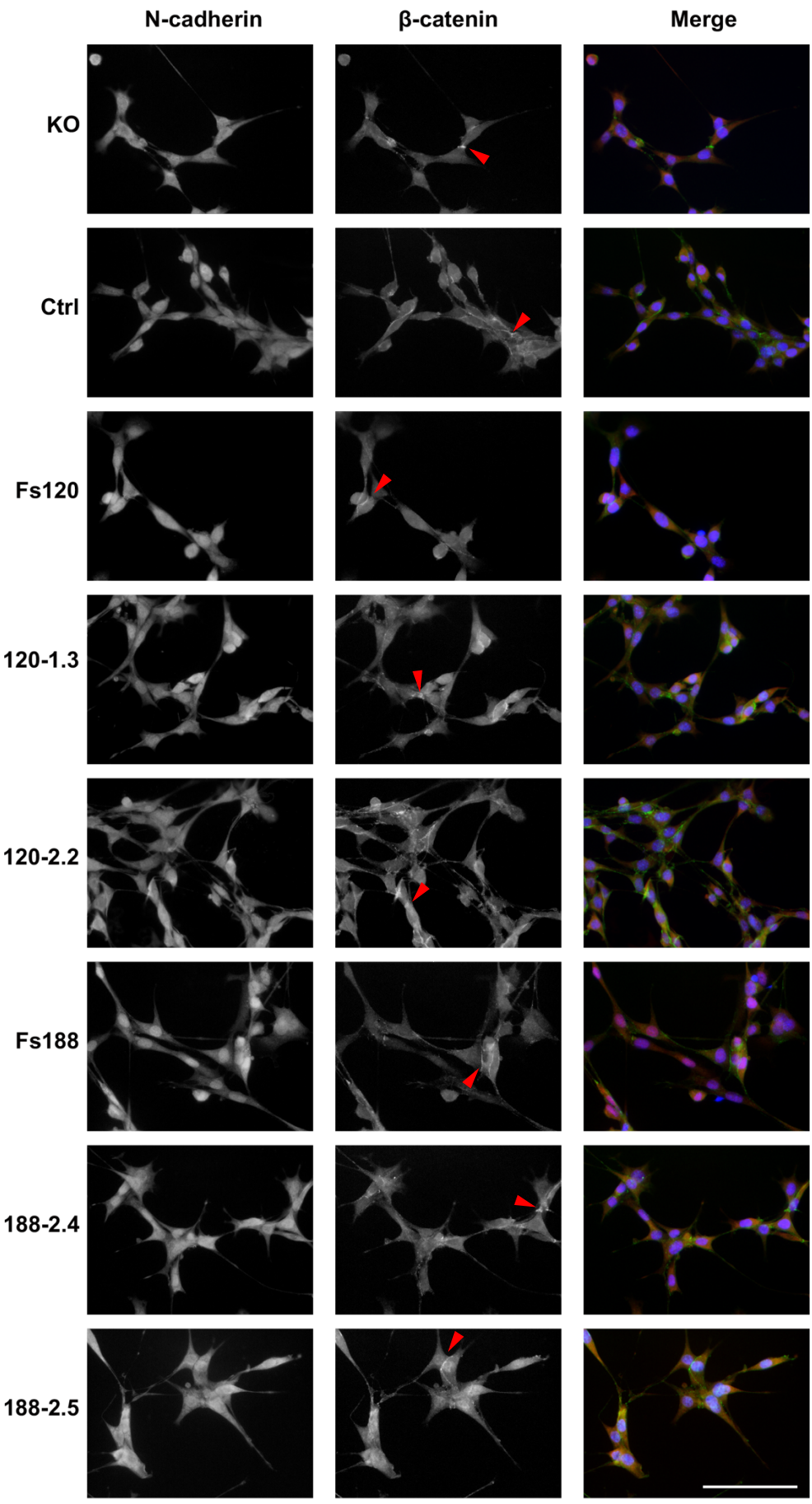
N-cadherin
β-catenin
Merge
KO
Ctrl
Fs120
120-1.3
120-2.2
Fs188
188-2.4
188-2.5

Figure 3.12 Co- staining of N-cadherin and β-catenin in cells grown on plastic

Immunofluorescent staining of N-cadherin (red) and β-catenin (green) of 8 selected clones on ibidi 8 Well μ-Slides. The red arrow indicates cell-cell junctions. Scale bar = 100 μm.

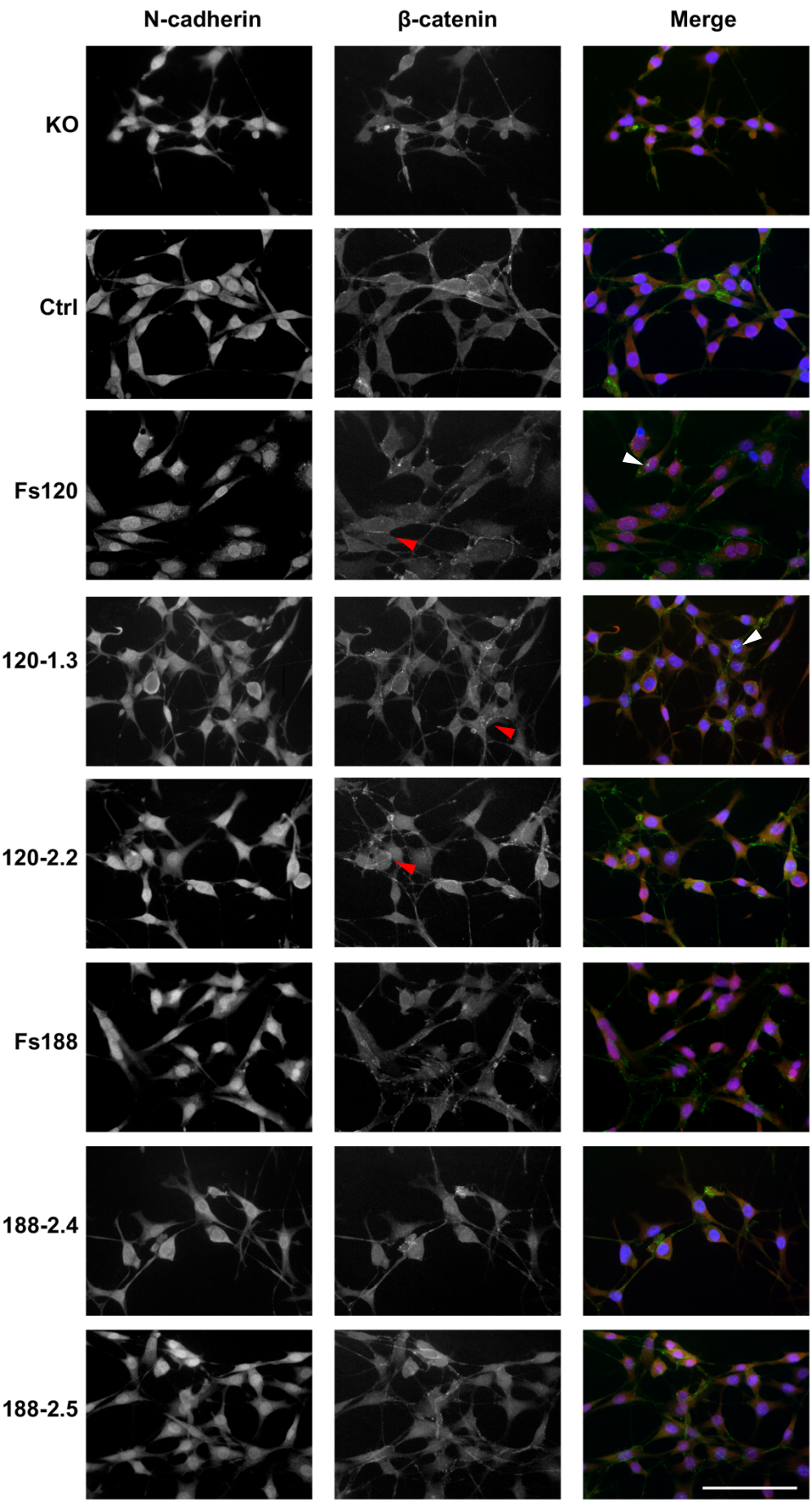
N-cadherin
β-catenin
Merge
KO
Ctrl
Fs120
120-1.3
120-2.2
Fs188
188-2.4
188-2.5

Figure 3.13 Immunofluorescent staining of N-cadherin and β-catenin in cells grown on laminin

Immunofluorescent staining of N-cadherin (red) and β-catenin (green) of 8 selected clones on ibidi 8 Well μ-Slides coated with 2.5 mL of laminin in the concentration of 5 μg/mL (w/v). The red arrow indicated the formation of cell-cell junctions. The white arrow indicates translocation of β-catenin to the nucleus. Scale bar = 100 μm.

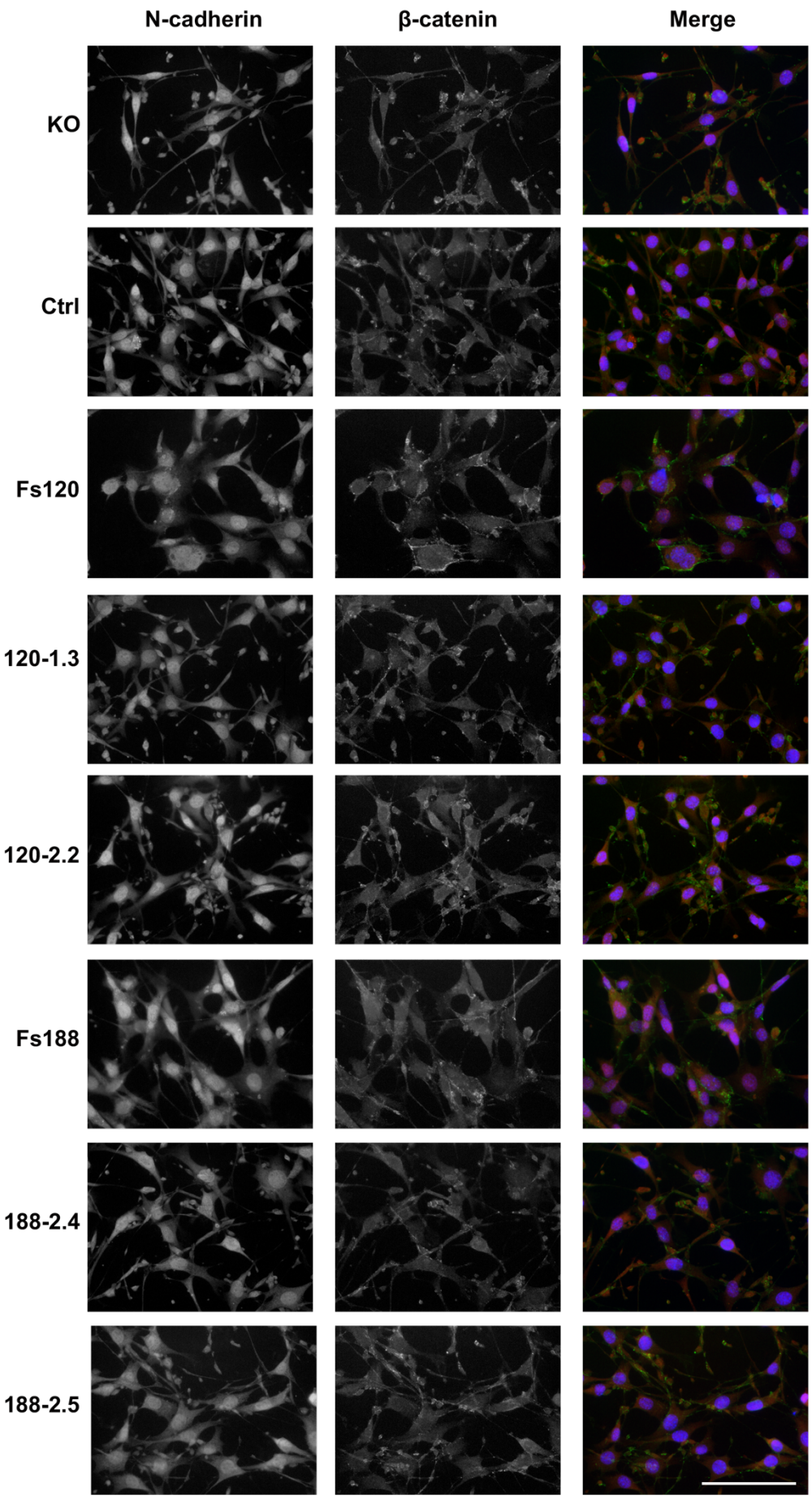
N-cadherin
β-catenin
Merge
KO
Ctrl
Fs120
120-1.3
120-2.2
Fs188
188-2.4
188-2.5

Figure 3.14 Immunofluorescent staining of N-cadherin and β-catenin in cells grown on fibronectin

Immunofluorescent staining of N-cadherin (red) and β-catenin (green) of 8 selected clones on ibidi 8 Well μ-Slides coated with 2.5 mL of fibronectin in the concentration of 5 μg/mL (w/v). The red arrow indicates cell-cell junctions. Scale bar = 100 μm.

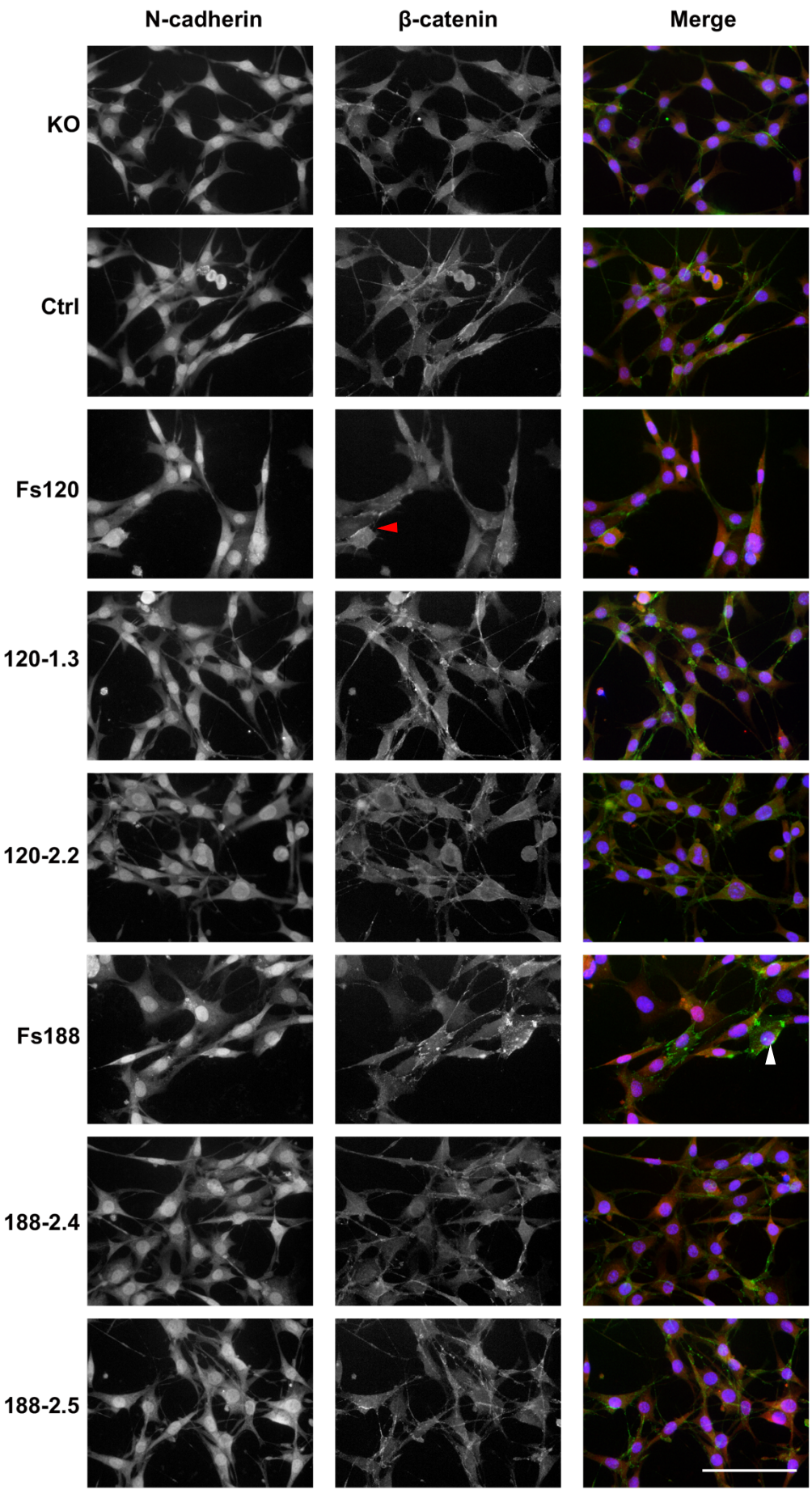
N-cadherin
β-catenin
Merge
KO
Ctrl
Fs120
120-1.3
120-2.2
Fs188
188-2.4
188-2.5

Figure 3.15 Immunofluorescent staining of N-cadherin and β-catenin in cells on collagen

Immunofluorescent staining of N-cadherin (red) and β-catenin (green) of 8 selected clones on ibidi 8 Well μ-Slides coated with 2.5 mL of collagen in the concentration of 20 μg/mL (w/v). The red arrow indicated the formation of cell-cell junctions. The white arrow indicated the translocation of β-catenin to the nucleus. Scale bar = 100 μm.

3.3.1.2 Localisation of focal adhesion proteins in fibrosarcomas expressing a single VEGFA isoform

Besides cell-cell interactions, the adhesion between cells and the ECM also regulates the morphology of cells and their migration capacity (Gumbiner, 1996; Hynes & Lander, 1992). Several types of receptors are expressed on the surface of cells involved in cell-ECM interactions. Heterodimeric integrins composed of a α- and a β-subunits show high binding affinity to the ECM (Takada, Ye, & Simon, 2007; Hynes, 2002). The extracellular domain of integrin subunits binds to extracellular proteins that are ligand specific. Whereas β_1-integrin binds to fibronectin, laminin and collagen, the binding specificity of α-integrin to those ligands is varied (Huttenlocher & Horwitz, 2011). The cytoplasmic domain interacts with proteins forming clusters called focal adhesions (FAs) that link to and regulate cytoskeletal functions. Paxillin, a scaffold protein in FAs, binds directly to either the integrin's cytoplasmic tail or the cytoskeleton and transduces ECM-induced signals to intercellular responses. Phosphorylated paxillin activated by ECM-integrin interactions regulates the cytoskeleton promoting cell migration through tyrosine kinases (Wozniak et al., 2004). To characterise the interaction between single VEGFA isoform expressing cells to different ECM proteins, the localization of FAs components β_1-integrin, p-paxillin and F-actin were analysed.

The expression of β1-integrin mediates the adhesion of cells to ECM proteins and is associated with the organization of the actin cytoskeleton. All fibrosarcomas strongly expressed β1-integrin across the different ECM protein-coated surfaces, but no distinct clusters were detected suggesting potential FA sites. F-actin, a major source of traction force for cell migration, was stained with phalloidin. Clear filamentous F-actin was visualized in both fs120 and fs188 cells while mainly diffuse in fibrosarcomas of VEGFA KO cell origin on uncoated plastic, laminin and collagen (Fig. 3.16, 3.17 and 3.19). Although there were some actin filaments detected in fibrosarcomas of VEGFA KO cell origin on fibronectin, these were mainly diffuse (Fig. 3.18). The p-paxillin clusters, indicators of FA sites, were detected at the edge of filopodia and partially at the projection of stress actin filaments in fs120 and fs188 cells across all coated surfaces. On the other hand, in fibrosarcomas from cells of VEGFA KO origin, p-paxillin clusters accumulated in the cytoplasm around the nucleus on uncoated plastic, laminin, and collagen (Fig. 3.16, 3.17 and 3.19) but located at the edge of filopodia on fibronectin (Fig. 3.18). Both VEGFA120- and VEGFA188-expressing cells had the highest

numbers of p-paxillin clusters on fibronectin (Fig. 3.18 and Table 3.1). The numbers of p-paxillin clusters observed in fs cells were significantly increased on collagen and fibronectin in comparison to on un-coated plastic (Fig. 3.16, 3.17 and 3.19). Whereas, both clones of VEGFA120 and VEGFA188 cells showed significantly upregulated numbers of p-paxillin clusters on fibronectin but downregulated on laminin compared with cells seeded on plastic (Table 3.1). Different to fs cells, rescued the expression of VEGFA in fibrosarcoma cells derived from total VEGFA KO mature skin fibroblasts successfully increased p-paxillin clusters in cells seeded on fibronectin but reduced on laminin.

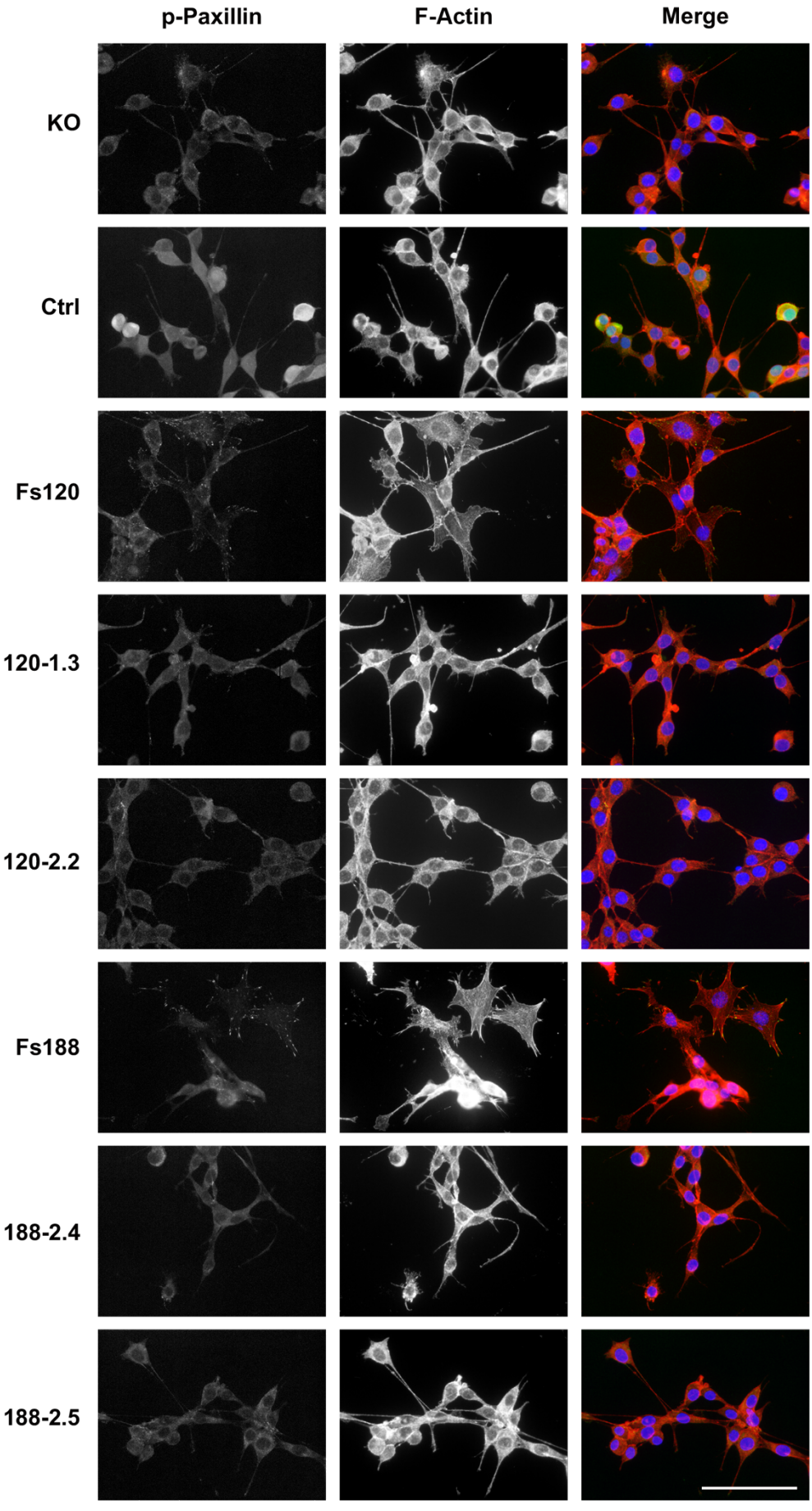
p-Paxillin
F-Actin
Merge
KO
Ctrl
Fs120
120-1.3
120-2.2
Fs188
188-2.4
188-2.5

Figure 3.16 Co- staining of p-paxillin and actin in cells on plastic

Immunofluorescent staining of p-paxillin (green), actin (red) and DAPI (blue) of 8 selected clones on ibidi 8 well μ-Slides. Scale bar = 100 μm.

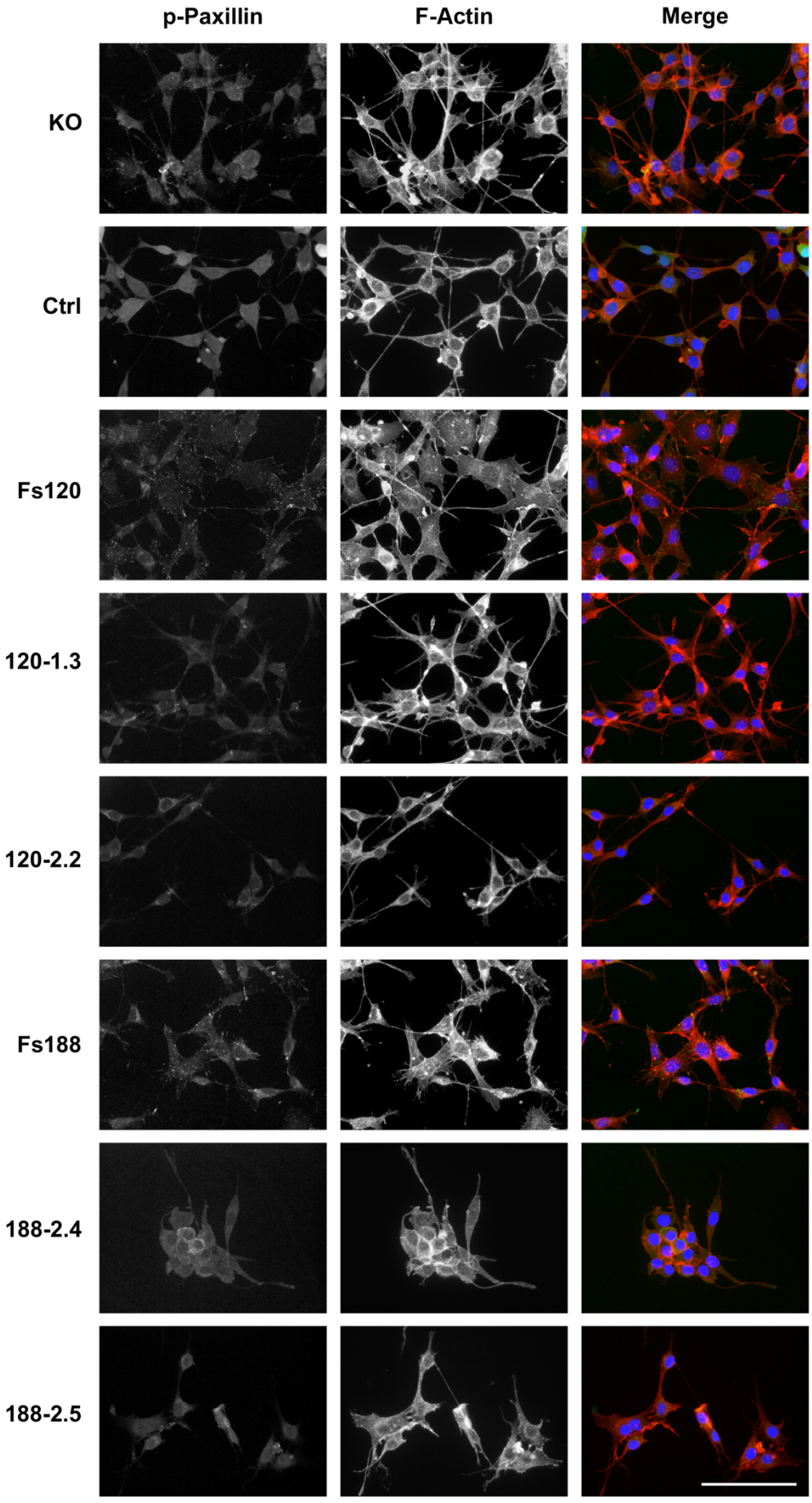
p-Paxillin
F-Actin
Merge
KO
Ctrl
Fs120
120-1.3
120-2.2
Fs188
188-2.4
188-2.5

Figure 3.17 Co- staining of p-paxillin and actin in cells on laminin

Immunofluorescent staining of p-paxillin (green), actin (red) and DAPI (blue) of 8 selected clones on ibidi 8 well μ-Slides. Scale bar = 100 μm.

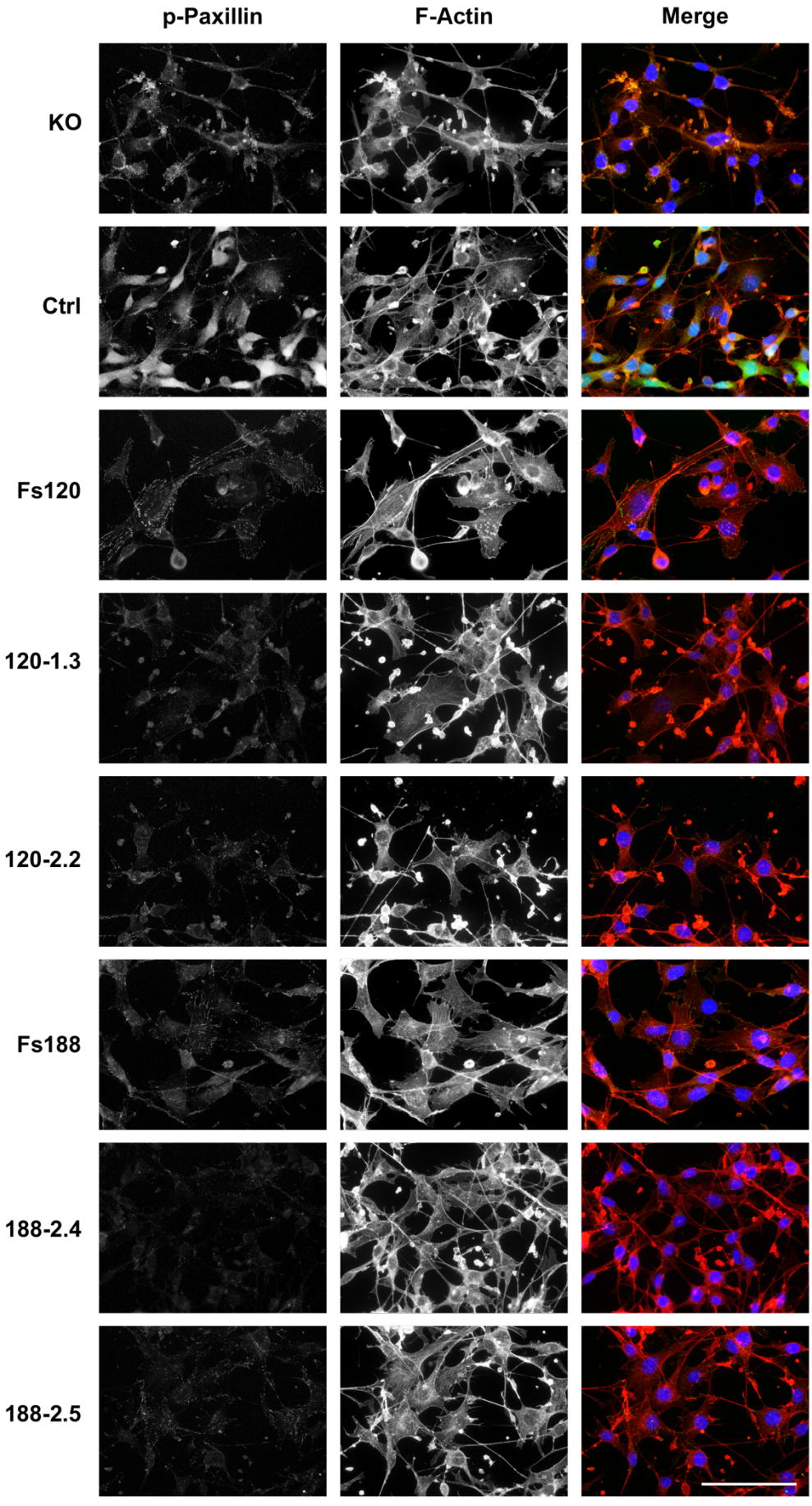
p-Paxillin
F-Actin
Merge
KO
Ctrl
Fs120
120-1.3
120-2.2
Fs188
188-2.4
188-2.5

Figure 3.18 Co- staining of p-paxillin and phalloidin in cells on fibronectin

Immunofluorescent staining of p-paxillin (green), actin (red) and DAPI (blue) of 8 selected clones on ibidi 8 well μ-Slides. Scale bar = 100 μm.

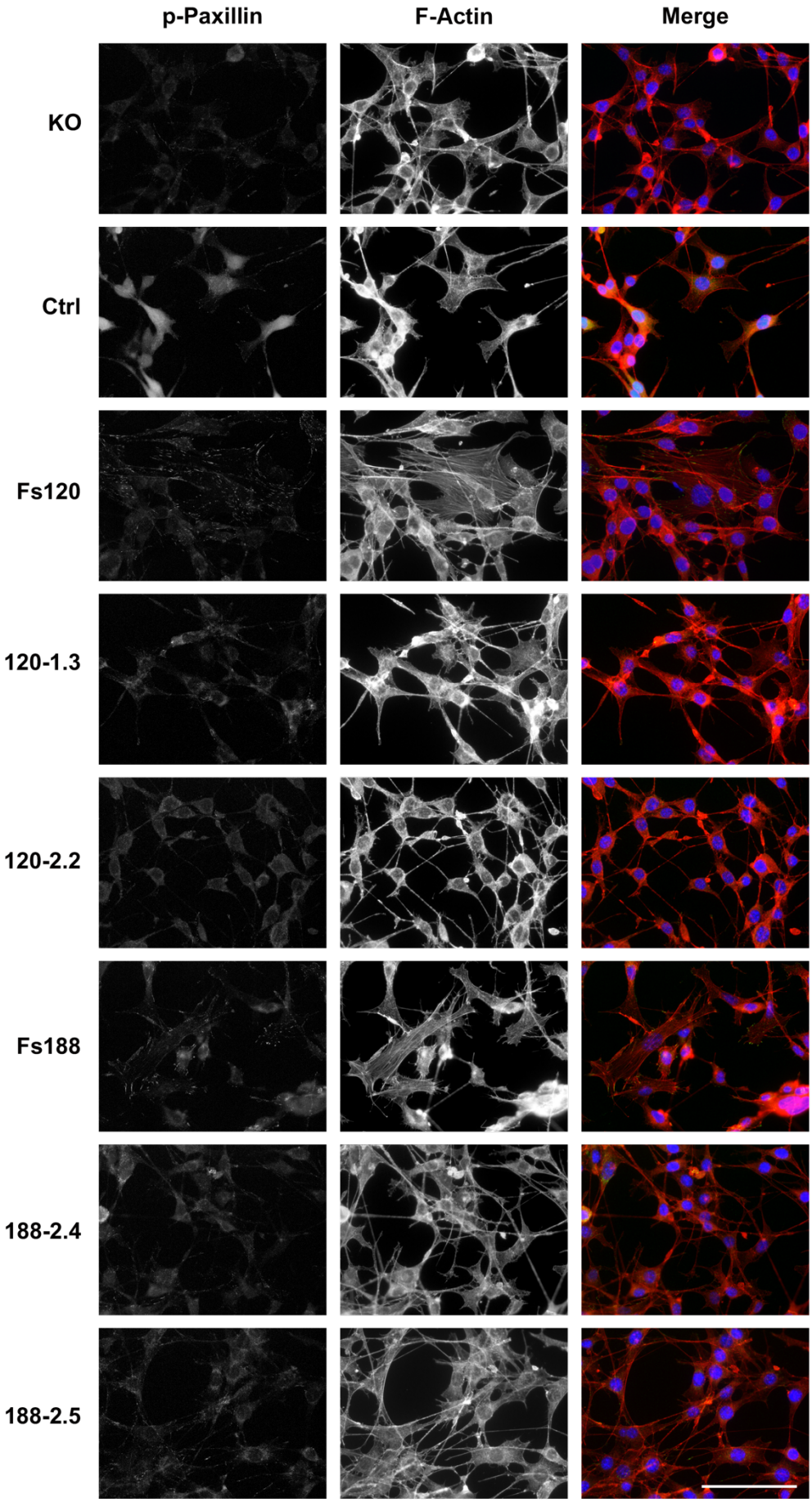
p-Paxillin
F-Actin
Merge
KO
Ctrl
Fs120
120-1.3
120-2.2
Fs188
188-2.4
188-2.5

Figure 3.19 Co- staining of p-paxillin and actin in cells on collagen

Immunofluorescent staining of p-paxillin (green), actin (red) and DAPI (blue) of 8 selected clones on ibidi 8 well μ-Slides. The red arrow indicated cell-cell junctions. Scale bar = 100 μm.

Table 3.1. Numbers of p-paxillin foci in cells on different ECM-coated surfaces

	Plastic	Laminin	Fibronectin	Collagen
Fs120	895.00±76.43	1002.33±58.77	****2188.00±93.30	****1790.33±77.15
Fs188	837.33±30.56	651.33±28.29	****2889.67±8.11	****1383.00±74.85
KO	794.00±34.20	****183.67±45.58	**1159.00±118.39	**1156.33±98.02
Control	648.67±27.91	469.33±52.92	482.33±45.83	*932.67±72.61
VEGFA120-1.3	806.00±33.26	****121.33±40.60	***1734.00±197.01	783.67±108.59
VEGFA120-2.2	849.67±111.62	****49.33±5.36	1057.00±112.78	703.33±43.63
VEGFA188-2.4	734.33±66.58	****81.67±4.06	****1878.00±136.84	810.00±49.27
VEGFA188-2.5	750.67±4.74	****74.33±1.86	****1776.00±282.93	931.67±48.17

Numbers of p-paxillin foci in cells were calculated by the plugin, Analyse Particles, in the Image J which presented in the means of foci counts from 3 images ± SEM. An ordinary two-way ANOVA test with multiple comparisons to fs120 and fs188 cells respectively was performed by an uncorrected Fisher's LSD test. * p-value <0.05, ** p-value <0.01, **** p-value <0.0001 values represent differences to cells seeded on plastic.

3.3.2 Proliferation of cells expressing single VEGFA isoforms *in vitro*

The proliferation rate of cells was determined by two different methods; directly calculating the number of viable cells by trypan blue staining and indirectly measuring cell metabolic activity by MTT.

Total viable cells across cell lines were first calculated 72 hours after seeding on plastic. There was no significant difference in the number of viable cells between VEGFA188 expressing VEGFA KO cells (clone 2.4 and clone 2.5). However, the expression of VEGFA120 in VEGFA KO cells showed a statistical difference between clones in their proliferation rate (clone 1.3 and clone 2.2). Interestingly, the proliferation rate of VEGFA KO cells with expression of VEGFA120 was inhibited at different levels compared with the transfection control. Furthermore, fs120 cells proliferated slightly faster than fs188 cells, although there was no statistically significant difference (Fig. 3.20).

Relative viable cell numbers were estimated at different time points by measuring the absorbance of purple metabolized MTT. The oxidoreductase enzymes in mitochondria in viable cells are able to metabolize MTT from yellow to purple insoluble particles. The more viable cells present, the higher the absorbance at 540 nm. VEGFA expressing VEGFA KO cells resulted in remarkable downregulation of cell proliferation similar to the observation by the Trypan blue staining method. Moreover, the MTT metabolizing assay also showed the VEGFA120-1.3 clone proliferated faster than the VEGFA120-2.2 clone. The proliferation rate of fs120 cells was consistently the fastest among cell lines (Fig. 3.21). Both methods used to characterize the proliferation rate of cell lines shared a similar pattern at 72 hours.

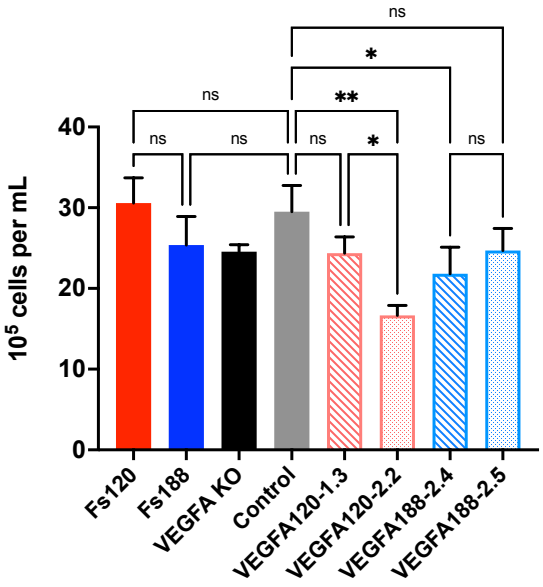

Figure 3.20 Numbers of viable cells expressing a single VEGFA isoform after 72 h

Viable cells after incubation for 72 hours were calculated by Trypan blue staining. Three independent replicates were expressed as mean ± SEM. A non-parametric Kruskal-Wallis test with multiple comparisons followed by an Uncorrected Dunn's test was performed to determine statistical differences. * p-value <0.05, ** p-value <0.01.

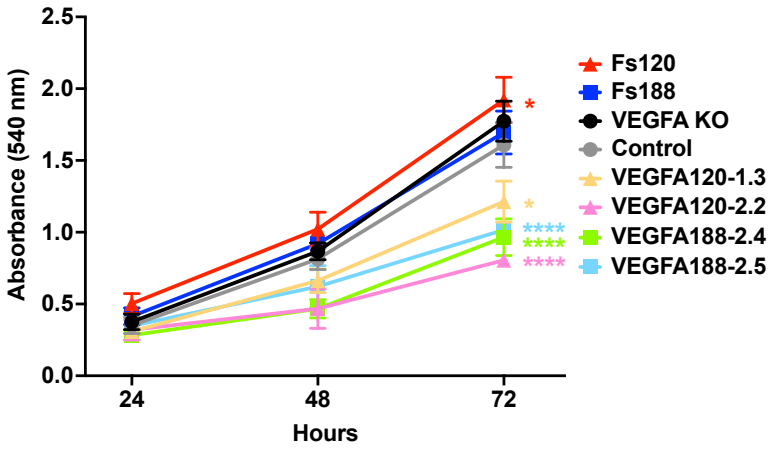

Figure 3.21 Proliferation assay of cells expressing a single VEGFA isoform determined by MTT assay

The relative changes in the number of viable cells at 24, 48 and 72 hours were estimated from the absorbance at 540 nm of insoluble MTT particles. Three independent replicates were expressed as mean ± SEM. A two-way ANOVA test with multiple comparisons to the control was performed by a Fisher's LSD test. * p-value <0.05, **** p-value <0.0001.

3.3.3 The expression of VEGFA receptors in VEGFA single isoform expressing cells

As described in the Introduction section 1.2.4, VEGFA isoforms can bind multiple receptors to trigger signal transduction. VEGFRs and their co-receptor NRP1 are the main receptors that interact with VEGFA isoforms. The expression of VEGFR1, VEGFR2 and NRP-1 across cell lines was characterized.

Western blotting analysis successfully detected the protein expression of VEGFR1 and NRP-1 among cell lines (Fig. 3.22). Even though there was no statistically significant difference in the expression of VEGFR1 across cell lines, VEGFA188-expressing cells showed higher expression levels of VEGFR1 compared with VEGFA120-expressing cells (Fig. 3.23A). The expression of NRP-1 was upregulated in fs188 cells compared with fs120 cells. However, the upregulation of NRP-1 was not observed in VEGFA188 expressing KO clones compared to the transfection control cell line. There was no difference in the expression of NRP-1 between fs120 and both VEGFA120-expressing KO clones (Fig. 3.23B).

The expression of VEGFR2 was unable to be detected by western blotting analysis across all cell lines, although the antibody successfully detected VEGFR2 in HUVEC cells. Instead of measuring the protein expression, the mRNA expression of both *Vegfr1* and *Vegfr2* across cell lines was determined by RT-PCR and gel electrophoresis. The clear band represented *Vegfr1* was detected across cell lines with two different primer pairs, but the band in the VEGFA120-2.2 clone was weak (Fig. 3.24A and B). Although there were bands across cell lines that represented *Vegfr2*, the PCR product size was smaller than the predicted 211 bp (Fig. 3.24C). Moreover, the band at 342 bp that represented *Vegfr2* was picked by other primer pairs only in the H5V cells (Fig. 3.24D). Therefore, if selected clones expressed VEGFR2 remained unclear.

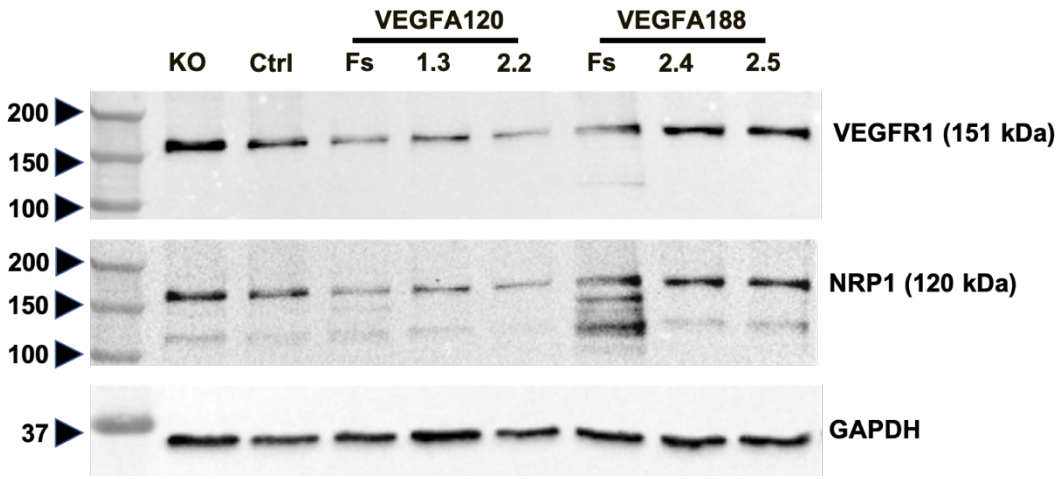

Figure 3. 22 Western blotting analysis of VEGFR1 and NRP-1 in cells expressing a single VEGFA isoform

Representative Western blot images of VEGFR1 and NRP-1 in cells expressing a single VEGFA isoform and the KO control are shown. GAPDH acted as a loading control. Three independent lysates were analysed by western blotting.

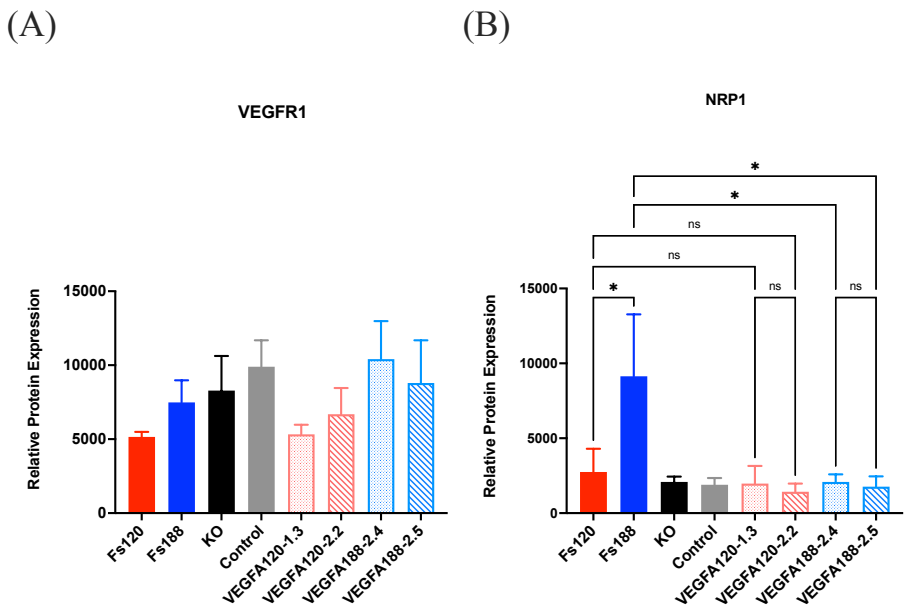

Figure 3.23 Quantification of relative VEGFR1 and NRP-1 expression in cells expressing a single VEGFA isoform

Relative protein expression of (A) VEGFR1 and (B) NRP-1 to GAPDH were quantified by Image J. The average of biological triplicates was expressed as mean ± SEM. A one-way ANOVA test with multiple comparisons by Fisher's LSD test was performed to detect statistical significance. * p-value <0.05.

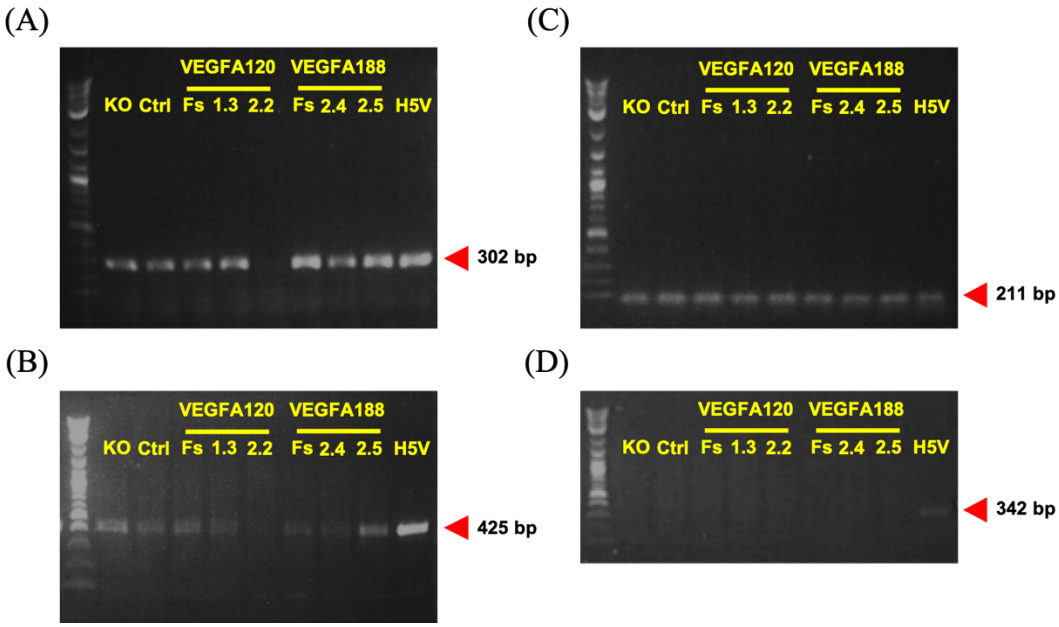

Figure 3.24 RT-PCR of VEGFR1/2 expression in cells expressing a single VEGFA isoform

Representative electrophoresis images of (A and B) VEGFR1 and (C and D) VEGFR2 PCR products in cells expressing a single VEGFA isoform, the transfection control and H5V cells were shown. (A) VEGFR1 primer set 1: 302 bp. (B) VEGFR1 primer set 2: 425 bp. (C) VEGFR2 primer set 1: 211 bp. (D) VEGFR2 primer set 2: 342 bP.

3.3.4 The protein level expression of cell migration-related markers in VEGFA single isoform expressing cells.

The importance of EMT in cancer cells, especially from epithelial origins, gains metastatic potential by enhancing migration capacity and invasiveness. Though fibrosarcoma cells are from mesenchymal origins, upregulated expression of mesenchymal markers has been shown to increase the invasiveness and metastasis in other subtypes of sarcomas (A. Shen et al., 2012; Masià et al., 2012). The expression of mesenchymal markers, fibronectin, N-cadherin and vimentin, across cell lines expressing different VEGFA isoforms were measured using Western blot.

There was no statistically significant difference in the protein expression of fibronectin between VEGFA120- and VEGFA188-expressing fibrosarcoma cells generated from embryonic or mature skin fibroblasts (Fig. 3.26A). Moreover, the expression of VEGFA in VEGFA KO cells upregulated the expression of fibronectin compared with the transfection control. The protein expression of N-cadherin was similar between VEGFA-expressing clones but increased expression in VEGFA120-expressing clones shared a similar trend seen between fs120 and fs188 cells (Fig. 3.26B). No statistically significant difference in the expression of vimentin between VEGFA-expressing clones was observed (Fig. 3.26C). However, an upregulation of vimentin in fs120 cells was detected compared with fs188 cells. A similar trend between was not seen in fibrosarcoma cells derived from mature skin VEGFA KO fibroblasts expressing VEGFA isoforms. These observations indicate the morphology of VEGFA120- and VEGFA188-expressing fibrosarcoma cells from different genetic backgrounds on plastic remained mesenchymal-like.

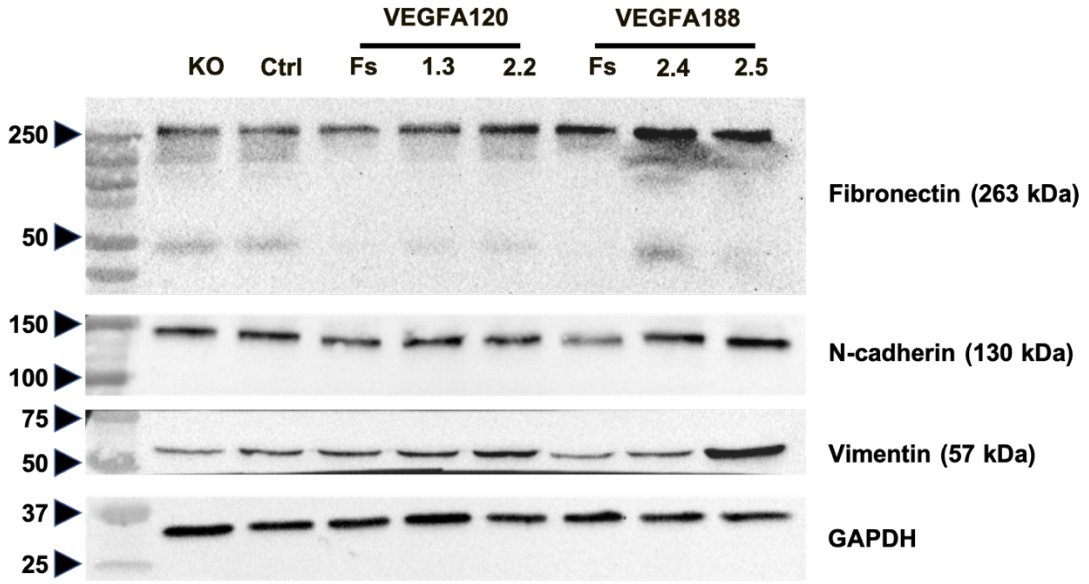

Figure 3.25 Western blotting analysis of mesenchymal markers in cells expressing a single VEGFA isoform

Representative Western blotting images of fibronectin, N-cadherin and vimentin in cells expressing a single VEGFA isoform and the VEGFA KO control are shown. GAPDH acted as a loading control. Three independent lysates were analysed by Western blotting.

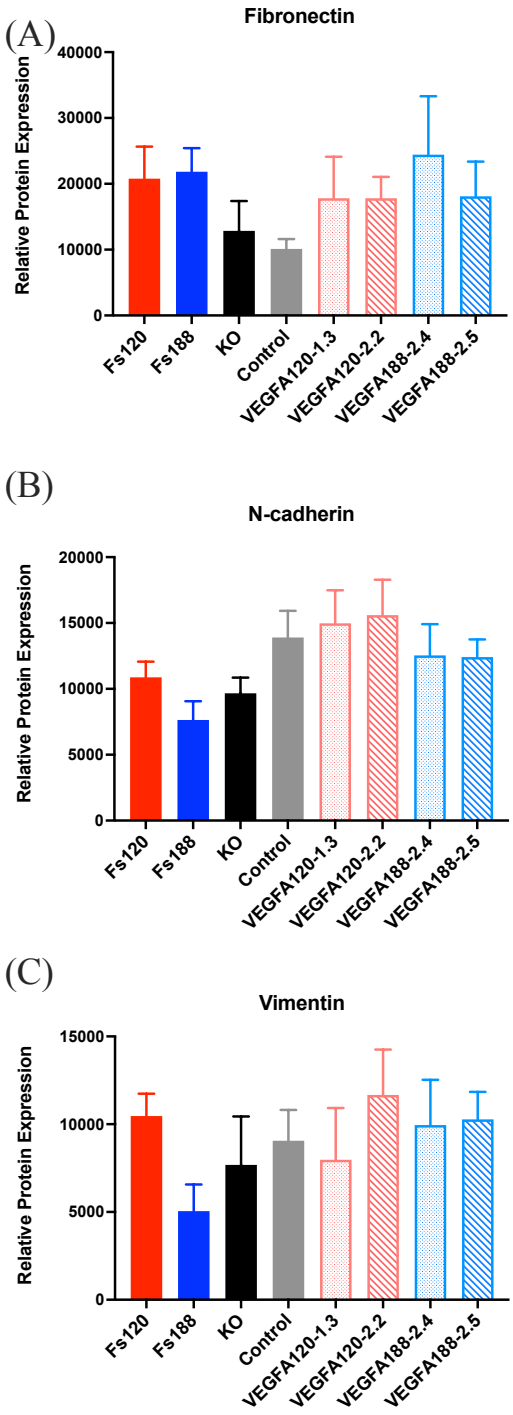

Figure 3.26 Quantification of mesenchymal markers in cells expressing a single VEGFA isoform

Relative protein expression of (A) fibronectin, (B) N-cadherin and (C) vimentin normalised to GAPDH were quantified by Image J. Three independent replicates were expressed as mean ± SEM. A one-way ANOVA test with multiple comparisons by using Fisher's LSD post-test was performed to detect statistically significant differences.

The Introduction has described in detail that PI3K/Akt, Src kinase and MAPK kinase (MEK)-ERK signalling cascades that regulate EMT and cell migration. (Gonzalez & Medici, 2014; Wang et al., 2011; Srinivasan et al., 2009; Liu, Huang, & Zhan, 1999). Various growth factors, such as PDGF, EGF and VEGF, may activate these signalling cascades through receptor tyrosine kinases (RTKs). VEGFA-induced migration and the expression of metastasis-related proteins through VEGFR1/2 were successfully abrogated by inhibiting the phosphorylation of Akt, Src and ERK1/2, indicating the important roles of these proteins in cell migration (Huang et al., 2018; Weddell, Chen, & Imoukhuede, 2018; Dellinger & Brekken, 2011; Ali et al., 2005). The expression of and phosphorylation of proteins that participate in VEGFA signalling pathways in fibrosarcoma cells expressing different VEGFA isoforms was measured by Western blotting (Fig. 3.27).

Overall, there were no statistically significant differences across all cell lines in the expression of the total and phosphorylated form of p44/42 (Thr^{202} and Tyr^{204}) and Src (Fig. 3.28A, B, C and D). However, phosphorylated Src (Tyr^{416}) expression was on average higher in fs120 cells than in fs188 cells (Fig. 3.28 C). In addition, the expression of the total and phosphorylated form of Akt (Tyr^{413})between VEGFA KO cells expressing VEGFA120 and VEGFA188 was similar. Interestingly, fs188 cells significantly increased the expression of phosphorylated Akt, whereas decreased the expression of total Akt in comparison to fs120 cells (Fig. 3.28E and F).

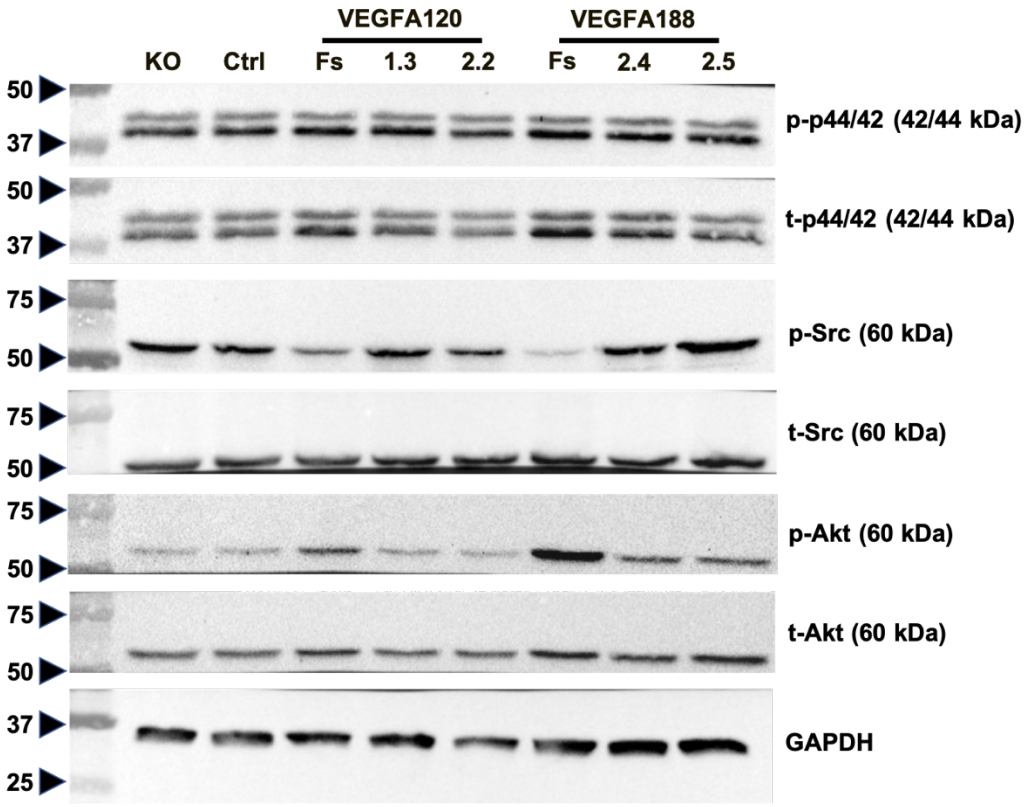

Figure 3.27 Western blot analysis of tyrosine kinases in cells expressing single VEGFA isoforms

Representative Western blotting images of p44/42, Src and Akt in both phosphorylated and total form in cells expressing single VEGFA isoforms and the VEGFA KO controls are shown. The total form was detected on the same membrane after the detection of the phosphorylated form. GAPDH acted as a loading control. Three independent lysates were analyzed by western blotting.

(A)

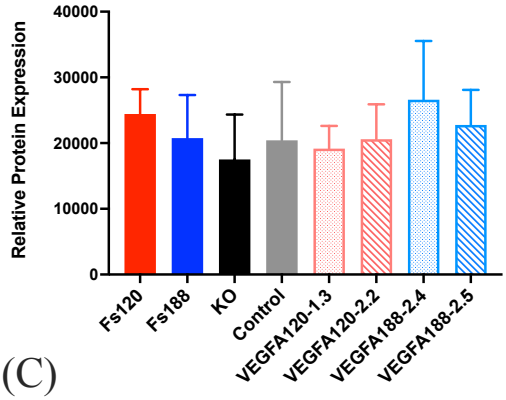
p-p44/42
Relative Protein Expression
40000
30000
20000
10000
0
Fs120
Fs188
KO
Control
VEGFA120-1.3
VEGFA120-2.2
VEGFA188-2.4
VEGFA188-2.5

(B)

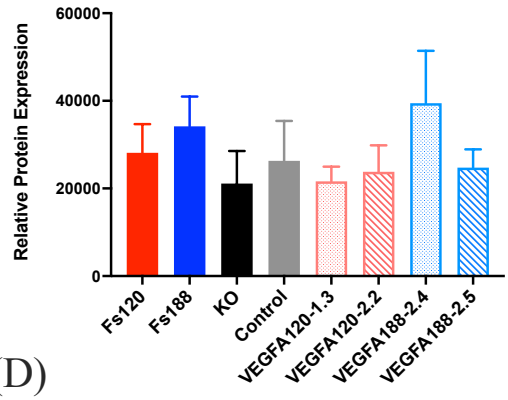
t-p44/42
Relative Protein Expression
60000
40000
20000
0
Fs120
Fs188
KO
Control
VEGFA120-1.3
VEGFA120-2.2
VEGFA188-2.4
VEGFA188-2.5

(C)

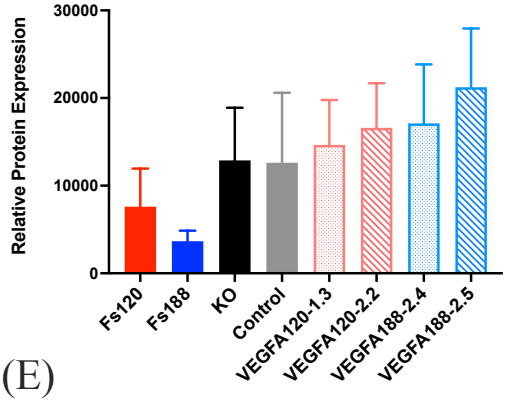
p-Src
Relative Protein Expression
30000
20000
10000
0
Fs120
Fs188
KO
Control
VEGFA120-1.3
VEGFA120-2.2
VEGFA188-2.4
VEGFA188-2.5

(D)

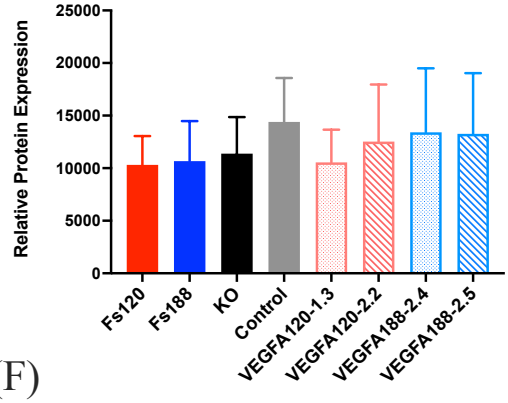
t-Src
Relative Protein Expression
25000
20000
15000
10000
5000
0
Fs120
Fs188
KO
Control
VEGFA120-1.3
VEGFA120-2.2
VEGFA188-2.4
VEGFA188-2.5

(E)

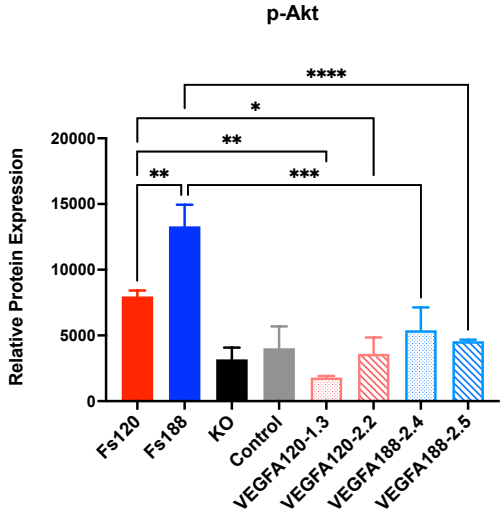
p-Akt
Relative Protein Expression
****
*
**
**
***
20000
15000
10000
5000
0
Fs120
Fs188
KO
Control
VEGFA120-1.3
VEGFA120-2.2
VEGFA188-2.4
VEGFA188-2.5

(F)

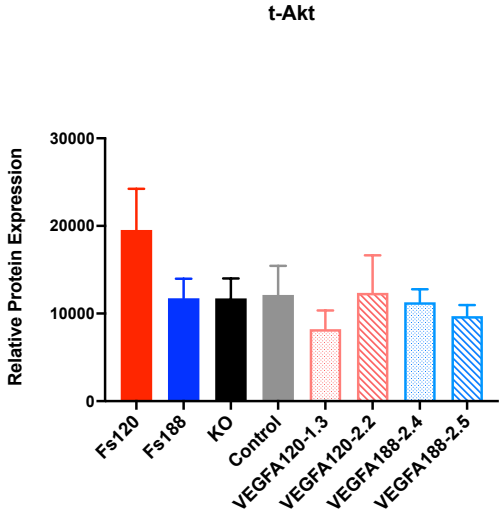
t-Akt
Relative Protein Expression
30000
20000
10000
0
Fs120
Fs188
KO
Control
VEGFA120-1.3
VEGFA120-2.2
VEGFA188-2.4
VEGFA188-2.5

Figure 3.28 Quantification of tyrosine kinases in cells expressing single VEGFA isoforms

Protein expression of (A) p-p44/42, (B) t-p44/42, (C) p-Src, (D) t-Src, (E) p-Akt and (F) t-Akt relative to GAPDH were quantified by Image J. Three independent replicates were expressed as mean ± SEM. A one-way ANOVA test with multiple comparisons by Fisher's LSD post-test was performed to detect statistical significance in t-p44/42, p-Src, t-Src and t-Akt. Non-parametric Kruskal-Wallis test with multiple comparisons by an Uncorrected Dunn's test was performed to detect statistical significance in p-p44/42 and p-Akt. * p-value <0.05, ** p-value <0.01, *** p-value <0.001, **** p-value <0.0001.

The RhoA and Rac GTPase subfamilies play major roles in the control of modes of cell migration through actomyosin contractility and actin polymerization, as mentioned in detail in the Introduction section 1.3.2.1 (Parri & Chiarugi, 2010). The activation of RhoA through ECM binding in cancer cells induced disease progression and metastasis. Furthermore, the migration of carcinomas was inhibited by the knockdown of Rac1 (Xu, Hao, & Gan, 2020). The regulation of RhoA and Rac1 in the migration of cancer cells is critical. VEGFA signalling through VEGFR1/2 modulated EMT and cell membrane protrusion by activating RhoA and Rac1 respectively. The binding of VEGFA to NRP1 also initiated the activation of RhoA inducing EMT (El Baba et al., 2020). Measuring the expression of RhoA and Rac1 induced by different VEGFA isoforms in selected clones may provide insights into which modes of cell migration were more favourable on the plastic surfaces (Fig. 3.29).

The expression of Rac1 and RhoA in both VEGFA120 and VEGFA188 expressing VEGFA KO cells were similar to the transfection control cells and had no difference between clones. Even though there was no statistically significant difference in the expression of Rac1 and RhoA between fs120 and fs188 cells, there was a small increase in the expression of Rac1 and RhoA in fs120 cells compared with fs188 cells (Fig. 3.30). Overall, the balance between Rac1 and RhoA across all cell lines remained relatively even, indicating a similar morphology and migration state.

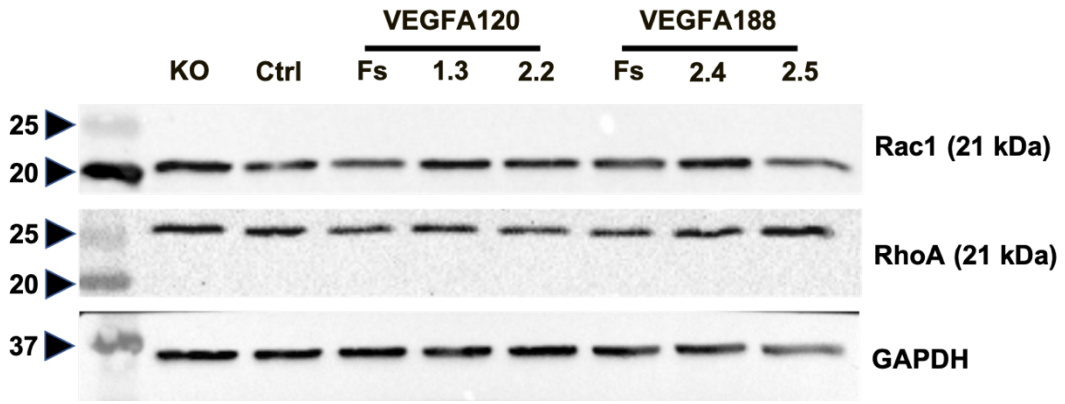

Figure 3.29 Western blot analysis of Rho/Rac expression in cells expressing a single VEGFA isoform

Representative Western blot images of Rac1 and RhoA in cells expressing single VEGFA isoforms and the control VEGFA KO cells are shown. GAPDH acted as a loading control. Three independent lysates were analyzed by Western blotting.

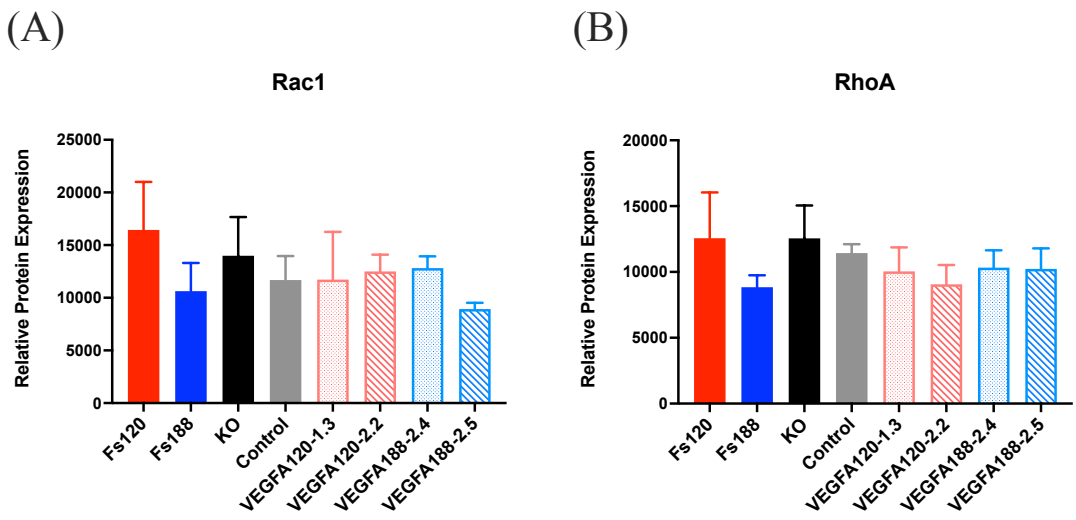

Figure 3.30 Quantification of Rho/Rac expression in cells expressing a single VEGFA isoform

Relative protein expression of (A) Rac1 and (B) RhoA to GAPDH were quantified by Image J. Three independent replicates were expressed as mean ± SEM. A one-way ANOVA test with multiple comparisons by a Fisher's LSD post-test was performed to determine statistical significance.

Cancer stem cells (CSCs), a subpopulation of cells in tumours, have been reported to share similar expression signatures to normal stem cells including self-renewal, regeneration and differentiation properties. The stem cell-like properties in CSCs can initiate EMT and metastasis (Mani et al., 2008; Morel et al., 2008). Sox2 is a transcription factor that plays a critical role in regulating cell pluripotency and differentiation in embryonic stem cells (Feng & Wen, 2015). The expression of Sox2 in fibrosarcomas and various cancer types aids their maintenance of a stem cell-like state (Liu et al., 2014; B. H. Feng et al., 2013; Bareiss et al., 2013; Leis et al., 2012). Induced expression of Sox2 promoted EMT, enhancing cell migration and invasiveness (Kim et al., 2017; Han et al., 2012). To this end, the expression of Sox2 was investigated in single VEGFA isoform-expressing cells detected by Western blotting (Fig. 3.31).

The expression of Sox2 in cells generated from VEGFA KO cells including the transfection control, VEGFA120-1.3/2.2 and VEGFA188-2.4/2.5 clones was at low levels. Interestingly, induced expression of VEGFA120 and VEGFA188 slightly repressed the Sox2 expression compared with the transfection control. In addition, unlike fs188 cells, fs120 cells expressed significantly higher levels of Sox2 suggesting they may have stem cell-like properties (Fig. 3.32).

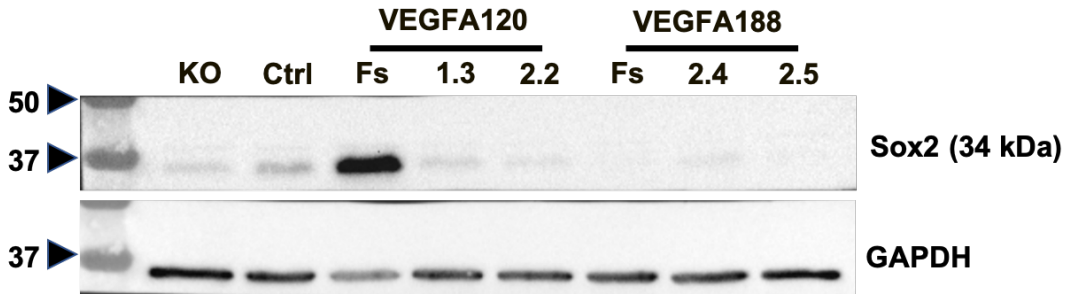

Figure 3.31 Western blotting analysis of Sox2 in cells expressing single VEGFA isoforms

Representative Western blot images of Sox2 expression in cells expressing single VEGFA isoforms and the VEGFA KO control cells are shown. GAPDH acted as a loading control. Three independent lysates were analyzed by western blotting.

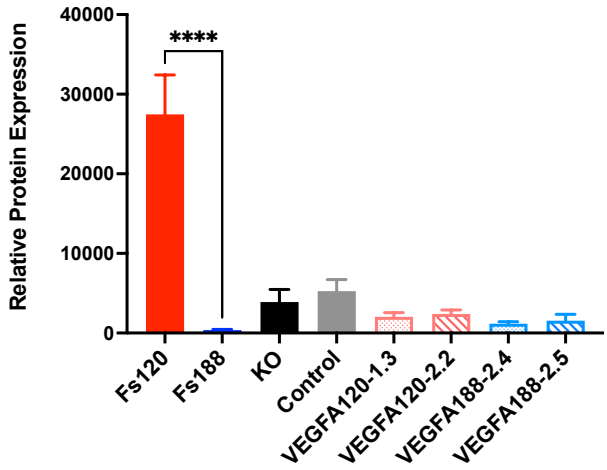

Figure 3.32 Quantification of Sox2 expression in single VEGFA isoform expressing cells

The relative protein expression of Sox2 to GAPDH was quantified by Image J. Three independent replicates were expressed as mean ± SEM. A one-way ANOVA test with multiple comparisons by a Fisher's LSD post-test was performed to determine statistical significance. **** p-value <0.0001.

3.4 Summary

In this thesis chapter, we successfully introduced the expression of a single VEGFA isoform in VEGFA KO cells by transfecting with plasmids containing hypoxia-inducible or a strong constitutively active promoter. Although expression of VEGFA was detected in VEGFA KO cells transfected with the plasmid containing the inducible promotor, [HRE]×5-minCMV, the expression of VEGFA did not reach a similar level to fs cells derived from genetically engineered embryonic fibroblasts we have previously characterised under atmospheric O_2. Low VEGFA expression may be due to the characteristic of the promotor which would only highly activate under hypoxic conditions in VEGFA KO fibrosarcoma cells derived from mature skin fibroblasts. Due to the time limitation and the COVID-19 pandemic lockdown, it was not determined if the expression of VEGFA in transfected cells reached a similar level as fs cells under hypoxia. On the contrary, VEGFA KO cells transfected with plasmids constructed with the strong constitutively active promotor, CMV, showed similar VEGFA expression to fs cells under atmospheric O_2. Despite the hypoxia-induced system potentially being more relevant to the physiological mechanisms by which tumour cells gain plasticity and increased metastatic potential within the TME (Schwab et al., 2012; Tsai & Wu, 2012), acquiring cells expressing equal VEGFA to fs cells was the priority because this project is focused on the role that VEGFA isoforms play in cell migration and metastasis *in vitro*. Therefore, the newly generated fibrosarcoma cells expressing a single VEGFA isoform sharing similar developmental and differential backgrounds stably transfected with plasmids carrying the CMV promotor would be a better system for further experiments.

New mouse fibrosarcoma cells, termed VEGFA120 and VEGFA188, were developed by inducing expression of a single VEGFA isoform in VEGFA KO cells by transfecting with plasmid pCLIIP-CMV-VEGFA. Clones VEGFA120-1.3 and VEGFA120-2.2 were selected as new fibrosarcoma cell lines expressing VEGFA120 because they expressed similar levels of total VEGFA to fs120 cells as measured by ELISA. Because VEGFA188 binds to the matrix and cell membrane, the amount of VEGFA detected by ELISA was low in these cells. To aid the selection of clones expressing a similar level of VEGFA188 to fs188 cells, QRT-PCR was used. Two different clones (VEGFA188-2.4 and VEGFA188-2.5) were selected which had similar mRNA expression for total VEGFA and VEGFA188. Moreover, with the support of suramin salt which enables the

release of ECM and cell-bound VEGFA188, the protein expression of total VEGFA in all selected cell lines was measured by ELISA to confirm similar levels were expressed at the protein level. Interestingly, the increased levels of VEGFA expression in fs188 cells compared with fs120 cells were also observed between the new VEGFA188 clones and VEGFA120 clones.

Overall, fibrosarcoma cells expressing different VEGFA isoforms shared alike phenotypes on the plastic. The morphology of all cell lines remained elongated and spindle-shaped, as well as similar cell areas. Abundant expression of mesenchymal markers, including fibronectin, N-cadherin and vimentin, were also detected in all cells by IF staining or Western blotting. However, classic mesenchymal properties were only displayed in fs188 cells, whereas other cell lines displayed atypical mesenchymal properties. In addition, VEGFA120 and VEGFA188 clones, VEGFA KO cells and their transfection control cells shared similar morphologies indicating that expression of VEGFA in VEGFA KO cells did not alter their morphology. Localization of β-catenin is an indicator of cell-cell interactions and its nuclear translocation can indicate activation of transcription programmes including EMT. Interestingly, clear AJs were only observed in VEGFA120-expressing cells on laminin and in fs120 cells on collagen. Fibrosarcomas expressing VEGFA120 on fibronectin gained classical mesenchymal morphologies. In addition to localizing at AJs, β-catenin was detected on the membrane, in the cytoplasm and in the nucleus. β-catenin bounding to N- or E-cadherin on the membrane or accumulating in the cytoplasm can indicate the inactivation of the Wnt signalling pathway (Kim et al., 2019; Tanaka et al., 2019). However, only a few events of β-catenin translocation to the nucleus were observed mainly in VEGFA120 clones on laminin. Translocation of β-catenin from cytoplasm to nucleus initiating the transcription of mesenchymal makers resulting cells gaining mesenchymal properties. Due to the COVID-19 pandemic lockdown, the images of IF staining were acquired only with the epifluorescence microscope. It was difficult to accurately determine the localization of β-catenin. The images may need to be acquired with confocal microscopy to better identify cell localisation. Furthermore, a positive staining control for N-cadherin may be necessary because the distribution of N-cadherin was in the cytoplasm instead of on the membrane.

Actin filaments play an essential role in providing forces to regulate multiple cellular processes, especially cell morphology and migration. The bundling of actin filaments

establishes stress fibres preferentially on rigid surfaces, typically in experimental culture systems, in response to mechanical stress (Walcott & Sun, 2010). All fibrosarcoma cells displayed stress fibres on fibronectin. However, distinct stress fibres were only detected in fs120 and fs188 cells on uncoated plastic, laminin and collagen. The diffuse actin seen in VEGFA120 and VEGFA188 cells may be caused by their Ras transformation (Pawlak & Helfman, 2001; Sahai, Olson, & Marshall, 2001). Although fs120 and fs188 cells were also Ras-transformed, either the rigidity of the surfaces or the interaction between cells and ECM proteins restored the formation of stress fibres, as well as seen in VEGFA120 and VEGFA188 cells on fibronectin. The adhesion of cells to the ECM regulates their morphology and is the first step in promoting the formation of FAs (Nagano et al., 2012). Lots of VEGFA188-expressing cells on laminin were lost while processing for IF staining, reflecting weak adhesiveness on laminin (data not shown), similar to the observation in cell adhesion assay from Kanthou *et al.* (Kanthou et al., 2014). It would be valuable to measure cell adhesion with new cell lines by using an adhesion assay. Paxillin is a scaffold protein in FAs and acts as an indicator of FA sites. Clusters of phosphorylated paxillin (pY118-paxillin) were observed predominantly at the edge of filopodia anchored to the stress fibres that distributed at the edge and the cell body in fs120 and fs188 across surfaces, as well as VEGFA120 and VEGFA188 cells on fibronectin (Tojkander, Gateva, & Lappalainen, 2012). Because of the low level of stress fibres, abrogation of maturation of FAs may lead to high FA turnover increasing the accumulation of paxillin in the cytoplasm and nucleus in VEGFA120 and VEGFA188 cells (Sathe, Shivashankar, & Sheetz, 2016; Short, 2012). The turnover rate of FAs could be identified by time-lapse imaging of the assembly of paxillin at the leading edge (Hu et al., 2017). In addition, the localization of β1-integrin in the cytoplasm instead of the membrane requires further investigation with positive controls by immunofluorescent staining.

In vitro cell proliferation assays were performed for all cell lines to compare the proliferation rate between cells expressing different VEGFA isoforms and between cells of different origins. The proliferation rate of fs120 cells was faster than fs188 cells, consistent with previous observations (Tozer et al., 2008). There was no significant difference in the numbers of proliferation between the VEGFA KO and transfection control cells after 72 h incubation. VEGFA is a key factor promoting cell proliferation, observed in multiple cancer cell types (Zeng et al., 2016; Lichtenberger et al., 2010).

However, the re-introduction of VEGFA into *Vegfa* KO cells, either VEGFA120-1.3/2.2 or VEGFA188-2.4/2.5, led to the cells proliferating significantly slower than the *Vegfa* KO transfection control cells on plastic. Autocrine VEGFA signalling may cause cytotoxic effects and repress cell proliferation in both VEGFA120 and VEGFA188 cell lines, requiring further studies to measure cytotoxicity and apoptosis.

Fibrosarcoma cells expressing a single VEGFA isoform derived from different origins all expressed similar levels of VEGF receptor 1 (VEGFR1/flt-1), whereas the highest expression of NRP-1, a co-receptor of VEGFR1, was observed in fs188 cells compared with the other cell lines. Kanthou *et al* observed the expression of VEGFR2 in both fs120 and fs188 cells (Kanthou et al., 2014). However, no protein expression of VEGFR2 (flk-1) was detected across all cell lines which may be due to the differences in the recipe of the protein lysis buffer. Even though PCR products amplifying VEGFR2 mRNA using specific primers (Zhang et al., 2014; Kim et al., 2011) were detected across cell lines, the product was not of the expected size. This could be because the product is not VEGFR2 or fibrosarcoma cells express an alternative splice variant of VEGFR2 to H5V cells. Further investigation into the expression of VEGFR2 in fibrosarcomas by executing RT-PCR with more VEGFR2-specific primer pairs is required along with sequencing of PCR products to identify if VEGFR2 is not expressed or an alternative splice variant is being produced.

Phosphorylation/activation of signalling pathways downstream of VEGFRs, including Src, Akt and p-44/42, in fibrosarcoma cells expressing different single VEGFA isoforms could be important in the regulation of cell migration (Zhang et al., 2014). There were no significant differences in the expression of phosphorylated p-44/42 across all cell lines. High levels of phosphorylated Akt linked to increased mesenchymal properties and induction of lamellipodia in nasopharyngeal carcinoma and endothelial cells (He et al., 2015; Chanvorachote, Chunhacha, & Pongrakhananon, 2014; Mendoza et al., 2011) were observed in fs188 cells. Interestingly, fibrosarcoma cells derived from mature fibroblasts had higher levels of phosphorylated Src. In addition, the expression of Rac1 and RhoA were similar across cells expressing different VEGFA isoforms. The steady balance between Rac1 and RhoA may be due to the absence of a chemotactic gradient triggering cell migration. Instead of measuring the protein expression of Rac1 and RhoA in cell lysates, localization of Rac1 and RhoA in cells by IF staining and measuring their activity in kinase assay may provide better information on which modes

of cell migration are dominant. The expression of stem cell-like properties indicating cell plasticity is critical in metastasis which requires adapting to different TME. Low expression of Sox was detected in fibrosarcoma cells derived from mature fibroblasts. However, induced expression of VEGFA120 in VEGFA KO cells failed to increase the expression of Sox2. Significant upregulation of Sox2 in fs120 cells compared with fs188 cells was observed, indicating that fs120 and fs188 cells had experienced different levels of development in the embryo before immortalization.

In summary, newly generated VEGFA120 and VEGFA188 cell lines transfected with plasmid pCLIIP-CMV-VEGFA successfully expressed a single VEGFA isoform to similar levels as fs120 and fs188 cells under atmospheric O_2. Expression of a single VEGFA isoform in VEGFA KO cells did not dramatically alter cell morphology, adhesion properties and endogenous protein expression but repressed cell proliferation compared with transfection control. Despite differences in the cell characteristics between fibrosarcoma cells expressing a single VEGFA isoform derived from different origins, the cell properties between newly generated clones expressing the same VEGFA isoform remained consistent. These differences probably reflect the varied developmental and differential backgrounds that influence the characteristics of cells. Therefore, VEGFA120 and VEGFA188 cell lines may be better cell lines to identify the roles that VEGFA isoforms play in cell migration and the plasticity in modes of cell migration.

Chapter 4

4. Recapitulation of the fibrillar collagen structure in the tumour microenvironment

4.1 Introduction

In the process of metastasis, the ECM plays critical roles in directly or indirectly modulating the behaviour of cancer cells, particularly during the stages of invasion, extravasation, and intravasation. Many studies have shown that ECM topography and biophysical properties directly regulate cellular functions such as proliferation, migration and differentiation (Li et al., 2012; Wang et al., 2011). Unique ECM structures assembled with architectures, pore sizes, stiffness and adhesiveness limit the migration capacity of cancer cells in the TME (Hwang et al., 2017; Nasrollahi et al., 2017; Bauer, Jackson, & Jiang, 2009). Many studies on the migration capacity of cancer cells have been made using wound healing assays and Boyden chamber (transwell) assays. However, these *in vitro* systems did not fully recapitulate the ECM features in TME *in vivo* and failed to reflect actual cancer cell behaviours (Wolf et al., 2013). Therefore, it is crucial to create a novel *in vitro* platform for studying cancer cell migration, that mimics the ECM properties found in the TME while being reproducible.

Collagen I is the most dominant ECM protein in TME. The upregulation of fibrous collagen correlated to tumour progression and increased the stiffness of stroma that facilitated cell invasion in breast and ovarian cancer (Sleeboom et al., 2018; Weigelt, Ghajar, & Bissell, 2014). Moreover, collagen fibrils can serve as a highway for cancer cells metastasizing to distant sites (Beunk et al., 2022; Y. Shen et al., 2012; Conklin et al., 2011; Provenzano et al., 2006). It has been reported that fibrosarcoma cells expressing the longer VEGFA188 isoform produced more collagen but had less metastatic potential (Wolf et al., 2009). Yet, the topography of collagen in TME was undefined. To address this, this chapter will measure the diameter and structure of collagen fibres in tumours of fibrosarcoma cells expressing a single VEGFA isoform within viable and necrotic areas to be used as a reference to develop an engineered microenvironment.

Electrospinning is a technique that fabricates polymer solutions into fibres in an electric field (English et al., 2017). Electrospinning fibres can be customized into varied diameters, densities, pore sizes and alignments by modifying different parameters, like the viscosity of polymer solutions, the voltage applied in the electric field and the

rotational speed of collectors. Polycaprolactone (PCL), a biocompatible and biodegradable polymer, is widely used in generating electrospinning fibre scaffolds for the study of cell proliferation, differentiation and migration (Xue et al., 2019). Moreover, the characteristics of low melting temperature and high thermal stability decrease difficulties in modifying the architecture of PCL fibre scaffolds.

In this chapter, I will characterize the topography of fibril collagen in fibrosarcoma tumours expressing different VEGFA isoforms and generate PCL fibre scaffolds mimicking collagen fibres observed in tumours as closely as possible. These fibre scaffolds will further be applied in single-cell migration assays.

4.2 Characterisation of the fibril collagen in mouse fibrosarcomas expressing a single VEGFA isoform

A nonlinear optical process is an intense laser light passing through a noncentrosymmetric structure that generates second harmonic generation (SHG) signals. The non-centrosymmetric molecular structure of type I and II fibril collagen fulfils the requirement that generates signals detected by SHG microscopy. Due to the wavelength specificity, samples for SHG microscopy are stain-free, which significantly decreases interference from the background signal and autofluorescence, enhancing image quality when compared with images taken by confocal microscopy. Moreover, mature and immature collagen fibres can be also detected in SHG microscopy in comparison to other imaging techniques that require antibody labelling. In addition, the samples are polarized with a laser, that is tuned to double the excitation wavelength used with other microscopy techniques, being able to penetrate through thicker samples. This advantage provides more information on the 3D structure of fibril collagen, especially in the study of the alteration of collagen topographies. The application of SHG microscopy in the study of the architecture of collagen fibres is simpler and time-saving (Garcia et al., 2018; Narice et al., 2016).

4.2.1 Haematoxylin & Eosin (H&E) staining of tumour sections

H&E staining is the most commonly used protocol in disease diagnosis that identifies the structure, shape and organization of cells in tissues via bright field microscopy. The nucleus stained by haematoxylin is displayed in purple. The cytoplasm and ECM stained by eosin are shown in pink. Under H&E staining, the loss of the nucleus caused by hypoxia-induced cell death transforms into cytoplasmic necrosis within tumours. (Ottosson, Jakobsson, & Johansson, 2017; Taskin et al., 2016; Borjigin et al., 2013). The H&E staining images that enable us to distinguish viability and necrosis in tumours were used as a reference to decide positions for SHG microscopy. In addition, there were significantly increased necrotic areas in fs188 tumours compared with fs120 tumours indicating more rapid cell death in fibrosarcoma cells expressing VEGFA188. Interestingly, most cancer cells in the necrotic area in fs188 tumours lost their nuclei and became cell ghosts (Fig. 4.1)

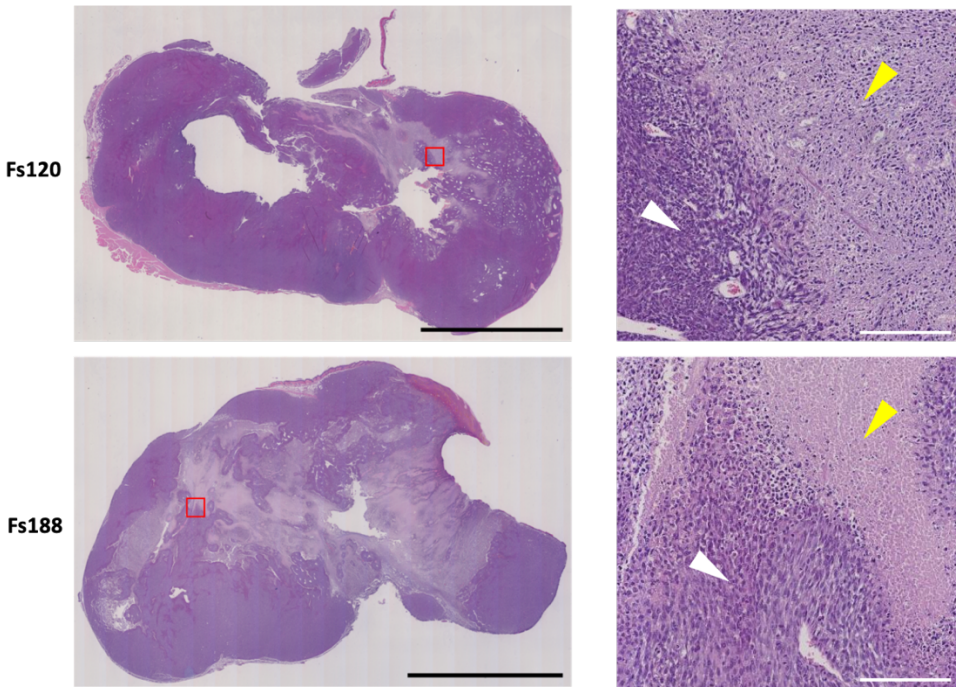

Figure 4.1 Representative H&E staining images of tumour sections from fs120 and fs188 cells

Tumour sections were scanned after H&E staining. The zoom-in of the position marked in red is displayed on the right. The yellow arrow points to the necrotic area, whereas the white arrow points to the viable area. Black scale bar = 1 cm. White scale bar = 200 μm.

4.2.2 Second harmonic generation (SHG) microscopy of tumour sections

Using H&E staining as references to identify necrotic and viable areas, the images of collagen fibres in mouse fibrosarcoma expressing different VEGFA isoforms were taken from adjacent stain-free sections by SHG microscopy. The specific SHG signals represented type I fibril collagen in tumour sections were detected with excitation and emersion at 940 nm and 470 nm.

Fibrillar collagen with different topographies was imaged in tumours expressing VEGFA120 and VEGFA188 between viable and necrotic areas (Fig. 4.2). The collagen fibres were increased in viable areas in fs120 tumours compared with fs188 tumours. The fibrillar collagen was reduced in necrotic areas but gained a strong background, especially in fs188 tumours. The average diameter of fibrillar collagen in viable areas was significantly increased in fs188 tumours but formed less branched and shorter fibres compared with fs120 tumours (Fig 4.4 A, B and D). In addition, a remarkable increase in the average diameter of fibrillar collagen in the necrotic areas was observed only in the fs120 tumours. Although fibrillar collagen showed different diameters between fs120 and fs188 tumours and between viable and necrotic areas, the average diameter of fibril collagen was in a small range between 2 to 3 μm. According to the analysis performed by the Image J plugin, Orientation J, fibrillar collagen was well-orientated in that long fibres aligned in the same direction with perpendicular branches in viable areas in fs120 tumours. On the contrary, fibrillar collagen was less orientated in fs188 tumours, as well as in areas of necrosis in fs120 tumours, which orientated in multiple directions but with two primary directions (Fig. 4.3). Moreover, collagen fibres in fs120 tumours seemed to have better alignment than fs188 tumours though there was no significant difference in the fibre alignment between fs120 and fs188 tumours and between viable and necrotic areas (Fig. 4.4 C). These observations indicated that fibrillar collagen in fibrosarcomas was structured in two dominant topographies: long-aligned and short-randomized architectures.

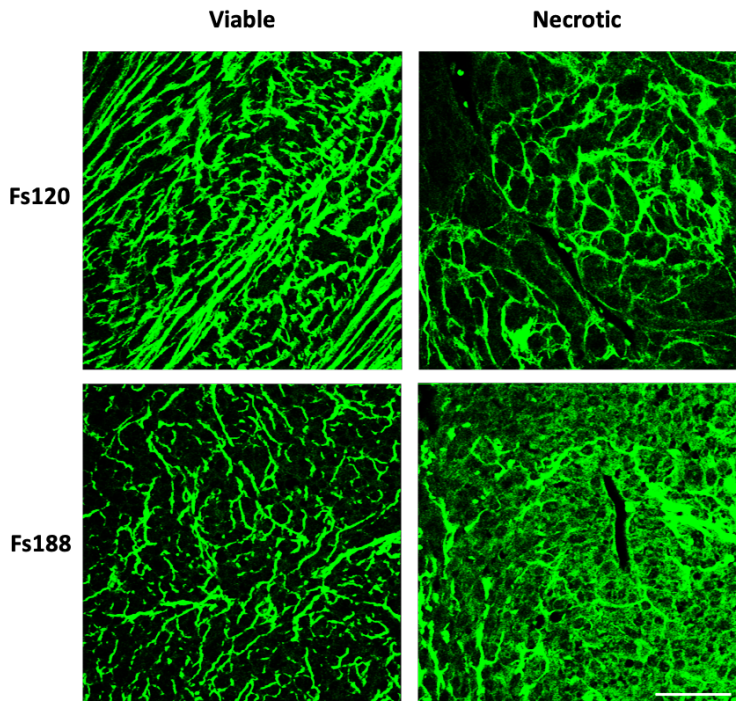

Figure 4.2 Representative SHG microscopy images of tumour sections from fs120 and fs188 cells

Dewaxed tumour sections were mounted in PBS and imaged by SHG microscopy with Chameleon sapphire laser exciting at 940 nm and emission at 470 nm. Scale bar = 50 μm.

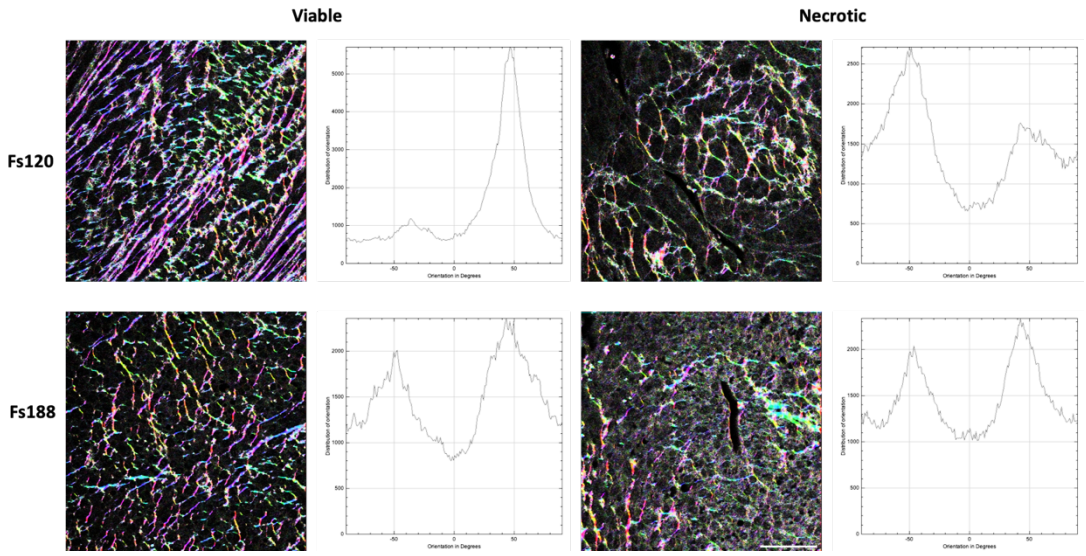

Figure 4.3 Orientation of collagen fibres in fs120 and fs188 tumours

The orientation of collagen fibres in each position was analysed by the Image J plugin, Orientation J. Fibres with similar orientations were marked in a similar colour in the colour survey (on the left). The distribution of angles between fibres and reference horizon was shown on the right. Scale bar = 50 μm.

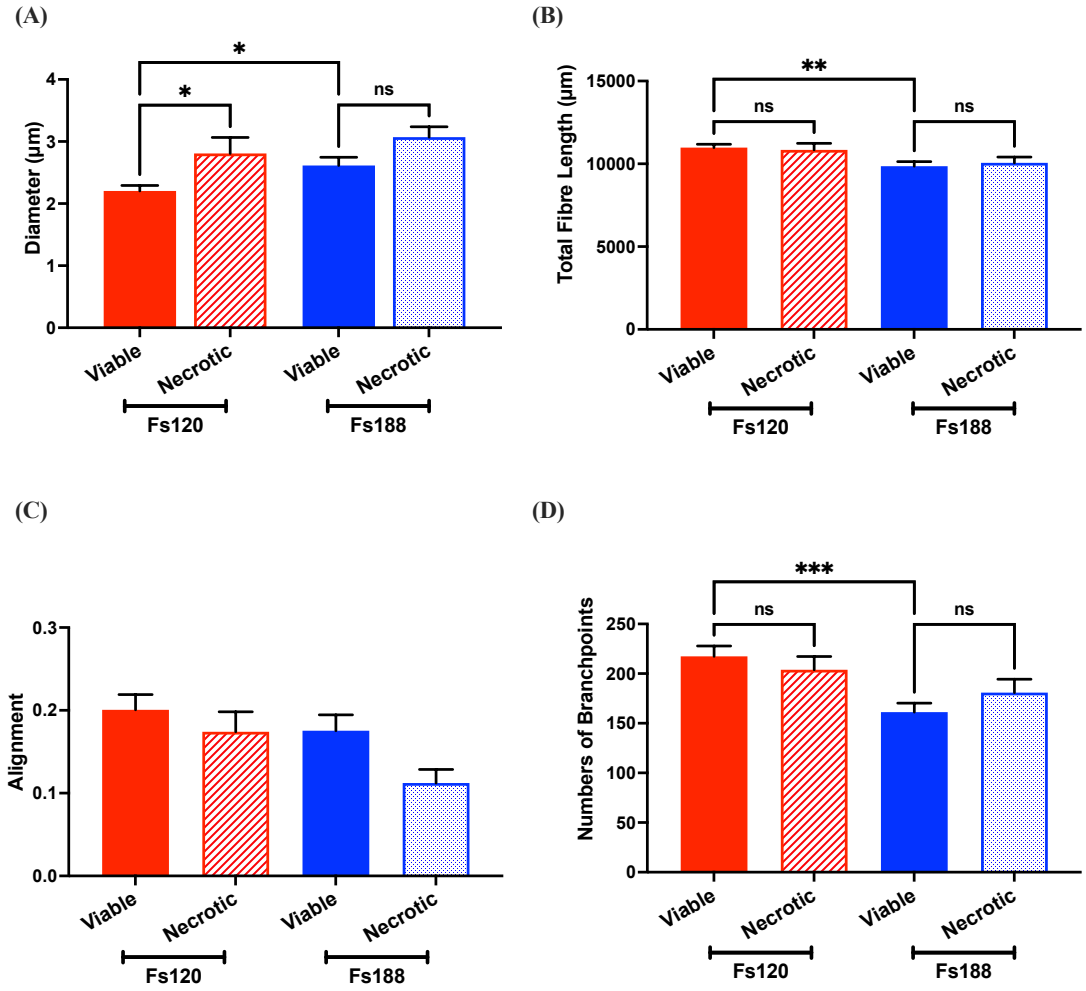

Figure 4.4 Characteristics of collagen fibres in fs120 and fs188 tumours

Quantification of (A) diameter, (B) total fibre length, (C) alignment and (D) numbers of branchpoints in images taken by SHG microscopy by the Image J plugin, Twombli v1. The average of measurements in all positions was expressed as mean ± SEM. A non-parametric Kruskal-Wallis test with multiple comparisons followed by an Uncorrected Dunn's test was performed to determine statistical differences. * p-value <0.05, ** p-value <0.01, *** p-value <0.001 (Viable: n=25, Necrotic: n=15).

4.3 Production and characterisation of electrospun fibre scaffolds

According to the characteristics of fibril collagen in fibrosarcoma tumours expressing different VEGFA isoforms analysed from SHG images, we aimed to generate fibre scaffolds with an average fibre diameter between 2 to 3 μm in two different orientations, aligned and randomized, by electrospinning (Fig 4.5 A). There are multiple factors that can play a role in determining the diameter of fibres. Based on experiences from Dr Claeyssens's group, different fibre scaffolds were generated by controlling the different ejection pump speeds of the PCL polymer solution. The average fibre diameter in electrospinning fibre scaffolds made under the pump speed at 1 mL/h was about 2 μm, whereas at 1.5 mL/h was about 4 μm (Fig. 4.5 B). The fibre scaffold generated with pump speed at 1 mL/h met the requirement of average fibre diameter of fibre collagen observed in TME.

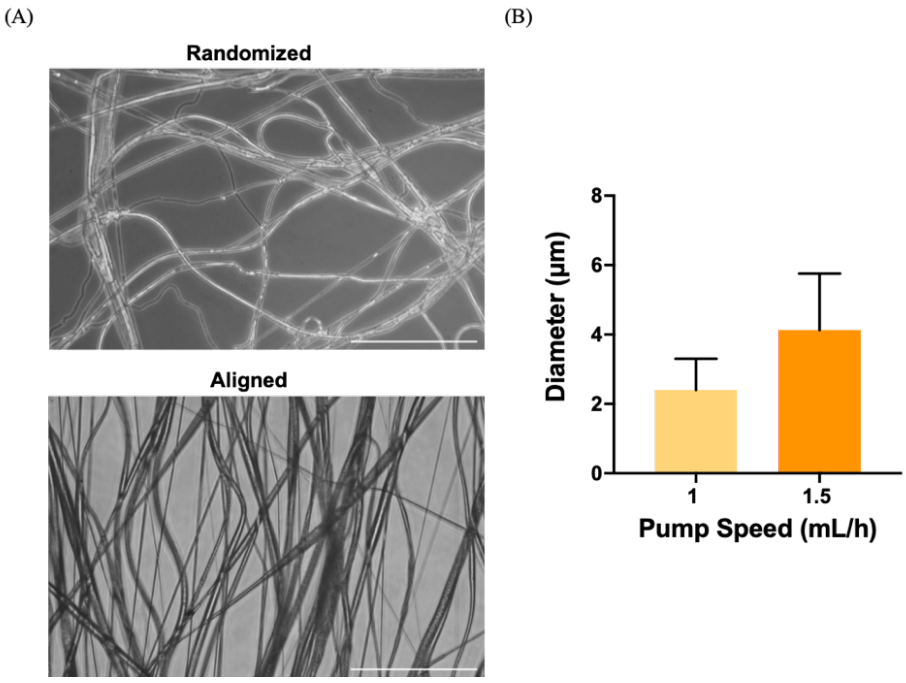

Figure 4.5 PCL Electrospinning fibre scaffold

(A) Phase-contrast images of PCL fibre scaffold with different orientations under 40X magnification. Scale bar = 100 μm. (B) The average fibre diameter was calculated from the measurements of 300 positions from 3 individual images and was expressed as mean ± SEM.

Although PCL is a biodegradable and nontoxic polymer, cells are unable to attach efficiently due to its hydrophobic properties. There are multiple methods for increasing the hydrophobicity of fibre scaffolds, such as air plasma and protein substrate coating. Plasma coating was widely used in improving cell attachment and binding affinities to substrates (Manakhov et al., 2017). However, during the process, fibre scaffolds were exposed to high pressure and voltage that heated the scaffolds leading to structural damage (data not shown). The alternative method was directly coating fibre scaffolds with fibronectin. The coating of fibronectin on PCL fibre scaffolds can not only enhance cell attachment but also there was fibronectin bounded on the surfaces of fibril collagen(Paten et al., 2019).

The fibre scaffolds were coated under three different temperatures overnight, 4℃, room temperature and 37 ℃ (data not shown). The scaffolds coated at room temperature showed the best outcome observed by immunofluorescent staining of fibronectin (Fig 4.6 B). The efficiency of cell attachment on fibronectin-coated fibre scaffolds was remarkably improved. Cells attached to fibre scaffolds were visualized under phase-contract images (Fig. 4.6 C). Moreover, cells that adhere to fibres were detected with the immunofluorescent staining (Fig. 4.6 D).

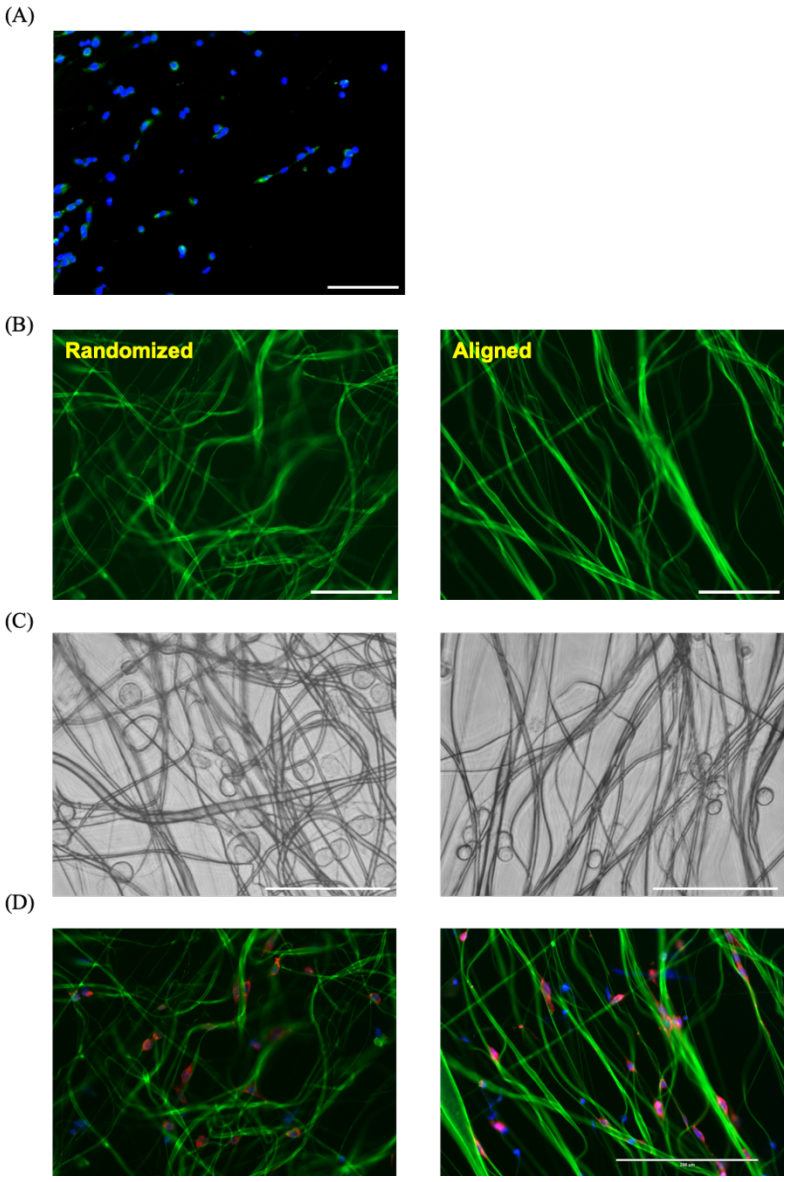

Figure 4.6 Fibronectin-coated fibre scaffold with fs120 cells

(A) Immunofluorescent staining of fibronectin (green) and DAPI of fs120 cells on uncoated fibre scaffolds after 24h as representative (B) Fibre scaffolds coated with fibronectin at room temperature were immunofluorescent stained with fibronectin (green). (C) Phase-contrast images of fs120 cells seeded on fibronectin-coated fibre scaffolds after 24h as representative (40X). (D) Immunofluorescent staining of phalloidin (red), fibronectin (green) and DAPI of fs120 cells on fibronectin-coated fibre scaffolds after 24h as representative. White scale bar = 100 μm.

4.4 Summary

Fibrillar collagen in the TME is composed of a complex 3D structure that influences the migration capacity of cells and the selection of cell migration modes (Yee et al., 2020; Eustace et al., 2013). However, most studies in tumour cell migration were performed on either 2D surfaces or in Boyden chambers. The lack of recapitulation of the 3D topography of the TME may lead to biased research outcomes and ultimately failure in clinical trials (Xie et al., 2017; Doyle et al., 2015). In this chapter, we analysed the architecture of collagen fibres in mouse tumours that had high (fs120) and low (fs188) levels of metastasis and demonstrated a newly engineered 3D environment that mimicked its architecture with the application of electrospinning techniques. According to SHG images, the fibril collagen in TME between fibrosarcomas expressing VEGFA120 and VEGFA188 were characterized by their diameter, length, branchpoint and alignment. Overall, the diameter of collagen fibres in fibrosarcomas was about 2 to 3 μm, though its diameter in fs188 tumours was statistically increased compared with in fs120 tumours. In addition, the structure of collagen fibres in fs120 tumours was longer, and better aligned with more branched points; on the contrary, in fs188 tumours, it was shorter with less branched and less organized. Engineered PCL fibre scaffolds successfully recapitulated the diameter and alignment of fibril collagen in tumours, which can regulate the mode of cell migration and directionality respectively (Morgan et al., 2018). This new 3D *in vitro* platform may be a better option in the study of the metastatic potential of cancer cells and their responses to the therapy.

The formation of necrosis in solid tumours results from rapid tumour growth leading to hypoxia and nutrient deprivation (Zhang et al., 2022; Doyle et al., 2009). Fibrosarcomas expressing VEGFA188 showed increased necrotic areas compared with tumours expressing VEGFA120 identified by H&E staining. Compared to fs188 cells, fs120 cells had better proliferation *in vitro* (Bredholt et al., 2015) and induced tumour growth in mice (Tozer et al., 2008) which may have a higher risk of experiencing hypoxia (Tozer et al., 2008). Moreover, enlarged and leaky vessels damaged vascular functions in fibrosarcomas expressing VEGFA120 and may be deficient in the transportation of oxygen (English et al., 2017). However, increased necrosis in VEGFA188-expressing tumours indicated fs188 cells may experience stronger hypoxic effects that conflicted with observations of induced proliferation and impaired vascular functions in VEGFA120-expressing tumours. On the other hand, cell apoptosis was primarily found

in fs188 cells *in vitro* and within viable areas in tumours (Tozer et al., 2008), which supports the increased necrosis in fs188 tumours. Apoptosis of cells may be a major driver of the formation of necrosis in tumours due to the size of the tumour is not big enough to induce hypoxia. To determine if fibrosarcoma cells were experiencing hypoxia in tumours, measuring the expression of HIF1 and CA9 in cancer cells extracted from tumours may provide better information (Forker et al., 2018).

ECM properties are key factors that regulate the metastatic potential of cancer cells. Cells successfully metastasising to distant sites can remodel ECM favouring cell migration and invasion (Kanthou et al., 2014). The distinct differences in the architecture of collagen fibres between fs120 and fs188 tumours were observed. Collagen-modifying enzymes, LOX and LOX-like proteins play a critical role in the alignment and linkage of collagen fibres (Winkler et al., 2020). Hypoxia-induced expression of these proteins facilitating modification of ECM promoted metastasis (Canty & Kadler, 2005). Better aligned and branched fibril collagen, accounting for the increased metastases seen in mice with fs120 tumours (Erler et al., 2006b), may be linked to the increased expression of modifying enzymes. Due to the time limitation, the expression of enzymes participating in collagen modification between fs120 and fs188 cells under hypoxia was not measured. Except for ECM modification, ECM disposition also regulates the cellular functions of cells. Fibronectin expressed by fibrosarcoma cells was detected on fibre scaffolds indicating the ability of cells to remodel the surface properties which favours the attachment and preparation for migration.

In summary, there was no remarkable difference in the average diameter of collagen fibres in fibrosarcomas expressing different VEGFA isoforms. Yet, the alignment of fibril collagen in fs120 tumours was better aligned in viable areas, whereas in fs188 tumours fibres were predominantly randomized. The electrospinning of PCL fibre scaffolds successfully recapitulated the diameter (between 2 to 3 μm) and the alignment (aligned and randomized) of collagen fibres observed in tumours expressing either VEGFA120 or VEGFA188. The attachment of cells on either aligned or randomized fibre scaffolds after fibronectin coating was significantly improved. Hence, the newly developed electrospinning PCL fibre scaffold coated with fibronectin reflecting characteristics of fibril collagen in TME may be used as a potential *in vitro* platform in

the study of cell migration in fibrosarcoma cells expressing different VEGFA isoforms and its response to anti-VEGFA therapy.

Chapter 5

5. Migration capacity of fibrosarcoma cells expressing single VEGFA isoforms on engineered microenvironments

5.1 Introduction

"Activating invasion and metastasis" is one of the hallmarks of cancer (Hanahan, 2022). Molecular mechanisms that regulate metastatic potential and invasiveness of cancer cells can be distinguished into four categories; EMT program, ECM remodelling, migration capacity and cell plasticity. Motility controlled by the EMT program, especially in carcinomas, is an essential process that evokes invasion and metastasis. Transcription factors such as Snail, Slug and Twist orchestrate EMT that elicits dissemination of cancer cells from the primary tumours and the alteration of morphology from epithelial to mesenchymal favouring penetration through the basal membrane and invading the stroma (Hanahan & Weinberg, 2011). The chemical and physical properties of the ECM act as a rate-limiting step of migration capacity and plasticity of cancer cells. In response to the restrictions from the ECM, cancer cells may activate ECM remodelling by promoting the expression of proteolytic enzymes from themselves or from infiltrated tumour-associated cells (Wolf et al., 2003) to maintain the efficiency of migration. On the other hand, cancer cells that are incapable of remodelling the ECM are required to change their migration mode to adapt to the ECM (Carragher et al., 2006). Cells also get trapped in the ECM because of the nucleus, at which point they require to express proteolytic enzymes to widen holes in the ECM or deform their nucleus to allow progress (Harada et al., 2014). The capability in these categories decides the metastatic potential of cancer cells.

The studies conducted using the *in vitro* platform established in this chapter only focus on the characterization of cell migration capacity on different modelled ECM topographies and its response to the anti-VEGFA antibody. Apart from wound healing and transwell assays, this platform provided different engineered microenvironments with chemotactic gradients that measure the single-cell migration capacity independently of cell proliferation.

Live cell imaging is a technique that can track the position of a single cell at each time point. According to the positions of cells, accumulated distance, Euclidean distance, migration speed and directionality can be calculated. The accumulated distance is the total distance travelled by the cells within the imaging period. Euclidean distance is the

distance between the points of origin and the endpoint. Different to the physical velocity, the migration speed of cells is calculated by the accumulated distance divided by the total time travelled. The directionality is the ratio between Euclidean and accumulated distance which can be used as a reference to identify the straightness of cell migration. The response to the chemotactic gradient is evaluated by the centre of mass, the direction of cell tracks and the distribution of cell endpoints in the trajectory plots and rose diagrams. In addition, the effects of chemotaxis on cell migration can be identified by the directionality. More straightness in cell migration correlates to a stronger response to the chemotactic gradient.

In this chapter, I will characterize the migration capacity and the plasticity in modes of migration in fibrosarcoma cells expressing different single VEGFA isoforms in the *in vitro* platform. The differences in migration capacity of fibrosarcoma cells expressing different VEGFA isoforms and between different origins is compared on aligned versus non-aligned fibres to replicate the differences in collagen fibres seen in tumours derived from fibrosarcomas expressing different VEGFA isoforms. In addition, the response to the anti-VEGFA therapy in the cell mobility in fibrosarcoma cells expressing different VEGFA isoforms is analysed.

5.2 Characterisation of the migration capacity of a single VEGFA isoform expressing fibrosarcomas on 2D ECM-coated surfaces

The aim of characterising cell migration capacity on 2D surfaces coated with different ECM proteins is to identify if cell mobility depends on the interaction between cells and ECM proteins. The expression of ECM proteins showed a distinct pattern between fibrosarcomas expressing different VEGFA isoforms (Yang & Weinberg, 2008). Moreover, fibrosarcoma cells expressing VEGFA120 displayed the altered morphology of mesenchymal- to epithelial-like in response to ECM proteins from fibronectin to collagen (English et al., 2017). Although the cell mobility of fibrosarcoma cells expressing different VEGFA isoforms had been characterized by wound healing and transwell migration assays (Kanthou et al., 2014), the effects of ECM proteins on the single-cell migration capacity needed further characterisation.

5.2.1 Migration on fibronectin-coated 2D surfaces with a chemotactic gradient

In the first instance migration on fibronectin was studied. A chemotactic gradient was set up to make the identification of differences in migration easier. There was no significant difference in the migration speed and accumulated distance between VEGFA isoform expressing and transfection control *VEGFA* KO fibrosarcoma cells derived from mature skin fibroblasts, whereas speed was significantly increased in comparison to fibrosarcoma cells derived from embryonic fibroblasts expressing single VEGFA isoforms. Moreover, the mobility of fibrosarcoma cells expressing VEGFA120 was comparable to cells expressing VEGFA188 on fibronectin-coated surfaces indicating cell mobility on fibronectin was VEGFA isoform independent. Interestingly, only VEGFA120-expressing fibrosarcoma cells responded to the anti-VEGFA antibody, B20-4.1.1, of which migration speed and accumulated distance were statistically decreased, consistent with previous observations in my MSc thesis (Fig. 5.1 A and B).

The centre of mass located on the right in the trajectory plots and the right-skewed distribution of cells displayed in the rose diagrams showed a small response to the chemotactic gradient was only observed in fibrosarcoma cells expressing VEGFA120 derived from mature skin fibroblasts. The response was impaired with the anti-VEGFA antibody (Fig. 5.2 and 5.3). Furthermore, there was no significant difference across cell lines in terms of directionality indicating they migrated with similar straightness (Fig. 5.1 D).

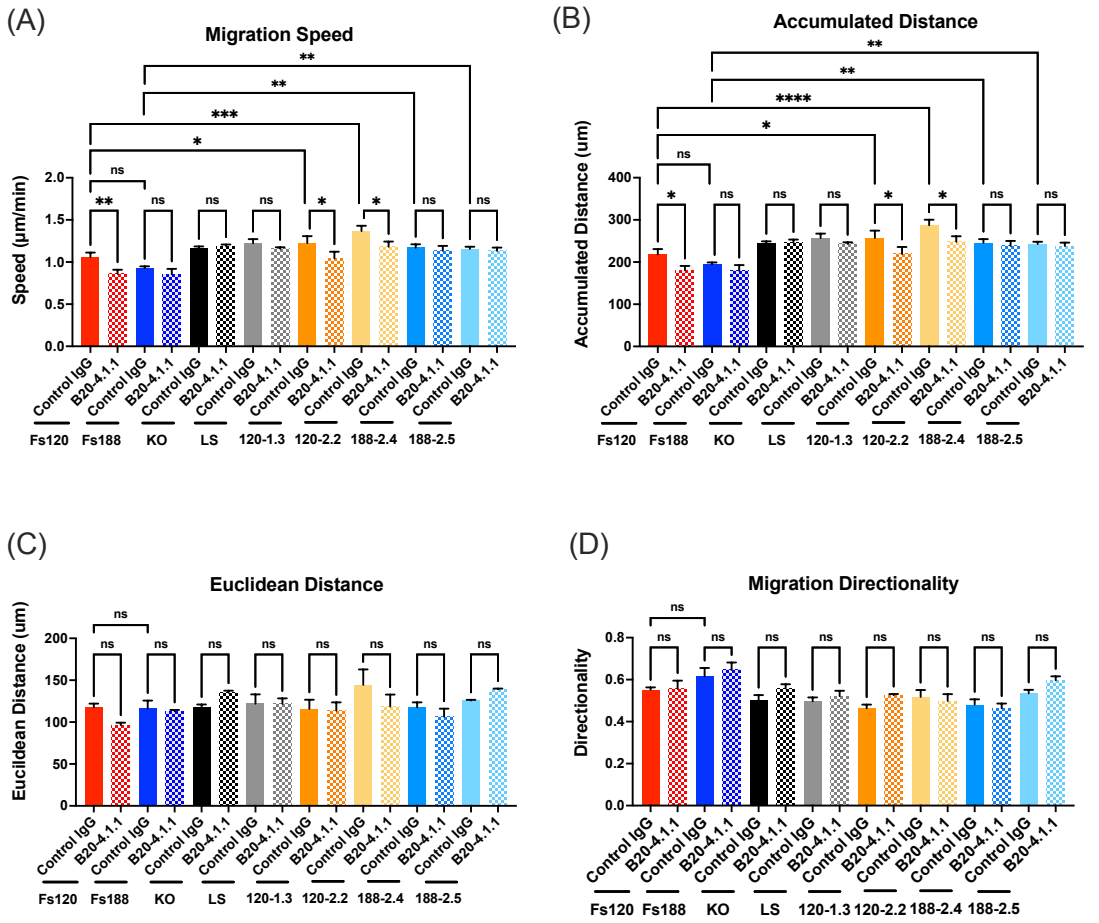

Figure 5.1 Migration capacity of fibrosarcoma cells expressing single VEGFA isoforms on 2D fibronectin-coated surfaces with chemotactic gradient.

Quantification of (A) migration speed, (B) accumulated distance, (C) Euclidean distance and (D) directionality in fibrosarcoma cells expressing different single VRGFA isoforms via single-cell live images by CD7 microscopy. 30 cells from different cell lines were analysed in each independent experiment. Three independent replicates were expressed as mean ± SEM. A one-way ANOVA test with multiple comparisons by Fisher's LSD test was performed to detect statistical significance in migration speed, accumulated distance and directionality. A non-parametric Kruskal-Wallis test with multiple comparisons followed by an Uncorrected Dunn's test was performed to detect statistical significance in Euclidean distance. * p-value <0.05, ** p-value <0.01, *** p-value <0.001, ns: no significant difference.

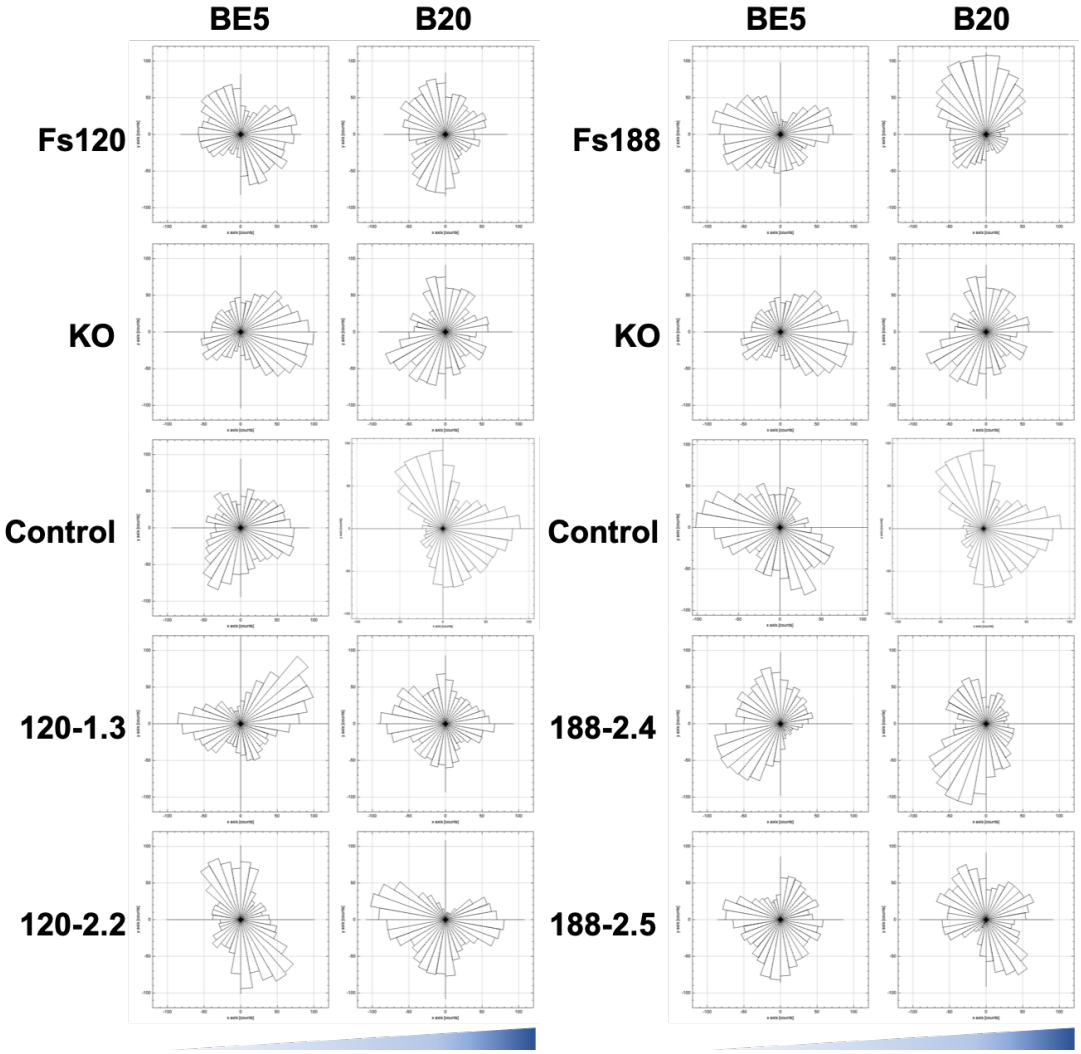

Figure 5.2 Representative Rose diagrams of cell migration direction in fibrosarcoma cells expressing single VEGFA isoforms on fibronectin-coated 2D surfaces.

Cell tracks from 30 cells of each cell line were analysed and plotted as a rose diagram according to the distribution of counted cells in each sector by the Chemotaxis Tool developed by Ibidi.

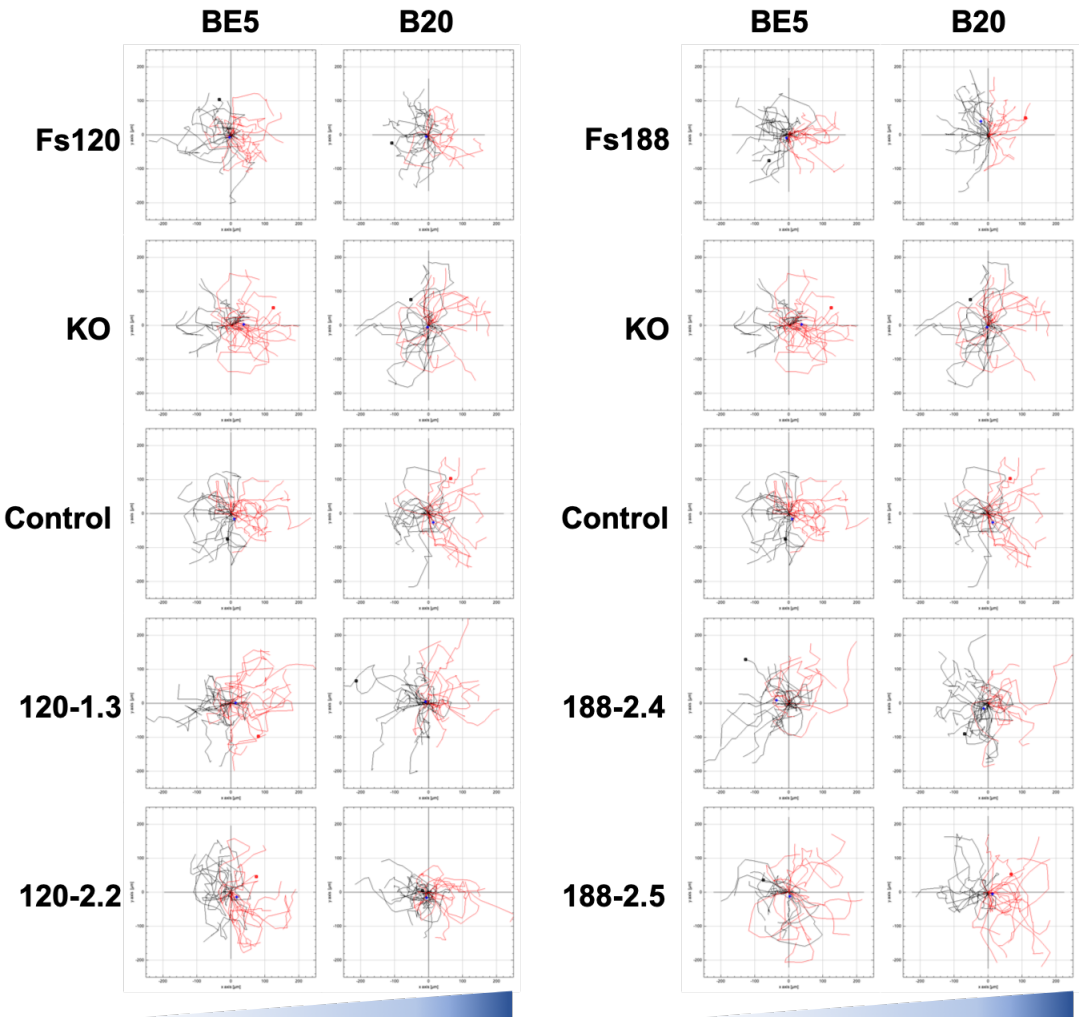

Figure 5.3 Representative trajectory plots of cell migration in fibrosarcoma cells expressing single VEGFA isoforms on fibronectin-coated 2D surfaces.

The trajectory of cell migration from 30 cells in each cell line was drawn from positions at each time point marked by the pointing cell tracking plugin in ImageJ. All tracks were centred on the origin. The tracks with cell endpoint on the right which migrated toward the chemotactic gradient were marked in red, whereas against the chemotactic gradient were marked in black. The centre of mass was marked in a blue cross.

5.2.2 Migration on collagen-coated 2D surfaces with chemotactic gradient

I next studied migration on collagen-coated surfaces. Similar to fibronectin-coated 2D surfaces, expression of VEGFA isoforms in *VEGFA* KO fibrosarcoma cells did not alter their travelled accumulated distance or migration speed on collagen-coated surfaces. Yet, a downregulation of migration speed and accumulated distance in fibrosarcoma cells derived from mature skin fibroblasts was observed in comparison to cells derived from embryonic fibroblasts. In addition, the expression of different VEGFA isoforms in fibrosarcoma cells generated from different origins did not affect cell mobility and the response to the anti-VEGFA antibody on collagen-coated surfaces (Fig. 5.4 A and B).

Other than the VEGFA120-1.3 and -2.2 clones, there were no distinct chemotactic effects on the direction of cell migration, indicated by the centre of mass located with respect to the origin in the trajectory plots and the cell endpoints were randomly distributed in the rose diagram. In addition, loss of the influence to the chemotaxis in VEGFA120-1.3 and -2.2 clones was detected with the application of an anti-VEGFA antibody (Fig, 5.5 and 5.6). However, all cell lines showed similar directionality that was independent of treatment with the anti-VEGFA antibody (Fig. 5.4 D).

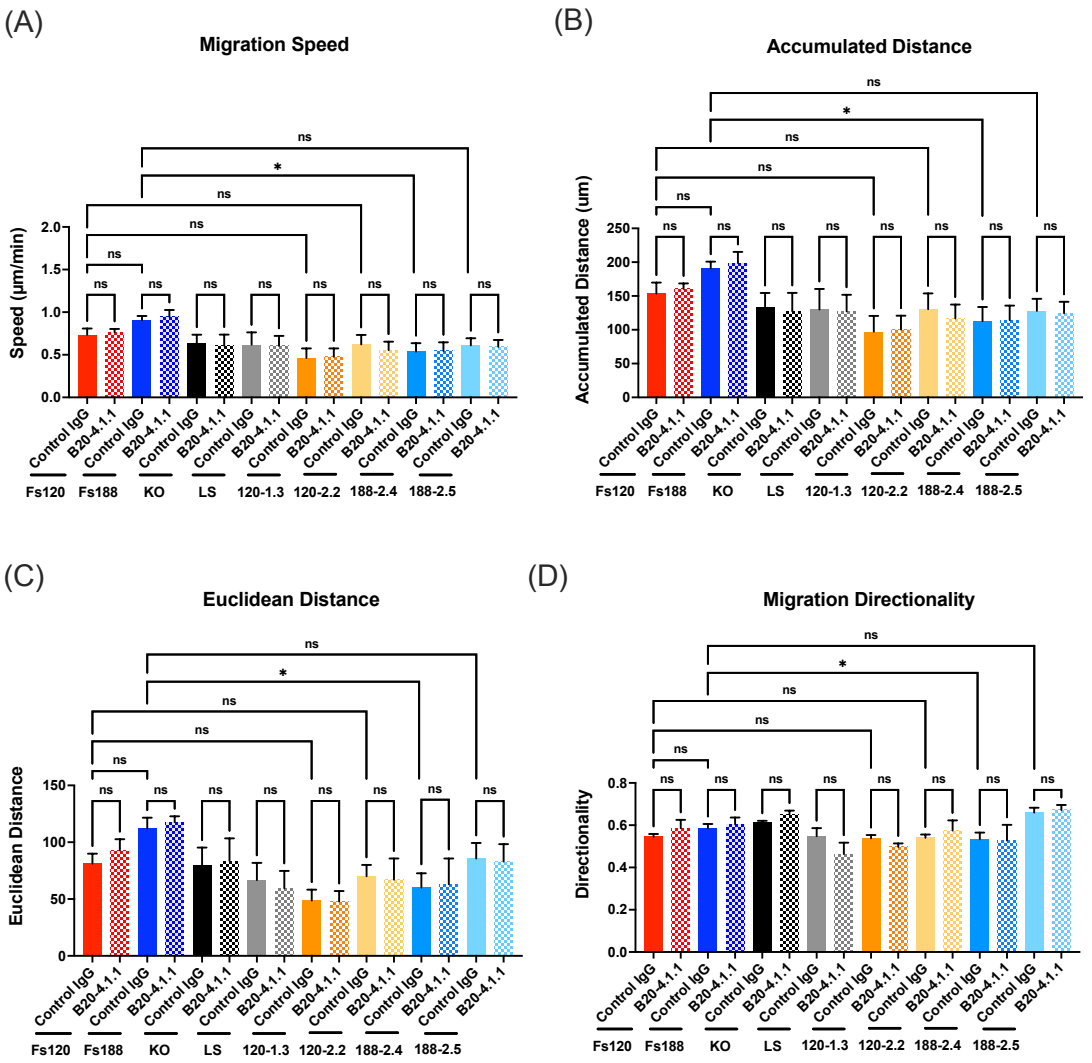

Figure 5.4 Migration capacity of fibrosarcoma cells expressing single VEGFA isoforms on 2D collagen-coated surfaces with chemotactic gradient.

Quantification of (A) migration speed, (B) accumulated distance, (C) Euclidean distance and (D) directionality in fibrosarcoma cells expressing different single VRGFA isoforms via single-cell live images by CD7 microscopy. 30 cells from different cell lines were analysed in each independent experiment. Three independent replicates were expressed as mean ± SEM. A non-parametric Kruskal-Wallis test with multiple comparisons followed by an Uncorrected Dunn's test was performed to detect statistical significance. * p-value <0.05, ns: no significant difference.

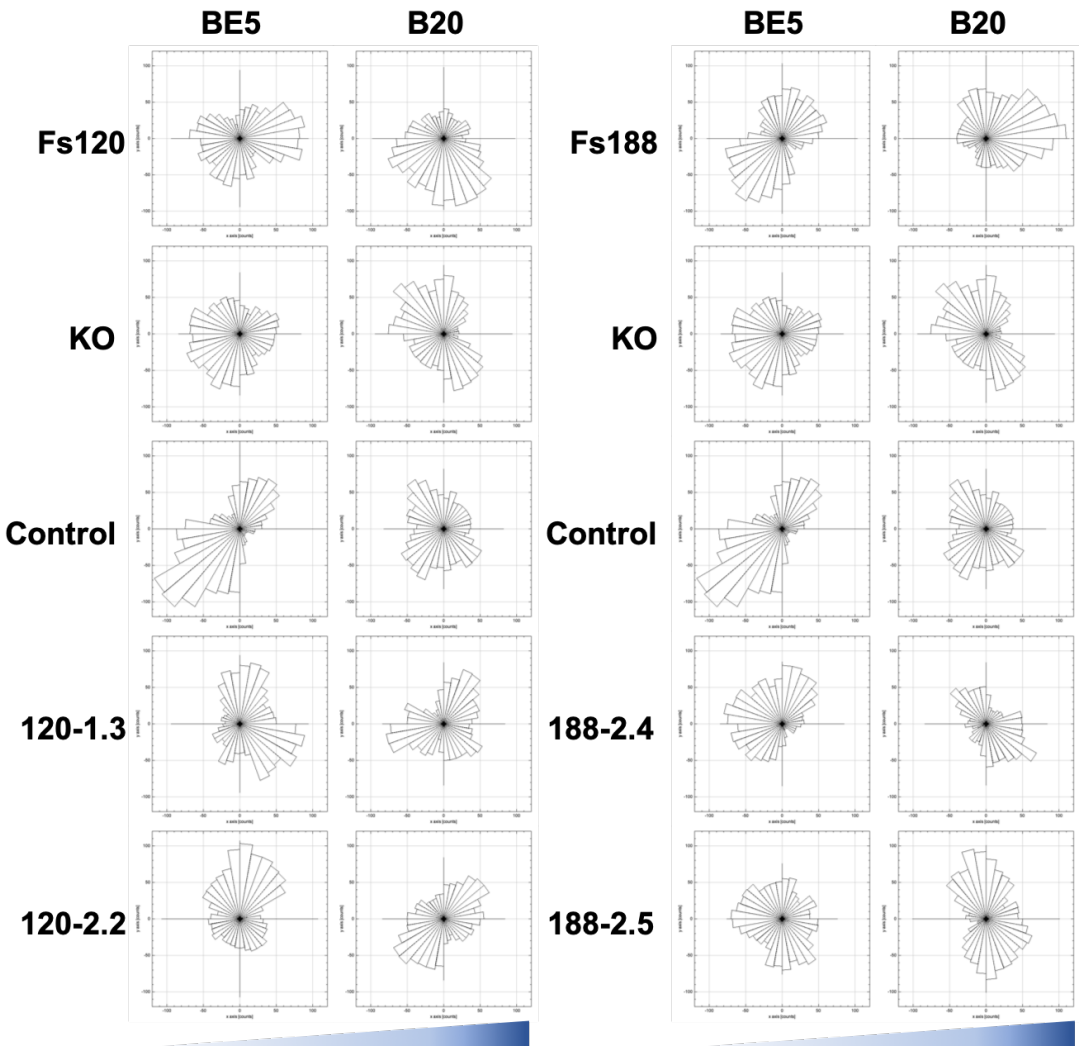

Figure 5.5 Representative Rose diagrams of cell migration direction in fibrosarcoma cells expressing single VEGFA isoforms on collagen-coated 2D surfaces.

Cell tracks from 30 cells in each cell line were analysed and plotted into a rose diagram according to the distribution of counted cells in each sector using the Chemotaxis tool developed by ibidi.

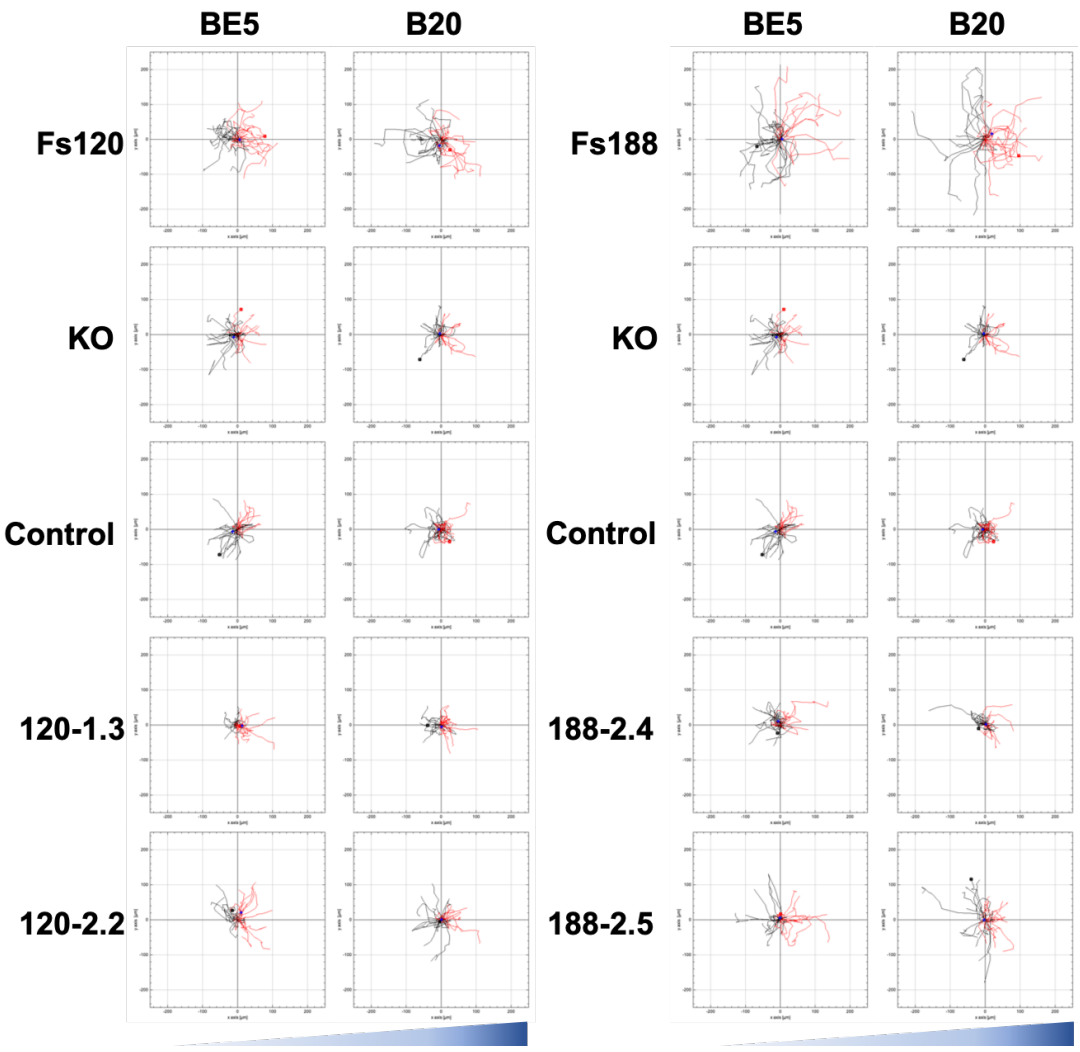

Figure 5.6 Representative trajectory plots of cell migration in fibrosarcoma cells expressing single VEGFA isoforms on collagen-coated 2D surfaces.

The trajectory of cell migration from 30 cells in each cell line was drawn from positions at each time point marked by the pointing cell tracking plugin in ImageJ. All tracks were centred on the origin. The tracks with cell endpoint on the right which migrated toward the chemotactic gradient were marked in red, whereas against the chemotactic gradient were marked in black. The centre of mass was marked in a blue cross.

5.3 Characterisation of the migration capacity of a single VEGFA isoform expressing fibrosarcomas on fibre scaffolds

Plasticity in cell migration modes is defined as cells being able to migrate in different methods to adapt to microenvironments. Diverse environmental conditions challenge cancer cells during metastasis. Therefore, gaining flexibility in the modes of migration of cancer cells is critical. Apart from 2D surfaces coated with different ECM proteins, fibrosarcoma cells expressing different VEGFA isoforms may be required to migrate on fibrillar collagen in fibrosarcoma tumours in mice. Comparing migration capacity on fibre scaffold versus 2D surfaces may help us understand which have better plasticity in modes of cell migration.

5.3.1 Studies of migration of single VEGFA isoform expressing fibrosarcoma cells on aligned fibre scaffolds coated with fibronectin and in a chemotactic gradient.

Induced expression of VEGFA in *VEGFA* KO cells did not alter their mobility. The migration speed and accumulated distance and therefore were VEGFA isoform independent. No statistical differences across cell lines expressing VEGFA isoforms on fibronectin-coated aligned fibre scaffold were seen (Fig 5.7 A and B). However, the responses to the anti-VEGFA antibody were VEGFA isoform dependent. Only the migration speed and the accumulated distance in VEGFA120 expressing cells were downregulated and were especially significant in the VEGFA120-2.2 clone (Fig 5.7 A and B).

The centre of mass and the distribution of cell endpoints did not show a consistent trend that pointed out that cells did not strongly interact with the chemotaxis gradient (Fig. 5.8 and 5.9). Furthermore, blocking signal transduction from VEGFA with the antibody B.20 failed to interrupt chemotactic gradient sensing across all fibrosarcoma cell lines. Although there was no clear evidence indicating cells migrated toward chemotaxis, fibrosarcoma cells expressing different isoforms migrated following the orientation of the fibre scaffolds which was parallel to the chemotactic gradient (Fig. 5.7 D and 5.9). Surprisingly, fibrosarcoma cells expressing VEGFA120 derived from mature skin fibroblasts had higher consistency in the direction of cell migration compared to cells derived from embryonic fibroblasts (Fig. 5.7 D).

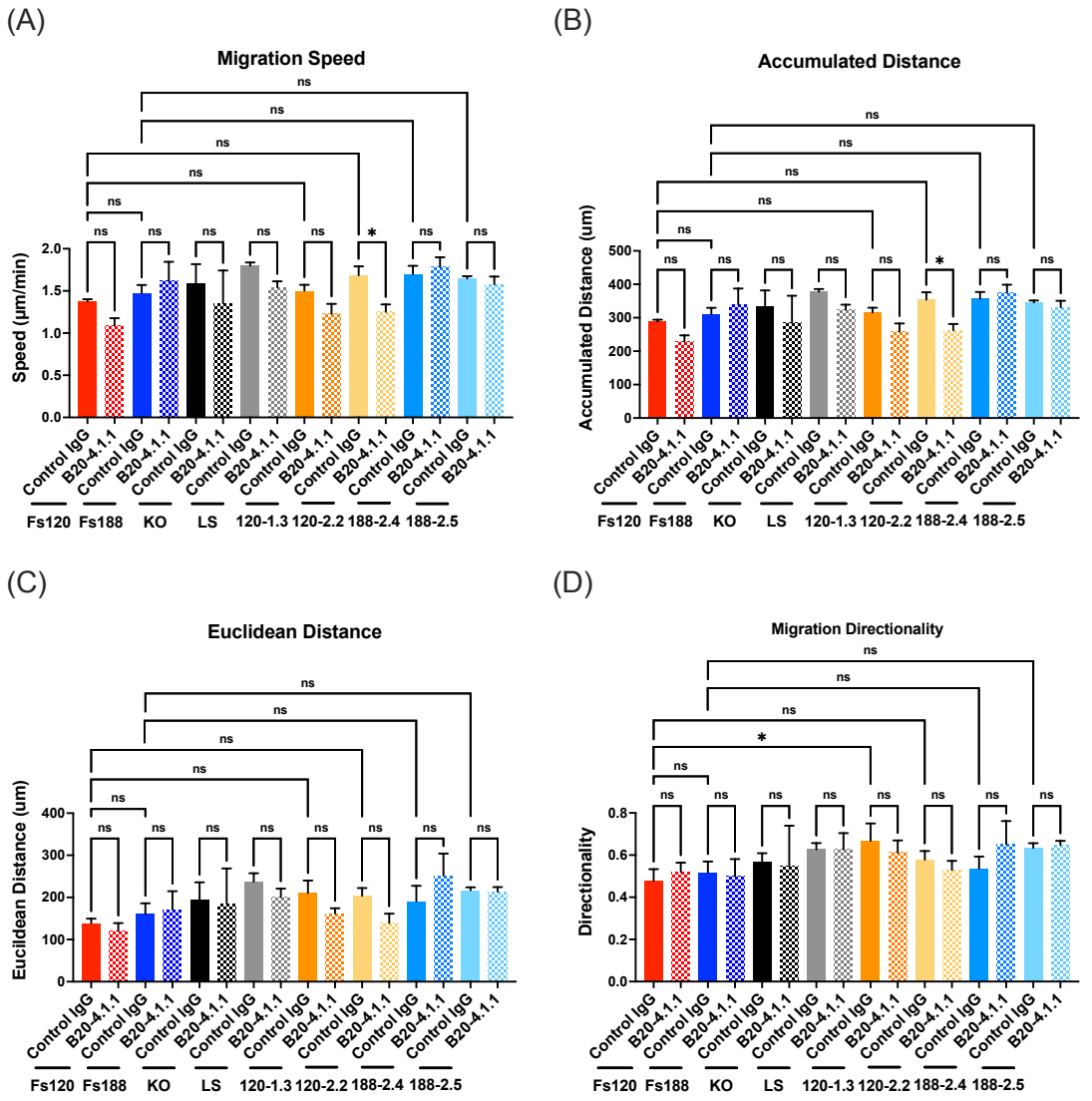

Figure 5.7 Migration capacity of fibrosarcoma cells expressing single VEGFA isoforms on fibronectin-coated aligned fibre scaffold with chemotactic gradient.

Quantification of (A) migration speed, (B) accumulated distance, (C) Euclidean distance and (D) directionality in fibrosarcoma cells expressing different single VEGFA isoforms via single-cell live images by CD7 microscopy. 30 cells from different cell lines were analysed in each independent experiment. Three independent replicates were expressed as mean ± SEM. A one-way ANOVA test with multiple comparisons by Fisher's LSD test was performed to detect statistical significance in the accumulated distance and Euclidean distance. A non-parametric Kruskal-Wallis test with multiple comparisons followed by an Uncorrected Dunn's test was performed to detect statistical significance in migration speed and directionality. * p-value <0.05, ns: no significant difference.

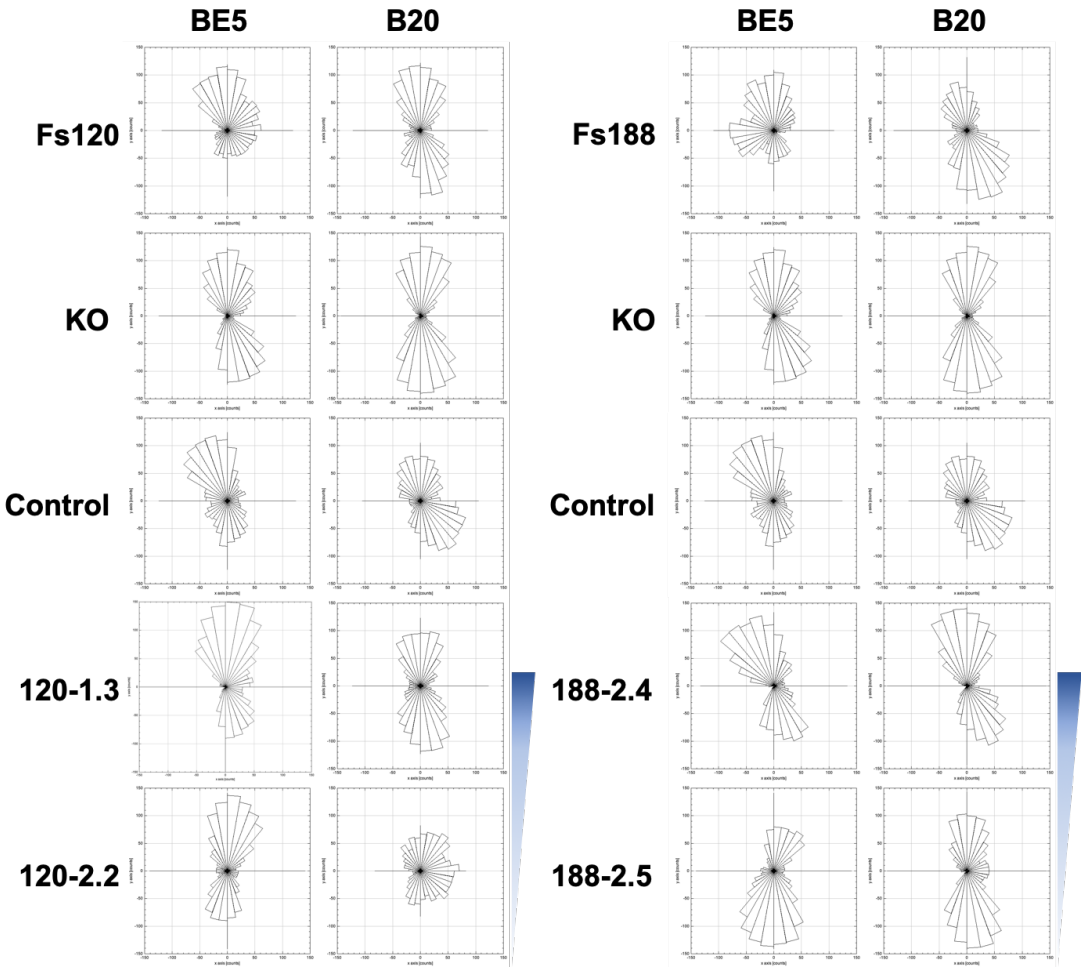

Figure 5.8 Representative Rose diagrams of cell migration direction in fibrosarcoma cells expressing single VEGFA isoforms on fibronectin-coated aligned fibre scaffold with chemotactic gradient.

Cell tracks from 30 cells in each cell line were analysed and plotted into a rose diagram according to the distribution of counted cells in each sector by the Chemotaxis tool developed by Ibidi.

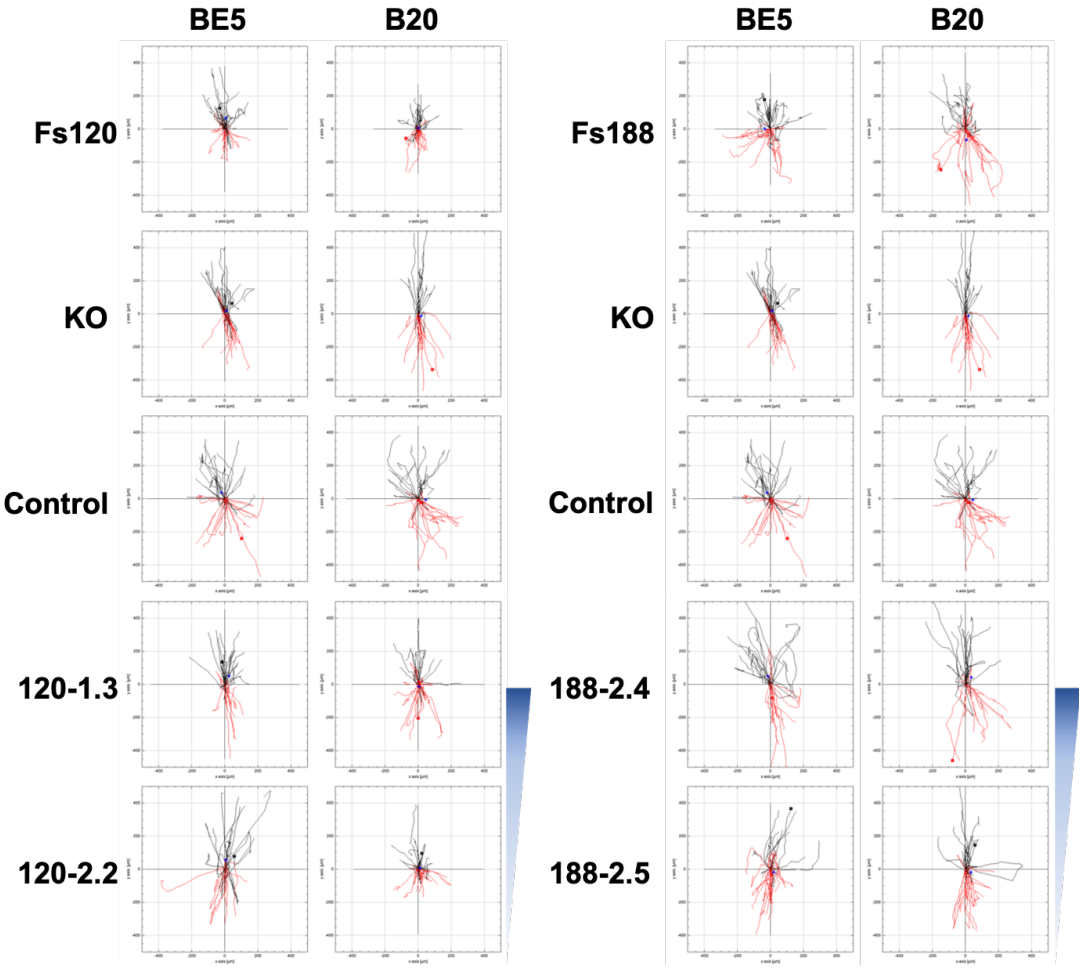

Figure 5.9 Representative trajectory plots of cell migration in fibrosarcoma cells expressing single VEGFA isoforms on fibronectin-coated aligned fibre scaffold with chemotactic gradient.

The trajectory of cell migration from 30 cells in each cell line was drawn from positions at each time point marked by the pointing cell tracking plugin in ImageJ. All tracks were centred on the origin. The tracks with cell endpoint on the top which migrated toward the chemotactic gradient were marked in black, whereas against the chemotactic gradient were marked in red. The centre of mass was marked in a blue cross.

5.4 Summary

The migration capacity of fibrosarcoma cells expressing different VEGFA isoforms was successfully characterized on different engineered microenvironments by measuring their migration speed, accumulated distance, Euclidean distance and directionality. Overall, there was no significant difference in the migration capacity between fibrosarcoma cells expressing VEGFA120 and VEGFA188, as well as between VEGFA expressing and transfection control cells, across microenvironments. Yet, the migration capacity of fibrosarcoma cells derived from mature skin fibroblasts on fibronectin was upregulated and downregulated on collagen compared with cells derived from embryonic fibroblasts. It had been reported in ovarian cancer cells that displayed varied morphology and migration capacity on surfaces coated with collagen, laminin and fibronectin (English et al., 2017; Kanthou et al., 2014). Moreover, the migration capacity of cells was repressed by blocking the specific integrin subunits, which play an important role in modulating cell interaction between cells and ECM, suggesting the migration capacity of cells on different ECM was integrin-dependent. The expression of integrin subunits that dominantly interacted with fibronectin and collagen may differ between fibrosarcoma cells derived from mature skin and embryonic fibroblasts, leading to distinct motility between fibronectin and collagen. However, due to the time limit, the expression of integrin subunits such as α_1, α_3, αv and β_1 in fibrosarcoma cells derived from different origins was not measured. Although there were differences in the migration capacity of fibronectin and collagen between fibrosarcoma cells generated from different origins, the migration capacity of cells from the same origin was VEGFA isoform independent.

The response to the chemotactic gradient is also essential to cell migration which directs cells migrating efficiently toward the final destination. An agarose gel containing horse serum acted as the chemoattractant in the single-cell migration assay. There was only a small attraction to serum observed in fibrosarcoma cells expressing VEGFA120 on fibronectin and collagen. On the contrary, VEGFA188-expressing cells showed no response to the chemotactic gradient. Previous data acquired during the master study showed a significant response to the chemotaxis gradient in fs120 cells on fibronectin and collagen (unpublished data, Yu-Chin Lee MSc thesis). The change of the brand of horse serum due to the impact of the shipping may be the reason for losing strong chemotactic effects. The differences in recipes between brands of serum suggest more

optimization in the concentration of horse serum acting as a chemoattractant is needed. Ibo *et. al* pointed out that chemotaxis was essential in the direction of cell blebbing, which is the dominant mode of cell migration on fibres (Ahmed et al., 2005). However, the direction of cell migration on the aligned fibre scaffold in fibrosarcoma cells expressing VEGFA120 or VEGFA188 was independent of the chemotaxis gradient and determined by the direction of fibres. Surprisingly, the direction of cell migration was guided by the orientation of fibres also observed in glioblastoma cells (Ibo et al., 2016). In comparison to the influence of the chemotaxis, the aligned fibres had a greater effect on the orientation of the distribution of focal adhesion uniaxially in cells (Estabridis et al., 2018), guiding cells migrating along the orientation of fibres.

Gaining plasticity in modes of cell migration favouring cancer cells rapidly adapts to the microenvironment during invasion and metastasis (Wang et al., 2018). Fibrosarcoma cells expressing different VEGFA isoforms were challenged on different engineered microenvironments, forcing cells to migrate in different migration modes. The adaptation to the microenvironment between cells expressing different VEGFA isoforms is identified by their migration capacity. There were no distinct differences in the migration capacity between VEGFA120- and VEGFA188-expression cells across 2D surfaces coated with fibronectin or collagen and fibronectin-coated aligned fibre scaffolds, indicating both VEGFA-expressing cells are well-adapted to changes in microenvironments. Therefore, the plasticity in modes of cell migration was VEGFA isoform independent. Yet, the results conflicted with previous observations done by English *et al* that fs120 cells resisted shear stress in the circulation system via undergoing mesenchymal-amoeboid transition suggesting better plasticity (Hanahan, 2022; Friedl & Alexander, 2011). It has been reported that increased fibre density (English et al., 2017) and decreased spacing between fibres (Doyle et al., 2009) altered cell morphology and the attachment of cells to fibres, enhancing migration capacity in fibroblasts and glioblastoma cells respectively. Even though we successfully recapitulated the diameter of fibrillar collagen detected in mouse fibrosarcomas expressing different VEGFA isoforms, the density and the gaps between fibres were not taken into consideration. Due to the time limit and technical difficulties, we were unable to generate fibre scaffolds that recapitulated all parameters of fibrillar collagen observed in mouse fibrosarcoma tumours, and the non-adherent chamber forced cells to migrate in the integrin-independent mode. Further characterization of the migration

capacity of fibrosarcoma cells in fibre scaffolds that recapitulated more parameters of fibrillar collagen and use of the non-adherent chamber may provide a better understanding if plasticity in modes of cell migration is VEGFA isoform dependent.

Anti-VEGFA therapy successfully inhibited fs120 cells metastasising from the primary subcutaneous tumour to the lung in mice, but with no effects on invasiveness (Estabridis et al., 2018). In this study we find VEGFA isoform-selective inhibition effects of B20-4.1.1 in the migration capacity of VEGFA120-expressing cells on fibronectin, collagen and fibronectin-coated fibre scaffolds compared to VEGFA188 expressing cells. In addition, VEGFA120 expression-dependent response to chemotaxis was abrogated by the application of B20.4.1.1. Downregulation of migration capacity and the directionality of movement by B20.4.1.1 may be a potential explanation for selectively repressed metastasis in the study of English et al (English et al., 2017).

According to the characteristics of engineered microenvironments, cells utilize different cell migration modes to move (English et al., 2017). The regulation of different modes of cells migration is discussed in detail in the introduction Section 1.3. On 2D surfaces, the mesenchymal mode is the primary mode in cell migration which highly relays on the force generated from the cell-ECM interaction. On the contrary, because of low adhesiveness in the 3D microenvironment, cells migrate in amoeboid/blebby mode that depends on the contractility of cells generated by actomyosin (Yamada & Sixt, 2019). We have successfully observed that fibrosarcoma cells had the fastest migration speed in the 3D fibre scaffolds followed by 2D surfaces coated with fibronectin and then collagen. The migration speed of cells in different environments is determined by the strength of focal adhesions suggesting rapid migration in amoeboid/blebby mode (Friedl, 2004) and slow migration in mesenchymal mode (Friedl, Zänker, & Bröcker, 1998), supporting our observations.

In summary, results obtained from this chapter showed fibrosarcoma cells expressing VEGFA120 or VEGFA188 had similar motility on 2D fibronectin- and collagen-coated surfaces and 3D-aligned fibre scaffolds. A reduced capacity for fibrosarcoma cells originating from mature skin fibroblasts to migrate was observed when compared to cells originating from embryonic fibroblasts when placed on collagen. Additionally, cells from both origins exhibited sensitivity to B20.4.1.1 on fibronectin and within 3D fibre scaffolds, with a dependency on VEGFA120. Furthermore, no differences in migration capacity across engineered environments between VEGFA120- and

VEGFA188-expressing cells were seen, indicating the plasticity in modes of cell migration was VEGFA isoform independent. Molecular mechanisms of VEGFA play in the regulation of cell migration will be identified by quantifying the expression of proteins that play roles in cell migration with the application of function blockades in the next chapter.

Chapter 6

6. Molecular mechanism of VEGFA/VEGFR signalling in cell migration

6.1 Introduction

Besides angiogenesis, VEGFA/VEGFR signalling also plays a role in the regulation of cell migration (Weddell, Chen, & Imoukhuede, 2018; Dellinger & Brekken, 2011). Several studies have shown that inhibition of signal transduction from VEGFA successfully represses the invasiveness and migration capacity of cancer cells *in vitro* (Kiso et al., 2018a; Zeng et al., 2016; Gong et al., 2014; Chen et al., 2009) and metastasis *in vivo* (Yu et al., 2022; English et al., 2017) suggesting VEGFA and its receptors may be a potential target for inhibiting metastasis. However, the efficacy of the inhibition in metastasis by anti-VEGFA therapy is cancer-type dependent in the clinic (Sitohy, Nagy, & Dvorak, 2012). Moreover, the normalized vascular network can occur in tumours after anti-VEGFA therapy, but the recall of the hypoxic condition after vascular normalisation increases the risk of again promoting metastasis (Pàez-Ribes et al., 2009). Therefore, understanding the mechanisms that VEGFA contributes to when orchestrating invasion and metastasis and how this responds to anti-VEGFA/VEGFR targeted therapy is crucial.

Several monoclonal antibodies and receptor tyrosine kinase inhibitors (RTKIs) have been developed and applied in the clinical setting that targets VEGFA and its receptors (Zirlik & Duyster, 2018). The developmental history and their efficacy in the treatment of cancers are introduced in detail in the Introduction Section 1.4.2. Blocking VEGFA signal transduction can be done by preventing either VEGFA binding to receptors or inhibiting RTK activity. Bevacizumab, a monoclonal antibody specific for human VEGFA, binds to VEGFA and blocks receptor interaction (Presta et al., 1997). B20.4.1.1 was developed by Genentech/Roche as a preclinical version of Bevacizumab. It binds to both mouse and human VEGFA at the same site and affinity as bevacizumab and has similar pharmacodynamic properties *in vivo* (Liang et al., 2006). On the contrary, pazopanib is a multitarget tyrosine kinase inhibitor, that mimics the adenine ring of ATP binding to tyrosine kinase receptor resulting in the abrogation of ATP-induced activation (Lee, Jones, & Huang, 2019). Unlike pazopanib, MF-1, a mouse monoclonal antibody, only interacts with VEGF receptor 1 to block ligand binding (Wu et al., 2006). Comparing the alteration in the expression and activation of VEGF-VEGFR signalling upon treatment with inhibitors may provide a better understanding

of the mechanisms of action of VEGFA signalling plays in cell migration and metastasis.

In this chapter, I will characterize the protein expression and phosphorylation of VEGFA-related signalling receptors and kinases in fibrosarcoma cells expressing single VEGFA isoforms with the application of the multi-RTKI pazopanib, the anti-VEGFA antibody B20.4.1.1 and the anti-VEGFR1 antibody MF-1. Through this the molecular mechanisms involved in VEGFA120-induced metastasis and selective response to B20.4.1.1 in cell migration may be identified.

6.2 RTK, kinase and phosphorylation and ECM expression in fibrosarcoma cells treated with VEGFA-VEGFR inhibitors

Inhibition of the signal transduction of VEGFA successfully selectively repressed metastasis in mice (English et al., 2017) and migration capacity (in Chapter 5) in fibrosarcoma cells expressing VEGFA120. However, the molecular mechanisms participating in the regulation of cell migration by VEGFA120 are unclear. The expression of p-VEGFR1 ($Tyr^{1213)}$, fibronectin, Akt (Tyr^{413}) and Src (Tyr^{416}) in VEGFA120- and VEGFA188-expressing fibrosarcoma cells treated with pazopanib (PZNB), and anti-VEGFA/VEGFR1 antibodies B20.4.1.1 and MF-1, was characterized by western blotting in this section.

6.2.1 Protein expression of p-VEGFR1

According to Section 3.3.3 in Chapter 3, the expression of VEGFR2 was unable to be confidently detected by western blotting and RT-PCR. In light of these results, the expression of VEGFR2 and its response to RTKIs and anti-VEGFA/VEGFR antibodies was not taken into account. It has been reported that phosphorylation of specific tyrosine sites, such as Tyr^{794} and Tyr^{1213}, in the cytoplasmic domain of VEGFR1 can promote the activation of PI3K/Akt and PLCγ resulting in migration in macrophage (Weddell, Chen, & Imoukhuede, 2018; Wang et al., 2011). However, only a few antibodies recognize specific phosphorylation sites in VEGFR1 available. Only one antibody I found commercially available detected mouse p-VEGFR1 at Tyr^{1213}. The molecular weight of full-length VEGFR1 is 180-kDa. Yet, several proteases can cleave VEGFR1 into two segments, the ectodomain and cytoplasmic fragments (Huang, 2021). The molecular weight of the cytoplasmic fragments comprising the phosphorylation sites in the kinase domain is approximately 60-KDa and 20-KDa in monomers and 70-KDa as a dimer (Han et al., 2015). Therefore, the expression of p-VEGFR1 at Tyr^{1213} in response to PZNB, B20.4.1.1 and MF-1 in fibrosarcoma cells expressing different VEGFA isoforms was measured (Fig. 6.1 A and 6.2 A).

Although there were no statistically statistical differences between cells treated with PZNB and DMSO, increased expression of p-VEGFR1 in VEGFA120-expressing fibrosarcoma cells and transfection control cells was seen. Additionally, the response to PZNB was different between the two VEGFA188-expressing clones. Clone 188-2.4 showed no sensitivity to PZNB, but downregulation of p-VEGFR1 was seen in clone

188-2.5 (Fig. 6.1 B).

No statistically significant differences were observed in the expression of p-VEGFR1 across fibrosarcoma cells after the treatment with control IgG, although induced expression of p-VEGFR1 was seen for the VEGFA120-expressing clone 2.2. Varied expression of p-VEGFR1 was observed between clones expressing VEGFA120 treated with the control IgG; however, both clones showed a similar pattern which induced p-VEGFR1 expression in cells treated with B20.4.1.1 was seen, but no effects with MF-1. Moreover, clones expressing VEGFA188 did not show a large effect on the expression of p-VEGFR1 (Fig. 6.2B).

(A)

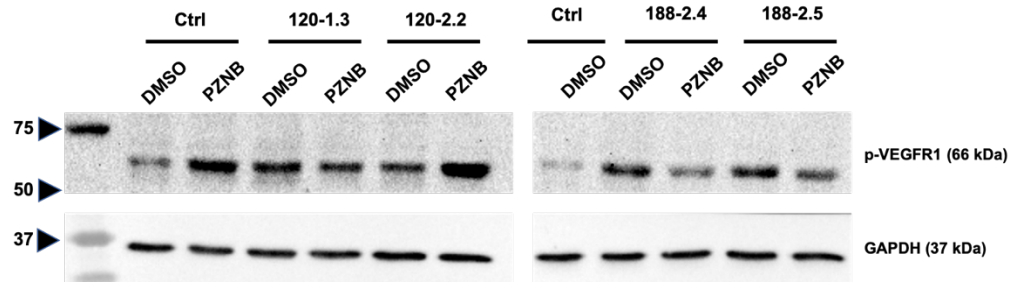

(B)

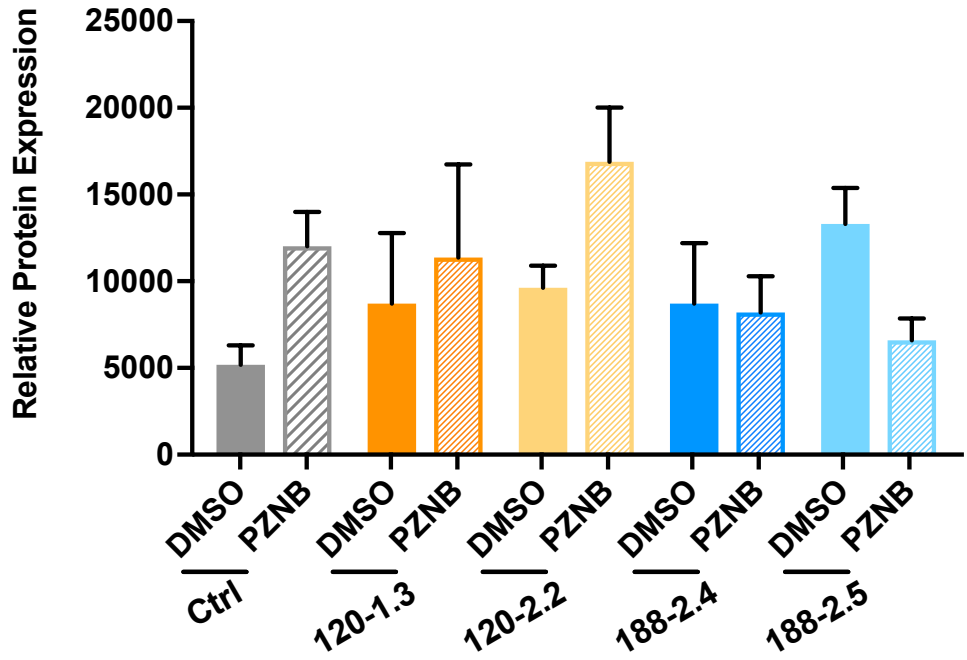

Figure 6.1 Western blotting analysis and quantification of p-VEGFR1(Tyr1213) expression in cells expressing a single VEGFA isoform with tyrosine kinase inhibitors

(A) Representative Western blotting images of p-VEGFR1 in cells expressing a single VEGFA isoform and the VEGFA KO control are shown. Due to the well limit, samples from the same experiment were run on different gels. The whole cell lysate from the control treated with DMSO acted as a control of variation between gels. GAPDH acted as a loading control. (B) Relative protein expression of fibronectin normalised to GAPDH was quantified by Image J. Three independent replicates were expressed as mean ± SEM. An ordinary two-way ANOVA test with multiple comparisons by uncorrected Fisher's LSD post-test was performed to detect statistically significant differences.

(A)

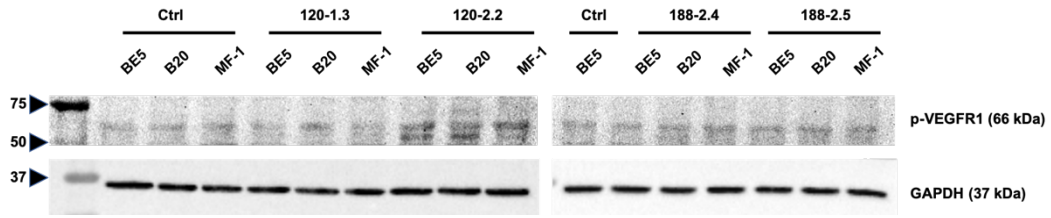

(B)

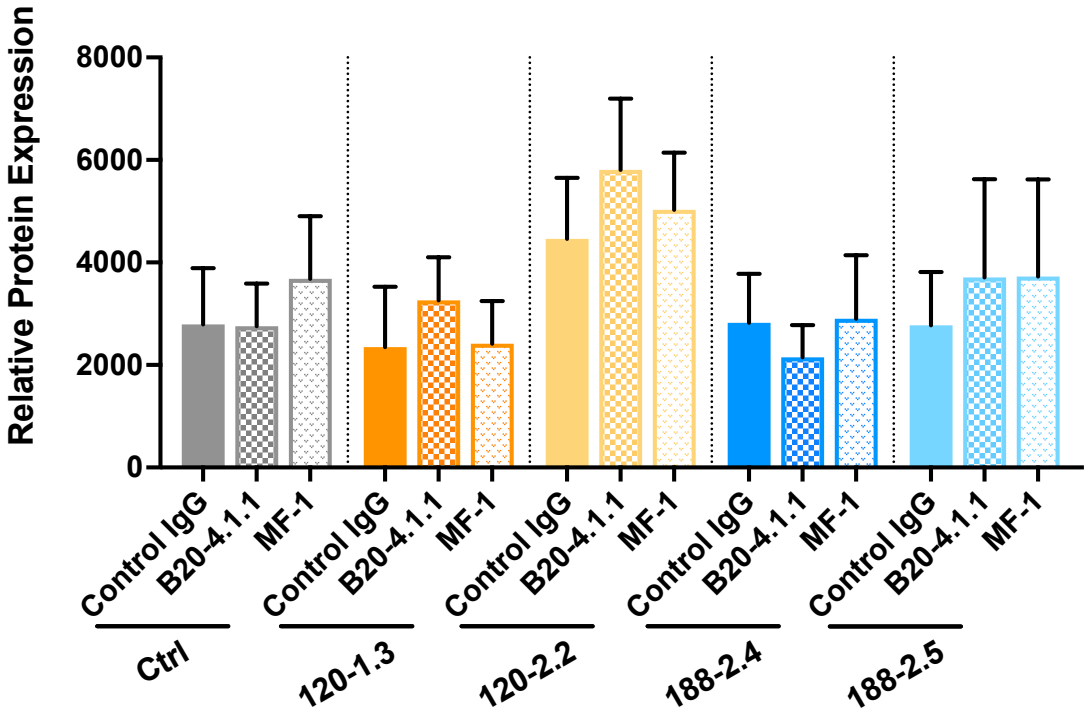

Figure 6.2 Western blotting analysis and quantification of p-VEGFR1 expression in cells expressing a single VEGFA isoform with anti-VEGFA/VEGFR1 inhibitors

(A) Representative Western blotting images of p-VEGFR1 in cells expressing a single VEGFA isoform and the VEGFA KO control are shown. Due to the well limit, samples from the same experiment were run on different gels. The whole cell lysate from the control treated with Control IgG acted as a control of variation between gels. GAPDH acted as a loading control. (B) Relative protein expression of fibronectin normalised to GAPDH was quantified by Image J. Three independent replicates were expressed as mean ± SEM. An ordinary two-way ANOVA test with multiple comparisons by uncorrected Fisher's LSD post-test was performed to detect statistically significant differences.

6.2.2 Expression of fibronectin

The expression of fibronectin in cells correlates with their morphology and the ability to modify the composition of the surrounding environment and how it affects cell migration is discussed in detail in Introduction section 1.3. The expression of fibronectin in response to PZNB, B20.4.1.1 and MF-1 in fibrosarcoma cells expressing different VEGFA isoforms was measured (Fig. 6.3 A and 6.4 A).

There was no difference in the expression of fibronectin across fibrosarcoma cells expressing different VEGFA isoforms or the transfection control cells with the application of DMSO. Surprisingly, downregulated expression of fibronectin was only detected in VEGFA120-expressing clone 2.2 with the application of PZNB. On the contrary, the treatment of PZNB did not alter the expression of fibronectin in either VEGFA188-expressing clone indicating a consistent response to PZNB (Fig. 6.3 B).

Expression of FN from fibrosarcoma cells expressing different VEGFA isoforms was not sensitive to B20.4.1.1 and MF-1 (6.4 B). However, there was an upregulation in the expression of fibronectin in the 188-2.5 clone compared with the 188-2.4 clone, suggesting these effects are clone rather than VEGFA isoform dependent.

(A)

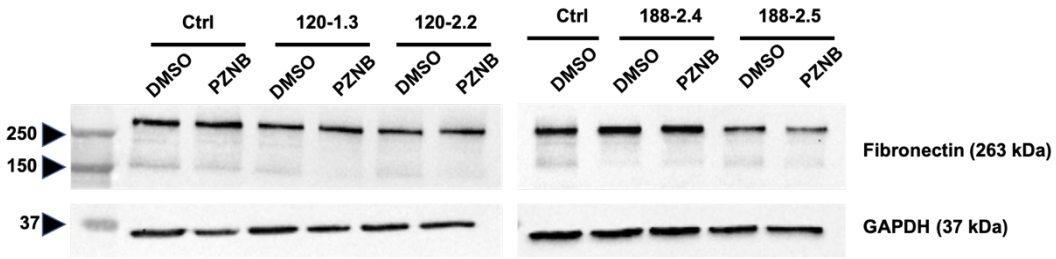

(B)

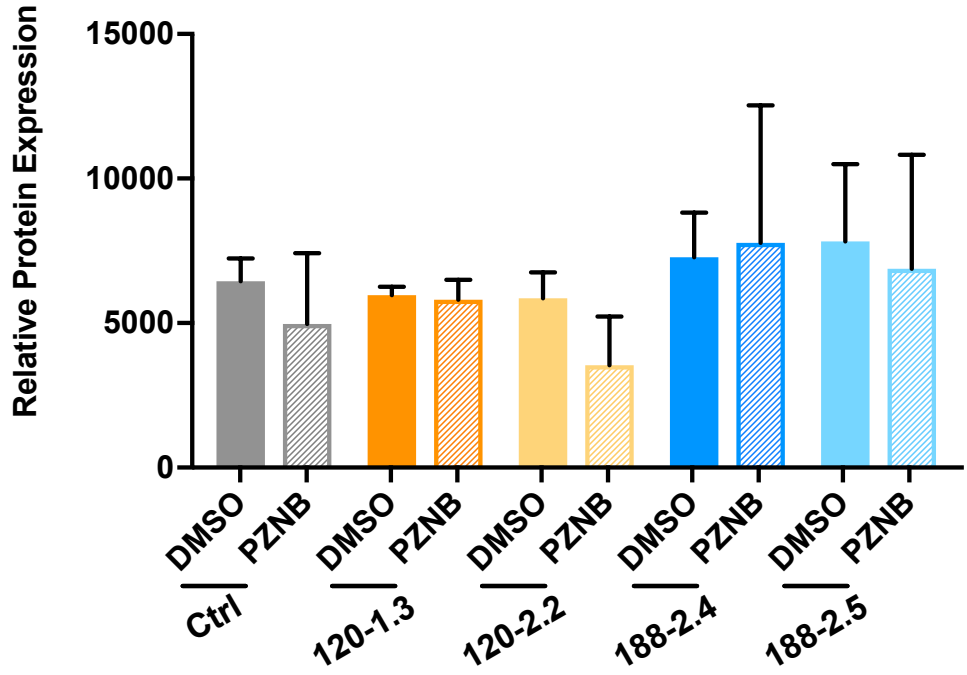

Figure 6.3 Western blotting analysis and quantification of fibronectin expression in cells expressing a single VEGFA isoform with tyrosine kinase inhibitors

(A) Representative Western blotting images of fibronectin in cells expressing a single VEGFA isoform and the VEGFA KO control are shown. Due to the well limit, samples from the same experiment were run on different gels. The whole cell lysate from the control treated with DMSO acted as a control of variation between gels. GAPDH acted as a loading control. (B) Relative protein expression of fibronectin normalised to GAPDH was quantified by Image J. Three independent replicates were expressed as mean ± SEM. An ordinary two-way ANOVA test with multiple comparisons by uncorrected Fisher's LSD post-test was performed to detect statistically significant differences.

(A)

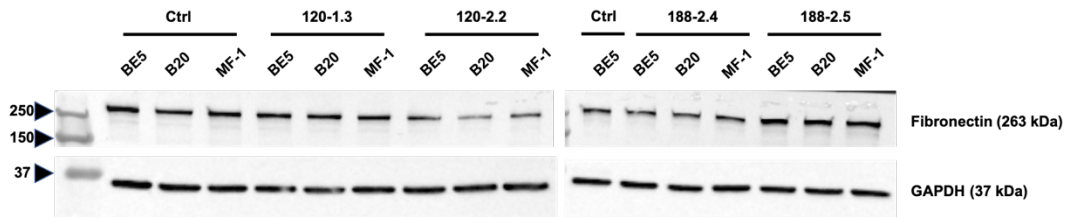

(B)

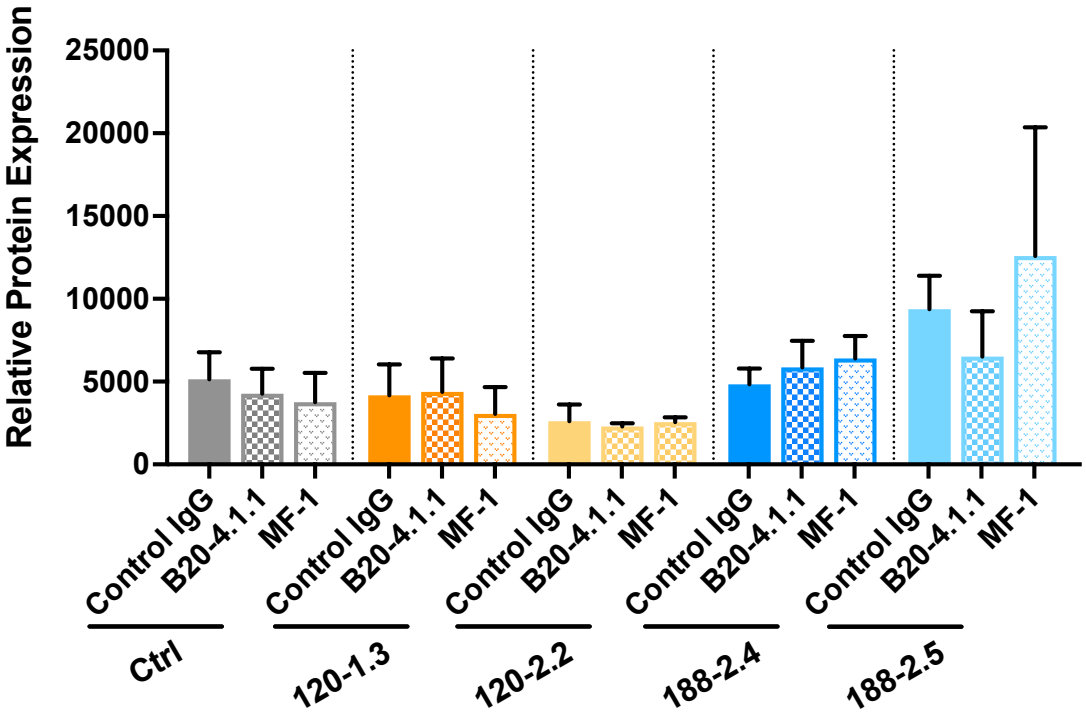

Figure 6.4 Western blotting analysis and quantification of fibronectin expression in cells expressing a single VEGFA isoform with anti-VEGFA/VEGFR1 inhibitors

(A) Representative Western blotting images of fibronectin in cells expressing a single VEGFA isoform and the VEGFA KO control are shown. Due to the well limit, samples from the same experiment were run on different gels. The whole cell lysate from the control treated with Control IgG acted as a control of variation between gels. GAPDH acted as a loading control. (B) Relative protein expression of fibronectin normalized to GAPDH was quantified by Image J. Three independent replicates were expressed as mean ± SEM. An ordinary two-way ANOVA test with multiple comparisons by uncorrected Fisher's LSD post-test was performed to detect statistically significant differences.

6.2.3 Protein expression of intracellular kinases downstream of RTKIs

The expression of kinases listed in Section 3.3.4 that regulates the VEGFA-induced cell migration was measured in fibrosarcoma cells expressing different VEGFA isoforms treated with RTKI and VEGFA/VEGFR inhibitors (Fig. 6.5 and 6.7).

Total Akt and Src were equally expressed in fibrosarcoma cells expressing VEGFA120 or VEGFA188, as well as transfection control, between DMSO and PZNB treatment (Fig 6.6 B and D). There was no dramatic alteration in the expression of p-Akt across fibrosarcoma cells treated with DMSO. Repressed expression of p-Akt was detected in cells with the application of PZNB, with the exception of VEGFA120-expressing clone 1.3 (Fig. 6.6 A). In addition, no effect was observed on the expression of p-Src in all fibrosarcoma cells treated with PZNB (Fig 6.6 C).

VEGFA188-expressing fibrosarcoma cells induced the expression of p-Akt compared with VEGFA120-expressing cells, whereas only VEGFA120-expressing clone 2.2 showed the induction of p-Src (Fig. 6.8 A and C). However, there were no statistical effects on the expression of p-Src in response to B20.4.1.1 and MF-1. The altered expression of p-Src to B20.4.1.1 and MF-1 had a similar trend between fibrosarcoma cells expressing VEGFA188, distinct from fibrosarcoma cells expressing VEGFA120. Furthermore, total Akt and Src expression were not differed between cells treated with B20.4.1.1. or MF-1 (Fig. 6.8 B and D).

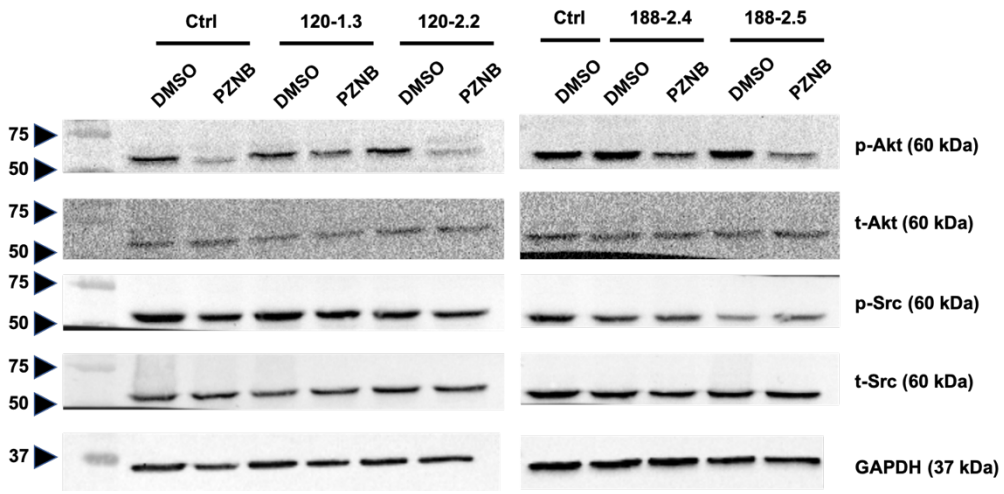

Figure 6.5 Western blotting analysis of tyrosine kinases in cells expressing a single VEGFA isoform with tyrosine kinase inhibitors

Representative Western blotting images of Akt and Src in both phosphorylated and total form in cells expressing single VEGFA isoforms and the VEGFA KO controls are shown. The total form was detected on the same membrane after the detection of the phosphorylated form. Due to the well limit, samples from the same experiment were run on different gels. The whole cell lysate from the control treated with DMSO acted as a control of variation between gels. GAPDH acted as a loading control. Three independent lysates were analysed by western blotting.

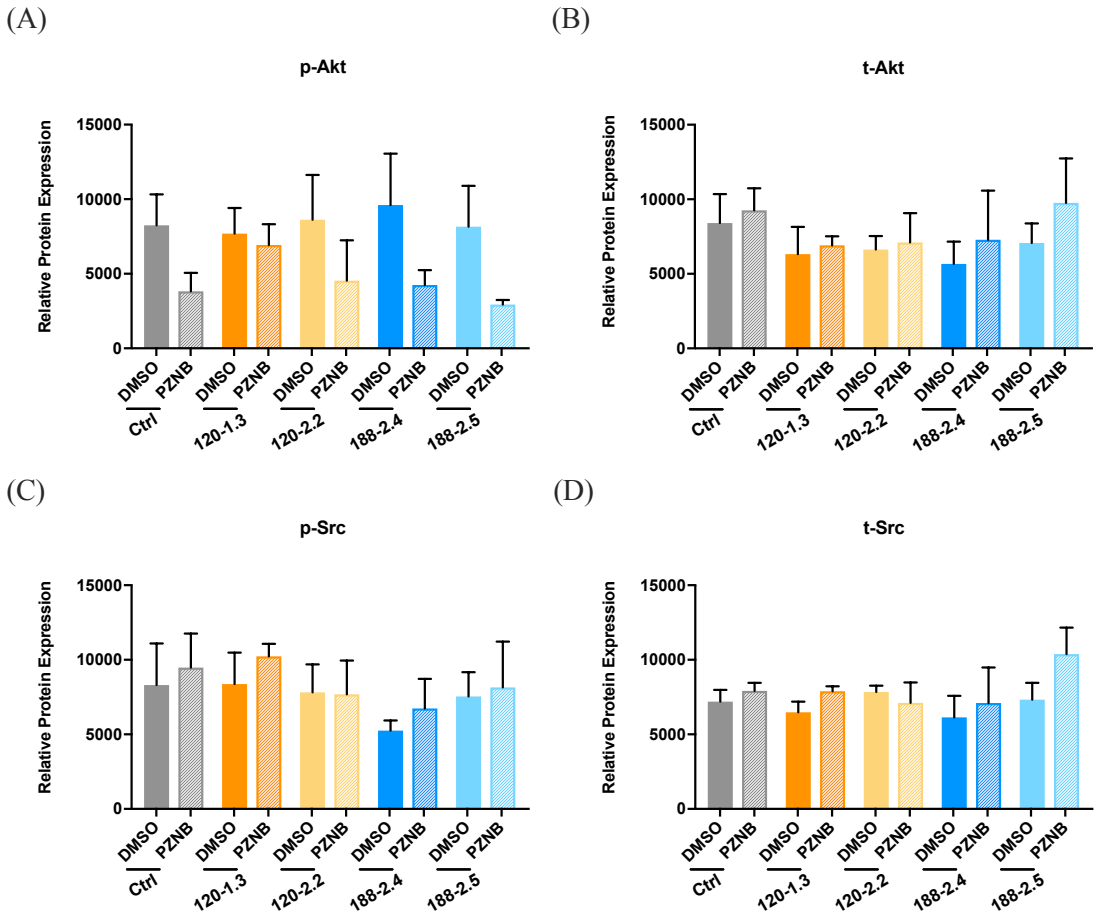

Figure 6.6 Quantification of kinases in cells expressing a single VEGFA isoform with pazopanib

Protein expression of (A) p-Akt (Tyr^{413}), (B) t-Akt, (C) p-Src (Tyr^{416}) and (D) t-Src relative to GAPDH were quantified by Image J. Three independent replicates were expressed as mean ± SEM. An ordinary two-way ANOVA test with multiple comparisons by uncorrected Fisher's LSD post-test was performed to detect statistically significant differences.

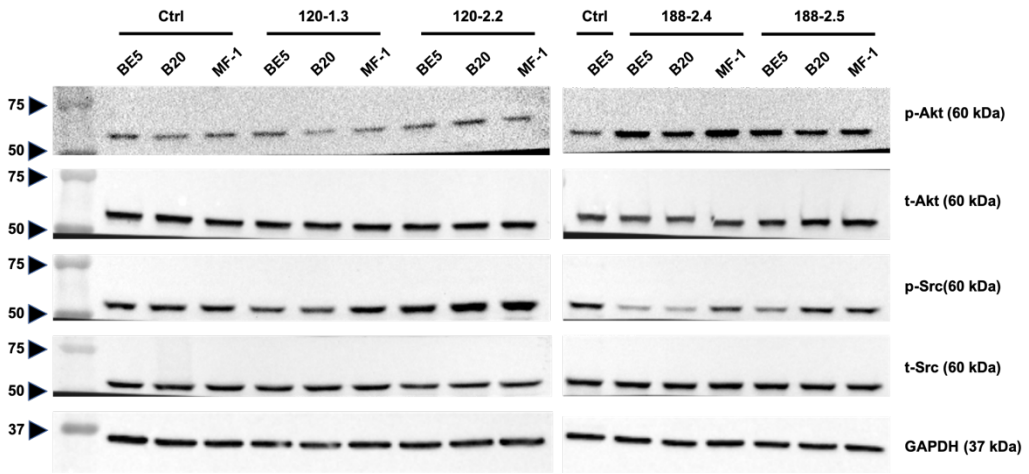

Figure 6.7 Western blotting analysis of tyrosine kinases in cells expressing a single VEGFA isoform with anti-VEGFA/VEGFR1 inhibitors

Representative Western blotting images of Akt and Src in both phosphorylated and total form in cells expressing single VEGFA isoforms and the VEGFA KO controls are shown. The total form was detected on the same membrane after the detection of the phosphorylated form. Due to the well limit, samples from the same experiment were run on different gels. The whole cell lysate from the control treated with Control IgG acted as a control of variation between gels. GAPDH acted as a loading control. Three independent lysates were analysed by western blotting.

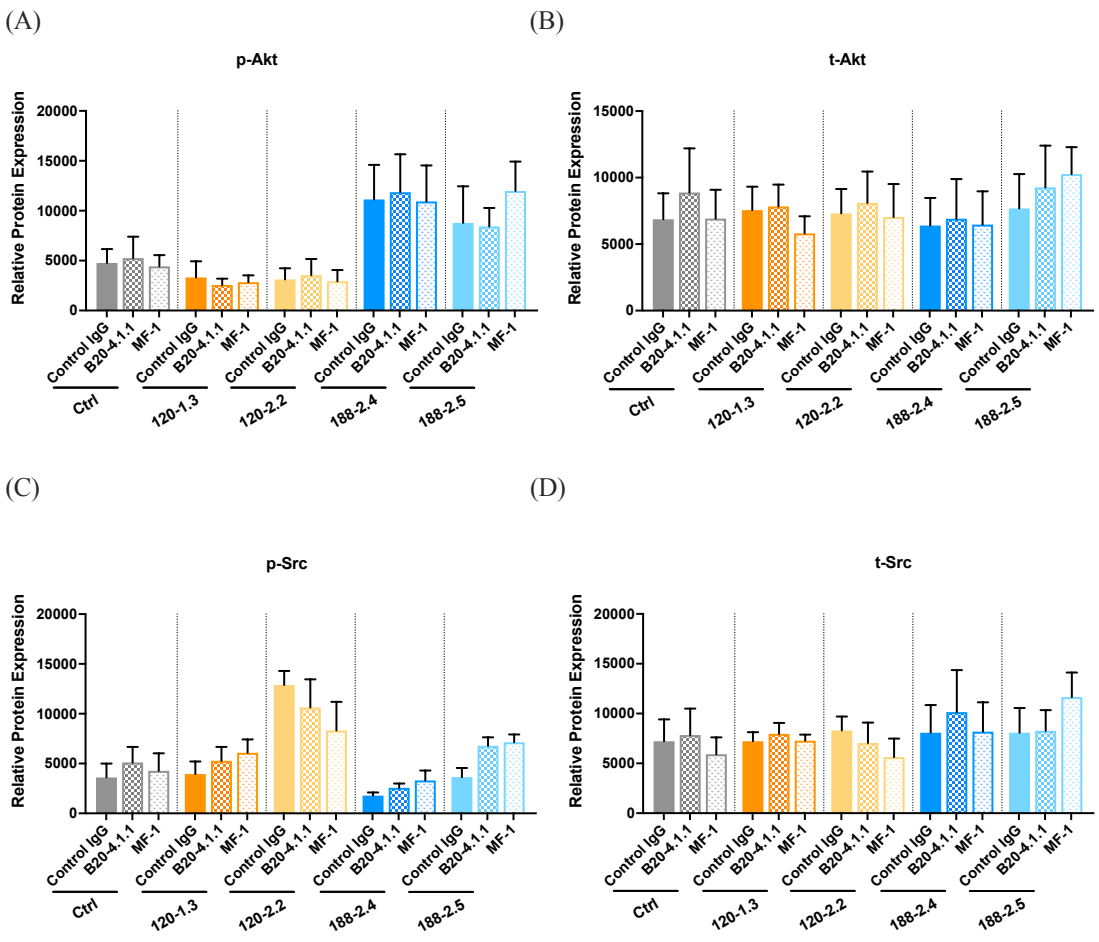

Figure 6.8 Quantification of tyrosine kinases in cells expressing a single VEGFA isoform with anti-VEGFA/VEGFR1 inhibitors

Protein expression of (A) p-Akt, (B) t-Akt, (C) p-Src and (D) t-Src relative to GAPDH were quantified by Image J. Three independent replicates were expressed as mean ± SEM. An ordinary two-way ANOVA test with multiple comparisons by uncorrected Fisher's LSD post-test was performed to detect statistically significant differences.

6.3 Summary

VEGFA not only binds to VEGFRs initiating its downstream signalling, but also other tyrosine kinase receptors such as PDGFRs, which may be a potential explanation for the failure in anti-angiogenic therapy with a single target (Mamer et al., 2017). Comparison of the altered protein expression between multitarget tyrosine kinase and VEGFA/VEGFR1-specific inhibitors may provide information to determine the target molecular mechanism that regulates VEGFA-induced cell migration. Overall, the tyrosine kinase inhibitor, pazopanib, inhibited the expression of p-Akt in fibrosarcoma cells expressing VEGFA120 or VEGFA188. However, no effects in the p-Akt were detected across cells dosing with the anti-VEGFA antibody, B20.4.1.1, and anti-VEGFR1 antibody, MF-1. Surprisingly, the expression of p-VEGFR1 was upregulated in VEGFA120-expressing cells with the treatment of pazopanib and B20.4.1.1 compared with VEGFA188-expressing cells. Fibronectin and Src expression were not sensitive to pazopanib nor B20.4.1.1 and MF-1.

The induced p-VEGFR1 in VEGF120-expressing cells treated between VEGFA120-selective and multitarget tyrosine kinase inhibitors, but not in cells treated with the VEGFR1-selective inhibitor, indicated the phosphorylation of VEGFR1 was highly correlated to VEGFA120 and independently to VEGFR1. Yet, the repressed expression of p-Akt was only observed in VEGFA120-expressing cells dosed with multitarget tyrosine kinase inhibitors suggesting VEGF120 did not link to the phosphorylation of Akt. Therefore, besides VEGFR1, other tyrosine kinase receptors that interacted with VEGFA may be involved in the activation of VEGFR1 and Akt.

There were trends of alteration between fibrosarcoma cells treated with the inhibitor and its control, but there was no statistical difference in the protein expression. The cause of weak variation in VEGFA-induced protein expression between the treatment and control groups may be due to the absence of the starvation process. Moreover, performing more replicates may power the statistical difference by decreasing the variation between each replicate. Although Kanthou *et al* had shown downregulation of p-Akt in fibrosarcoma cells derived from embryonic fibroblasts treated with inhibitors without starvation (Kanthou et al., 2014), the process of serum-starving cells in reduced or absent serum overnight was executed in studies of the efficiency of inhibition in VEGFA-induced protein phosphorylation in endothelial cells (Ruan &

Kazlauskas, 2012; Dellinger & Brekken, 2011). Different cell lines may require different handling processes. VEGFA-induced protein phosphorylation in fibrosarcoma cells derived from mature skin fibroblasts with overnight serum starvation may display significant differences between cells treated with inhibitors and its control.

In summary, the target molecular mechanism that contributed to B20-inhibited metastasis in mice and migration capacity on fibronectin of fibrosarcoma cells expressing VEGFA120 was still unclear. There may be other signalling pathways involved in VEGFA-induced migration that did not address in this chapter. Therefore, further investigations are required.

Chapter 7

7. Discussion

7.1 The challenges in the study of metastasis

More than 90% of patients with cancer die from metastasis (Dillekås et al., 2019). Although more and more metastatic-initiating mechanisms have been discovered, early prevention, detection and targeting of metastasis remain challenging. Metastasis is a highly inefficient process in that less than 0.1 % of tumour cells metastasise to distant sites successfully (Labelle et al., 2012). On the other hand, metastatic cancer cells arriving at the distant site may enter dormancy which could only be detected until forming secondary tumour. Because of the small tumour mass of metastases, it is difficult to detect in the early stage by non-invasive imaging techniques (Ganesh et al., 2022). Detecting biomarkers in the fluid from cancer patients has been used as a reference to monitor cancer progression and metastasis in clinics (Menezes et al., 2016). However, because of its low accuracy and specificity, the occurrence of metastasis cannot be determined by measuring the level of biomarkers alone. Therefore, blocking mechanisms in which cancer cells acquire metastatic potential trap cancer cells remaining at the primary site.

Metastasis is a dynamic process involving five general steps, invasive to the surrounding tissue, intravasation through the endothelium, survival in the circulation system, extravasation to the distant site, and the formation of metastatic colonisation (Labelle et al., 2012; Fares et al., 2020). Animal models have widely been used as *in vivo* models to study metastasis which fully recapitulates complexity of metastatic process. Apart from the high cost, there are limitations in the animal models. The subcutaneous injection model can be established by transplanting cancer cells from mice origin into host mice or from human origin into immunocompromised mice. However, the differential cellular behaviours between cells from humans and mice may have a different response to the therapy, which may explain failure in clinical trials (Chung et al., 2010; Gibney et al., 2016). On the other hand, infiltrated immune cells in the TME have been documented playing supportive roles during metastasis (Orr et al., 2010; Cai et al., 2019; Liu et al., 2021). Transplanting human cancer cells into immunocompromised mice eliminates the participation of the immune system in the metastatic process. Intravenous injection of cancer cells through the tail vein has been used to examine the ability of cells to survive in the circulation system, extravasation

and colonisation in distant sites. Nevertheless, cancer cells may arrive in distant sites that are different from those observed in human patients (Kang, 2009). There is also a high risk of forming coagulation of cancer cells that kills mice during experiments. In addition, dissecting the mechanisms involved in regulating metastasis in animal models is challenging.

In vitro models are well-controlled and convenient for identifying mechanisms in the modulation of particular events in cancer cells during metastasis. Scratch and transwell assays are the most dominant *in vitro* 2D platforms utilised to understand mechanisms regulating cell migration and invasion. Yet, these models do not recapitulate the topography of ECM, which is an essential determinant in cell migration and invasion. Later, the 3D tumour spheroid model was developed to investigate invasion and metastasis, aiming to replicate the heterogeneity seen *in vivo*. Nonetheless, the model's shortcomings persist, including the absence of intricate ECM surroundings and the spatial arrangement of diverse cell populations within the spheroids. 3D *in vitro* platforms were developed with the application of techniques from tissue engineering recently. Application of 3D bioprinting, we can identify the interaction between cancer cells and other cell types under the complex 3D structures and their influence on the cellular behaviours of cancer cells. Furthermore, a recently established 3D organ-on-chip has multiple chambers connected with fluidic channels (Zhang et al., 2022). The chamber on the chip allows the building of a microenvironment that shares characteristics of either primary or secondary sites. The fluidic channels between chambers resemble vascular structures creating gradients of biochemical cues. With different settings in chambers and fluidic channels, we can recapitulate factors involved in each step of metastasis.

The inhibition of cancer cells from gaining metastatic potential resulting in cancer cells being trapped in the surrounding ECM in the TME would be an efficient strategy to prevent metastasis. Understanding the regulation of plasticity in modes of cell migration can provide potential targets to abrogate the ability of cells to adapt to different TME and suppress metastatic potential. We established different *in vitro* platforms, including 2D ECM-coated surfaces and 3D fibre scaffolds, which restricted cells to travel in a specific migration mode. Apart from general 2D surfaces, the fibre scaffolds were specifically developed to mimic the structure of fibrillar collagen observed in mouse tumours. The adaptation of cells to different environments was

determined by the migration capacity of cells. Cells that adapted well to the environments had better migration capacity. The plasticity in migration modes was determined by the migration capacity in different engineered environments. Cells that maintained comparable migration capacity across environments had better plasticity. Therefore, by comparing migration capacity across different environments between fibrosarcoma cells expressing different VEGFA isoforms, we could identify if cell plasticity was VEGFA isoform-dependent. Moreover, the molecular mechanism in VEGFA-induced cell migration was characterised by Western blotting with the application of B20.4.1.1, an anti-VEGFA antibody, MF-1, an anti-VEGFR1 antibody, and pazopanib, an RTKI that inhibits VEGFR1, PDGFR-β and FGFR. Hence, the identified mechanism has the potential to be a target to repress cell plasticity, leading to the inhibition of metastasis.

7.2 Association between the expression of different VEGFA isoforms and cell migration

Migration on fibres is termed “contact guidance”, in which migration capacity is dominantly regulated by the orientation of fibres (Yamada et al., 2019). Cells on aligned fibres polarised in a uniaxial efficiently guiding cell migration. On the contrary, the formation of protrusions in multiple directions in response to random fibres disrupts contraction in a uniform order leading to suppressed migration capacity. There was no significant difference in the migration capacity between fibrosarcoma cells expressing different VEGFA isoforms on aligned fibre scaffolds (Fig. 5.7). However, the architecture of fibrillar collagen displays varied features between tumours expressing VEGFA120 and VEGFA188 (Fig. 4.2, 4.3 and 4.4). Even though the migration capacity is comparable between VEGFA120- and VEGFA188-expressing cells on aligned fibre scaffolds, the fibrillar collagen in the tumour expressing VEGFA188 is randomly distributed. Fibrosarcoma cells expressing VEGFA188 may be able to adapt to the fibrillar collagen environment, but downregulation of enzymes that participate in ECM modification may lead to impaired metastatic potential (Barker et al., 2012; Qi et al., 2018). Cells expressing different VEGFA isoforms diversely modified the surrounding ECM structure resulting in a pro-metastasis or anti-metastasis microenvironment between VEGFA120- and VEGFA188-expressing fibrosarcoma cells *in vivo*. In comparison, measuring the expression of ECM-modifying enzymes between cells

expressing VEGFA120 and VEGFA188 and the migration capacity of cells on random fibre scaffold may reveal if the differential expression of ECM-modifying enzymes is a factor that modulates metastatic potential.

7.3 Investigating the potential molecular mechanisms in VEGFA-induced cell migration

The induced expression of Sox2 acquires stemness and cell plasticity, facilitating EMT and increasing migration capacity and invasiveness in breast and colorectal cancer (Basu-Roy et al., 2012; Kim et al., 2017). The expression of Sox2 was increased in fs120 cells compared with VEGFA120-1.3 and -2.2 clones. However, the plasticity in modes of cell migration was comparable across VEGFA120-expressing cells, suggesting VEGFA120-induced Sox2 expression in fs120 cells is independent of the regulation of cell plasticity. Although the expression of Sox2 enhances cell plasticity in cancer cells from epithelial origins, it may promote cell renewal in fibroblast-derived cancer cells, resulting in resistance to chemotherapy (Basu-Roy et al., 2012; Feng et al., 2013).

Downregulation of migration capacity in VEGFA120-expressing cells treated with B20.4.1.1, an anti-VEGFA antibody, was observed on 2D fibronectin-coated surfaces and 3D fibre scaffolds, indicating VEGFA120 may participate in the regulation of VEGFA-induced cell migration. VEGFA-induced autophosphorylation of Y794 and Y1213 in VEGFR1 promotes cell migration through PLCγ and PI3K/Akt signalling pathway in endothelial cells (Weddell et al., 2018) and colorectal cancer (Zhou et al., 2015). The expression of p-Akt in VEGFA120-expressing cells was only decreased with pazopanib treatment, an RTKI that inhibits VEGFR1, PDGFR-β and FGFR, whereas there was no effect in the expression of p-Akt treated with B20.4.1.1, anti-VEGFA antibody, and MF-1, an anti-VEGFR1 antibody. These observations illustrate that receptors other than VEGFR1 are activated by VEGFA120 binding and regulate cell migration.

7.4 Future Direction

7.4.1 Animal study

English *et al*. suggested fibrosarcoma cells expressing VEGFA120 have better

plasticity in cell migration correlated to better metastatic potential (English et al., 2017; unpublished data, Yu-Chin Lee MSc thesis). However, these cells derived from embryonic fibroblasts may have experienced different levels of differentiation, supported by the varied expression of Sox2 between fs120 and fs188 cells (Fig. 3.31). This raises the concern of whether the differential plasticity in cell migration relies on the expression of different VEGFA isoforms. Although we have successfully developed new fibrosarcoma cell lines that express a single VEGFA isoform from VEGFA knockout adult fibroblasts, their cellular behaviours and metastatic potential in animal models are undefined due to time limitations. We so far conclude the migration capacity of new fibrosarcoma cells that express VEGFA120 or VEGFA188 on 2D ECM-coated surfaces or 3D fibre scaffolds is comparable to fs120 and fs188 cells used in the previous study and shares a similar response pattern to anti-VEGFA therapy, suggesting newly developed VEGFA120-expressing cells may have better metastatic potential. After characterising the efficiency of metastasis in new cell lines *in vivo* in the future, we can confirm if the regulation of cell plasticity is VEGFA isoform-dependent.

To solidify the links between metastatic potential and plasticity in modes of cell migration, we can examine the cell plasticity of metastatic fibrosarcoma cells isolated from either lung capillaries post 48 hours intravenous injection or metastases in the distant site by forcing them to utilize different migration modes on the different engineered environments. Our hypothesis strengthens if cells with better metastatic potential adapt to altered microenvironments with different migration modes. Furthermore, later we can send non-metastatic and metastatic fibrosarcoma cells sorted in animal models to proteomic analysis for differences in phosphoproteome, which may provide a better hint at the mechanisms regulating cell plasticity. In addition, our designed *in vitro* platform can be utilised to determine the metastatic potential of cancer cells and their response to the metastasis inhibitory therapies in an animal-free manner, reaching the 3Rs recommended by NC3Rs.

7.4.2 Alternative molecular mechanism in the regulation of cell migration

It has been suggested that other receptors interact with VEGFA and respond to pazopanib participating in the regulation of cell migration. PDGFRs, c-Kit and FGFR are the receptors most sensitive to pazopanib and initiate signal transduction down to PI3K kinase (Lee et al., 2019), which modulates cell migration (Zhou et al., 2015). Ball

et al. have shown the binding of VEGFA to PDGFRs induces cell migration in mesenchymal stem cells (Ball et al., 2007). Moreover, the inhibition of signal transduction through PDGFRs and VEGFRs by pazopanib represses the outgrowth of brain metastases in breast cancer (Gril et al., 2011). Therefore, PDGFRs may be a promising target that involves in the control of VEGFA-induced cell migration. Performing single-cell migration assay across cell lines on different environments with pazopanib or inhibitors specifically targeting PDGFRs would provide supportive information if PDGFRs contribute to the mediation of cell migration. Together with measuring the protein expression of p-PDGFRs and p-Akt across cell lines treated with pazopanib and PDGFRs-specific inhibitors may provide enough information to confirm if VEGFA-activated PDGFRs and its downstream Akt is the key regulation of cell migration.

7.5 Conclusion

Characterisation of embryonic versus adult fibroblast-derived fibrosarcomas expressing a single VEGFA isoform has shown there are VEGFA isoform-independent changes between the model systems. However, reduced migration in fibrosarcoma cells expressing VEGFA120 in response to the anti-VEGFA antibody, B20.4.1.1, was independent of cell origin, suggesting the suppression of metastasis *in vivo* published previously could be a universal phenomenon in fibrosarcoma and perhaps more widely in sarcomas and other cancers. Data from this thesis comparing 2D migration with fibre migration indicates the differential expression of single VEGFA isoforms may not contribute to the modulation of plasticity in cell migration. However, in results from my previous MSc thesis, the motility of fs188 cells was significantly reduced in the confined non-adherent chambers compared with fs120 cells. Sadly, time did not allow this to be repeated with the new, adult-derived single isoform expressing fibrosarcomas, but regulation of cell plasticity could be confirmed to be VEGFA isoform-dependent if these experiments are conducted in future. Characterisation of changes in signalling pathways associated with VEGFA showed upregulation of p-VEGFR1 in VEGFA120-expressing cells treated with anti-VEGFA and pazopanib, whereas downregulation of p-Akt was observed only with pazopanib treatment. These effects were not seen with MF-1. These results suggest receptors other than VEGFR1 could interact with VEGFA120 to regulate pVEGFR1, pAkt and cell migration. In conclusion, the

expression of VEGFA120 may potentially increase cell migration and plasticity through another receptor, besides VEGFR1 interacting with VEGFA. This signalling pathway is affected explicitly by the anti-VEGFA antibody and pazopanib, an RTKI that inhibits VEGFR1, PDGFR-β and FGFR, suggesting new avenues for investigation.

References

Aceto, N. et al. (2014). Circulating Tumor Cell Clusters Are Oligoclonal Precursors of Breast Cancer Metastasis. *Cell*, 158(5), 1110–1122.

Afik, R., Zigmond, E., Vugman, M., Klepfish, M., Shimshoni, E., Pasmanik-Chor, M., Shenoy, A., Bassat, E., Halpern, Z., Geiger, T., Sagi, I. & Varol, C. (2016). Tumor Macrophages Are Pivotal Constructors of Tumor Collagenous Matrix. *The Journal of experimental medicine*, 213(11), 2315–2331.

Ahmed, N., Riley, C., Rice, G. & Quinn, M. (2005). Role of Integrin Receptors for Fibronectin, Collagen and Laminin in the Regulation of Ovarian Carcinoma Functions in Response to a Matrix Microenvironment. *Clinical and Experimental Metastasis*, 22(5), 391–402.

Akerman, S., Fisher, M., Daniel, R. A., Lefley, D., Reyes-Aldasoro, C. C., Lunt, S. J., Harris, S., Bjorndahl, M., Williams, L. J., Evans, H., Barber, P. R., Prise, V. E., Vojnovic, B., Kanthou, C. & Tozer, G. M. (2013). Influence of Soluble or Matrix-Bound Isoforms of Vascular Endothelial Growth Factor-A on Tumor Response to Vascular-Targeted Strategies. *International Journal of Cancer*, 133(11), 2563–2576.

Akiri, G., Sabo, E., Dafni, H., Vadasz, Z., Kartvelishvily, Y., Gan, N., Kessler, O., Cohen, T., Resnick, M., Neeman, M. & Neufeld, G. (2003). Lysyl Oxidase-Related Protein-1 Promotes Tumor Fibrosis and Tumor Progression in Vivo. *Cancer research*, 63(7), 1657–1666.

Albritton, J. L. & Miller, J. S. (2017). 3D Bioprinting: Improving in Vitro Models of Metastasis with Heterogeneous Tumor Microenvironments. *Disease Models & Mechanisms*, 10(1), 3–14. Retrieved from https://doi.org/10.1242/dmm.025049

Ali, N., Yoshizumi, M., Fujita, Y., Izawa, Y., Kanematsu, Y., Ishizawa, K., Tsuchiya, K., Yano, S., Sone, S. & Tamaki, T. (2005). A Novel Src Kinase Inhibitor, M475271, Inhibits VEGF-Induced Human Umbilical Vein Endothelial Cell Proliferation and Migration. *Journal of Pharmacological Sciences*, 98(2), 130–141.

Amin, E. M. et al. (2011). WT1 Mutants Reveal SRPK1 to Be a Downstream Angiogenesis Target by Altering VEGF Splicing. *Cancer Cell*.

Asghar, W., El Assal, R., Shafiee, H., Pitteri, S., Paulmurugan, R. & Demirci, U. (2015). Engineering Cancer Microenvironments for in Vitro 3-D Tumor Models. *Materials Today*, 18(10), 539–553.

El Baba, N., Farran, M., Khalil, E. A., Jaafar, L., Fakhoury, I. & El-Sibai, M. (2020). The Role of Rho GTPases in VEGF Signaling in Cancer Cells. *Analytical Cellular Pathology*, 2020.

Bambace, N. M. & Holmes, C. E. (2011). The Platelet Contribution to Cancer Progression. *Journal of thrombosis and haemostasis : JTH*, 9(2), 237–249.

Bareiss, P. M., Paczulla, A., Wang, H., Schairer, R., Wiehr, S., Kohlhofer, U., Rothfuss, O. C., Fischer, A., Perner, S., Staebler, A., Wallwiener, D., Fend, F., Fehm, T., Pichler, B., Kanz, L., Quintanilla-Martinez, L., Schulze-Osthoff, K., Essmann, F. & Lengerke, C. (2013). SOX2 Expression Associates with Stem Cell State in Human Ovarian Carcinoma. *Cancer Research*, 73(17), 5544–5555.

Barker, H. E., Cox, T. R. & Erler, J. T. (2012). The Rationale for Targeting the LOX Family in Cancer. *Nature reviews. Cancer*, 12(8), 540–552.

Bauer, A. L., Jackson, T. L. & Jiang, Y. (2009). Topography of Extracellular Matrix Mediates Vascular Morphogenesis and Migration Speeds in Angiogenesis. *PLoS Computational Biology*, 5(7).

Benckert, C., Jonas, S., Cramer, T., Von Marschall, Z., Schäfer, G., Peters, M., Wagner, K., Radke, C., Wiedenmann, B., Neuhaus, P., Höcker, M. & Rosewicz, S. (2003). Transforming Growth Factor Beta 1 Stimulates Vascular Endothelial Growth Factor Gene Transcription in Human Cholangiocellular Carcinoma Cells. *Cancer research*, 63(5), 1083–1092.

Bergamaschi, A., Tagliabue, E., Sørlie, T., Naume, B., Triulzi, T., Orlandi, R., Russnes, H. G., Nesland, J. M., Tammi, R., Auvinen, P., Kosma, V. M., Ménard, S. & Børresen-Dale, A. L. (2008). Extracellular Matrix Signature Identifies Breast Cancer Subgroups with Different Clinical Outcome. *Journal of Pathology*, 214(3), 357–367.

Beunk, L., Helvert, S. Van, Bekker, B., Ran, L., Kang, R., Paulat, T., Syga, S., Deutsch, A., Friedl, P. & Wolf, K. (2022). Extracellular Matrix Guidance Determines Proteolytic and Non-Proteolytic Cancer Cell Patterning. *bioRxiv preprint*.

Borjigin, M., Eskridge, C., Niamat, R., Strouse, B., Bialk, P. & Kmiec, E. B. (2013). Electrospun Fiber Membranes Enable Proliferation of Genetically Modified Cells. *International Journal of Nanomedicine*, 8, 855–864.

Brabletz, T., Jung, A., Reu, S., Porzner, M., Hlubek, F., Kunz-Schughart, L. A., Knuechel, R. & Kirchner, T. (2001). Variable β-Catenin Expression in Colorectal Cancers Indicates Tumor Progression Driven by the Tumor Environment. *Proceedings of the National Academy of Sciences*, 98(18), 10356–10361.

Bredholt, G., Mannelqvist, M., Stefansson, I. M., Birkeland, E., Bø, T. H., Øyan, A. M., Trovik, J., Kalland, K. H., Jonassen, I., Salvesen, H. B., Wik, E. & Akslen, L. A. (2015). Tumor Necrosis Is an Important Hallmark of Aggressive Endometrial Cancer and Associates with Hypoxia, Angiogenesis and Inflammation Responses. *Oncotarget*, 6(37), 39676–39691.

Brennan, S. E., Kuwano, Y., Alkharouf, N., Blackshear, P. J., Gorospe, M. & Wilson, G. M. (2009). The MRNA-Destabilizing Protein Tristetraprolin Is Suppressed in Many Cancers, Altering Tumorigenic Phenotypes and Patient Prognosis. *Cancer research*, 69(12), 5168–5176.

Bryan, B. A., Walshe, T. E., Mitchell, D. C., Havumaki, J. S., Saint-Geniez, M., Maharaj, A. S., Maldonado, A. E. & D'Amore, P. A. (2007). Coordinated Vascular Endothelial Growth Factor Expression and Signaling During Skeletal Myogenic Differentiation. *Molecular Biology of the Cell*, 19(3), 994–1006.

Budczies, J., von Winterfeld, M., Klauschen, F., Bockmayr, M., Lennerz, J. K., Denkert, C., Wolf, T., Warth, A., Dietel, M., Anagnostopoulos, I., Weichert, W., Wittschieber, D. & Stenzinger, A. (2015). The Landscape of Metastatic Progression Patterns across Major Human Cancers. *Oncotarget*, 6(1), 570–583.

Burke, R. M., Madden, K. S., Perry, S. W., Zettel, M. L. & Brown, E. B. 3rd. (2013). Tumor-Associated Macrophages and Stromal TNF-α Regulate Collagen Structure in a Breast Tumor Model as Visualized by Second Harmonic Generation. *Journal of biomedical optics*, 18(8), 86003.

Cai, J., Xia, L., Li, J., Ni, S., Song, H. & Wu, X. (2019). Tumor-Associated Macrophages Derived TGF-β-Induced Epithelial to Mesenchymal Transition in Colorectal Cancer Cells through Smad2,3-4/Snail Signaling Pathway. *Cancer Research and Treatment*, 51(1), 252–256.

Caicedo-Carvajal, C. E., Liu, Q., Remache, Y., Goy, A. & Suh, K. S. (2011). Cancer Tissue Engineering: A Novel 3D Polystyrene Scaffold for In Vitro Isolation and Amplification of Lymphoma Cancer Cells from Heterogeneous Cell Mixtures. *Journal of tissue engineering*, 2011, 362326.

Calvo, F., Ege, N., Grande-Garcia, A., Hooper, S., Jenkins, R. P., Chaudhry, S. I., Harrington, K., Williamson, P., Moeendarbary, E., Charras, G. & Sahai, E. (2013). Mechanotransduction and YAP-Dependent Matrix Remodelling Is Required for the Generation and Maintenance of Cancer-Associated Fibroblasts. *Nature Cell Biology*, 15(6), 637–646.

Canty, E. G. & Kadler, K. E. (2005). Procollagen Trafficking, Processing and Fibrillogenesis. *Journal of Cell Science*, 118(7), 1341–1353.

Carmeliet, P., Ferreira, V., Breier, G., Pollefeyt, S., Kieckens, L., Gertsenstein, M., Fahrig, M., Vandenhoeck, A., Harpal, K., Eberhardt, C., Declercq, C., Pawling, J., Moons, L., Collen, D., Risau, W. & Nagy, A. (1996). Abnormal Blood Vessel Development and Lethality in Embryos Lacking a Single VEGF Allele. *Nature*, 380(6573), 435–439.

Carmeliet, P. & Jain, R. K. (2011). Molecular Mechanisms and Clinical Applications of Angiogenesis. *Nature*, 473(7347), 298–307.

Carmeliet, P., Ng, Y. S., Nuyens, D., Theilmeier, G., Brusselmans, K., Cornelissen, I., Ehler, E., Kakkar, V. V., Stalmans, I., Mattot, V., Perriard, J. C., Dewerchin, M., Flameng, W., Nagy, A., Lupu, F., Moons, L., Collen, D., D'Amore, P. A. & Shima, D. T. (1999). Impaired Myocardial Angiogenesis and Ischemic Cardiomyopathy in Mice Lacking the Vascular Endothelial Growth Factor Isoforms VEGF164 and VEGF188. *Nature Medicine*.

Carragher, N. O., Walker, S. M., Scott Carragher, L. A., Harris, F., Sawyer, T. K., Brunton, V. G., Ozanne, B. W. & Frame, M. C. (2006). Calpain 2 and Src Dependence Distinguishes Mesenchymal and Amoeboid Modes of Tumour Cell Invasion: A Link to Integrin Function. *Oncogene*, 25(42), 5726–5740.

Ceci, C., Atzori, M. G., Lacal, P. M. & Graziani, G. (2020). Role of VEGFs/VEGFR-1 Signaling and Its Inhibition in Modulating Tumor Invasion: Experimental Evidence in Different Metastatic Cancer Models. *International journal of molecular sciences*, 21(4).

Chamoun, K., Kantarjian, H., Atallah, R., Gonzalez, G. N., Issa, G. C., Rios, M. B., Garcia-Manero, G., Borthakur, G., Ravandi, F., Jain, N., Daver, N., Konopleva, M., DiNardo, C. D., Kadia, T., Pemmaraju, N., Jabbour, E. & Cortes, J. (2019). Tyrosine Kinase Inhibitor Discontinuation in Patients with Chronic Myeloid Leukemia: A Single-Institution Experience. *Journal of hematology & oncology*, 12(1), 1.

Chanvorachote, P., Chunhacha, P. & Pongrakhananon, V. (2014). Caveolin-1 Induces Lamellipodia Formation via an Akt-Dependent Pathway. *Cancer Cell International*, 14(1), 1–9.

Chekhonin, V. P., Shein, S. A., Korchagina, A. A. & Gurina, O. I. (2013). VEGF in Tumor Progression and Targeted Therapy. *Current cancer drug targets*, 13(4), 423–443.

Chen, C. H., Lai, J. M., Chou, T. Y., Chen, C. Y., Su, L. J., Lee, Y. C., Cheng, T. S., Hong, Y. R., Chou, C. K., Whang-Peng, J., Wu, Y. C. & Huang, C. Y. F. (2009). VEGFA Upregulates FLJ10540 and Modulates Migration and Invasion of Lung

Cancer via PI3K/AKT Pathway. *PLoS ONE*, 4(4).

Chen, H., Cheng, Y., Wang, X., Wang, J., Shi, X., Li, X., Tan, W. & Tan, Z. (2020). 3D Printed in Vitro Tumor Tissue Model of Colorectal Cancer. *Theranostics*, 10(26), 12127–12143.

Chen, L., Liu, S. & Tao, Y. (2020). Regulating Tumor Suppressor Genes: Post-Translational Modifications. *Signal Transduction and Targeted Therapy*, 5(1).

Choi, J. Y., Jang, Y. S., Min, S. Y. & Song, J. Y. (2011). Overexpression of MMP-9 and Hif-1α in Breast Cancer Cells under Hypoxic Conditions. *Journal of Breast Cancer*, 14(2), 88–95.

Conacci-Sorrell, M., Zhurinsky, J. & Ben-Ze'ev, A. (2002). The Cadherin-Catenin Adhesion System in Signaling and Cancer. *Journal of Clinical Investigation*, 109(8), 987–991.

Conklin, M. W., Eickhoff, J. C., Riching, K. M., Pehlke, C. A., Eliceiri, K. W., Provenzano, P. P., Friedl, A. & Keely, P. J. (2011). Aligned Collagen Is a Prognostic Signature for Survival in Human Breast Carcinoma. *American Journal of Pathology*.

Cooke, V. G., LeBleu, V. S., Keskin, D., Khan, Z., O'Connell, J. T., Teng, Y., Duncan, M. B., Xie, L., Maeda, G., Vong, S., Sugimoto, H., Rocha, R. M., Damascena, A., Brentani, R. R. & Kalluri, R. (2012). Pericyte Depletion Results in Hypoxia-Associated Epithelial-to-Mesenchymal Transition and Metastasis Mediated by Met Signaling Pathway. *Cancer Cell*, 21(1), 66–81. Retrieved from http://dx.doi.org/10.1016/j.ccr.2011.11.024

Cox, T. R., Bird, D., Baker, A.-M., Barker, H. E., Ho, M. W.-Y., Lang, G. & Erler, J. T. (2013). LOX-Mediated Collagen Crosslinking Is Responsible for Fibrosis-Enhanced Metastasis. *Cancer research*, 73(6), 1721–1732.

Dardente, H., English, W. R., Valluru, M. K., Kanthou, C. & Simpson, D. (2020). Debunking the Myth of the Endogenous Antiangiogenic Vegfaxxxb Transcripts. *Trends in endocrinology and metabolism: TEM*, 31(6), 398–409.

Darland, D. C., Cain, J. T., Berosik, M. A., Saint-Geniez, M., Odens, P. W., Schaubhut, G. J., Frisch, S., Stemmer-Rachamimov, A., Darland, T. & D'Amore, P. A. (2011). Vascular Endothelial Growth Factor (VEGF) Isoform Regulation of Early Forebrain Development. *Developmental biology*, 358(1), 9–22.

Dellinger, M. T. & Brekken, R. A. (2011). Phosphorylation of Akt and ERK1/2 Is Required for VEGF-A/VEGFR2-Induced Proliferation and Migration of Lymphatic Endothelium. *PLoS ONE*, 6(12).

Denève, E., Riethdorf, S., Ramos, J., Nocca, D., Coffy, A., Daurès, J.-P., Maudelonde, T., Fabre, J.-M., Pantel, K. & Alix-Panabières, C. (2013). Capture of Viable Circulating Tumor Cells in the Liver of Colorectal Cancer Patients. *Clinical chemistry*, 59(9), 1384–1392.

Derksen, P. W. B., Liu, X., Saridin, F., van der Gulden, H., Zevenhoven, J., Evers, B., van Beijnum, J. R., Griffioen, A. W., Vink, J., Krimpenfort, P., Peterse, J. L., Cardiff, R. D., Berns, A. & Jonkers, J. (2006). Somatic Inactivation of E-Cadherin and P53 in Mice Leads to Metastatic Lobular Mammary Carcinoma through Induction of Anoikis Resistance and Angiogenesis. *Cancer Cell*, 10(5), 437–449.

Doyle, A. D., Carvajal, N., Jin, A., Matsumoto, K. & Yamada, K. M. (2015). Local 3D Matrix Microenvironment Regulates Cell Migration through Spatiotemporal Dynamics of Contractility-Dependent Adhesions. *Nature Communications*, 6.

Doyle, A. D., Kutys, M. L., Conti, M. A., Matsumoto, K., Adelstein, R. S. & Yamada, K. M. (2012). Micro-Environmental Control of Cell Migration - Myosin IIA Is Required for Efficient Migration in Fibrillar Environments through Control of Cell Adhesion Dynamics. *Journal of Cell Science*, 125(9), 2244–2256.

Doyle, A. D., Wang, F. W., Matsumoto, K. & Yamada, K. M. (2009). One-Dimensional Topography Underlies Three-Dimensional Fibrillar Cell Migration. *Journal of Cell Biology*, 184(4), 481–490.

Duda, D. G., Duyverman, A. M. M. J., Kohno, M., Snuderl, M., Steller, E. J. A., Fukumura, D. & Jain, R. K. (2010). Malignant Cells Facilitate Lung Metastasis by Bringing Their Own Soil. *Proceedings of the National Academy of Sciences of the United States of America*, 107(50), 21677–21682.

Dvinge, H., Kim, E., Abdel-Wahab, O. & Bradley, R. K. (2016). RNA Splicing Factors as Oncoproteins and Tumour Suppressors. *Nature reviews. Cancer*, 16(7), 413–430.

Eisinger-Mathason, T. S. K., Zhang, M., Qiu, Q., Skuli, N., Nakazawa, M. S., Karakasheva, T., Mucaj, V., Shay, J. E. S., Stangenberg, L., Sadri, N., Puré, E., Yoon, S. S., Kirsch, D. G. & Simon, M. C. (2013). Hypoxia-Dependent Modification of Collagen Networks Promotes Sarcoma Metastasis. *Cancer Discovery*, 3(10), 1190–1205.

Ellerbroek, S. M., Wu, Y. I., Overall, C. M. & Stack, M. S. (2001). Functional Interplay between Type I Collagen and Cell Surface Matrix Metalloproteinase Activity. *Journal of Biological Chemistry*, 276(27), 24833–24842.

English, W. R., Lunt, S. J., Fisher, M., Lefley, D. V., Dhingra, M., Lee, Y. C., Bingham,

K., Hurrell, J. E., Lyons, S. K., Kanthou, C. & Tozer, G. M. (2017). Differential Expression of VEGFA Isoforms Regulates Metastasis and Response to Anti-VEGFA Therapy in Sarcoma. *Cancer Research*, 77(10), 2633–2646.

Erler, J. T., Bennewith, K. L., Nicolau, M., Dornhöfer, N., Kong, C., Le, Q.-T., Chi, J.-T. A., Jeffrey, S. S. & Giaccia, A. J. (2006a). Lysyl Oxidase Is Essential for Hypoxia-Induced Metastasis. *Nature*, 440(7088), 1222–6.

Erler, J. T., Bennewith, K. L., Nicolau, M., Dornhöfer, N., Kong, C., Le, Q.-T., Chi, J.-T. A., Jeffrey, S. S. & Giaccia, A. J. (2006b). Lysyl Oxidase Is Essential for Hypoxia-Induced Metastasis. *Nature*, 440(7088), 1222–6. Retrieved from http://www.ncbi.nlm.nih.gov/pubmed/16642001

Esbona, K., Yi, Y., Saha, S., Yu, M., Van Doorn, R. R., Conklin, M. W., Graham, D. S., Wisinski, K. B., Ponik, S. M., Eliceiri, K. W., Wilke, L. G. & Keely, P. J. (2018). The Presence of Cyclooxygenase 2, Tumor-Associated Macrophages, and Collagen Alignment as Prognostic Markers for Invasive Breast Carcinoma Patients. *The American journal of pathology*, 188(3), 559–573.

Estabridis, H. M., Jana, A., Nain, A. & Odde, D. J. (2018). Cell Migration in 1D and 2D Nanofiber Microenvironments. *Annals of Biomedical Engineering*, 46(3), 392–403.

Eustace, A., Irlam, J. J., Taylor, J., Denley, H., Agrawal, S., Choudhury, A., Ryder, D., Ord, J. J., Harris, A. L., Rojas, A. M., Hoskin, P. J. & West, C. M. L. (2013). Necrosis Predicts Benefit from Hypoxia-Modifying Therapy in Patients with High Risk Bladder Cancer Enrolled in a Phase III Randomised Trial. *Radiotherapy and Oncology*, 108(1), 40–47.

Fackler, O. T. & Grosse, R. (2008). Cell Motility through Plasma Membrane Blebbing. *The Journal of cell biology*, 181(6), 879–884.

Fares, J., Fares, M. Y., Khachfe, H. H., Salhab, H. A. & Fares, Y. (2020). Molecular Principles of Metastasis: A Hallmark of Cancer Revisited. *Signal Transduction and Targeted Therapy*, 5(1). Retrieved from http://dx.doi.org/10.1038/s41392-020-0134-x

Fearnley, G. W., Bruns, A. F., Wheatcroft, S. B. & Ponnambalam, S. (2015). VEGF-A Isoform-Specific Regulation of Calcium Ion Flux, Transcriptional Activation and Endothelial Cell Migration. *Biology Open*, 4(6), 731–742.

Fearnley, G. W., Smith, G. A., Abdul-Zani, I., Yuldasheva, N., Mughal, N. A., Homer-Vanniasinkam, S., Kearney, M. T., Zachary, I. C., Tomlinson, D. C., Harrison, M. A., Wheatcroft, S. B. & Ponnambalam, S. (2016). VEGF-A Isoforms Program

Differential VEGFR2 Signal Transduction, Trafficking and Proteolysis. *Biology Open*, 5(5), 571–583.

Feinberg, T. Y., Zheng, H., Liu, R., Wicha, M. S., Yu, S. M. & Weiss, S. J. (2018). Divergent Matrix-Remodeling Strategies Distinguish Developmental from Neoplastic Mammary Epithelial Cell Invasion Programs. *Developmental Cell*, 47(2), 145-160.e6.

Feng, B. H., Liu, A. G., Gu, W. G., Deng, L., Cheng, X. G., Tong, T. J. & Zhang, H. Z. (2013). CD133+ Subpopulation of the HT1080 Human Fibrosarcoma Cell Line Exhibits Cancer Stem-like Characteristics. *Oncology Reports*, 30(2), 815–823.

Feng, R. & Wen, J. (2015). Overview of the Roles of Sox2 in Stem Cell and Development. *Biological Chemistry*, 396(8), 883–891.

Feng, S., Duan, X., Lo, P.-K., Liu, S., Liu, X., Chen, H. & Wang, Q. (2013). Expansion of Breast Cancer Stem Cells with Fibrous Scaffolds. *Integrative Biology*, 5(5), 768–777.

Ferrara, N. (2010). Binding to the Extracellular Matrix and Proteolytic Processing: Two Key Mechanisms Regulating Vascular Endothelial Growth Factor Action. *Molecular Biology of the Cell*, 21(5), 687–690.

Ferrara, N. & Davis-Smyth, T. (1997). The Biology of Vascular Endothelial Growth Factor. *Endocrine Reviews*, 18(1), 4–25.

Ferrara, N., Gerber, H. P. & LeCouter, J. (2003). The Biology of VEGF and Its Receptors. *Nature Medicine*, 9(6), 669–676.

Ferrara, N. & Henzel, W. J. (1989). Pituitary Follicular Cells Secrete a Novel Heparin-Binding Growth Factor Specific for Vascular Endothelial Cells. *Biochemical and biophysical research communications*, 161(2), 851–858.

Ferreira, L. P., Gaspar, V. M. & Mano, J. F. (2020). Decellularized Extracellular Matrix for Bioengineering Physiomimetic 3D in Vitro Tumor Models. *Trends in biotechnology*, 38(12), 1397–1414.

Ferreira, L. P., Gaspar, V. M., Mendes, L., Duarte, I. F. & Mano, J. F. (2021). Organotypic 3D Decellularized Matrix Tumor Spheroids for High-Throughput Drug Screening. *Biomaterials*, 275, 120983.

Fidalgo, M. F., Fonseca, C. G., Caldas, P., Raposo, A. A., Balboni, T., Henao-Mišíková, L., Grosso, A. R., Vasconcelos, F. F. & Franco, C. A. (2022). Aerocyte Specification and Lung Adaptation to Breathing Is Dependent on Alternative Splicing Changes. *Life science alliance*, 5(12).

Fischbach, C., Chen, R., Matsumoto, T., Schmelzle, T., Brugge, J. S., Polverini, P. J. & Mooney, D. J. (2007). Engineering Tumors with 3D Scaffolds. *Nature Methods*, 4(10), 855–860.

Fong, G. H., Rossant, J., Gertsenstein, M. & Breitman, M. L. (1995). Role of the Flt-1 Receptor Tyrosine Kinase in Regulating the Assembly of Vascular Endothelium. *Nature*, 376(6535), 66–70.

Forker, L., Gaunt, P., Sioletic, S., Shenjere, P., Potter, R., Roberts, D., Irlam, J., Valentine, H., Hughes, D., Hughes, A., Billingham, L., Grimer, R., Seddon, B., Choudhury, A., Robinson, M. & West, C. M. L. (2018). The Hypoxia Marker CAIX Is Prognostic in the UK Phase III VorteX-Biobank Cohort: An Important Resource for Translational Research in Soft Tissue Sarcoma. *British journal of cancer*, 118(5), 698–704.

Forsythe, J. A., Jiang, B. H., Iyer, N. V, Agani, F., Leung, S. W., Koos, R. D. & Semenza, G. L. (1996). Activation of Vascular Endothelial Growth Factor Gene Transcription by Hypoxia-Inducible Factor 1. *Molecular and Cellular Biology*, 16(9), 4604–4613.

Fouad, Y. A. & Aanei, C. (2017). Revisiting the Hallmarks of Cancer. *American journal of cancer research*, 7(5), 1016–1036.

Freire-de-Lima, L., Gelfenbeyn, K., Ding, Y., Mandel, U., Clausen, H., Handa, K. & Hakomori, S.-I. (2011). Involvement of O-Glycosylation Defining Oncofetal Fibronectin in Epithelial-Mesenchymal Transition Process. *Proceedings of the National Academy of Sciences of the United States of America*, 108(43), 17690–17695.

Friedl, P. (2004). Prespecification and Plasticity: Shifting Mechanisms of Cell Migration. *Current Opinion in Cell Biology*, 16(1), 14–23.

Friedl, P. & Alexander, S. (2011). Cancer Invasion and the Microenvironment: Plasticity and Reciprocity. *Cell*.

Friedl, P. & Gilmour, D. (2009). Collective Cell Migration in Morphogenesis, Regeneration and Cancer. *Nature Reviews Molecular Cell Biology*, 10(7), 445–457.

Friedl, P. & Weigelin, B. (2008). Interstitial Leukocyte Migration and Immune Function. *Nature immunology*, 9(9), 960–969.

Friedl, P., Zänker, K. S. & Bröcker, E. B. (1998). Cell Migration Strategies in 3-D Extracellular Matrix: Differences in Morphology, Cell Matrix Interactions, and Integrin Function. *Microscopy Research and Technique*, 43(5), 369–378.

Gao, Y., Wang, Z., Hao, Q., Li, W., Xu, Y., Zhang, J., Zhang, Wangqian, Wang, S., Liu, S., Li, M., Xue, X., Zhang, Wei, Zhang, C. & Zhang, Y. (2017). Loss of ERα Induces Amoeboid-like Migration of Breast Cancer Cells by Downregulating Vinculin. *Nature communications*, 8, 14483.

Garcia, A. M., Magalhes, F. L., Soares, J. S., Junior, E. P., Lima, M. F. R. D., Mamede, M. & Paula, A. M. D. (2018). Second Harmonic Generation Imaging of the Collagen Architecture in Prostate Cancer Tissue. *Biomedical Physics and Engineering Express*, 4(2).

Gay, L. J. & Felding-Habermann, B. (2011). Contribution of Platelets to Tumour Metastasis. *Nature Reviews Cancer*.

Gerber, H. P., Condorelli, F., Park, J. & Ferrara, N. (1997). Differential Transcriptional Regulation of the Two Vascular Endothelial Growth Factor Receptor Genes. Flt-1, but Not Flk-1/KDR, Is up-Regulated by Hypoxia. *The Journal of biological chemistry*, 272(38), 23659–23667.

Gerhardt, H., Golding, M., Fruttiger, M., Ruhrberg, C., Lundkvist, A., Abramsson, A., Jeltsch, M., Mitchell, C., Alitalo, K., Shima, D. & Betsholtz, C. (2003). VEGF Guides Angiogenic Sprouting Utilizing Endothelial Tip Cell Filopodia. *The Journal of cell biology*, 161(6), 1163–1177.

Gilbert, M. R. et al. (2014). A Randomized Trial of Bevacizumab for Newly Diagnosed Glioblastoma. *The New England journal of medicine*, 370(8), 699–708.

Goel, H. L. & Mercurio, A. M. (2013). VEGF Targets the Tumour Cell. *Nature Reviews Cancer*, 13(12), 871–882.

Gong, J., Zhu, S., Zhang, Y. & Wang, J. (2014). Interplay of VEGFa and MMP2 Regulates Invasion of Glioblastoma. *Tumor Biology*, 35(12), 11879–11885.

Gonzalez, D. M. & Medici, D. (2014). Signaling Mechanisms of the Epithelial-Mesenchymal Transition. *Science Signaling*, 7(344), re8.

Graziani, V., Rodriguez-Hernandez, I., Maiques, O. & Sanz-Moreno, V. (2022). The Amoeboid State as Part of the Epithelial-to-Mesenchymal Transition Programme. *Trends in Cell Biology*, 32(3), 228–242.

Grossman, M., Ben-Chetrit, N., Zhuravlev, A., Afik, R., Bassat, E., Solomonov, I., Yarden, Y. & Sagi, I. (2016). Tumor Cell Invasion Can Be Blocked by Modulators of Collagen Fibril Alignment That Control Assembly of the Extracellular Matrix. *Cancer Research*, 76(14), 4249–4258.

Gumbiner, B. M. (1996). Cell Adhesion: The Molecular Basis of Tissue Architecture and Morphogenesis. *Cell*, 84(3), 345–357.

Gumbiner, B. M. (2005). Regulation of Cadherin-Mediated Adhesion in Morphogenesis. *Nature Reviews Molecular Cell Biology*, 6(8), 622–634.

Gupta, G. P., Nguyen, D. X., Chiang, A. C., Bos, P. D., Kim, J. Y., Nadal, C., Gomis, R. R., Manova-Todorova, K. & Massagué, J. (2007). Mediators of Vascular Remodelling Co-Opted for Sequential Steps in Lung Metastasis. *Nature*, 446(7137), 765–70.

Guyot, M. & Pagès, G. (2015). VEGF Splicing and the Role of VEGF Splice Variants: From Physiological-Pathological Conditions to Specific Pre-MRNA Splicing. *Methods in molecular biology (Clifton, N.J.)*, 1332, 3–23.

Han, K. Y., Dugas-Ford, J., Lee, H., Chang, J. H. & Azar, D. T. (2015). MMP14 Cleavage of VEGFR1 in the Cornea Leads to a VEGF-Trap Antiangiogenic Effect. *Investigative Ophthalmology and Visual Science*, 56(9), 5450–5456.

Han, X., Fang, X., Lou, X., Hua, D., Ding, W., Foltz, G., Hood, L., Yuan, Y. & Lin, B. (2012). Silencing SOX2 Induced Mesenchymal-Epithelial Transition and Its Expression Predicts Liver and Lymph Node Metastasis of CRC Patients. *PLoS ONE*, 7(8).

Hanahan, D. (2022). Hallmarks of Cancer: New Dimensions. *Cancer Discovery*, 12(1), 31–46.

Hanahan, D. & Weinberg, R. A. (2011). Hallmarks of Cancer: The next Generation. *Cell*, 144(5), 646–674.

Harada, T., Swift, J., Irianto, J., Shin, J.-W., Spinler, K. R., Athirasala, A., Diegmiller, R., Dingal, P. C. D. P., Ivanovska, I. L. & Discher, D. E. (2014). Nuclear Lamin Stiffness Is a Barrier to 3D Migration, but Softness Can Limit Survival. *The Journal of cell biology*, 204(5), 669–682.

Harris, S., Craze, M., Newton, J., Fisher, M., Shima, D. T., Tozer, G. M. & Kanthou, C. (2012). Do Anti-Angiogenic VEGF (VEGFxxxb) Isoforms Exist? A Cautionary Tale. *PloS one*, 7(5), e35231.

Hashimoto, N., Kitai, R., Fujita, S., Yamauchi, T., Isozaki, M. & Kikuta, K. I. (2022). Single-Cell Analysis of Unidirectional Migration of Glioblastoma Cells Using a Fiber-Based Scaffold. *ACS Applied Bio Materials*.

Hatcher, J. M., Wu, G., Zeng, C., Zhu, J., Meng, F., Patel, S., Wang, W., Ficarro, S. B., Leggett, A. L., Powell, C. E., Marto, J. A., Zhang, K., Ki Ngo, J. C., Fu, X.-D., Zhang, T. & Gray, N. S. (2018). SRPKIN-1: A Covalent SRPK1/2 Inhibitor That Potently Converts VEGF from Pro-Angiogenic to Anti-Angiogenic Isoform. *Cell chemical biology*, 25(4), 460-470.e6.

Hayakawa, K., Pham, L.-D. D., Som, A. T., Lee, B. J., Guo, S., Lo, E. H. & Arai, K. (2011). Vascular Endothelial Growth Factor Regulates the Migration of Oligodendrocyte Precursor Cells. *The Journal of neuroscience : the official journal of the Society for Neuroscience*, 31(29), 10666–10670.

Hazan, R. B., Qiao, R., Keren, R., Badano, I. & Suyama, K. (2004). Cadherin Switch in Tumor Progression. *Annals of the New York Academy of Sciences*, 1014, 155–163.

He, Y., Ren, Y., Wu, B., Decourt, B., Lee, A. C., Taylor, A. & Suter, D. M. (2015). Src and Cortactin Promote Lamellipodia Protrusion and Filopodia Formation and Stability in Growth Cones. *Molecular Biology of the Cell*, 26(18), 3229–3244.

Herzog, B., Pellet-Many, C., Britton, G., Hartzoulakis, B. & Zachary, I. C. (2011). VEGF Binding to NRP1 Is Essential for VEGF Stimulation of Endothelial Cell Migration, Complex Formation between NRP1 and VEGFR2, and Signaling via FAK Tyr407 Phosphorylation. *Molecular Biology of the Cell*, 22(15), 2766–2776.

Hill, R. M. et al. (2015). Combined MYC and P53 Defects Emerge at Medulloblastoma Relapse and Define Rapidly Progressive, Therapeutically Targetable Disease. *Cancer Cell*, 27(1), 72–84.

Hiratsuka, S., Maru, Y., Okada, A., Seiki, M., Noda, T. & Shibuya, M. (2001). Involvement of Flt-1 Tyrosine Kinase (Vascular Endothelial Growth Factor Receptor-1) in Pathological Angiogenesis. *Cancer research*, 61(3), 1207–1213.

Hiratsuka, S., Minowa, O., Kuno, J., Noda, T. & Shibuya, M. (1998). Flt-1 Lacking the Tyrosine Kinase Domain Is Sufficient for Normal Development and Angiogenesis in Mice. *Proceedings of the National Academy of Sciences of the United States of America*, 95(16), 9349–9354.

Hiratsuka, S., Nakamura, K., Iwai, S., Murakami, M., Itoh, T., Kijima, H., Shipley, J. M., Senior, R. M. & Shibuya, M. (2002). MMP9 Induction by Vascular Endothelial Growth Factor Receptor-1 Is Involved in Lung-Specific Metastasis. *Cancer Cell*, 2(4), 289–300.

Holle, A. W., Govindan Kutty Devi, N., Clar, K., Fan, A., Saif, T., Kemkemer, R. & Spatz, J. P. (2019). Cancer Cells Invade Confined Microchannels via a Self-Directed Mesenchymal-to-Amoeboid Transition. *Nano Letters*, 19(4), 2280–2290.

Holliday, D. L., Brouilette, K. T., Markert, A., Gordon, L. A. & Jones, J. L. (2009). Novel Multicellular Organotypic Models of Normal and Malignant Breast: Tools for Dissecting the Role of the Microenvironment in Breast Cancer Progression. *Breast cancer research : BCR*, 11(1), R3.

Holmqvist, K., Cross, M. J., Rolny, C., Hägerkvist, R., Rahimi, N., Matsumoto, T., Claesson-Welsh, L. & Welsh, M. (2004). The Adaptor Protein Shb Binds to Tyrosine 1175 in Vascular Endothelial Growth Factor (VEGF) Receptor-2 and Regulates VEGF-Dependent Cellular Migration. *The Journal of biological chemistry*, 279(21), 22267–22275.

Hu, Y., Lu, J., Xu, X., Lyu, J. & Zhang, H. (2017). Regulation of Focal Adhesion Turnover in SDF-1α-Stimulated Migration of Mesenchymal Stem Cells in Neural Differentiation. *Scientific Reports*, 7(1), 1–14.

Huang, H. (2021). Proteolytic Cleavage of Receptor Tyrosine Kinases. *Biomolecules*, 11(5), 1–24.

Huang, M., Fu, M., Wang, J., Xia, C., Zhang, H., Xiong, Y., He, J., Liu, J., Liu, B., Pan, S. & Liu, F. (2021). TGF-B1-Activated Cancer-Associated Fibroblasts Promote Breast Cancer Invasion, Metastasis and Epithelial-Mesenchymal Transition by Autophagy or Overexpression of FAP-α. *Biochemical Pharmacology*, 188.

Huang, M., Huang, B., Li, G. & Zeng, S. (2018). Apatinib Affect VEGF-Mediated Cell Proliferation, Migration, Invasion via Blocking VEGFR2/RAF/MEK/ERK and PI3K/AKT Pathways in Cholangiocarcinoma Cell. *BMC Gastroenterology*, 18(1), 1–10.

Hutmacher, D. W., Loessner, D., Rizzi, S., Kaplan, D. L., Mooney, D. J. & Clements, J. A. (2010). Can Tissue Engineering Concepts Advance Tumor Biology Research? *Trends in Biotechnology*, 28(3), 125–133.

Huttenlocher, A. & Horwitz, A. R. (2011). Integrins in Cell Migration. *Cold Spring Harbor Perspectives in Biology*, 3(9), 1–16.

Hwang, Y., Seo, T., Hariri, S., Choi, C. & Varghese, S. (2017). Matrix Topographical Cue-Mediated Myogenic Differentiation of Human Embryonic Stem Cell Derivatives. *Polymers*, 9(11).

Hynes, R. O. (2002). Integrins: Bidirectional, Allosteric Signaling Machines. *Cell*, 110(6), 673–687.

Hynes, R. O. & Lander, A. D. (1992). Contact and Adhesive Specificities in the Associations, Migrations, and Targeting of Cells and Axons. *Cell*, 68(2), 303–322.

Ibo, M., Srivastava, V., Robinson, D. N. & Gagnon, Z. R. (2016). Cell Blebbing in Confined Microfluidic Environments. *PLoS ONE*, 11(10), 1–18.

Jansson, S., Bendahl, P.-O., Larsson, A.-M., Aaltonen, K. E. & Rydén, L. (2016). Prognostic Impact of Circulating Tumor Cell Apoptosis and Clusters in Serial Blood Samples from Patients with Metastatic Breast Cancer in a Prospective

Observational Cohort. *BMC cancer*, 16, 433.

Kanapathipillai, M., Mammoto, A., Mammoto, T., Kang, J. H., Jiang, E., Ghosh, K., Korin, N., Gibbs, A., Mannix, R. & Ingber, D. E. (2012). Inhibition of Mammary Tumor Growth Using Lysyl Oxidase-Targeting Nanoparticles to Modify Extracellular Matrix. *Nano Letters*, 12(6), 3213–3217.

Kanthou, C., Dachs, G. U., Lefley, D. V., Steele, A. J., Coralli-Foxon, C., Harris, S., Greco, O., Dos Santos, S. A., Reyes-Aldasoro, C. C., English, W. R. & Tozer, G. M. (2014). Tumour Cells Expressing Single VEGF Isoforms Display Distinct Growth, Survival and Migration Characteristics. *PLoS ONE*, 9(8).

Kasurinen, A., Tervahartiala, T., Laitinen, A., Kokkola, A. & Sorsa, T. (2018). High Serum MMP-14 Predicts Worse Survival in Gastric Cancer. *PLoS ONE*, 13(12), 1–11.

Keck, P. J., Hauser, S. D., Krivi, G., Sanzo, K., Warren, T., Feder, J. & Connolly, D. T. (1989). Vascular Permeability Factor, an Endothelial Cell Mitogen Related to PDGF. *Science (New York, N.Y.)*, 246(4935), 1309–1312.

Keely, P. J., Westwick, J. K., Whitehead, I. P., Der, C. J. & Parise, L. V. (1997). Cdc42 and Rac1 Induce Integrin-Mediated Cell Motility and Invasiveness through PI(3)K. *Nature*, 390(6660), 632–636.

Kendall, R. L. & Thomas, K. A. (1993). Inhibition of Vascular Endothelial Cell Growth Factor Activity by an Endogenously Encoded Soluble Receptor. *Proceedings of the National Academy of Sciences of the United States of America*, 90(22), 10705–10709.

Keyt, B. A., Berleau, L. T., Nguyen, H. V., Chen, H., Heinsohn, H., Vandlen, R. & Ferrara, N. (1996). The Carboxyl-Terminal Domain (111-165) of Vascular Endothelial Growth Factor Is Critical for Its Mitogenic Potency. *Journal of Biological Chemistry*.

Kim, E., Lisby, A., Ma, C., Lo, N., Ehmer, U., Hayer, K. E., Furth, E. E. & Viatour, P. (2019). Promotion of Growth Factor Signaling as a Critical Function of β-Catenin during HCC Progression. *Nature Communications*, 10(1), 1909.

Kim, H. W., Lim, J. H., Kim, M. Y., Chung, S., Shin, S. J., Chung, H. W., Choi, B. S., Kim, Y.-S., Chang, Y. S. & Park, C. W. (2011). Long-Term Blockade of Vascular Endothelial Growth Factor Receptor-2 Aggravates the Diabetic Renal Dysfunction Associated with Inactivation of the Akt/ENOS-NO Axis. *Nephrology Dialysis Transplantation*, 26(4), 1173–1188.

Kim, M., Jang, K., Miller, P., Picon-Ruiz, M., Yeasky, T. M., El-Ashry, D. &

Slingerland, J. M. (2017). VEGFA Links Self-Renewal and Metastasis by Inducing Sox2 to Repress MiR-452, Driving Slug. *Oncogene*, 36(36), 5199–5211.

Kiso, M., Tanaka, S., Saji, S., Toi, M. & Sato, F. (2018a). Long Isoform of VEGF Stimulates Cell Migration of Breast Cancer by Filopodia Formation via NRP1/ARHGAP17/Cdc42 Regulatory Network. *International Journal of Cancer*, 143(11), 2905–2918.

Kiso, M., Tanaka, S., Saji, S., Toi, M. & Sato, F. (2018b). Long Isoform of VEGF Stimulates Cell Migration of Breast Cancer by Filopodia Formation via NRP1/ARHGAP17/Cdc42 Regulatory Network. *International Journal of Cancer*.

Kontomanolis, E. N., Koutras, A., Syllaios, A., Schizas, D., Mastoraki, A., Garmpis, N., Diakosavvas, M., Angelou, K., Tsatsaris, G., Pagkalos, A., Ntounis, T. & Fasoulakis, Z. (2020). Role of Oncogenes and Tumor-Suppressor Genes in Carcinogenesis: A Review. *Anticancer Research*, 40(11), 6009–6015.

Kosla, J., Paňková, D., Plachý, J., Tolde, O., Bicanová, K., Dvořák, M., Rösel, D. & Brábek, J. (2013). Metastasis of Aggressive Amoeboid Sarcoma Cells Is Dependent on Rho/ROCK/MLC Signaling. *Cell communication and signaling : CCS*, 11, 51.

Kraning-Rush, C. M., Califano, J. P. & Reinhart-King, C. A. (2012). Cellular Traction Stresses Increase with Increasing Metastatic Potential. *PloS one*, 7(2), e32572.

Krishnamachary, B., Zagzag, D., Nagasawa, H., Rainey, K., Okuyama, H., Baek, J. H. & Semenza, G. L. (2006). Hypoxia-Inducible Factor-1-Dependent Repression of E-Cadherin in von Hippel-Lindau Tumor Suppressor-Null Renal Cell Carcinoma Mediated by TCF3, ZFHX1A, and ZFHX1B. *Cancer Research*, 66(5), 2725–2731.

Kubow, K. E., Shuklis, V. D., Sales, D. J. & Horwitz, A. R. (2017). Contact Guidance Persists under Myosin Inhibition Due to the Local Alignment of Adhesions and Individual Protrusions. *Scientific Reports*, 7(1), 1–15.

Labelle, M., Begum, S. & Hynes, R. O. (2011). Direct Signaling between Platelets and Cancer Cells Induces an Epithelial-Mesenchymal-Like Transition and Promotes Metastasis. *Cancer Cell*, 20(5), 576–590.

Labelle, M. & Hynes, R. O. (2012). The Initial Hours of Metastasis: The Importance of Cooperative Host-Tumor Cell Interactions during Hematogenous Dissemination. *Cancer discovery*, 2(12), 1091–1099.

Lamalice, L., Houle, F. & Huot, J. (2006). Phosphorylation of Tyr1214 within VEGFR-2 Triggers the Recruitment of Nck and Activation of Fyn Leading to SAPK2/P38 Activation and Endothelial Cell Migration in Response to VEGF. *Journal of*

Biological Chemistry.

Lamalice, L., Houle, F., Jourdan, G. & Huot, J. (2004). Phosphorylation of Tyrosine 1214 on VEGFR2 Is Required for VEGF-Induced Activation of Cdc42 Upstream of SAPK2/P38. *Oncogene*, 23(2), 434–445.

Langer, E. M., Allen-Petersen, B. L., King, S. M., Kendsersky, N. D., Turnidge, M. A., Kuziel, G. M., Riggers, R., Samatham, R., Amery, T. S., Jacques, S. L., Sheppard, B. C., Korkola, J. E., Muschler, J. L., Thibault, G., Chang, Y. H., Gray, J. W., Presnell, S. C., Nguyen, D. G. & Sears, R. C. (2019). Modeling Tumor Phenotypes In Vitro with Three-Dimensional Bioprinting. *Cell reports*, 26(3), 608-623.e6.

Langley, R. R. & Fidler, I. J. (2011). The Seed and Soil Hypothesis Revisited-The Role of Tumor-Stroma Interactions in Metastasis to Different Organs. *International Journal of Cancer*, 128(11), 2527–2535.

Lee, A. T. J., Jones, R. L. & Huang, P. H. (2019). Pazopanib in Advanced Soft Tissue Sarcomas. *Signal Transduction and Targeted Therapy*, 4(1), 1–10. Retrieved from http://dx.doi.org/10.1038/s41392-019-0049-6

Lee, E. Y. H. P. & Muller, W. J. (2010). Oncogenes and Tumor Suppressor Genes. *Cold Spring Harbor perspectives in biology*, 2(10), a003236.

Lee, S., Jilan, S. M., Nikolova, G. V., Carpizo, D. & Luisa Iruela-Arispe, M. (2005). Processing of VEGF-A by Matrix Metalloproteinases Regulates Bioavailability and Vascular Patterning in Tumors. *Journal of Cell Biology*.

Leis, O., Eguiara, A., Lopez-Arribillaga, E., Alberdi, M. J., Hernandez-Garcia, S., Elorriaga, K., Pandiella, A., Rezola, R. & Martin, A. G. (2012). Sox2 Expression in Breast Tumours and Activation in Breast Cancer Stem Cells. *Oncogene*, 31(11), 1354–1365.

Leung, D. W., Cachianes, G., Kuang, W. J., Goeddel, D. V & Ferrara, N. (1989). Vascular Endothelial Growth Factor Is a Secreted Angiogenic Mitogen. *Science (New York, N.Y.)*, 246(4935), 1306–1309.

Levental, K. R., Yu, H., Kass, L., Lakins, J. N., Egeblad, M., Erler, J. T., Fong, S. F. T., Csiszar, K., Giaccia, A., Weninger, W., Yamauchi, M., Gasser, D. L. & Weaver, V. M. (2009). Matrix Crosslinking Forces Tumor Progression by Enhancing Integrin Signaling. *Cell*, 139(5), 891–906.

Li, R., Zhuang, Y., Han, M., Xu, T. & Wu, X. (2013). PiggyBac as a High-Capacity Transgenesis and Gene-Therapy Vector in Human Cells and Mice. *DMM Disease Models and Mechanisms*, 6(3), 828–833.

Li, T., Zhu, Y., Han, L., Ren, W., Liu, H. & Qin, C. (2015). VEGFR-1 Activation-

Induced MMP-9-Dependent Invasion in Hepatocellular Carcinoma. *Future Oncology*, 11(23), 3143–3157.

Li, W., Gupta, S. K., Han, W., Kundson, R. A., Nelson, S., Knutson, D., Greipp, P. T., Elsawa, S. F., Sotomayor, E. M. & Gupta, M. (2019). Targeting MYC Activity in Double-Hit Lymphoma with MYC and BCL2 and/or BCL6 Rearrangements with Epigenetic Bromodomain Inhibitors. *Journal of Hematology and Oncology*, 12(1), 1–13.

Li, X. J., Peng, L. X., Shao, J. Y., Lu, W. H., Zhang, J. X., Chen, S., Chen, Z. Y., Xiang, Y. Q., Bao, Y. N., Zheng, F. J., Zeng, M. S., Kang, T. B., Zeng, Y. X., Teh, B. T. & Qian, C. N. (2012). As an Independent Unfavorable Prognostic Factor, IL-8 Promotes Metastasis of Nasopharyngeal Carcinoma through Induction of Epithelial-Mesenchymal Transition and Activation of AKT Signaling. *Carcinogenesis*, 33(7), 1302–1309.

Liang, W. C., Wu, X., Peale, F. V., Lee, C. V., Meng, Y. G., Gutierrez, J., Fu, L., Malik, A. K., Gerber, H. P., Ferrara, N. & Fuh, G. (2006). Cross-Species Vascular Endothelial Growth Factor (VEGF)-Blocking Antibodies Completely Inhibit the Growth of Human Tumor Xenografts and Measure the Contribution of Stromal VEGF. *Journal of Biological Chemistry*, 281(2), 951–961.

Lichtenberger, B. M., Tan, P. K., Niederleithner, H., Ferrara, N., Petzelbauer, P. & Sibilia, M. (2010). Autocrine VEGF Signaling Synergizes with EGFR in Tumor Cells to Promote Epithelial Cancer Development. *Cell*, 140(2), 268–279.

Liu, C., Zhang, W., Wang, J., Si, T. & Xing, W. (2021). Tumor-Associated Macrophage-Derived Transforming Growth Factor-β Promotes Colorectal Cancer Progression through HIF1-TRIB3 Signaling. *Cancer Science*, 112(10), 4198–4207.

Liu, J., Huang, C. & Zhan, X. (1999). Src Is Required for Cell Migration and Shape Changes Induced by Fibroblast Growth Factor. *Oncogene*, 18(48), 6700–6706.

Liu, X. F., Yang, W. T., Xu, R., Liu, J. T. & Zheng, P. S. (2014). Cervical Cancer Cells with Positive Sox2 Expression Exhibit the Properties of Cancer Stem Cells. *PLoS ONE*, 9(1), 1–12.

Liu, Y., Berendsen, A. D., Jia, S., Lotinun, S., Baron, R., Ferrara, N. & Olsen, B. R. (2012). Intracellular VEGF Regulates the Balance between Osteoblast and Adipocyte Differentiation. *Journal of Clinical Investigation*, 122(9), 3101–3113.

Liu, Y., Cox, S. R., Morita, T. & Kourembanas, S. (1995). Hypoxia Regulates Vascular Endothelial Growth Factor Gene Expression in Endothelial Cells. *Circulation*

research, 77(3), 638–643.

Long, T. J., Sprenger, C. C., Plymate, S. R. & Ratner, B. D. (2014). Prostate Cancer Xenografts Engineered from 3D Precision-Porous Poly(2-Hydroxyethyl Methacrylate) Hydrogels as Models for Tumorigenesis and Dormancy Escape. *Biomaterials*, 35(28), 8164–8174.

Lyu, Y., Xiao, Q., Yin, L., Yang, L. & He, W. (2019). Potent Delivery of an Mmp Inhibitor to the Tumor Microenvironment with Thermosensitive Liposomes for the Suppression of Metastasis and Angiogenesis. *Signal Transduction and Targeted Therapy*, 4(1). Retrieved from http://dx.doi.org/10.1038/s41392-019-0054-9

Malandrino, A., Mak, M., Trepat, X. & Kamm, R. D. (2017). Non-Elastic Remodeling of the 3D Extracellular Matrix by Cell-Generated Forces. *bioRxiv*.

Mamer, S. B., Chen, S., Weddell, J. C., Palasz, A., Wittenkeller, A., Kumar, M. & Imoukhuede, P. I. (2017). Discovery of High-Affinity PDGF-VEGFR Interactions: Redefining RTK Dynamics. *Scientific Reports*, 7(1), 1–14.

Manakhov, A., Kedroňová, E., Medalová, J., Černochová, P., Obrusník, A., Michlíček, M., Shtansky, D. V & Zajíčková, L. (2017). Carboxyl-Anhydride and Amine Plasma Coating of PCL Nanofibers to Improve Their Bioactivity. *Materials and Design*, 132, 257–265.

Mani, S. A., Guo, W., Liao, M. J., Eaton, E. N., Ayyanan, A., Zhou, A. Y., Brooks, M., Reinhard, F., Zhang, C. C., Shipitsin, M., Campbell, L. L., Polyak, K., Brisken, C., Yang, J. & Weinberg, R. A. (2008). The Epithelial-Mesenchymal Transition Generates Cells with Properties of Stem Cells. *Cell*, 133(4), 704–715.

Maragathavally, K. J., Kaminski, J. M., Coates, C. J., Maragathavally, K. J., Kaminski, J. M. & Coates, C. J. (2006). Chimeric Mos1 and PiggyBac Transposases Result in Site-directed Integration . *The FASEB Journal*, 20(11), 1880–1882.

Masià, A., Almazán-Moga, A., Velasco, P., Reventós, J., Torán, N., Sánchez De Toledo, J., Roma, J. & Gallego, S. (2012). Notch-Mediated Induction of N-Cadherin and A9-Integrin Confers Higher Invasive Phenotype on Rhabdomyosarcoma Cells. *British Journal of Cancer*, 107(8), 1374–1383.

Massagué, J. & Obenauf, A. C. (2016). Metastatic Colonization by Circulating Tumour Cells. *Nature*, 529(7586), 298–306.

Matsumoto, T., Bohman, S., Dixelius, J., Berge, T., Dimberg, A., Magnusson, P., Wang, L., Wikner, C., Qi, J. H., Wernstedt, C., Wu, J., Bruheim, S., Mugishima, H., Mukhopadhyay, D., Spurkland, A. & Claesson-Welsh, L. (2005). VEGF

Receptor-2 Y951 Signaling and a Role for the Adapter Molecule TSAd in Tumor Angiogenesis. *The EMBO journal*, 24(13), 2342–2353.

Matsuoka, J., Yashiro, M., Doi, Y., Fuyuhiro, Y., Kato, Y., Shinto, O., Noda, S., Kashiwagi, S., Aomatsu, N., Hirakawa, T., Hasegawa, T., Shimizu, K., Shimizu, T., Miwa, A., Yamada, N., Sawada, T. & Hirakawa, K. (2013). Hypoxia Stimulates the EMT of Gastric Cancer Cells through Autocrine TGFβ Signaling. *PLoS ONE*, 8(5).

Di Matteo, A., Belloni, E., Pradella, D., Cappelletto, A., Volf, N., Zacchigna, S. & Ghigna, C. (2020). Alternative Splicing in Endothelial Cells: Novel Therapeutic Opportunities in Cancer Angiogenesis. *Journal of Experimental and Clinical Cancer Research*, 39(1), 1–19.

Mazzocchi, A., Devarasetty, M., Herberg, S., Petty, W. J., Marini, F., Miller, L., Kucera, G., Dukes, D. K., Ruiz, J., Skardal, A. & Soker, S. (2019). Pleural Effusion Aspirate for Use in 3D Lung Cancer Modeling and Chemotherapy Screening. *ACS biomaterials science & engineering*, 5(4), 1937–1943.

Mendoza, M. C., Er, E. E., Zhang, W., Ballif, B. A., Elliott, H. L., Danuser, G. & Blenis, J. (2011). ERK-MAPK Drives Lamellipodia Protrusion by Activating the WAVE2 Regulatory Complex. *Molecular Cell*, 41(6), 661–671.

Milanini, J., Viñals, F., Pouysségur, J. & Pagès, G. (1998). P42/P44 MAP Kinase Module Plays a Key Role in the Transcriptional Regulation of the Vascular Endothelial Growth Factor Gene in Fibroblasts. *The Journal of biological chemistry*, 273(29), 18165–18172.

Morel, A. P., Lièvre, M., Thomas, C., Hinkal, G., Ansieau, S. & Puisieux, A. (2008). Generation of Breast Cancer Stem Cells through Epithelial-Mesenchymal Transition. *PLoS ONE*, 3(8), 1–7.

Morgan, P., Brown, D. G., Lennard, S., Anderton, M. J., Barrett, J. C., Eriksson, U., Fidock, M., Hamrén, B., Johnson, A., March, R. E., Matcham, J., Mettetal, J., Nicholls, D. J., Platz, S., Rees, S., Snowden, M. A. & Pangalos, M. N. (2018). Impact of a Five-Dimensional Framework on R&D Productivity at AstraZeneca. *Nature Reviews Drug Discovery*, 17(3), 167–181.

Motzer, R. J. et al. (2013). Pazopanib versus Sunitinib in Metastatic Renal-Cell Carcinoma. *The New England journal of medicine*, 369(8), 722–731.

Murlidhar, V., Reddy, R. M., Fouladdel, S., Zhao, L., Ishikawa, M. K., Grabauskiene, S., Zhang, Z., Lin, J., Chang, A. C., Carrott, P., Lynch, W. R., Orringer, M. B., Kumar-Sinha, C., Palanisamy, N., Beer, D. G., Wicha, M. S., Ramnath, N., Azizi,

E. & Nagrath, S. (2017). Poor Prognosis Indicated by Venous Circulating Tumor Cell Clusters in Early-Stage Lung Cancers. *Cancer research*, 77(18), 5194–5206.

Naba, A., Clauser, K. R., Hoersch, S., Liu, H., Carr, S. A. & Hynes, R. O. (2012). The Matrisome: In Silico Definition and in Vivo Characterization by Proteomics of Normal and Tumor Extracellular Matrices. *Molecular and Cellular Proteomics*, 11(4), 1–18.

Nagano, M., Hoshino, D., Koshikawa, N., Akizawa, T. & Seiki, M. (2012). Turnover of Focal Adhesions and Cancer Cell Migration (J. Chung, Ed.). *International Journal of Cell Biology*, 2012, 310616. Retrieved from https://doi.org/10.1155/2012/310616

Nagy, A., Rossant, J., Nagy, R., Abramow-Newerly, W. & Roder, J. C. (1993). Derivation of Completely Cell Culture-Derived Mice from Early-Passage Embryonic Stem Cells. *Proceedings of the National Academy of Sciences of the United States of America*, 90(18), 8424–8428.

Nam, S., Lee, J., Brownfield, D. G. & Chaudhuri, O. (2016). Viscoplasticity Enables Mechanical Remodeling of Matrix by Cells. *Biophysical Journal*, 111(10), 2296–2308.

Narice, B. F., Green, N. H., MacNeil, S. & Anumba, D. (2016). Second Harmonic Generation Microscopy Reveals Collagen Fibres Are More Organised in the Cervix of Postmenopausal Women. *Reproductive Biology and Endocrinology*, 14(1), 1–8.

Nasrollahi, S., Banerjee, S., Qayum, B., Banerjee, P. & Pathak, A. (2017). Nanoscale Matrix Topography Influences Microscale Cell Motility through Adhesions, Actin Organization, and Cell Shape. *ACS Biomaterials Science and Engineering*, 3(11), 2980–2986.

Neufeld, G., Cohen, T., Shraga, N., Lange, T., Kessler, O. & Herzog, Y. (2002). The Neuropilins: Multifunctional Semaphorin and VEGF Receptors That Modulate Axon Guidance and Angiogenesis. *Trends in cardiovascular medicine*, 12(1), 13–19.

Nieswandt, B., Hafner, M., Echtenacher, B. & Männel, D. N. (1999). Lysis of Tumor Cells by Natural Killer Cells in Mice Is Impeded by Platelets. *Cancer research*, 59(6), 1295–1300.

Nobes, C. D. & Hall, A. (1999). Rho GTPases Control Polarity, Protrusion, and Adhesion during Cell Movement. *Journal of Cell Biology*, 144(6), 1235–1244.

Okikawa, S., Morine, Y., Saito, Y., Yamada, S., Tokuda, K., Teraoku, H., Miyazaki, K., Yamashita, S., Ikemoto, T., Imura, S. & Shimada, M. (2022). Inhibition of the VEGF Signaling Pathway Attenuates Tumor-associated Macrophage Activity in Liver Cancer. *Oncology reports*, 47(4).

Oltean, S., Gammons, M., Hulse, R., Hamdollah-Zadeh, M., Mavrou, A., Donaldson, L., Salmon, A. H., Harper, S. J., Ladomery, M. R. & Bates, D. O. (2012). SRPK1 Inhibition in Vivo: Modulation of VEGF Splicing and Potential Treatment for Multiple Diseases, in: *Biochemical Society Transactions*.

Onder, T. T., Gupta, P. B., Mani, S. A., Yang, J., Lander, E. S. & Weinberg, R. A. (2008). Loss of E-Cadherin Promotes Metastasis via Multiple Downstream Transcriptional Pathways. *Cancer Research*, 68(10), 3645–3654.

Oommen, S., Gupta, S. K. & Vlahakis, N. E. (2011). Vascular Endothelial Growth Factor A (VEGF-A) Induces Endothelial and Cancer Cell Migration through Direct Binding to Integrin A9β1: Identification of a Specific A9β1 Binding Site. *Journal of Biological Chemistry*, 286(2), 1083–1092.

Orgaz, J. L., Pandya, P., Dalmeida, R., Karagiannis, P., Sanchez-Laorden, B., Viros, A., Albrengues, J., Nestle, F. O., Ridley, A. J., Gaggioli, C., Marais, R., Karagiannis, S. N. & Sanz-Moreno, V. (2014). Diverse Matrix Metalloproteinase Functions Regulate Cancer Amoeboid Migration. *Nature communications*, 5, 4255.

Orr, M. T. & Lanier, L. L. (2010). Natural Killer Cell Education and Tolerance. *Cell*, 142(6), 847–856.

Ottosson, M., Jakobsson, A. & Johansson, F. (2017). Accelerated Wound Closure - Differently Organized Nanofibers Affect Cell Migration and Hence the Closure of Artificial Wounds in a Cell Based in Vitro Model. *PLoS ONE*, 12(1), 1–15.

Pa, P. (2003). Matrix Metalloproteinase-2 (MMP-2) Is Associated with Survival in Breast Carcinoma. , 2, 1270–1275.

Padmanaban, V., Krol, I., Suhail, Y., Szczerba, B. M., Aceto, N., Bader, J. S. & Ewald, A. J. (2019). E-Cadherin Is Required for Metastasis in Multiple Models of Breast Cancer. *Nature*, 573(7774), 439–444.

Padua, D., Zhang, X. H.-F., Wang, Q., Nadal, C., Gerald, W. L., Gomis, R. R. & Massagué, J. (2008). TGFbeta Primes Breast Tumors for Lung Metastasis Seeding through Angiopoietin-like 4. *Cell*, 133(1), 66–77.

Pàez-Ribes, M., Allen, E., Hudock, J., Takeda, T., Okuyama, H., Viñals, F., Inoue, M., Bergers, G., Hanahan, D. & Casanovas, O. (2009). Antiangiogenic Therapy Elicits

Malignant Progression of Tumors to Increased Local Invasion and Distant Metastasis. *Cancer Cell*, 15(3), 220–231.

Paget, S. (1989). The Distribution of Secondary Growths in Cancer of the Breast. 1889. *Cancer metastasis reviews*, 8(2), 98–101.

Pan, Q. et al. (2007). Blocking Neuropilin-1 Function Has an Additive Effect with Anti-VEGF to Inhibit Tumor Growth. *Cancer cell*, 11(1), 53–67.

Parekh, A., Ruppender, N. S., Branch, K. M., Sewell-Loftin, M. K., Lin, J., Boyer, P. D., Candiello, O. E., Merryman, W. D., Guelcher, S. A. & Weaver, A. M. (2011). Sensing and Modulation of Invadopodia across a Wide Range of Rigidities. *Biophysical Journal*, 100(3), 573–582.

Parri, M. & Chiarugi, P. (2010). Rac and Rho GTPases in Cancer Cell Motility Control. *Cell Communication and Signaling*, 8, 1–14.

Paten, J. A., Martin, C. L., Wanis, J. T., Siadat, S. M., Figueroa-Navedo, A. M., Ruberti, J. W. & Deravi, L. F. (2019). Molecular Interactions between Collagen and Fibronectin: A Reciprocal Relationship That Regulates De Novo Fibrillogenesis. *Chem*, 5(8), 2126–2145.

Pawlak, G. & Helfman, D. M. (2001). Cytoskeletal Changes in Cell Transformation and Tumorigenesis. *Current Opinion in Genetics and Development*, 11(1), 41–47.

Pein, M., Insua-Rodríguez, J., Hongu, T., Riedel, A., Meier, J., Wiedmann, L., Decker, K., Essers, M. A. G., Sinn, H. P., Spaich, S., Sütterlin, M., Schneeweiss, A., Trumpp, A. & Oskarsson, T. (2020). Metastasis-Initiating Cells Induce and Exploit a Fibroblast Niche to Fuel Malignant Colonization of the Lungs. *Nature Communications*, 11(1), 1–18. Retrieved from http://dx.doi.org/10.1038/s41467-020-15188-x

Peppas, N. A., Hilt, J. Z., Khademhosseini, A. & Langer, R. (2006). Hydrogels in Biology and Medicine: From Molecular Principles to Bionanotechnology. *Advanced Materials*, 18(11), 1345–1360.

Perren, T. J. et al. (2011). A Phase 3 Trial of Bevacizumab in Ovarian Cancer. *The New England journal of medicine*, 365(26), 2484–2496.

Placke, T., Örgel, M., Schaller, M., Jung, G., Rammensee, H. G., Kopp, H. G. & Salih, H. R. (2012). Platelet-Derived MHC Class I Confers a Pseudonormal Phenotype to Cancer Cells That Subverts the Antitumor Reactivity of Natural Killer Immune Cells. *Cancer Research*.

Plouët, J., Schilling, J. & Gospodarowicz, D. (1989). Isolation and Characterization of a Newly Identified Endothelial Cell Mitogen Produced by AtT-20 Cells. *The*

EMBO journal, 8(12), 3801–3806.

Presta, L. G., Chen, H., O'Connor, S. J., Chisholm, V., Meng, Y. G., Krummen, L., Winkler, M. & Ferrara, N. (1997). Humanization of an Anti-Vascular Endothelial Growth Factor Monoclonal Antibody for the Therapy of Solid Tumors and Other Disorders. *Cancer Research*, 57(20), 4593–4599.

Provenzano, P. P., Eliceiri, K. W., Campbell, J. M., Inman, D. R., White, J. G. & Keely, P. J. (2006). Collagen Reorganization at the Tumor-Stromal Interface Facilitates Local Invasion. *BMC Medicine*.

Provenzano, P. P., Inman, D. R., Eliceiri, K. W., Knittel, J. G., Yan, L., Rueden, C. T., White, J. G. & Keely, P. J. (2008). Collagen Density Promotes Mammary Tumor Initiation and Progression. *BMC Medicine*, 6, 1–15.

Pylayeva-Gupta, Y., Grabocka, E. & Bar-Sagi, D. (2011). RAS Oncogenes: Weaving a Tumorigenic Web. *Nature Reviews Cancer*, 11(11), 761–774.

Pylayeva, Y., Gillen, K. M., Gerald, W., Beggs, H. E., Reichardt, L. F. & Giancotti, F. G. (2009). Ras- and PI3K-Dependent Breast Tumorigenesis in Mice and Humans Requires Focal Adhesion Kinase Signaling. *Journal of Clinical Investigation*, 119(2), 252–266.

Qi, Y. & Xu, R. (2018). Roles of PLODs in Collagen Synthesis and Cancer Progression. *Frontiers in cell and developmental biology*, 6, 66.

Qin, G., Luo, M., Chen, J., Dang, Y., Chen, G., Li, L., Zeng, J., Lu, Y. & Yang, J. (2016). Reciprocal Activation between MMP-8 and TGF-B1 Stimulates EMT and Malignant Progression of Hepatocellular Carcinoma. *Cancer letters*, 374(1), 85–95.

Rak, J., Yu, J. L., Klement, G. & Kerbel, R. S. (2000). Oncogenes and Angiogenesis: Signaling Three-Dimensional Tumor Growth. *The journal of investigative dermatology. Symposium proceedings*, 5(1), 24–33.

Ramirez-San Juan, G. R., Oakes, P. W. & Gardel, M. L. (2017). Contact Guidance Requires Spatial Control of Leading-Edge Protrusion. *Molecular Biology of the Cell*, 28(8), 1043–1053.

Rebelo, S. P., Pinto, C., Martins, T. R., Harrer, N., Estrada, M. F., Loza-Alvarez, P., Cabeçadas, J., Alves, P. M., Gualda, E. J., Sommergruber, W. & Brito, C. (2018). 3D-3-Culture: A Tool to Unveil Macrophage Plasticity in the Tumour Microenvironment. *Biomaterials*, 163, 185–197.

Riching, K. M., Cox, B. L., Salick, M. R., Pehlke, C., Riching, A. S., Ponik, S. M., Bass, B. R., Crone, W. C., Jiang, Y., Weaver, A. M., Eliceiri, K. W. & Keely, P. J. (2015).

3D Collagen Alignment Limits Protrusions to Enhance Breast Cancer Cell Persistence. *Biophysical Journal*, 107(11), 2546–2558.

Richter, P., Junker, K., Franz, M., Berndt, Angela, Geyer, C., Gajda, M., Kosmehl, H., Berndt, Alexander & Wunderlich, H. (2008). IIICS de Novo Glycosylated Fibronectin as a Marker for Invasiveness in Urothelial Carcinoma of the Urinary Bladder (UBC). *Journal of cancer research and clinical oncology*, 134(10), 1059–1065.

Rodenhizer, D., Dean, T., D'Arcangelo, E. & McGuigan, A. P. (2018). The Current Landscape of 3D In Vitro Tumor Models: What Cancer Hallmarks Are Accessible for Drug Discovery? *Advanced healthcare materials*, 7(8), e1701174.

Rodrigues, J., Heinrich, M. A., Teixeira, L. M. & Prakash, J. (2021). 3D In Vitro Model (R)Evolution: Unveiling Tumor–Stroma Interactions. *Trends in Cancer*, 7(3), 249–264.

Rosen, L. S. (2002). Clinical Experience with Angiogenesis Signaling Inhibitors: Focus on Vascular Endothelial Growth Factor (VEGF) Blockers. *Cancer control : journal of the Moffitt Cancer Center*, 9(2 Suppl), 36–44.

Ruan, G. X. & Kazlauskas, A. (2012). Axl Is Essential for VEGF-A-Dependent Activation of PI3K/Akt. *EMBO Journal*, 31(7), 1692–1703.

Ruhrberg, C., Gerhardt, H., Golding, M., Watson, R., Ioannidou, S., Fujisawa, H., Betsholtz, C. & Shima, D. T. (2002). Spatially Restricted Patterning Cues Provided by Heparin-Binding VEGF-A Control Blood Vessel Branching Morphogenesis. *Genes and Development*.

Sabeh, F., Ota, I., Holmbeck, K., Birkedal-Hansen, H., Soloway, P., Balbin, M., Lopez-Otin, C., Shapiro, S., Inada, M., Krane, S., Allen, E., Chung, D. & Weiss, S. J. (2004). Tumor Cell Traffic through the Extracellular Matrix Is Controlled by the Membrane-Anchored Collagenase MT1-MMP. *Journal of Cell Biology*, 167(4), 769–781.

Sahai, E. & Marshall, C. J. (2003). Differing Modes of Tumour Cell Invasion Have Distinct Requirements for Rho/ROCK Signalling and Extracellular Proteolysis. *Nature cell biology*, 5(8), 711–719.

Sahai, E., Olson, M. F. & Marshall, C. J. (2001). Cross-Talk between Ras and Rho Signalling Pathways in Transformation Favours Proliferation and Increased Motility. *EMBO Journal*, 20(4), 755–766.

Sanz-Moreno, V., Gadea, G., Ahn, J., Paterson, H., Marra, P., Pinner, S., Sahai, E. & Marshall, C. J. (2008). Rac Activation and Inactivation Control Plasticity of

Tumor Cell Movement. *Cell*, 135(3), 510–523.

Sase, H., Watabe, T., Kawasaki, K., Miyazono, K. & Miyazawa, K. (2009). VEGFR2-PLCgamma1 Axis Is Essential for Endothelial Specification of VEGFR2+ Vascular Progenitor Cells. *Journal of cell science*, 122(Pt 18), 3303–3311.

Sathe, A. R., Shivashankar, G. V. & Sheetz, M. P. (2016). Nuclear Transport of Paxillin Depends on Focal Adhesion Dynamics and FAT Domains. *Journal of Cell Science*, 129(10), 1981–1988.

Schumacher, D., Strilic, B., Sivaraj, K., Wettschureck, N. & Offermanns, S. (2013). Platelet-Derived Nucleotides Promote Tumor-Cell Transendothelial Migration and Metastasis via P2Y2 Receptor. *Cancer Cell*, 24(1), 130–137.

Schwab, L. P., Peacock, D. L., Majumdar, D., Ingels, J. F., Jensen, L. C., Smith, K. D., Cushing, R. C. & Seagroves, T. N. (2012). Hypoxia-Inducible Factor 1α Promotes Primary Tumor Growth and Tumor-Initiating Cell Activity in Breast Cancer. *Breast Cancer Research*, 14(1), R6.

Seetharam, L., Gotoh, N., Maru, Y., Neufeld, G., Yamaguchi, S. & Shibuya, M. (1995). A Unique Signal Transduction from FLT Tyrosine Kinase, a Receptor for Vascular Endothelial Growth Factor VEGF. *Oncogene*, 10(1), 135–147.

Senger, D. R., Galli, S. J., Dvorak, A. M., Perruzzi, C. A., Susan Harvey, V. & Dvorak, H. F. (1983). Tumor Cells Secrete a Vascular Permeability Factor That Promotes Accumulation of Ascites Fluid. *Science*, 219(4587), 983–985.

Shalaby, F., Rossant, J., Yamaguchi, T. P., Gertsenstein, M., Wu, X. F., Breitman, M. L. & Schuh, A. C. (1995). Failure of Blood-Island Formation and Vasculogenesis in Flk-1-Deficient Mice. *Nature*, 376(6535), 62–66.

Shan, Y., You, B., Shi, S., Shi, W., Zhang, Z., Zhang, Q., Gu, M., Chen, J. & Bao, L. (2018). Hypoxia-Induced Matrix Metalloproteinase- 13 Expression in Exosomes from Nasopharyngeal Carcinoma Enhances Metastases. *Cell Death and Disease*.

Sharma, V. P., Beaty, B. T., Patsialou, A., Liu, H., Clarke, M., Cox, D., Condeelis, J. S. & Eddy, R. J. (2012). Reconstitution of in Vivo Macrophage-Tumor Cell Pairing and Streaming Motility on One-Dimensional Micro-Patterned Substrates. *Intravital*, 1(1), 77–85.

Shen, A., Zhang, Y., Yang, H., Xu, R. & Huang, G. (2012). Overexpression of ZEB1 Relates to Metastasis and Invasion in Osteosarcoma. *Journal of Surgical Oncology*, 105(8), 830–834.

Shen, Y., Shen, R., Ge, L., Zhu, Q. & Li, F. (2012). Fibrillar Type i Collagen Matrices Enhance Metastasis/Invasion of Ovarian Epithelial Cancer via B1 Integrin and

PTEN Signals. *International Journal of Gynecological Cancer*, 22(8), 1316–1324.

Shi, F., Harman, J., Fujiwara, K. & Sottile, J. (2010). Collagen I Matrix Turnover Is Regulated by Fibronectin Polymerization. *American Journal of Physiology - Cell Physiology*, 298(5), 1265–1275.

Shiau, J.-P., Wu, C.-C., Chang, S.-J., Pan, M.-R., Liu, W., Ou-Yang, F., Chen, F.-M., Hou, M.-F., Shih, S.-L. & Luo, C.-W. (2021). FAK Regulates VEGFR2 Expression and Promotes Angiogenesis in Triple-Negative Breast Cancer. *Biomedicines*, 9(12).

Shibata, T., Akiyama, N., Noda, M., Sasai, K. & Hiraoka, M. (1998). Enhancement of Gene Expression under Hypoxic Conditions Using Fragments of the Human Vascular Endothelial Growth Factor and the Erythropoietin Genes. *International Journal of Radiation Oncology, Biology, Physics*, 42(4), 913–916.

Shibata, T., Giaccia, A. J. & Brown, J. M. (2000). Development of a Hypoxia-Responsive Vector for Tumor-Specific Gene Therapy. *Gene Therapy*, 7(6), 493–498.

Shima, D. T., Kuroki, M., Deutsch, U., Ng, Y. S., Adamis, A. P. & D'Amore, P. A. (1996). The Mouse Gene for Vascular Endothelial Growth Factor. Genomic Structure, Definition of the Transcriptional Unit, and Characterization of Transcriptional and Post-Transcriptional Regulatory Sequences. *The Journal of biological chemistry*, 271(7), 3877–3883.

Shiozawa, Y., Nie, B., Pienta, K. J., Morgan, T. M. & Taichman, R. S. (2013). Cancer Stem Cells and Their Role in Metastasis. *Pharmacology and Therapeutics*, 138(2), 285–293.

Short, B. (2012). Stress Fibers Guide Focal Adhesions to Maturity. *Journal of Cell Biology*, 196(3), 301.

Shortt, J. & Johnstone, R. W. (2012). Oncogenes in Cell Survival and Cell Death. *Cold Spring Harbor Perspectives in Biology*, 4(12).

Simons, M., Gordon, E. & Claesson-Welsh, L. (2016). Mechanisms and Regulation of Endothelial VEGF Receptor Signalling. *Nature Reviews Molecular Cell Biology*, 17(10), 611–625.

Sitohy, B., Nagy, J. A. & Dvorak, H. F. (2012). Anti-VEGF/VEGFR Therapy for Cancer: Reassessing the Target. *Cancer research*, 72(8), 1909–1914.

Sleeboom, J. J. F., Amirabadi, H. E., Nair, P., Sahlgren, C. M. & Den Toonder, J. M. J. (2018). Metastasis in Context: Modeling the Tumor Microenvironment with Cancer-on-a-Chip Approaches. *DMM Disease Models and Mechanisms*, 11(3).

Soker, S., Fidder, H., Neufeld, G. & Klagsbrun, M. (1996). Characterization of Novel Vascular Endothelial Growth Factor (VEGF) Receptors on Tumor Cells That Bind VEGF165 via Its Exon 7-Encoded Domain. *The Journal of biological chemistry*, 271(10), 5761–5767.

Soker, S., Miao, H.-Q., Nomi, M., Takashima, S. & Klagsbrun, M. (2002). VEGF165 Mediates Formation of Complexes Containing VEGFR-2 and Neuropilin-1 That Enhance VEGF165-Receptor Binding. *Journal of cellular biochemistry*, 85(2), 357–368.

Soker, S., Takashima, S., Miao, H. Q., Neufeld, G. & Klagsbrun, M. (1998). Neuropilin-1 Is Expressed by Endothelial and Tumor Cells as an Isoform-Specific Receptor for Vascular Endothelial Growth Factor. *Cell*, 92(6), 735–745.

Srinivasan, R., Zabuawala, T., Huang, H., Zhang, J., Gulati, P., Fernandez, S., Karlo, J. C., Landreth, G. E., Leone, G. & Ostrowski, M. C. (2009). Erk1 and Erk2 Regulate Endothelial Cell Proliferation and Migration during Mouse Embryonic Angiogenesis. *PLoS ONE*, 4(12).

Stadlmann, S., Pollheimer, J., Moser, P. L., Raggi, A., Amberger, A., Margreiter, R., Offner, F. A., Mikuz, G., Dirnhofer, S. & Moch, H. (2003). Cytokine-Regulated Expression of Collagenase-2 (MMP-8) Is Involved in the Progression of Ovarian Cancer. *European journal of cancer (Oxford, England : 1990)*, 39(17), 2499–2505.

Stalmans, I., Ng, Y. S., Rohan, R., Fruttiger, M., Bouché, A., Ÿuce, A., Fujisawa, H., Hermans, B., Shani, M., Jansen, S., Hicklin, D., Anderson, D. J., Gardiner, T., Hammes, H. P., Moons, L., Dewerchin, M., Collen, D., Carmeliet, P. & D'Amore, P. A. (2002). Arteriolar and Venular Patterning in Retinas of Mice Selectively Expressing VEGF Isoforms. *Journal of Clinical Investigation*.

Strasser, A., Harris, A. W., Bath, M. L. & Cory, S. (1990). Novel Primitive Lymphoid Tumours Induced in Transgenic Mice by Cooperation between Myc and Bcl-2. *Nature*, 348(6299), 331–333.

Szarvas, T., Hoffmann, M. J., Olah, C., Szekely, E., Kiss, A., Hess, J., Tschirdewahn, S., Hadaschik, B., Grotheer, V., Nyirady, P., Csizmarik, A., Varadi, M. & Reis, H. (2021). Mmp-7 Serum and Tissue Levels Are Associated with Poor Survival in Platinum-Treated Bladder Cancer Patients. *Diagnostics*, 11(1), 10–15.

Takada, Y., Ye, X. & Simon, S. (2007). The Integrins. *Genome Biology*, 8(5).

Takafuji, V., Forgues, M., Unsworth, E., Goldsmith, P. & Wang, X. W. (2007). An Osteopontin Fragment Is Essential for Tumor Cell Invasion in Hepatocellular Carcinoma. *Oncogene*, 26(44), 6361–6371.

Takahashi, T. & Shibuya, M. (1997). The 230 KDa Mature Form of KDR/Flk-1 (VEGF Receptor-2) Activates the PLC-Gamma Pathway and Partially Induces Mitotic Signals in NIH3T3 Fibroblasts. *Oncogene*, 14(17), 2079–2089.

Takahashi, T., Yamaguchi, S., Chida, K. & Shibuya, M. (2001). A Single Autophosphorylation Site on KDR/Flk-1 Is Essential for VEGF-A-Dependent Activation of PLC-Gamma and DNA Synthesis in Vascular Endothelial Cells. *The EMBO journal*, 20(11), 2768–2778.

Tambe, D. T., Hardin, C. C., Angelini, T. E., Rajendran, K., Park, C. Y., Serra-Picamal, X., Zhou, E. H., Zaman, M. H., Butler, J. P., Weitz, D. A., Fredberg, J. J. & Trepat, X. (2011). Collective Cell Guidance by Cooperative Intercellular Forces. *Nature materials*, 10(6), 469–475.

Tanaka, H., Kawaguchi, M., Shoda, S., Miyoshi, T., Iwasaki, R., Hyodo, F., Mori, T., Hara, A., Tomita, H. & Matsuo, M. (2019). Nuclear Accumulation of β-Catenin in Cancer Stem Cell Radioresistance and Stemness in Human Colon Cancer. *Anticancer Research*, 39(12), 6575–6583.

Tanaka, M., Gertsenstein, M., Rossant, J. & Nagy, A. (1997). Mash2 Acts Cell Autonomously in Mouse Spongiotrophoblast Development. *Developmental Biology*, 190(1), 55–65.

Taskin, M. B., Xu, R., Gregersen, H., Nygaard, J. V., Besenbacher, F. & Chen, M. (2016). Three-Dimensional Polydopamine Functionalized Coiled Microfibrous Scaffolds Enhance Human Mesenchymal Stem Cells Colonization and Mild Myofibroblastic Differentiation. *ACS Applied Materials and Interfaces*, 8(25), 15864–15873.

Testorelli, C., Bussini, S., De Filippi, R., Marelli, O., Orlando, L., Greiner, J. W., Grohmann, U., Tentori, L., Giuliani, A., Bonmassar, E. & Graziani, G. (1997). Dacarbazine-Induced Immunogenicity of a Murine Leukemia Is Attenuated in Cells Transfected with Mutated K-Ras Gene. *Journal of experimental & clinical cancer research : CR*, 16(1), 15–22.

Theveneau, E. & Mayor, R. (2013). Collective Cell Migration of Epithelial and Mesenchymal Cells. *Cellular and Molecular Life Sciences*, 70(19), 3481–3492.

Toi, M., Matsumoto, T. & Bando, H. (2001). Vascular Endothelial Growth Factor: Its Prognostic, Predictive, and Therapeutic Implications. *The Lancet. Oncology*, 2(11), 667–673.

Tojkander, S., Gateva, G. & Lappalainen, P. (2012). Actin Stress Fibers - Assembly, Dynamics and Biological Roles. *Journal of Cell Science*, 125(8), 1855–1864.

Tozer, G. M., Akerman, S., Cross, N. A., Barber, P. R., Björndahl, M. A., Greco, O., Harris, S., Hill, S. A., Honess, D. J., Ireson, C. R., Pettyjohn, K. L., Prise, V. E., Reyes-Aldasoro, C. C., Ruhrberg, C., Shima, D. T. & Kanthou, C. (2008). Blood Vessel Maturation and Response to Vascular-Disrupting Therapy in Single Vascular Endothelial Growth Factor-A Isoform-Producing Tumors. *Cancer Research*, 68(7), 2301–2311.

Trepat, X. & Fredberg, J. J. (2011). Plithotaxis and Emergent Dynamics in Collective Cellular Migration. *Trends in cell biology*, 21(11), 638–646.

Trisciuoglio, D., Iervolino, A., Zupi, G. & Del Bufalo, D. (2005). Involvement of PI3K and MAPK Signaling in Bcl-2-Induced Vascular Endothelial Growth Factor Expression in Melanoma Cells. *Molecular biology of the cell*, 16(9), 4153–4162.

Tsai, Y.-P. & Wu, K.-J. (2012). Hypoxia-Regulated Target Genes Implicated in Tumor Metastasis. *Journal of Biomedical Science*, 19(1), 102.

Ueyama, Y. & Nakamura, M. (2000). Ribozyme-Mediated Inactivation of Mutant K-Ras Oncogene in a Colon Cancer Cell Line. , 83, 833–839.

Velling, T., Risteli, J., Wennerberg, K., Mosher, D. F. & Johansson, S. (2002). Polymerization of Type I and III Collagens Is Dependent on Fibronectin and Enhanced by Integrins A11β1 and A2β1. *Journal of Biological Chemistry*, 277(40), 37377–37381.

Vempati, P., Popel, A. S. & Mac Gabhann, F. (2014). Extracellular Regulation of VEGF: Isoforms, Proteolysis, and Vascular Patterning. *Cytokine and Growth Factor Reviews*.

Viloria-Petit, A., Miquerol, L., Yu, J. L., Gertsenstein, M., Sheehan, C., May, L., Henkin, J., Lobe, C., Nagy, A., Kerbel, R. S. & Rak, J. (2003). Contrasting Effects of VEGF Gene Disruption in Embryonic Stem Cell-Derived versus Oncogene-Induced Tumors. *EMBO Journal*, 22(16), 4091–4102.

Vincenti, V., Cassano, C., Rocchi, M. & Persico, G. (1996). Assignment of the Vascular Endothelial Growth Factor Gene to Human Chromosome 6p21.3. *Circulation*, 93(8), 1493–1495.

Vita, M. & Henriksson, M. (2006). The Myc Oncoprotein as a Therapeutic Target for Human Cancer. *Seminars in Cancer Biology*, 16(4), 318–330.

Volz, C. et al. (2020). Inhibition of Tumor VEGFR2 Induces Serine 897 EphA2-Dependent Tumor Cell Invasion and Metastasis in NSCLC. *Cell reports*, 31(4), 107568.

Wagner, K.-D., El Maï, M., Ladomery, M., Belali, T., Leccia, N., Michiels, J.-F. &

Wagner, N. (2019). Altered VEGF Splicing Isoform Balance in Tumor Endothelium Involves Activation of Splicing Factors Srpk1 and Srsf1 by the Wilms' Tumor Suppressor Wt1. *Cells*, 8(1).

Walcott, S. & Sun, S. X. (2010). A Mechanical Model of Actin Stress Fiber Formation and Substrate Elasticity Sensing in Adherent Cells. *Proceedings of the National Academy of Sciences of the United States of America*, 107(17), 7757–7762.

Waltenberger, J., Claesson-Welsh, L., Siegbahn, A., Shibuya, M. & Heldin, C. H. (1994). Different Signal Transduction Properties of KDR and Flt1, Two Receptors for Vascular Endothelial Growth Factor. *The Journal of biological chemistry*, 269(43), 26988–26995.

Wang, Bin, Ding, Y., Fan, P., Wang, Bing, Xu, J. & Wang, W. (2014). Expression and Significance of MMP2 and HIF-1α in Hepatocellular Carcinoma. *Oncology Letters*, 8(2), 539–546.

Wang, C., Mu, Z., Chervoneva, I., Austin, L., Ye, Z., Rossi, G., Palazzo, J. P., Sun, C., Abu-Khalaf, M., Myers, R. E., Zhu, Z., Ba, Y., Li, B., Hou, L., Cristofanilli, M. & Yang, H. (2017). Longitudinally Collected CTCs and CTC-Clusters and Clinical Outcomes of Metastatic Breast Cancer. *Breast cancer research and treatment*, 161(1), 83–94.

Wang, F., Yamauchi, M., Muramatsu, M., Osawa, T., Tsuchida, R. & Shibuya, M. (2011). RACK1 Regulates VEGF/Flt1-Mediated Cell Migration via Activation of a PI3K/Akt Pathway. *Journal of Biological Chemistry*.

Wang, J. & Schneider, I. C. (2017). Myosin Phosphorylation on Stress Fibers Predicts Contact Guidance Behavior across Diverse Breast Cancer Cells. *Biomaterials*, 120, 81–93.

Wang, W. Y., Pearson, A. T., Kutys, M. L., Choi, C. K., Wozniak, M. A., Baker, B. M. & Chen, C. S. (2018). Extracellular Matrix Alignment Dictates the Organization of Focal Adhesions and Directs Uniaxial Cell Migration. *APL Bioengineering*, 2(4).

Wang, X., Bove, A. M., Simone, G. & Ma, B. (2020). Molecular Bases of VEGFR-2-Mediated Physiological Function and Pathological Role. *Frontiers in Cell and Developmental Biology*, 8(November), 1–12.

Webb, A. H., Gao, B. T., Goldsmith, Z. K., Irvine, A. S., Saleh, N., Lee, R. P., Lendermon, J. B., Bheemreddy, R., Zhang, Q., Brennan, R. C., Johnson, D., Steinle, J. J., Wilson, M. W. & Morales-Tirado, V. M. (2017). Inhibition of MMP-2 and MMP-9 Decreases Cellular Migration, and Angiogenesis in in Vitro Models

of Retinoblastoma. *BMC Cancer*, 17(1), 1–11.

Weddell, J. C., Chen, S. & Imoukhuede, P. I. (2018). VEGFR1 Promotes Cell Migration and Proliferation through PLCγ and PI3K Pathways. *npj Systems Biology and Applications*, 4(1), 1–11.

Weigelin, B., Bakker, G.-J. & Friedl, P. (2012). Intravital Third Harmonic Generation Microscopy of Collective Melanoma Cell Invasion: Principles of Interface Guidance and Microvesicle Dynamics. *Intravital*, 1(1), 32–43.

Weigelt, B., Ghajar, C. M. & Bissell, M. J. (2014). The Need for Complex 3D Culture Models to Unravel Novel Pathways and Identify Accurate Biomarkers in Breast Cancer. *Advanced Drug Delivery Reviews*, 69–70, 42–51.

Weis, S., Cui, J., Barnes, L. & Cheresh, D. (2004). Endothelial Barrier Disruption by VEGF-Mediated Src Activity Potentiates Tumor Cell Extravasation and Metastasis. *The Journal of cell biology*, 167(2), 223–229.

Winkler, J., Abisoye-Ogunniyan, A., Metcalf, K. J. & Werb, Z. (2020). Concepts of Extracellular Matrix Remodelling in Tumour Progression and Metastasis. *Nature Communications*, 11(1), 1–19.

Wirtz, D., Konstantopoulos, K. & Searson, P. C. (2011). The Physics of Cancer: The Role of Physical Interactions and Mechanical Forces in Metastasis. *Nature Reviews Cancer*.

Wolf, K., Alexander, S., Schacht, V., Coussens, L. M., von Andrian, U. H., van Rheenen, J., Deryugina, E. & Friedl, P. (2009). Collagen-Based Cell Migration Models in Vitro and in Vivo. *Seminars in Cell and Developmental Biology*, 20(8), 931–941.

Wolf, K. & Friedl, P. (2011). Extracellular Matrix Determinants of Proteolytic and Non-Proteolytic Cell Migration. *Trends in Cell Biology*, 21(12), 736–744.

Wolf, K., te Lindert, M., Krause, M., Alexander, S., te Riet, J., Willis, A. L., Hoffman, R. M., Figdor, C. G., Weiss, S. J. & Friedl, P. (2013). Physical Limits of Cell Migration: Control by ECM Space and Nuclear Deformation and Tuning by Proteolysis and Traction Force. *Journal of Cell Biology*.

Wolf, K., Mazo, I., Leung, H., Engelke, K., Von Andrian, U. H., Deryugina, E. I., Strongin, A. Y., Bröcker, E. B. & Friedl, P. (2003). Compensation Mechanism in Tumor Cell Migration: Mesenchymal-Amoeboid Transition after Blocking of Pericellular Proteolysis. *Journal of Cell Biology*, 160(2), 267–277.

Wolf, K., Wu, Y. I., Liu, Y., Geiger, J., Tam, E., Overall, C., Stack, M. S. & Friedl, P. (2007). Multi-Step Pericellular Proteolysis Controls the Transition from

Individual to Collective Cancer Cell Invasion. *Nature cell biology*, 9(8), 893–904.

Wozniak, M. A., Modzelewska, K., Kwong, L. & Keely, P. J. (2004). Focal Adhesion Regulation of Cell Behavior. *Biochimica et Biophysica Acta - Molecular Cell Research*, 1692(2–3), 103–119.

Wu, Y., Zhong, Z., Huber, J., Bassi, R., Finnerty, B., Corcoran, E., Li, H., Navarro, E., Balderes, P., Jimenez, X., Koo, H., Mangalampalli, V. R. M., Ludwig, D. L., Tonra, J. R. & Hicklin, D. J. (2006). Anti-Vascular Endothelial Growth Factor Receptor-1 Antagonist Antibody as a Therapeutic Agent for Cancer. *Clinical Cancer Research*, 12(21), 6573–6584.

Xia, Y., Lian, S., Khoi, P. N., Yoon, H. J., Joo, Y. E. & Chay, K. O. (2015). Chrysin Inhibits Tumor Promoter-Induced MMP-9 Expression by Blocking AP-1 via Suppression of ERK and JNK Pathways in Gastric Cancer Cells. , 10(4), 1–16.

Xie, J., Bao, M., Bruekers, S. M. C. & Huck, W. T. S. (2017). Collagen Gels with Different Fibrillar Microarchitectures Elicit Different Cellular Responses. *ACS Applied Materials and Interfaces*, 9(23), 19630–19637.

Xu, Z. dong, Hao, T. & Gan, Y. H. (2020). RhoG/Rac1 Signaling Pathway Involved in Migration and Invasion of Salivary Adenoid Cystic Carcinoma Cells. *Oral Diseases*, 26(2), 302–312.

Xue, J., Wu, T., Dai, Y. & Xia, Y. (2019). Electrospinning and Electrospun Nanofibers: Methods, Materials, and Applications. *Chemical Reviews*, 119(8), 5298–5415.

Yalak, G., Shiu, J.-Y., Schoen, I., Mitsi, M. & Vogel, V. (2019). Phosphorylated Fibronectin Enhances Cell Attachment and Upregulates Mechanical Cell Functions. *PloS one*, 14(7), e0218893.

Yalak, G. & Vogel, V. (2015). Ectokinases as Novel Cancer Markers and Drug Targets in Cancer Therapy. *Cancer medicine*, 4(3), 404–414.

Yamada, K. M. & Sixt, M. (2019). Mechanisms of 3D Cell Migration. *Nature Reviews Molecular Cell Biology*, 20(12), 738–752.

Yamaguchi, T., Fushida, S., Kinoshita, J., Okazaki, M., Ishikawa, S., Ohbatake, Y., Terai, S., Okamoto, K., Nakanuma, S., Makino, I., Nakamura, K., Miyashita, T., Tajima, H., Takamura, H., Ninomiya, I. & Ohta, T. (2020). Extravasated Platelet Aggregation Contributes to Tumor Progression via the Accumulation of Myeloid-Derived Suppressor Cells in Gastric Cancer with Peritoneal Metastasis. *Oncology Letters*, 20(2), 1879–1887.

Yamahana, H., Terashima, M., Takatsuka, R., Asada, C., Suzuki, T., Uto, Y. & Takino, T. (2021). TGF-B1 Facilitates MT1-MMP-Mediated ProMMP-9 Activation and

Invasion in Oral Squamous Cell Carcinoma Cells. *Biochemistry and biophysics reports*, 27, 101072.

Yang, J. & Weinberg, R. A. (2008). Epithelial-Mesenchymal Transition: At the Crossroads of Development and Tumor Metastasis. *Developmental Cell*, 14(6), 818–829.

Yang, X., Zhang, Y., Yang, Y., Lim, S., Cao, Z., Rak, J. & Cao, Y. (2013). Vascular Endothelial Growth Factor-Dependent Spatiotemporal Dual Roles of Placental Growth Factor in Modulation of Angiogenesis and Tumor Growth. *Proceedings of the National Academy of Sciences of the United States of America*, 110(34), 13932–13937.

Yang, Y., Zhang, Y., Iwamoto, H., Hosaka, K., Seki, T., Andersson, P., Lim, S., Fischer, C., Nakamura, M., Abe, M., Cao, R., Skov, P. V., Chen, F., Chen, X., Lu, Y., Nie, G. & Cao, Y. (2016). Discontinuation of Anti-VEGF Cancer Therapy Promotes Metastasis through a Liver Revascularization Mechanism. *Nature Communications*.

Yee, P. P., Wei, Y., Kim, S. Y., Lu, T., Chih, S. Y., Lawson, C., Tang, M., Liu, Z., Anderson, B., Thamburaj, K., Young, M. M., Aregawi, D. G., Glantz, M. J., Zacharia, B. E., Specht, C. S., Wang, H. G. & Li, W. (2020). Neutrophil-Induced Ferroptosis Promotes Tumor Necrosis in Glioblastoma Progression. *Nature Communications*, 11(1), 1–22.

Yu, B., Zhu, N., Fan, Z., Li, J., Kang, Y. & Liu, B. (2022). MiR-29c Inhibits Metastasis of Gastric Cancer Cells by Targeting VEGFA. *Journal of Cancer*, 13(14), 3566–3574.

Yu, Y., Xiao, C. H., Tan, L. D., Wang, Q. S., Li, X. Q. & Feng, Y. M. (2014). Cancer-Associated Fibroblasts Induce Epithelial-Mesenchymal Transition of Breast Cancer Cells through Paracrine TGF-β Signalling. *British Journal of Cancer*, 110(3), 724–732.

Zeng, F. C., Zeng, M. Q., Huang, L., Li, Y. L., Gao, B. M., Chen, J. J., Xue, R. Z. & Tang, Z. Y. (2016). Downregulation of VEGFA Inhibits Proliferation, Promotes Apoptosis, and Suppresses Migration and Invasion of Renal Clear Cell Carcinoma. *OncoTargets and Therapy*, 9, 2131–2141.

Zhang, D., Sheng, Y., Piano, N., Jakuszeit, T., Cozens, E. J., Dong, L., Buell, A. K., Pollet, A., Lei, I. M., Wang, W., Terentjev, E. & Huang, Y. Y. S. (2022). Cancer Cell Migration on Straight, Wavy, Loop and Grid Microfibre Patterns. *Biofabrication*, 14(2).

Zhang, L., Huang, G., Li, X., Zhang, Y., Jiang, Y., Shen, J., Liu, J., Wang, Q., Zhu, J., Feng, X., Dong, J. & Qian, C. (2013). Hypoxia Induces Epithelial-Mesenchymal Transition via Activation of SNAI1 by Hypoxia-Inducible Factor -1α in Hepatocellular Carcinoma. *BMC Cancer*, 13, 24–27.

Zhang, L., Yu, D., Hu, M., Xiong, S., Lang, A., Ellis, L. M. & Pollock, R. E. (2000). Wild-Type P53 Suppresses Angiogenesis in Human Leiomyosarcoma and Synovial Sarcoma by Transcriptional Suppression of Vascular Endothelial Growth Factor Expression. *Cancer research*, 60(13), 3655–3661.

Zhang, Q., Bai, X., Chen, W., Ma, T., Hu, Q., Liang, C., Xie, S., Chen, C., Hu, L., Xu, S. & Liang, T. (2013). Wnt/β-Catenin Signaling Enhances Hypoxia-Induced Epithelial-Mesenchymal Transition in Hepatocellular Carcinoma via Crosstalk with Hif-1α Signaling. *Carcinogenesis*, 34(5), 962–973.

Zhang, W., Shi, X., Peng, Y., Wu, M., Zhang, P., Xie, R., Wu, Y., Yan, Q., Liu, S. & Wang, J. (2015). HIF-1α Promotes Epithelial-Mesenchymal Transition and Metastasis through Direct Regulation of ZEB1 in Colorectal Cancer. *PLoS ONE*, 10(6), 1–16.

Zhang, Y., Qian, J., Gu, C. & Yang, Y. (2021). Alternative Splicing and Cancer: A Systematic Review. *Signal Transduction and Targeted Therapy*, 6(1).

Zhang, Z., Hao, C., Liu, P., Tian, X., Wang, L., Zhao, L. & Zhu, C. (2014). Valproic Acid Inhibits Tumor Angiogenesis in Mice Transplanted with Kasumi-1 Leukemia Cells. *Mol Med Rep*, 9(2), 443–449.

Zhao, S., Jiang, E., Chen, S., Gu, Y., Shangguan, A. J., Lv, T., Luo, L. & Yu, Z. (2016). PiggyBac Transposon Vectors: The Tools of the Human Gene Encoding. *Translational Lung Cancer Research*, 5(1), 120–125.

Zheng, B., Zhou, C., Qu, G., Ren, C., Yan, P., Guo, W. & Yue, B. (2020). VEGFR2 Promotes Metastasis and PD-L2 Expression of Human Osteosarcoma Cells by Activating the STAT3 and RhoA-ROCK-LIMK2 Pathways. *Frontiers in oncology*, 10, 543562.

Zhou, X., Zhu, W., Nowicki, M., Miao, S., Cui, H., Holmes, B., Glazer, R. I. & Zhang, L. G. (2016). 3D Bioprinting a Cell-Laden Bone Matrix for Breast Cancer Metastasis Study. *ACS Applied Materials & Interfaces*, 8(44), 30017–30026. Retrieved from https://doi.org/10.1021/acsami.6b10673

Zhou, Z. H., Ji, C. D., Xiao, H. L., Zhao, H. Bin, Cui, Y. H. & Bian, X. W. (2017). Reorganized Collagen in the Tumor Microenvironment of Gastric Cancer and Its Association with Prognosis. *Journal of Cancer*, 8(8), 1466–1476.

Zips, D., Eicheler, W., Geyer, P., Hessel, F., Dörfler, A., Thames, H. D., Haberey, M. & Baumann, M. (2005). Enhanced Susceptibility of Irradiated Tumor Vessels to Vascular Endothelial Growth Factor Receptor Tyrosine Kinase Inhibition. *Cancer Research*, 65(12), 5374–5379.

Zirlik, K. & Duyster, J. (2018). Anti-Angiogenics: Current Situation and Future Perspectives. *Oncology Research and Treatment*, 41(4), 166–171.